# Implication de l'inflammasome NLRP3 dans la détection des toxines bactériennes et dans l'évolution du COVID-19

Océane Dufies

UNIVERSITÉ CÔTE D'AZUR

ÉCOLE DOCTORALE
SCIENCES DE LA VIE ET DE LA SANTÉ

# THÈSE DE DOCTORAT

# Implication de l'inflammasome NLRP3 dans la détection des toxines bactériennes et dans l'évolution du COVID-19


**Océane DUFIES**

Centre Méditerranéen de Médecine Moléculaire


Présentée en vue de l'obtention

**du grade de docteur en** Immunologie et Microbiologie

**d'**Université Côte d'Azur

**Dirigée par** : Dr Laurent Boyer

**Soutenue le** : 11 février 2022

Devant le jury, composé de :

Dr Patrick Auberger, DRCE, C3M, Inserm

Dr Nicolas Manel, DR1, Institut Curie, Inserm

Dr Thomas Henry, DR2, CIRI, Inserm

Dr Laurent Boyer, DR2, C3M, Inserm

Inserm

Implication de l'inflammasome NLRP3 dans la détection des toxines bactériennes et dans l'évolution du COVID-19

Jury :

Président du jury :

Dr. Patrick Auberger, DRCE, C3M, Inserm

Rapporteurs :

Dr. Nicolas Manel, DR1, Institut Curie, Inserm

Dr. Thomas Henry, DR2, CIRI, Inserm

Directeur de thèse :

Dr. Laurent Boyer, DR2, C3M, Inserm

Implication de l'inflammasome NLRP3 dans la détection des toxines bactériennes et dans l'évolution du COVID-19

# Résumé

Lors d'une infection, les mécanismes innés de détection des microorganismes pathogènes sont indispensables à la réponse immunitaire innée et à l'initiation de l'immunité adaptative. Une réponse immunitaire physiologique est définie comme une réponse proportionnelle et adaptée à la stimulation microbienne et doit conduire à une résolution effective de l'inflammation. Pour cela, l'hôte doit être capable de détecter quantitativement et qualitativement les micro-organismes. Du point de vue quantitatif, l'hôte détecte des motifs structuraux conservés au sein d'une classe de micro-organismes comme le lipopolysaccharide des bactéries Gram négatives. D'autre part, la détection de l'activité des facteurs de virulence – spécifiques aux pathogènes – permet une détection qualitative.

La découverte des PRR et plus précisément des inflammasomes a permis une avancée majeure dans la compréhension des mécanismes de détection des pathogènes et des signaux de danger liés aux dommages cellulaires produits lors de l'infections. Les inflammasomes sont des complexes macromoléculaires à l'origine de l'activation de la Caspase-1 et de la maturation des Interleukines (IL)-1ß et -18. L'inflammasome le mieux caractérisé est NLRP3. Cet inflammasome est régulé par des modifications post-traductionnelles qui régulent sa localisation, stabilité, changement de conformation et ses interactions protéiques. Initialement découverts pour leur implication dans des pathologies auto-inflammatoires, les inflammasomes sont également impliqués dans la détection de l'activité des facteurs de virulence notamment ceux ciblant les RhoGTPases.

Les Rho GTPases sont situées au carrefour de grandes voies de signalisation cellulaire ; en régulant la migration cellulaire, la phagocytose ou encore la transcription des gènes, ceux sont des acteurs majeurs de l'immunité. Cela en fait des cibles préférentielles pour les micro-organismes pathogènes. En effet, plus de 30 facteurs de virulence bactériens manipulent les Rho GTPases en utilisant diverses stratégies menant à leur inhibition ou leur activation.

La bactérie *Escherichia coli* (*E. coli*) uropathogène est la première cause de cystites et pyélonéphrites et dans les cas les plus graves de bactériémies. Plus d'un tiers des *E. coli* uropathogènes possèdent la toxine CNF1, une dé-amidase activant les Rho GTPases. Cette modification détruit l'activité GTPase intrinsèque et stimulée par les GAPs (GTPase-activating protein) de Rho, Rac et Cdc42.

Avant mon arrivée au laboratoire, l'équipe du Dr Laurent Boyer a montré que la toxine CNF1 induit une réponse immunitaire. En effet, au cours de la bactériémie chez la souris ou de l'infection systémique

chez la drosophile, les *E. coli* exprimant CNF1 sont éliminées plus rapidement que les *E. coli* ne possédant par CNF1. Au niveau cellulaire, l'activation des Rho GTPases par CNF1 est responsable de la production de cytokines pro-inflammatoires. En parallèle de cette réponse transcriptionnelle, la toxine CNF1 provoque la maturation de l'IL-1ß de façon dépendante de la Caspase-1, suggérant l'implication d'un inflammasome.

Mon projet de thèse était d'identifier l'inflammasome impliqué dans la détection de la toxine CNF1 et de caractériser la voie de signalisation menant à cette activation.

Nous avons identifié l'inflammasome NLRP3 comme étant responsable de la détection de l'activation de la Rho GTPase Rac2 par la toxine CNF1. Nous avons ensuite étudié le rôle de la kinase Pak1, effecteur majeur de Rac2, dans cette voie de signalisation et nous avons pu montrer que Pak1 joue un rôle crucial dans l'activation de l'inflammasome NLRP3 par CNF1. Pak1 phosphoryle la Thr659 du récepteur NLRP3 et cette phosphorylation est déterminante pour le recrutement de la protéine régulatrice Nek7 et l'activation de l'inflammasome NLRP3 en aval de la détection de CNF1. Finalement, nous avons pu montrer le rôle majeur de la voie Pak1-NLRP3 dans la mise en place d'une réponse immunitaire anti-virulence au cours de la bactériémie.

De plus, nous avons utilisé notre expertise pour étudier l'activation de l'inflammasome NLRP3 chez les patients infectés par le SARS-CoV-2. Cette étude nous a permis d'établir la signature de la réponse NLRP3 dans les cellules myéloïdes circulantes des patients COVID-19 et d'utiliser ces paramètres pour définir un score permettant de prédire l'évolution des patients.

En résumé, mon travail sur l'implication de l'inflammasome NLRP3 dans la détection de la virulence a permis une meilleure compréhension des mécanismes mis en jeu lors d'une réponse immunitaire anti-infectieuse.

Mots clés : Inflammasome – Rho-GTPases – Facteurs de virulence – COVID-19

Implication of the NLRP3 inflammasome in the sensing of RhoGTPase-activating toxins and clinical evolution of COVID-19

# Abstract

The innate immune detection of pathogenic microbes is crucial to enhance the immune response. During an infection, the activation of the innate immune system is the first step to establish an adaptative immune response. A physiological immune response is defined as adapted to the microbial environment and as an effectively resolved inflammation. To do so, the host must be able to detect qualitatively and quantitatively microbes. The detection of conserved microbial-associated molecular patterns (MAMPs) such as lipopolysaccharide of Gram-negative bacteria allows the host to evaluate the number of microbes. On the other hand, the detection of virulence factors' activity – pathogen-specific – give a qualitative view of microbes.

The discovery of inflammasomes has allowed a major advance in the understanding of the mechanisms of detection of pathogen- and danger-associated molecular patterns. Inflammasomes are macromolecular complexes responsible for the activation of Caspase-1 and the maturation of Interleukins (IL) -1ß and -18. The best characterized inflammasome is NLRP3. This inflammasome is regulated by post-translational modifications which regulate its localization, stability, conformational change and its protein interactions. Initially discovered for their involvement in autoinflammatory pathologies, there is growing evidence for the role of inflammasomes in detecting the activity of toxins and microbial effectors including those targeting Rho GTPases.

Rho GTPases are located at the crossroads of major cell signaling pathways; by regulating cell migration, phagocytosis or even gene transcription, these are major players in immunity. This makes them preferential targets for pathogenic microorganisms. Indeed, more than 30 bacterial virulence factors manipulate Rho GTPases using various strategies leading to their inhibition or activation.

The uropathogenic *Escherichia coli* (*E. coli*) bacterium is the primary cause of cystitis and pyelonephritis and in the most severe cases of bacteremia. More than a third of uropathogenic *E. coli* possess the CNF1 toxin, a de-amidase that activates Rho GTPases. This modification destroys the intrinsic GTPase activity stimulated by the GAPs (GTPase-activating protein) of Rho, Rac and Cdc42.

Before my arrival at the laboratory, Dr. Laurent Boyer's team showed that the CNF1 toxin induces an immune response. Indeed, during bacteremia in mice or systemic infection in drosophila, *E. coli* expressing CNF1 are eliminated more quickly than *E. coli* deleted for CNF1. At the cellular level, the activation of Rho GTPases by CNF1 is responsible for the production of pro-inflammatory cytokines.

Alongside this transcriptional response, the CNF1 toxin causes IL-1β to mature in a Caspase-1 dependent fashion, suggesting the involvement of an inflammasome.

My thesis project was to identify the inflammasome involved in the detection of the CNF1 toxin and to characterize the signaling pathway leading to this activation.

We have identified the NLRP3 inflammasome as being responsible for the detection of Rho GTPase Rac2 activation by the CNF1 toxin. We then studied the role of the kinase Pak1, a major effector of Rac2, in this signaling pathway and we were able to show that Pak1 plays a crucial role in the activation of the inflammasome NLRP3 by CNF1. Pak1 phosphorylates Thr659 of the NLRP3 receptor and this phosphorylation is critical for the recruitment of the regulatory protein Nek7 and the activation of the NLRP3 inflammasome downstream of the detection of CNF1. Finally, we were able to show the major role of the Pak1-NLRP3 pathway in the establishment of an anti-virulence immune response during mice bacteremia.

In addition, we used our expertise to study the activation of the NLRP3 inflammasome in patients infected with SARS-CoV-2. This study allowed us to establish the signature of the NLRP3 response in the circulating myeloid cells of COVID-19 patients and to use these parameters to define a score to predict the outcome of the patients.

In summary, my work on the involvement of the NLRP3 inflammasome in the detection of virulence has provided a better understanding of the mechanisms involved in an anti-infective response.

Keywords : Inflammasome – Rho-GTPases – Virulence factors – COVID-19

# Remerciements

Aux Dr Nicolas Manel et Dr Thomas Henry, je vous remercie d'avoir accepté d'évaluer cette thèse en tant que Rapporteurs, j'en suis honorée et j'espère être à la hauteur de vos attentes.

Au Dr Patrick Auberger, Examinateur et Président du jury, je te remercie d'avoir accepté cette fonction ! On se connaît depuis quelques années maintenant… Après avoir encadré la thèse de Maëva il y a presque 10ans, te voilà Président du jury de sa sœur ! Merci pour ta bienveillance.

A Laurent Boyer, Directeur de thèse, merci pour TOUT ! Et d'abord pour m'avoir supportée (dans les deux sens du terme !) pendant toutes ces années. Tu nous pousses à toujours donner le meilleur et nous encourage sans fin. Merci pour les looooongues conversations et pour tous tes précieux conseils. Toute l'équipe est d'accord sur un point : tu es un chef d'équipe parfait, tu nous fais confiance, tu as des idées brillantes et ton soutien est indéfectible ! Ce sera difficile de trouver un futur chef d'équipe à ta hauteur, autant scientifiquement qu'humainement ! Tu vas beaucoup me manquer !

A toute l'équipe, les « piliers » : Laurent, Anne, Patrick , Orane, Céline, Johan, Greg et les « jeunes plus si jeunes » : Cédric, Juan, Alissa, Loïc, Alex et Eva. Merci pour ces moments du quotidien et merci à tous pour cette bonne ambiance où on est tous proches les uns des autres et où l'entraide est toujours présente. Vous allez terriblement me manquer et j'espère pouvoir vous retrouver un jour ! En attendant, je vous souhaite beaucoup de belle science et beaucoup de bonheur ! *P.S. : Il ne fait pas très chaud à Boston, mais ça me ferait plaisir de vous y accueillir !*

Cédric, merci pour toutes ces discussions (où je t'empêchais de te concentrer… oups !), ton soutien et tes bonnes blagues. Tu as su apaiser mon tempérament « fougueux » plus d'une fois… ! Tes chaussettes et ta précision (et toi aussi) vont me manquer. Mais surtout tes macarons !!! Tu as l'étoffe d'un excellent chercheur et je te souhaite le meilleur pour la suite. *P.S. : on attend toujours le retour du Ruinart.*

Anne, que serait le labo sans toi ! Tu es notre référente à tous ! Tu nous impressionne par ta gentillesse, ton altruisme, ta disponibilité et la MASSE de travail que tu abats ! Ma thèse n'aurait pas été la même sans toi, autant techniquement qu'humainement ! Tu vas me manquer !

Patrick, j'ai adoré passer ces moments à l'animalerie avec toi ! Ton passage ne sera pas très facile à lire, mais je voulais te rendre hommage. Tes jeux de mots et ta constante bonne humeur et ta pédagogie vont me manquer !

Orane, ou « sosie de caractère » ! Tu vas énormément me manquer, autant ta bonne humeur que ton « exigence ». Dans ma dictature, tu serais la co-dictatrice… ça promet des bons moments ! Félicitations pour la naissance du petit Elyo ! Je te souhaite beaucoup de bonheur pour la suite et promis, je te

ramènerai des chewing-gums – ignobles – à la cannelle ( Patrick pourra aussi en profiter, il les… adore) ! *PS : un jour tu auras ta bouteille de Ruinart au Santa Swap*.

Céline, référente biologie moléculaire ET potins ! Tu as (presque) toujours un coup d'avance sur nous ! Tes potins, ta gentillesse et ta disponibilité vont me manquer (et me manquent déjà…). Je te souhaite beaucoup de bonheur avec Séb et Malo !

Johan, tu es une sorte de génie. On a vécu une belle expérience pendant le projet sur le COVID-19 et sans toi ça n'aurait jamais été possible ! Félicitations pour ton doctorat, ton poste de MCU-PH et pour la naissance de Capucine ! 2021 aura été une année plus que riche pour toi ! Félicitations ! Tu nous impressionnes ! Tu vas me manquer ! *P.S. : garde la prochaine bouteille de Ruinart pour le Santa Swap pour Orane !*

Greg, merci pour ton aide à l'animalerie et pour ta gentillesse. Dès que tu peux nous aider tu le fais, tu es quelqu'un de d'excessivement altruiste et on l'apprécie tous ! Je te souhaite le meilleur.

La team des « jeunes ou presque jeunes » : Juan, Alissa (Dr Majoor !), Loïc, Alex[3], Eva et Cédric (tu fais encore partie des jeunes, mais plus pour très longtemps !). Merci pour ces bons moments, les fous rires, les expériences pas très scientifiques et le soutient les uns envers les autres ! Vous allez me manquer !

Eva, je suis extrêmement heureuse de t'avoir rencontrée au labo ! On aurait pu se connaître bien plus tôt, mais on a rattrapé ça ! Tu nous as tous impressionnés pendant ton stage ! Tu me manques déjà énormément mais je sais que cette amitié durera longtemps ! Félicitations à toi et Sam pour la belle Elsie et je vous souhaite beaucoup de bonheur en Martinique !

A Maëva, la grande sœur, pour ton soutien et ton éclairage. Tu as su me guider dans mes choix et même si je n'ai pas toujours suivi tes conseils tu es toujours là pour m'encourager. BRAVO pour ton poste de CR, pour la création de la start-up et pour les prix ! Je souhaite le meilleur pour toi et pour Kévin, Giulia et Matteo.

A mon père, merci pour tout. Tu as toujours tout fait pour nous, tu as fait des choix en pensant avant tout à nous, merci pour ça. En plus de ça tu nous as toujours soutenues quelques soit nos choix. Je te souhaite beaucoup de bonheur.

Aux copains de longue date de Montpellier : Adrien, Ariane, Alex, Amine & Rémi, Olivier, Maxime et Victor. Merci pour tous ces bons moments passés ensemble et pour cette amitié qui dure maintenant depuis le début de la fac… ! Je vous souhaite beaucoup de bonheur et j'espère que vous viendrez faire un petit tour vers Boston !

# Table des matières

# Liste des figures



# Liste des tableaux

# Abréviations

| | |
|---|---|
| ADN | Acide désoxyribonucléique |
| ADP | Adenosine diphosphate |
| AIM2 | Absent In Melanoma 2 |
| ALR | Absent in melanoma 2 (AIM2)-like receptors |
| AMPc | Adenosine monophosphate cyclique |
| ARN | Acide ribonucléique |
| ASC | Apoptosis-associated speck-like protein containing a CARD |
| ATP | Adenosine triphosphate |
| CARD | Caspase recruitment domain |
| CD | Cluster of differentiation |
| CLR | C-type lectin receptors |
| CNF1 | Cytotoxic necrotizing factor 1 |
| COVID-19 | Coronavirus disease 2019 |
| DAMP | Danger-associated molecular patterns |
| ETI | Effector-triggered immunity |
| FMF | Familial Mediterranean fever |
| GBP | Guanylate-binding proteins |
| GDP | Guanosine diphosphate |
| GSDMD | Gasdermin D |
| GTP | Guanosine triphosphate |
| IFN | Interferon |
| IL | Interleukin |
| IL-1RA | Interleukin 1 receptor antagonist |
| ISGs | Interferon-stimulated gene |
| LPS | Lipopolysaccharides |
| LRR | Leucine-rich repeat |
| MAM | Mitochondria-associated membranes |
| MAMP | Microbe-associated molecular patterns |
| MAPK | Mitogen-activated protein kinase |
| MSU | Monosodium urate |
| MTOC | Microtubule-organizing center |
| NADPH | Nicotinamide Adenine Dinucleotide Phosphate |
| NBD | Nucleotide-binding domain |
| Nek7 | NIMA related kinase 7 |
| NET | Neutrophil extracellular trap |
| NLR | Nucleotide-binding oligomerization domain (NOD)-like receptor |
| NLRP | NOD, Leucine rich repeat and pyrin domain containing receptor |
| Pak1/2 | P21 activated kinase 1/2 |
| PAMP | Pathogen-associated molecular patterns |
| PBMC | Peripheral blood mononuclear cells |

| | |
|---|---|
| PKN1/2 | Serine/threonine-protein kinase N1/2 |
| PRR | Pattern recognition receptor |
| PTI | Pattern-triggered immunity |
| PYD | Pyrin domain |
| RLR | Retinoic acid-inducible gene I (RIG-I)-like receptors |
| ROCK | Rho-associated protein kinase |
| SARS-CoV-2 | Severe acute respiratory syndrome coronavirus 2 |
| SDRA | Syndrome de détresse respiratoire aiguë |
| TGN | Trans-Golgi network |
| TLR | Toll-like receptor |
| TNF | Tumor necrosis factor |

# Introduction

## 1. Immunité innée au cours de l'infection

L'immunité innée constitue la première ligne de défense au cours d'une infection. Celle-ci est mise en place dans les premières heures et fait intervenir différents types cellulaires. Les barrières épithéliales sont le premier obstacle qu'un micro-organisme rencontre. Si le pathogène parvient à franchir cette barrière, les cellules de l'immunité innée sont mises en jeu afin de combattre l'infection. L'activation de l'immunité innée est cruciale pour la mise en place, en aval, d'une immunité adaptative.

### 1.1. La théorie des MAMPs et PRRs

Les cellules de l'immunité innée détectent des motifs microbiens hautement conservés appelés PAMPS (Pathogen-Associated Molecular Patterns) (Janeway, 1989). En raison de leur présence chez les micro-organismes pathogènes et non pathogènes le terme MAMPs (Microbial-Associated Molecular Patterns) a été proposé ; celui-ci est maintenant privilégié pour désigner ces motifs (Ausubel, 2005). Les MAMPs sont des molécules systématiquement associées à une classe de micro-organismes, comme par exemple, le lipopolysaccharide (LPS) de la paroi des bactéries Gram négatives.

Les récepteurs cellulaires responsables de la reconnaissance des MAMPs ont été nommés « Pattern Recognition Receptors » (PRRs) par le Pr Charles Janeway qui formula cette hypothèse en 1989 (Janeway, 1989). Celle-ci fût confirmée par la découverte du récepteur Toll chez *Drosophila Melanogaster* (Lemaitre et al., 1996). Un an plus tard, le premier homologue de Toll chez l'humain (aujourd'hui nommé TLR4) est découvert (Medzhitov et al., 1997). Nous connaissons aujourd'hui 13 homologues de Toll nommés TLRs (Toll-like receptors) chez la souris et 10 TLRs chez l'homme (Medzhitov, 2009). Ces récepteurs jouent un rôle essentiel dans la réponse à l'infection en activant des voies de signalisation permettant la synthèse de cytokines et chimiokines pro-inflammatoires (Takeda and Akira, 2015).

Les PRRs regroupent actuellement un grand nombre de protéines classées en différentes classes : les TLRs, les récepteurs de type RIG-I (RLRs), les lectines de type C (CLR), les récepteurs de type Nod (NLRs), les récepteurs de type AIM2 (ALRs) ou encore cGAS (Brubaker et al., 2015; Fitzgerald and Kagan, 2020). Ces récepteurs reconnaissent ensemble un large panel de motifs microbiens, tel que détaillé dans le tableau 1. Les récepteurs formant des inflammasomes seront abordés dans la section « Inflammasomes » (page 17).

En reconnaissant des motifs microbiens conservés, l'immunité déclenchée par la détection de ceux-ci ne permet pas au système immunitaire de différencier les micro-organismes pathogènes et non-pathogènes, ni même de savoir s'ils sont vivants ou non. Comment le système immunitaire peut-il distinguer les microorganismes virulents et avirulents, et ainsi adapter sa réponse ?

| PRR | MAMP(s) reconnu(s) | Référence |
|---|---|---|
| **Récepteurs de type Toll** | | |
| TLR1/2* | Lipoprotéines | (Takeuchi et al., 2002) |
| TLR2/6* | Lipoprotéines | (Ozinsky et al., 2000) |
| TLR3 | ARN double brin | (Alexopoulou et al., 2001) |
| TLR4 | LPS | (Medzhitov et al., 1997; Poltorak et al., 1998) |
| TLR5 | Flagelline | (Hayashi et al., 2001) |
| TLR7 | ARN simple brin | (Diebold et al., 2004; Heil et al., 2004) |
| TLR8 | ARN simple brin | (Heil et al., 2004) |
| TLR9 | ADN (îlots CpG non méthylés) | (Hemmi et al., 2000) |
| TLR10/2* | Lipoprotéines | (Guan et al., 2010) |
| TLR11 | Profilin (*Toxoplasma gondii*) | (Yarovinsky et al., 2005) |
| TLR12 | Profilin (*Toxoplasma gondii*) | (Koblansky et al., 2013) |
| TLR13 | ARN ribosomal bactérien | (Hidmark et al., 2012) |
| **Récepteurs de type RIG-I** | | |
| RIG-I | ARN double brin et simple brin | (Yoneyama et al., 2004) |
| MDA5 | ARN double brin | (Kato et al., 2006) |
| LGP2 | ARN double brin | (Rothenfusser et al., 2005) |
| **Lectines de type C** | | |
| Dectin-1 | ß-glucanes | (Brown and Gordon, 2001) |
| Dectin-2 | Mannanes α | (Saijo et al., 2010) |
| DC-SIGN | N-glycanes riches en mannose | (Feinberg et al., 2001) |
| **cGAS** | ADN double brin | (Sun et al., 2013) |

*Tableau 1 : Détection des motifs microbiens par les PRRs*
* : dimérisation du TLR2 avec un autre TLR.

### 1.2. Détection de la virulence des microorganismes

Il est avant tout nécessaire de définir la notion de virulence. La virulence d'un microorganisme se définit par sa capacité à causer des dommages à l'hôte. Cependant la virulence d'un pathogène est directement en lien avec la susceptibilité de l'hôte (Bhavsar et al., 2007; Casadevall and Pirofski, 2019; Stuart et al., 2013). Les facteurs de virulence bactériens sont des molécules promouvant la dissémination, l'invasion ou encore l'échappement au système immunitaire de l'hôte.

Chez la plante, il existe une théorie permettant au système immunitaire de distinguer si un microorganisme est virulent ou non. Celle-ci oppose l'immunité dite « médiée par les motifs microbiens » (ou PTI pour « Pattern-Triggered Immunity ») à l'immunité dite « médiée par les effecteurs microbiens » (ou ETI pour « Effector-Triggered Immunity »). L'ETI permet la détection de l'activité des facteurs de virulence microbiens exprimés exclusivement par les pathogènes *via* des protéines de type « NB-LRR » (Jones and Dangl, 2006).

Jusque dans les années 2000, la théorie des PRRs proposée par le Pr Charles Janeway était prédominante et ne permettait pas à elle seule d'expliquer la modulation de réponse du système immunitaire face à un micro-organisme non pathogène chez les métazoaires. La découverte de mécanismes moléculaires permettant la détection des facteurs de virulence bactériens ou des dommages cellulaires a permis l'émergence de nouvelles hypothèses. Celles-ci permettent d'expliquer la différence d'amplitude de réponse immunitaire observée entre un micro-organisme pathogène et non pathogène (Fischer et al., 2020; Matzinger, 2002a; Stuart et al., 2013; Vance et al., 2009). Parmi ces hypothèses, l'immunité dirigée contre les effecteurs microbiens décrite chez les plantes semble être conservée chez les métazoaires (Boyer et al., 2011; Diabate et al., 2015; Stuart et al., 2013).

## 2. Les inflammasomes

En 2002, l'équipe de Jürg Tschopp découvre des plateformes de signalisation macromoléculaires appelées inflammasomes (Martinon et al., 2002). Les inflammasomes sont impliqués dans la détection des signaux de dangers (DAMPs) (Tableau 2). Ils permettent l'activation de la Caspase-1 et la maturation des cytokines pro-inflammatoires Interleukine-1ß (IL-1ß) et Interleurkine-18 (IL-18) via leur clivage par la Caspase-1 (Lamkanfi and Dixit, 2014).

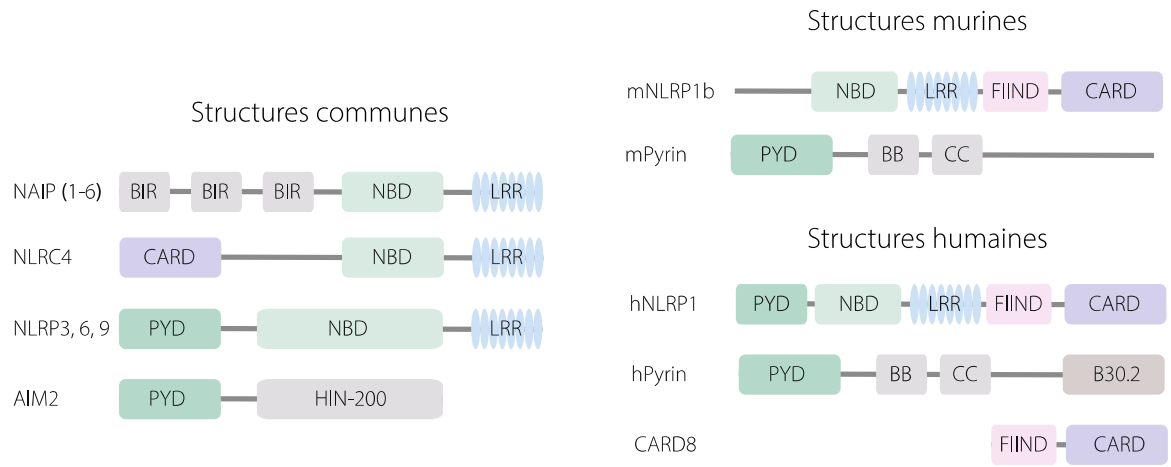


*Figure 1 : Structures des récepteurs formant un inflammasome chez l'homme et la souris*

Les inflammasomes sont composé d'un récepteur de type NLR, Pyrin ou PYHIN (ex : AIM2) (Figure 1), d'un adaptateur ASC lorsqu'il est nécessaire et d'un effecteur, la Caspase-1. La majorité des récepteurs s'oligomérisant en un inflammasome comportent un domaine de type « NB-LRR » également retrouvé chez les végétaux et possèdent une activité ATPase portée par leur domaine NBD (Duncan et al., 2007; Jones et al., 2016). Cependant, tous les récepteurs possédant un domaine NBD n'ont pas été décrits pour former un inflammasome et tous les récepteurs formant un inflammasome ne comportent pas de domaine NBD (ex : AIM2, Pyrin, CARD8). Cette partie se consacrera donc aux récepteurs dont la capacité à former un inflammasome a été démontrée.

| Récepteur | Détection | Références |
|---|---|---|
| NLRP1/1b | Protéases, E3-ligases et ARN double brin | (Bauernfried et al., 2021; Levinsohn et al., 2012; Robinson et al., 2020; Tsu et al., 2021) |
| CARD8 | Protéases | (Liu et al., 2021) |
| NLRP3 | Divers signaux de dangers stériles et microbiens | Revu dans (Swanson et al., 2019) |
| NLRP6 | Acide lipoteichoïque et ARN double brin | (Hara et al., 2018; Wang et al., 2015) |
| NAIP1/NLRC4 | Aiguille du SST3 | (Kofoed and Vance, 2011) |
| NAIP2/NLRC4 | Corps basal du SST3 | (Kofoed and Vance, 2011) |
| NAIP5/NLRC4 | Flagelline | (Kofoed and Vance, 2011) |
| NAIP6/NLRC4 | Flagelline | (Kofoed and Vance, 2011) |
| DDX17/NLRC4 | Petits éléments nucléaires intercalés | (Wang et al., 2021b) |
| AIM2 | ADN double brin cytosolique | (Bürckstümmer et al., 2009; Fernandes-Alnemri et al., 2009; Hornung et al., 2009; Roberts et al., 2009) |

*Tableau 2 : Activation des différents inflammasomes*
SST3 : Système de sécrétion de type III

### 2.1. La Caspase-1

La Caspase 1 est une protéase à cystéines nécessaire au clivage des cytokines pro-inflammatoires IL-1ß et IL-18. Ce clivage permet leur maturation, essentielle à leur activité biologique. La Caspase-1 nécessite également d'être clivée pour être active. En effet, elle est composée d'un domaine CARD et d'un domaine catalytique constitué d'une sous unité p10 et p20. Le domaine CARD de cette protéase est essentiel pour son recrutement au sein d'un inflammasome dont le but est la dimérisation de la Caspase-1 nécessaire pour son clivage (Boucher et al., 2018), la Caspase-1 subit ensuite différents clivages (Figure 2).

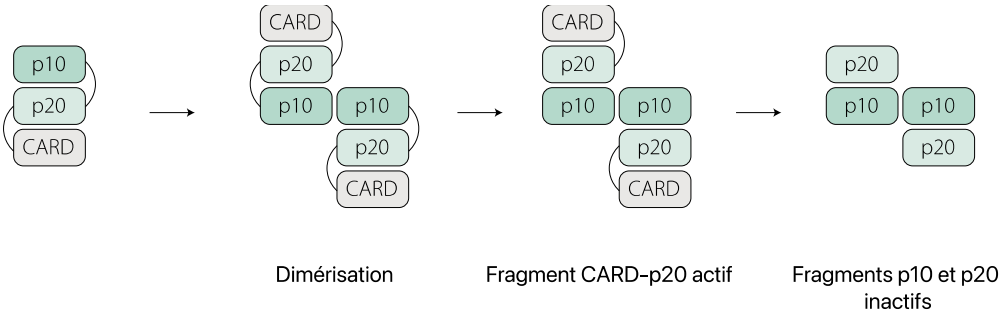


*Figure 2 : Mécanisme d'activation de la Caspase 1*

### 2.2. La protéine adaptatrice ASC

Certains PRRs intracellulaires possèdent un domaine CARD leur permettant une interaction directe homotypique CARD-CARD avec la Caspase-1, cependant, une grande partie n'en possède pas.

L'adaptateur ASC est nécessaire pour permettre l'interaction entre les récepteurs ne possédant pas de domaine CARD et la Caspase-1. ASC est composé d'un domaine Pyrin (PYD) interagissant avec le domaine PYD du récepteur et un domaine CARD (Caspase recruitment domain) liant le domaine CARD de la Caspase-1 (Oroz et al., 2016) (Figure 3). Lorsque l'inflammasome s'active et s'oligomérise, l'adaptateur ASC forme des structures punctiformes nommées « specks ». La nucléation des oligomères d'ASC permet d'amplifier le signal. En effet, cela permet une augmentation localisée de la concentration de la Caspase-1 et facilite la dimérisation et l'autoprotéolyse de cette dernière (Dick et al., 2016).

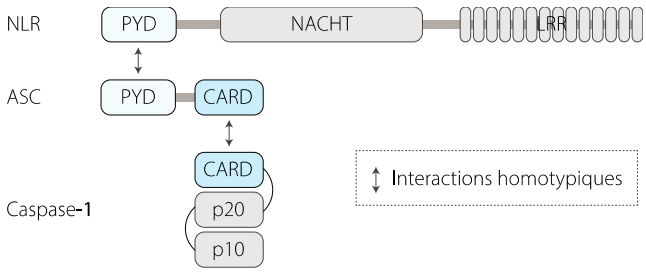


*Figure 3 : L'adaptateur ASC*

## 2.3. Les Interleukines 1ß et 18

### 2.3.1. Fonctions biologiques

L'IL-1ß est une cytokine pyrogénique, l'augmentation de la température corporelle accentue la migration des leucocytes. De plus, l'IL-1ß induit l'expression de molécules d'adhérence telles que ICAM-1 et VCAM-1 par les cellules endothéliales afin de promouvoir l'infiltration des leucocytes au site d'infection (Kupper and Groves, 1995). En se fixant à son récepteur, l'IL-1ß induit également l'activation de la voie NF-κB et donc sa propre transcription ainsi que d'autres cytokines et chimiokines pro-inflammatoires comme l'IL-6 (O'Neill, 2002).

### 2.3.2. Synthèse et maturation

Les Interleukines 1ß et 18 sont deux cytokines inflammatoires. La transcription de l'IL-1ß est induite par l'activation des TLRs, la cascade du complément et la signalisation en aval du récepteur de l'IL-1 (IL- 1R) (Weber et al., 2010). Contrairement à l'IL-1ß, l'IL-18 est exprimée de façon constitutive (Marshall et al., 1999).

Ces cytokines sont synthétisées dans le cytosol sous la forme d'un précurseur (pro-IL-1ß/pro-IL-18) nécessitant l'action de la Caspase 1 pour être clivé en forme mature. Seule la forme mature peut se fixer au Récepteur à l'IL-1 (IL-1R) ou à l'IL-18 (IL-18R) et activer ces derniers (Mosley et al., 1987).

### 2.3.3.Sécrétion

Les deux formes (précurseur et forme active) sont sécrétées. Les cytokines IL-1ß et IL-18 ne comportent pas de peptide signal permettant leur sécrétion par la voie conventionnelle (Hazuda et al., 1988; Stevenson et al., 1992). Le mécanisme de sécrétion de l'IL-1ß le mieux caractérisé implique les pores de Gasdermine D (GSDMD). Cependant, des mécanismes alternatifs de sécrétion ont été décrits.

#### 2.3.3.1. Sécrétion dépendante de la GSDMD

La Gasdermine D est clivée par les caspases inflammatoires 1 et 11 lorsque celles-ci sont activées. Ce clivage produit un fragment N-terminal (Gasdermine-N) et un fragment C-terminal (Gasdermine-C) (He et al., 2015; Shi et al., 2015) . Les fragments Gasdermine-N forment des oligomères qui s'ancrent dans la membrane plasmique afin de former un pore (Liu et al., 2016b). L'ancrage membranaire de la GSDMD provoque un gonflement de la cellule et une libération contrôlée de protéines comme l'IL-1ß ou l'IL-18 (He et al., 2015; Shi et al., 2015, 2017). Dans un deuxième temps, la Ninjurine 1 (NINJ1) s'ancre à son tour dans la membrane plasmique et provoque la lyse des cellules et ainsi une libération non contrôlée du contenu cellulaire (LDH, HMGB1…) (Bjanes et al., 2021; Kayagaki et al., 2021). Le mécanisme d'activation de NINJ1 n'est cependant pas encore élucidé (Newton et al., 2021).

La GSDMD est la mieux caractérisée dans le contexte infectieux mais d'autres Gasdermines comme la GSDMB ou la GSDME jouent également un rôle lors d'infections virales ou bactériennes. Alors que la GSDMD est clivée par les Caspases-1 et -11, la GSDMB et la GSDME sont respectivement clivées par le Granzyme A et la Caspase-3, de façon indépendante des inflammasomes (Hansen et al., 2021; Orzalli et al., 2021).

Étant donné le rôle important de la pyroptose dans l'élimination des pathogènes intracellulaires, par destruction de leur niche, il n'est pas étonnant de constater que la GSDMD est la cible de pathogènes. En effet, l'E3-ligase IpaH7.8 de *Shigella flexneri* ubiquitine la GSDMD et provoque sa dégradation par le protéasome, inhibant ainsi la pyroptose en aval de l'activation des inflammasomes NLRC4 et NLRP3 (non canonique) et la destruction de sa niche réplicative. De manière intéressante, la GSDMD murine n'est pas un substrat de IpaH7.8 et les souris sont résistantes à l'infection par *Shigella* (Luchetti et al., 2021). L'entérovirus 71 et le SARS-CoV-2 inhibent également la pyroptose en ciblant GSDMD : leurs protéases de type 3C clivent la GSDMD en 2 fragments inactifs (Lei et al., 2017; Planès et al., 2021).

Cependant, l'activation d'un inflammasome, l'ancrage de la GSDMD et la sécrétion d'IL-1ß ne sont pas toujours synonymes de mort cellulaire (Conos et al., 2016; Evavold et al., 2018; Monteleone et al., 2018; Wolf et al., 2016; Zanoni et al., 2016). En effet, il existe un mécanisme de réparation des pores de GSDMD dans la membrane plasmique par la machinerie ESCRT-III (Rühl et al., 2018). La GSDMD est également régulée négativement par succination (Humphries et al., 2020).

#### 2.3.3.2. Sécrétion indépendante de la GSDMD

Récemment, l'équipe de Kate Schroder a révélé un mécanisme pouvant expliquer à la fois la sécrétion d'IL-1ß GSDMD-dépendante et indépendante (Monteleone et al., 2018) . La maturation de l'IL-1ß induirait sa relocalisation au niveau de la membrane plasmique enrichie en PtdInsP2 (Phosphatidylinositol-4,5-bisphosphate) grâce à des interactions électrostatiques. Cependant, cela ne permet d'expliquer la présence de pro-IL-1ß dans le milieu extracellulaire.

Il a été observé qu'après stimulation, l'IL-1ß est localisé au niveau du cytosol mais également dans des vésicules présentant des marqueurs endolysosomaux (Cathespines D, LAMP-1) (Andrei et al., 1999). Bien que cette cytokine soit synthétisée dans le cytosol, l'implication d'autophagosomes ou de corps multivésiculaires qui fusionneraient avec la membrane plasmique dans un second temps pourrait être un nouveau mécanisme de sécrétion (Lopez-Castejon and Brough, 2011).

### 2.4. L'inflammasome NLRP1

NLRP1 a été le premier récepteur montré pour former un inflammasome responsable de l'activation de la Caspase-1 (Martinon et al., 2002). Chez l'homme il existe un unique gène codant pour NLRP1 tandis que la souris possède deux gènes orthologues *NLRP1A* et *NLRP1B* ainsi qu'un pseudogène *NLRP1C*. La principale différence est l'absence d'un domaine PYD chez les rongeurs. Le récepteur NLRP1 humain possède à la fois un domaine CARD ainsi qu'un domaine PYD, qui théoriquement, permettent le recrutement de la Caspase-1 et de l'adaptateur ASC respectivement (Chavarría-Smith and Vance, 2015). Le récepteur NLRP1/1b possède un domaine FIIND qui est clivé par autoprotéolyse et composé des domaines ZU5 et UPA. Ces domaines restent associés de façon non covalente après autoprotéolyse (D'Osualdo et al., 2011; Finger et al., 2012; Frew et al., 2012).

L'inflammasome NLRP1/1b est activé par clivage direct (protéases virales et bactériennes) ou par ubiquitination (E3-ligases). En effet, le facteur létal (LF) de *Bacillus anthracis* et la protéase de type 3C des entérovirus et betacoronavirus clivent la partie N-terminale de NLRP1b et le domaine NACHT de NLRP1 respectivement (Levinsohn et al., 2012; Planès et al., 2021; Robinson et al., 2020; Tsu et al., 2021). De plus, l'effecteur IpaH7.8 de *Shigella* a également été montré pour ubiquitiner NLRP1b (Sandstrom et al., 2019).

Ces modifications entrainent la déstabilisation du récepteur et la dégradation du fragment N-terminal par le protéasome à la suite de la règle du N-terminal (Chui et al., 2019; Sandstrom et al., 2019; Xu et al., 2019). Grâce à l'autoprotéolyse du domaine ZU5-UPA, le fragment C-terminal (UPA-CARD), associé de façon non covalente, est libéré et non dégradé par le protéasome. Enfin, ce fragment C-terminal UPA-CARD s'oligomérise et recrute l'adaptateur ASC pour former un inflammasome (Figure 4). La nécessité de l'interaction avec l'adaptateur ASC s'explique par l'incapacité – étonnante – du domaine

CARD de NLRP1 à recruter directement la Caspase-1 (Ball et al., 2020; Robert Hollingsworth et al., 2021). Il est intéressant de noter que le récepteur NLRP1 humain, en plus du domaine CARD, possède un domaine PYD situé à l'extrémité N-terminale. Le domaine PYD de NLRP1 semble jouer un rôle inhibiteur puisque son ablation induit l'activation spontanée de l'inflammasome NLRP1 (Bauernfried et al., 2021; Zhong et al., 2016).

Le récepteur NLRP1/1b est régulé par les peptidases DPP8 et DPP9. En effet, l'inhibition de DPP8/9 accélère l'ubiquitination et la dégradation du domaine N-terminal de NLRP1. Deux études récentes ont démontré que DPP9 s'associe au domaine C-terminal UPA-CARD en combinaison avec un monomère de NLRP1 (via son domaine ZU5) afin d'inhiber l'oligomérisation des fragments UPA-CARD en un inflammasome actif (Hollingsworth et al., 2021; Huang et al., 2021) (Figure 4). Il semblerait que le ratio cellulaire entre le récepteur NLRP1 dans sa forme entière et le domaine UPA-CARD de NLRP1 agissent comme un verrou de l'activation intempestive de l'inflammasome NLRP1.

Chez l'homme, l'inflammasome NLRP1 détecte également les ARN viraux doubles brins lors de la réplication virale de virus simple brins à polarité positive (Bauernfried et al., 2021). L'activation de l'inflammasome NLRP1 dans ce contexte nécessite l'action du protéasome mais n'implique pas la règle du N-terminal. Il a été montré que NLRP1 interagit directement avec l'ARN double brin, avec pour conséquence l'activation de son activité ATPase (contenue dans le domaine NACHT).

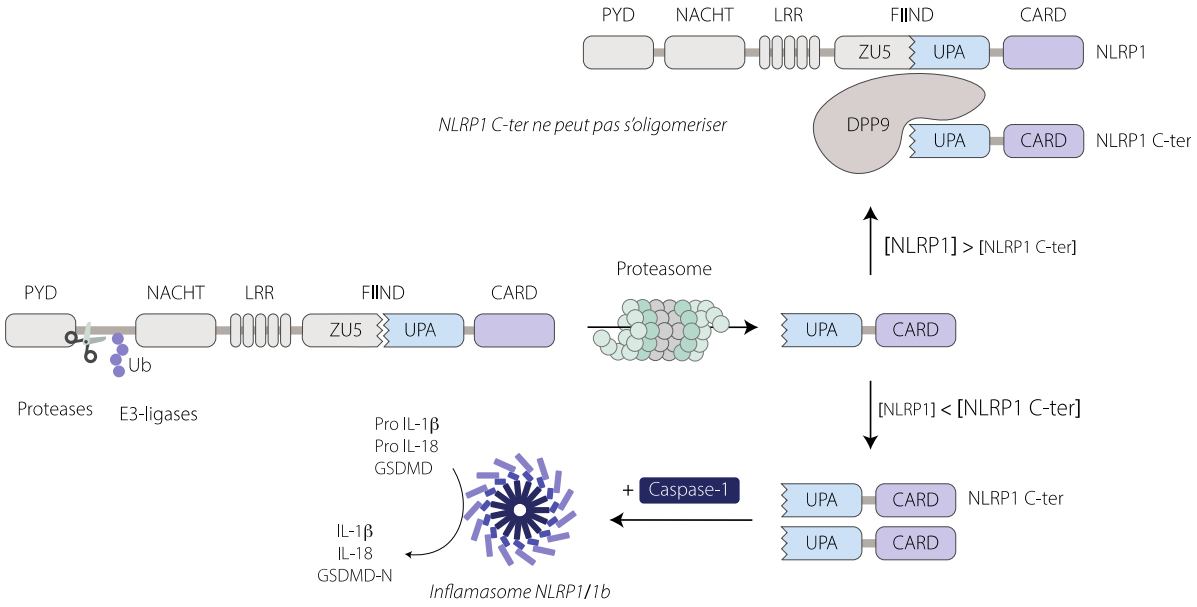


*Figure 4 : Mécanisme d'activation de l'inflammasome NLRP1*

### 2.5. L'inflammasome CARD8

L'inflammasome CARD8 est présent chez l'homme mais absent chez la souris et présente de grandes similarités avec l'inflammasome NLRP1. En effet, CARD8 est structurellement proche de NLRP1 : il

possède également un domaine FIIND qui est auto-clivé et composé des sous-domaines ZU5 et UPA (D'Osualdo et al., 2011). Cet inflammasome est également régulé par les peptidases DPP8/9 (Johnson et al., 2020; Sharif et al., 2021).

Il existe néanmoins des différences entre CARD8 et NLRP1. En effet, le récepteur CARD8 ne possède que les domaines FIIND et CARD. De plus, l'activation de cet inflammasome ne fait pas intervenir l'adaptateur ASC, mais le domaine CARD de CARD8 recrute directement la Caspase-1 (Ball et al., 2020; Robert Hollingsworth et al., 2021).

L'inflammasome CARD8 a été montré pour être activé par la protéase du VIH-1 (Virus de l'immunodéficience humaine) dans des lymphocytes T $CD4^+$ non activés et les macrophages humains (Wang et al., 2021a). La protéase du VIH clive CARD8 sur deux sites : le premier est situé au niveau du domaine N-terminal et le deuxième est situé dans le domaine ZU5. Le clivage du domaine N-terminal de CARD8 est nécessaire à son activation qui dépend de la règle du N-terminal et de sa dégradation par le protéasome. L'activation de CARD8 induit la maturation de l'IL-1ß et la mort cellulaire par pyroptose des lymphocytes T $CD4^+$ (Linder et al., 2020).

### 2.6. L'inflammasome NLRP3

L'inflammasome NLRP3 nécessite deux signaux pour être activé : le premier signal ou signal de « priming » correspond à la détection de MAMPs par les TLRs et un second signal ou signal d'activation correspondant à la détection d'un signal de danger.

#### 2.6.1. Signal de priming

Le premier signal permet tout d'abord la transcription du récepteur NLRP3 et de la pro-IL-1ß via l'activation du facteur de transcription NF-κB en aval de l'activation des PRRs ou du récepteur à l'IL-1 (IL-1R).

Lors du priming, l'engagement des TLRs induit également la transcription de CMPK2, responsable de la synthèse de désoxyribonucleotides requis pour la synthèse d'ADN mitochondrial. L'oxydation de l'ADN mitochondrial est un signal de danger détecté par l'inflammasome NLRP3 (Zhong et al., 2018).

Le premier signal de priming a été décrit pour induire une régulation post-traductionnelle de NLRP3. En effet, NLRP3 est régulé par de nombreuses modifications post-traductionnelles comme l'ubiquitination, la phosphorylation ou encore la SUMOylation (Figure 5). Lorsque ces modifications sont induites par une stimulation des TLRs, celles-ci sont regroupées sous le terme de « priming non-transcriptionnel ». Cet événement intervient dans les premières minutes de la stimulation des TLRs et repose sur l'activation de la kinase IRAK1 en aval de Myd88 (Fernandes-Alnemri et al., 2013).

Lors de l'activation des TLRs au cours du priming, il semblerait que les kinases IKKε et AKT (en aval de TBK1) soient activées et phosphorylent NLRP3, notamment sur la Ser5 (Fischer et al., 2021; Zhao et al., 2020a). Cette modification située dans le domaine Pyrin (PYD) empêche l'interaction du domaine PYD de NLRP3 avec le domaine PYD de la protéine adaptatrice ASC par répulsion électrostatique (Stutz et al., 2017; Zhao et al., 2020a). La phosphorylation de ce résidu inhibe NLRP3 afin d'empêcher son activation intempestive. Dans un second temps, lors du signal d'activation, PP2A déphosphoryle la Ser5 de NLRP3 pour permettre son activation (Stutz et al., 2017).

Les kinases JNK1/2 phosphorylent NLRP3 sur la Ser198 en réponse au premier signal. Cette phosphorylation a été décrite comme nécessaire à l'activation de l'inflammasome NLRP3 (Song et al., 2017). Il a été montré que cette phosphorylation permet de recruter le complexe BRISC (BRCC3, BRE, HSPC142 et ABRO1) et d'induire la dé-ubiquitination du domaine LRR de NLRP3 par BRCC3, nécessaire à l'activation de l'inflammasome (Py et al., 2013; Ren et al., 2019). Lors du priming, la Ser806 est phosphorylée par CSNK1A1. Au cours de l'étape d'activation, la déphosphorylation de ce résidu est nécessaire au recrutement de Nek7 puis de la dé-ubiquitinase BRCC3 (Niu et al., 2021).

De plus, il a été montré que l'E3-ligase Pellino2 forme des chaines d'ubiquitine de type K63 sur NLRP3 en réponse à un signal de priming (Humphries et al., 2018). De manière étonnante, l'utilisation de MCC950 (un inhibiteur de l'activité ATPase de NLRP3) inhibe cette ubiquitination.

L'inflammasome NLRP3 est également régulé par SUMOylation. En réponse au LPS, l'E3-ligase TRIM28 ajoute des SUMO1, 2 et 3 sur NLRP3. Cette modification inhibe l'ajout de chaines d'ubiquitine de type K48 sur NLRP3 avec pour conséquence l'inhibition de la dégradation de NLRP3 par le protéasome et sa stabilisation (Qin et al., 2021).

Enfin, la phosphorylation de la Ser728 de NLRP3 lors du priming par la kinase Msn (MINK1) a été montrée pour être une étape critique à son activation (Zhu et al., 2021).

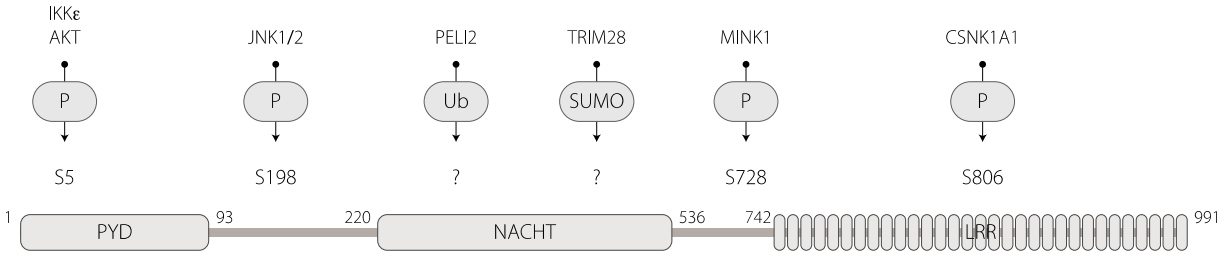


*Figure 5 : Modifications post-traductionnelles et priming de l'inflammasome NLPR3*

Les résidus modifiés correspondent à la protéine NLRP3 humaine. Ub : ubiquitination, deUb : déubiquitination, P : phosphorylation ; deP : déphosphorylation, SUMO : sumoylation.

### 2.6.2. Signaux d'activation

A la suite de la détection d'un signal de danger, le récepteur NLRP3 subit des modifications post-traductionnelles régulant son interaction avec l'adaptateur ASC puis le recrutement de la Caspase 1. Il a été montré que la protéine Nek7 est nécessaire à l'activation de l'inflammasome NLRP3 (Hauwermeiren and Lamkanfi, 2016; He et al., 2016) via son interaction avec le domaine LRR du récepteur (Sharif et al., 2019). Cette interaction intervient en amont du recrutement de l'adaptateur ASC (He et al., 2016).

L'inflammasome NLRP3 peut être activé par un large panel de signaux de dangers stériles (urate de sodium, ATP extracellulaire, cristaux de cholestérol, stress mitochondrial, amyloïde bêta…) ou microbiens (Nigéricine, *S. aureus*, *L. monocytogenes*…) (Hornung et al., 2008; Lamkanfi and Dixit, 2014). Étant donné la diversité des signaux détectés par cet inflammasome, il semblerait que NLRP3 se comporte plus comme un intégrateur de signal plutôt qu'un réel récepteur de motif (PRR). Plusieurs évènements semblent agir en amont de l'activation de l'inflammasome NLRP3 (Figure 6)

#### 2.6.2.1. Flux ioniques

- *Efflux de potassium et de chlore*

La toxine ionophore Nigéricine de *Streptomyces hygroscopicus* agit comme un antiport $H^+/K^+$. Son ancrage membranaire provoque un efflux de potassium (Budunova and Mittelman, 1992). D'autres signaux comme l'ATP extracellulaire, via sa fixation au récepteur P2X7R, ou les cristaux sont connus pour induire un efflux de potassium (Yang et al., 2019b).

L'efflux de potassium est un élément nécessaire à l'activation de l'inflammasome NLRP3 (Katsnelson et al., 2012; Muñoz-Planillo et al., 2013; Pétrilli et al., 2007). La kinase Nek7 semble permettre un changement de conformation de NLRP3 en aval de l'efflux de potassium, de façon indépendante de son activité kinase (Hauwermeiren and Lamkanfi, 2016; He et al., 2016; Sharif et al., 2019; Shi et al., 2016). Il semblerait néanmoins que certains activateurs de l'inflammasome NLRP3, comme le stress mitochondrial induit par l'imiquimod, ne nécessitent pas d'efflux de potassium pour induire un signal de danger alors que Nek7 demeure nécessaire pour l'activation de l'inflammasome (Groß et al., 2016).

Cependant, la voie de signalisation impliquée dans l'activation de l'inflammasome NLRP3 par l'efflux potassique n'était pas clairement décrite jusqu'à récemment. Il a été montré que les activateurs de l'inflammasome NLRP3 (Nigéricine, ATP, cristaux d'urate de sodium) induisent une dispersion du réseau trans-golgien (TGN). Ce mécanisme sera détaillé dans la partie 2.6.2.2.

L'efflux de chlore a également été décrit pour jouer un rôle dans l'activation de l'inflammasome NLRP3. Les ROS mitochondriaux provoqués par les activateurs de l'inflammasome NLRP3 (Nigéricine, ATP,

MSU…) induisent une translocation des canaux chlore de type CLIC du cytosol vers la membrane plasmique, provoquant un efflux de chlore impliqué dans l'activation de l'inflammasome NLRP3 (Tang et al., 2017). Il semblerait que l'efflux de chlore permette l'oligomérisation d'ASC en un speck de façon NLRP3-dépendante. En revanche ce dernier ne contiendrait ni Nek7 ni la Caspase-1 avant que l'efflux de potassium induise le recrutement de Nek7 et l'activation du complexe (Green et al., 2018).

Il existe une voie de régulation négative de l'activation de l'inflammasome NLRP3 en aval de l'efflux de potassium et de chlore. En effet, la protéine WNK1 détecte la chute de la concentration intracellulaire de chlore et active les protéines OSR1 et STK39 qui régulent les canaux co-transporteurs $Na^+/K^+/Cl^-$ SLC12A1, SLC12A2 et SLC12A3 afin de rétablir l'équilibre osmotique (Mayes-Hopfinger et al., 2021).

- *Mobilisation du calcium*

Le calcium est un second messager jouant un rôle important dans différents processus cellulaires. De nombreux activateurs de l'inflammasome NLRP3 induisent une mobilisation du calcium. (Lee et al., 2012; Murakami et al., 2012). Les cristaux provoquent la rupture des lysosomes qui libèrent du calcium dans le cytosol tandis que la mobilisation du calcium en aval de l'ATP ou de la Nigéricine semble impliquer le réticulum endoplasmique, un réservoir majeur de calcium intracellulaire. L'inflammasome NLRP3 est activé à la suite d'une hausse du calcium intracellulaire et une baisse de l'AMP cyclique (AMPc) (Lee et al., 2012). L'excès de calcium intracellulaire et la surcharge en calcium des mitochondries pourrait induire un dysfonctionnement mitochondrial (Murakami et al., 2012). De plus, l'AMPc semble agir comme un inhibiteur de NLRP3 via l'activation de la kinase PKA qui phosphoryle NLRP3 sur la Ser295. Cette phosphorylation induit l'ubiquitination subséquente du domaine LRR de NLRP3 par l'E3-ligase MARCH7 et sa dégradation par autophagie (Guo et al., 2016; Yan et al., 2015).

#### 2.6.2.2. Dysfonction des organelles

- *Rupture lysosomale*

La phagocytose de particules cristallines telles que les cristaux d'acide urique, de silice ou encore d'alun induit une déstabilisation des phagolysosomes et la libération d'enzymes lysosomales telles que les cathepsines B (Hornung et al., 2008; Sharp et al., 2009). Ces deux évènements sont nécessaires à l'activation de l'inflammasome NLRP3 en aval de la phagocytose de cristaux.

- *Dysfonctionnement mitochondrial*

Les mitochondries sont au centre de la régulation du métabolisme cellulaire comme le cycle de Krebs, la voie des pentoses phosphates ou encore la phosphorylation oxydative. Ces voies de signalisations sont étroitement liées à la polarisation des macrophages (O'Neill et al., 2016).

Les mitochondries jouent un rôle prépondérant dans l'activation de l'inflammasome NLRP3. En effet, des composés ciblant directement la machinerie mitochondriale activent NLRP3 mais les mitochondries jouent également un rôle dans l'activation de cet inflammasome en aval de toxines ou particules cristallines (Gurung et al., 2015).

L'imiquimod, connu pour être un agoniste du TLR7, est également un inhibiteur du complexe I de la chaine respiratoire mitochondriale et de NQO2 (quinone oxidoreductase) qui active l'inflammasome NLRP3 (Groß et al., 2016). La production de ROS mitochondriaux et l'inhibition du complexe I de la chaine respiratoire sont deux évènements requis pour l'activation de l'inflammasome NLRP3 par l'imiquimod de façon TLR7-indépendante. La perturbation du flux glycolytique par des composés chimique a également été décrite pour activer l'inflammasome NLRP3 (Sanman et al., 2016). L'inhibition de la GAPDH et de l'$\alpha$-enolase, impliquées dans la glycolyse, conduit à une chute de la concentration de NADH et à la production de ROS mitochondriaux, responsables de l'activation de NLRP3.

L'activation de l'inflammasome NLRP3 décrite dans ces deux études est indépendante de l'efflux de potassium. Il est intéressant de noter que cette activation est néanmoins dépendante de la protéine Nek7, décrite pour agir en aval de l'efflux de potassium (He et al., 2016).

Les dommages mitochondriaux induisent la libération et l'oxydation de l'ADN mitochondrial ainsi que l'externalisation de la cardiolipine. Ces événements sont également des signaux d'activation de l'inflammasome NLRP3 (Iyer et al., 2013; Shimada et al., 2012; Zhong et al., 2018).

Au cours du priming NLRP3 se localise au niveau des MAMs (mitochondria-associated ER membranes). Il a été montré que la PKD est activée en aval des dommages mitochondriaux et phosphoryle NLRP3 sur la Ser295. Cette modification post-traductionnelle induit une relocalisation de NLRP3 des MAMs vers le speck au niveau du MTOC (Microtubule-organizing center) (Zhang et al., 2017). Ces résultats sont à remettre en perspective d'autres résultats montrant que la PKA phosphoryle NLRP3 sur ce même résidu afin de l'inhiber (Guo et al., 2016).

La mitophagie permet d'éliminer les mitochondries endommagées. Il a été montré que la cellule utilise ce type d'autophagie comme rétrocontrôle négatif de l'activation de l'inflammasome NLRP3 (Kim et al., 2016; Lupfer et al., 2013).

- *Dispersion du réseau trans-golgien*

Comme décrit précédemment, l'efflux de potassium induit la dispersion du réseau trans-golgien. NLRP3 est recruté au réseau trans-golgien dispersé via l'interaction d'un domaine polybasique (chargé positivement) du récepteur (situé entre le PYD et le NACHT) et le phosphatidylinositol-4-phosphate (PtdIns4P) du TGN chargé négativement (Chen and Chen, 2018; Tapia-Abellán et al., 2021). Ce

recrutement est médié par l'efflux de potassium. En effet, les auteurs font l'hypothèse qu'une déplétion du potassium intracellulaire induit une baisse de la force ionique intracellulaire favorable à cette interaction (Chen and Chen, 2018). Après activation, NLRP3 est transporté via les microtubules au niveau du MTOC grâce à HDAC6 et MARK4 pour former un inflammasome (Li et al., 2017; Magupalli et al., 2020).

Il est intéressant de noter que la Tyr132 de NLRP3, située dans le domaine polybasique nécessaire au recrutement de NLRP3 au réseau trans-golgien, est phosphorylée par la kinase EphA2 pour inhiber NLRP3 (Zhang et al., 2020a).

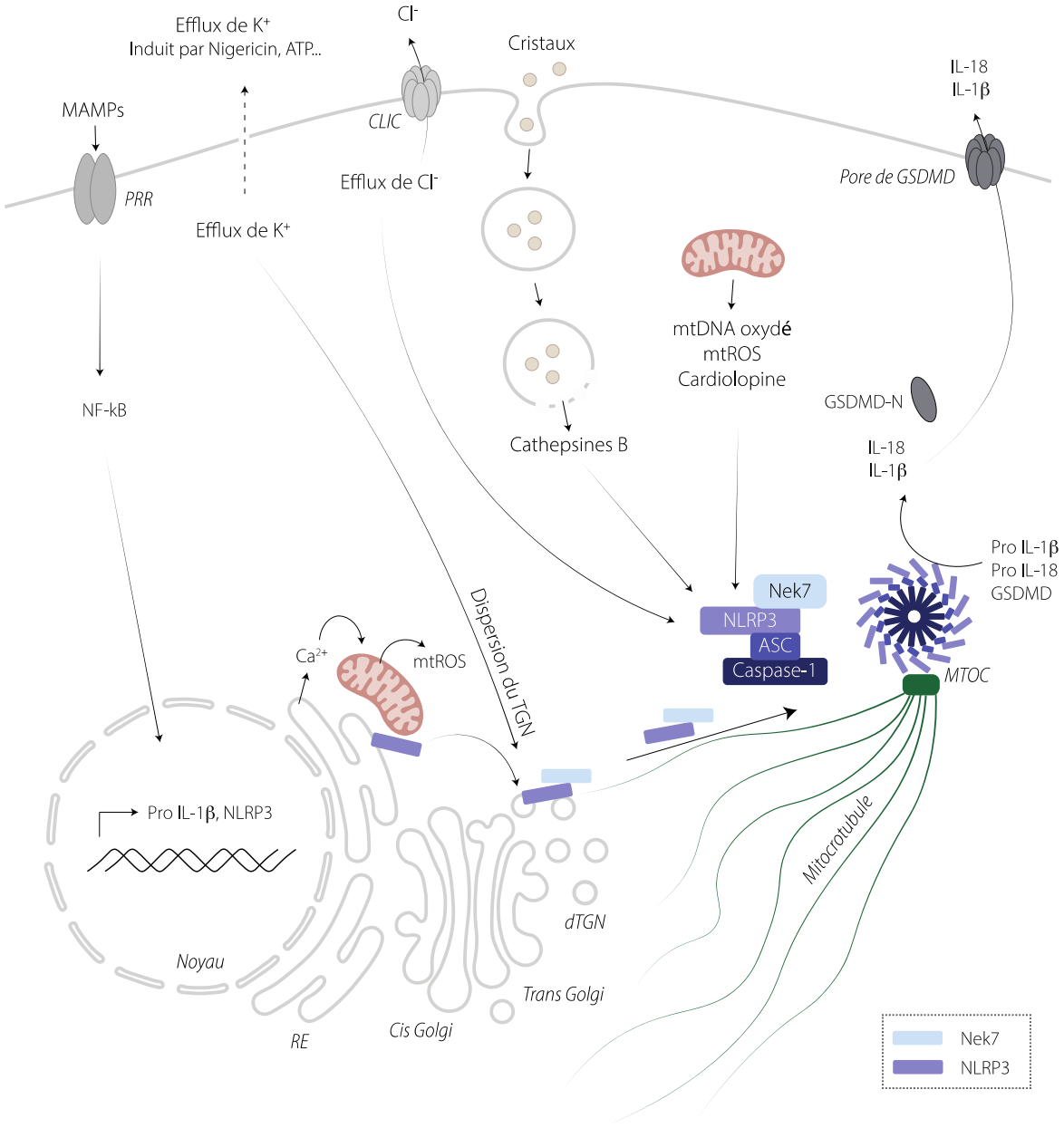


*Figure 6 : Activation de l'inflammasome NLRP3*

dTGN : Réseau trans-golgien dispersé ; MTOC : centre organisateur des microtubules

#### 2.6.2.1. Modifications post-traductionnelles supplémentaires

Dans cette partie je listerai les modifications post-traductionnelles nécessaires à l'étape d'activation de l'inflammasome NLRP3 qui, à ce jour, ne sont pas liées à des perturbations ioniques ou une dysfonction des organelles.

Au cours de la phase d'activation, la phosphatase PTPN22 déphosphoryle la Tyr861 de NLRP3. Cet événement est crucial pour l'activation de l'inflammasome en aval des cristaux ou de l'ATP extracellulaire (Spalinger et al., 2016).

La phase d'activation de l'inflammasome NLRP3 est également régulée par SUMOylation. En effet, la Lys204 est SUMOylée en aval du traitement des macrophages par ATP, Nigéricine ou encore des cristaux d'acide urique (Shao et al., 2020). Cette modification est nécessaire à l'activation de l'inflammasome NLRP3. La dé-SUMOylation par la protéase SENP3 est inhibitrice, mais les auteurs n'ont pas déterminé si SENP3 retire la SUMO1 du résidu Lys204 ou d'un autre résidu. Alors que la SUMOylation de la Lys204 est activatrice, la SUMOylation (SUMO-2/3) du domaine LRR de NLRP3 par MAPL inhibe l'activation de l'inflammasome (Barry et al., 2018). Les protéases SENP6/7 sont impliquées dans la dé-SUMOylation de résidus (non identifiés) afin de permettre l'assemblage de l'inflammasome NLRP3 (Barry et al., 2018).

De nombreuses E3-ligases agissent en tant que frein de l'activation de l'inflammasome NLRP3 en dirigeant NLRP3 vers la dégradation par le protéasome. En effet, l'E3-ligase TRIM31, dont la transcription est induite par le LPS, ubiquitine NLRP3 pour dégrader le récepteur (Song et al., 2016). C'est également le cas des E3-ligases ARIH2, Cbl-b, RNF125, Cul1 et FBXL2 qui ubiquitinent NLRP3 (Han et al., 2015; Kawashima et al., 2017; Tang et al., 2020; Wan et al., 2019).

L'exposition prolongée des macrophages au LPS induit une tolérance de l'inflammasome NLRP3. Il a été montré que le monoxyde d'azote (NO) inhibe l'activation de l'inflammasome NLRP3 par *S*-nitrosylation après une exposition prolongée au LPS ou aux Interférons de type I et II (Hernandez-Cuellar et al., 2012; Mishra et al., 2013). D'autre part, une exposition soutenue au LPS induit la production d'itaconate par Irg1, provoquant une tolérance des macrophages. Il a été montré que l'itaconate, en plus d'inhiber la transcription de gènes codant pour des cytokines pro-inflammatoires, est capable de modifier la Cys548 de NLRP3 pour inhiber son interaction avec Nek7 (Hooftman et al., 2020; Mills et al., 2018). En plus d'inhiber NLRP3, l'itaconate modifie également la Cys77 de la GSDMD et ainsi inhibe la pyroptose (Bambouskova et al., 2021).

### 2.6.3. Activation non canonique de l'inflammasome NLRP3

L'inflammasome NLRP3 peut également être activé en aval de la détection de LPS intracellulaire par la Caspase-11 chez la souris et les Caspase-4 et -5 chez l'homme. La Caspase-11 détecte le lipide A hexa-

acétylé du LPS par liaison directe à celui-ci via son domaine CARD (Hagar et al., 2013; Kayagaki et al., 2013; Shi et al., 2014). Chez l'homme, la Caspase-4 détecte également le lipide A tétra-acétylé contrairement à la Caspase-11 murine (Lagrange et al., 2018).

Une fois activée, la Caspase-11 clive la Gasdermine D et permet l'ancrage du fragment N-terminal dans la membrane plasmique qui s'oligomérise pour former un pore (Kayagaki et al., 2015). La formation du pore de Gasdermine D provoque un efflux de potassium responsable de l'activation de l'inflammasome NLRP3 (Rühl and Broz, 2015).

La transfection de LPS est une façon artificielle d'étudier la détection de LPS intracellulaire. En effet, lorsqu'une bactérie Gram négative pénètre dans une cellule hôte, celle-ci est contenue dans une vacuole. La Caspase-11, étant cytosolique, ne peut alors pas détecter la présence de LPS. Il est donc nécessaire que les bactéries s'échappent de la vacuole (Meunier et al., 2014).

L'activation de la Caspase-11 est dépendante de la présence d'Interférons γ. En effet, les GBPs (Guanylate binding protein), des GTPases inductibles par l'IFNγ, sont nécessaires à l'activation de la Caspase-11. Les GBPs ont été décrites pour être impliquées dans la rupture de la vacuole bactérienne (Meunier et al., 2014). De plus, les GBPs jouent un rôle dans le recrutement de la Caspase-11 au niveau des bactéries cytosoliques. La GTPase GBP1 se lie aux bactéries cytosoliques et est nécessaire au recrutement séquentiel de GBP2, 3 et 4 responsables du recrutement de la Caspase-11 (Santos et al., 2020; Wandel et al., 2020).

Il a été récemment montré que le LPS de *Salmonella* est ubiquitiné par l'E3-ligase RNF213. Le recrutement de RNF213 se produit en aval du recrutement de la Galectine 8, recrutée à la suite de la rupture de la vacuole bactérienne par exposition de ß-galactosides (Otten et al., 2021; Thurston et al., 2012). Le rôle de l'ubiquitination du LPS par RNF213 dans l'activation de la Caspases -11, -4 et -5 reste à déterminer.

La voie non canonique de l'inflammasome NLRP3 est également activée par des lipides endogènes. En effet, la Caspase-11 lie la forme oxydée du 1-palmitoyl-2-arachidonoyl-*sn*-glycero-3-phosphorylcholine (oxPAPC) retrouvé à la suite d'un stress oxydant notamment chez les cellules mourantes. De manière intéressante la Caspase-11 ne lie pas les oxPAPC via son domaine CARD comme pour le LPS mais via son domaine catalytique et son activité protéolytique n'est pas requise pour l'activation de l'inflammasome NLRP3 (Zanoni et al., 2016). L'activation de l'inflammasome NLRP3 dans ce contexte n'induit pas de pyroptose des cellules dendritiques, cet état a été nommé « hyperactivation ».

### 2.7. Les inflammasomes NAIPs-NLRC4

Le récepteur NLRC4 s'associe à un récepteur de type NAIP afin de former un inflammasome. Il s'agit de l'unique exemple de deux récepteurs différents s'oligomérisant et formant un inflammasome (Vance, 2015). L'inflammasome NAIP-NLRC4 détecte la flagelline ainsi que les systèmes de sécrétion de type III et IV permettant la libération d'effecteurs bactériens dans le cytosol de la cellule cible. Le récepteur NAIP confère à l'inflammasome NLRC4 sa spécificité de ligand. En effet, NAIP1 et NAIP2 détectent l'aiguille et le corps basal du système de sécrétion de type III respectivement tandis que NAIP5 et NAIP6 détectent la flagelline (Kofoed and Vance, 2011) . Chez l'homme il existe un unique NAIP reconnaissant l'aiguille du système de sécrétion de type III (Yang et al., 2013; Zhao et al., 2011).

Récemment, une étude a montré que l'inflammasome NLRC4 est également activé par des petits éléments nucléaires intercalés (SINE). Cependant cette détection est indépendante des protéines NAIPs (Wang et al., 2021b). En effet, l'ARN de ces rétrotransposons est détecté par l'hélicase DDX17 qui active NLRC4.

En étudiant la formation de l'inflammasome NLRC4 chez la souris, deux équipes ont montré que la détection du corps basal du système de sécrétion de type III par NAIP2 induit l'interaction d'un monomère de NAIP2 avec un monomère de NLRC4. Cette interaction induit un changement de conformation de NLRC4. Le premier monomère de NLRC4 dans une conformation « ouverte » peut alors recruter d'autres monomères afin de former l'inflammasome (Hu et al., 2015; Zhang et al., 2015) (Figure 7). Une fois l'inflammasome formé, le domaine CARD de NLRC4 permet de recruter et d'activer directement la Caspase 1 (Broz et al., 2010).

Le récepteur NLRC4 est également régulé par modification post-traductionnelle. En effet, au cours de l'infection par *Salmonella typhimurium*, NLRC4 est phosphorylé par la PKCδ sur la Ser533, un résidu conservé au cours de l'évolution (Qu et al., 2012). Cette phosphorylation est nécessaire pour l'activation de l'inflammasome NLRC4 en amont de la liaison des NAIPs (Matusiak et al., 2015).

Il est intéressant de noter que bien que NLRC4 puisse recruter directement la Caspase-1, des specks ASC ont été observés lorsque cet inflammasome est activé. ASC semble permettre d'augmenter la maturation d'IL-1ß via l'assemblage d'une plateforme plus propice à l'activation de la Caspase-1 (Dick et al., 2016; Miao et al., 2010).

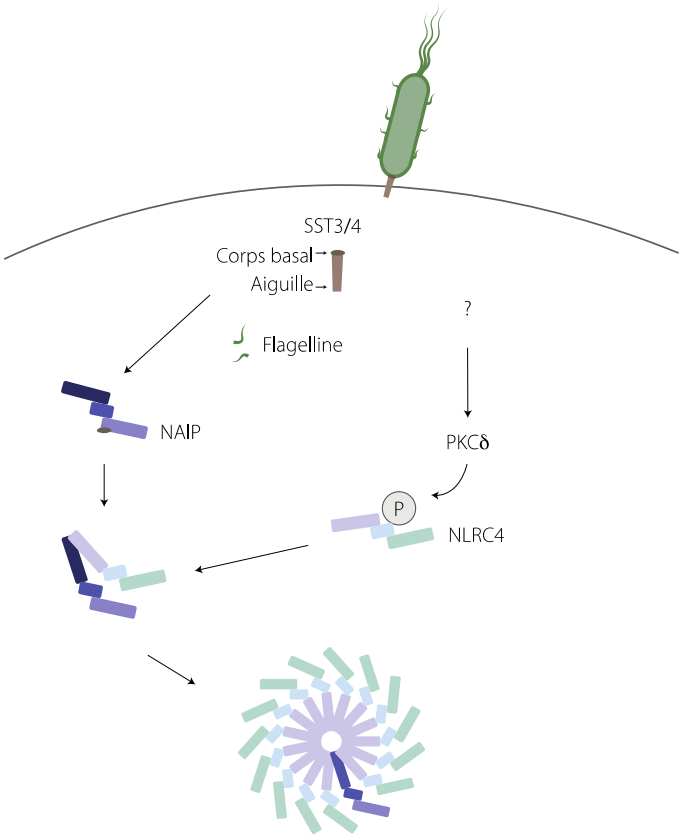


*Figure 7 : Activation de l'inflammasome NLRC4-NAIP*

### 2.8. L'inflammasome NLRP6

L'inflammasome NLRP6 est impliqué dans la régulation de l'immunité et de l'homéostasie intestinale. Il est fortement exprimé dans les cellules épithéliales intestinales.

Cet inflammasome détecte la présence cytosolique d'acide lipotéichoïque (LTA) associé aux bactéries Gram positives par liaison directe (Hara et al., 2018; Shen et al., 2021). De manière étonnante, NLRP6 recrute à la fois la Caspase-1 et la Caspase-11, l'activation de cet inflammasome conduit à la sécrétion d'IL-18 par les macrophages. La liaison de NLRP6 au LTA induit l'ubiquinitation du récepteur pour l'activer, la déubiquitinase CYLD retire ces chaines d'ubiquitine de type K63 afin d'inhiber l'activation de l'inflammasome NLRP6 (Mukherjee et al., 2020).

En plus de pouvoir former un inflammasome, NLRP6 semble réguler négativement les voies de signalisation ERK et NF-κB au cours de l'infection bactérienne (Anand et al., 2012). Cependant, il n'a pas été étudié si cette inhibition est liée à la capacité de NLRP6 à former un inflammasome.

NLRP6 joue également un rôle protecteur au cours de l'infection virale intestinale. Son expression est induite par les interférons. NLRP6 lie de façon directe l'ARN double brin viral via les domaines NACHT-LRR. L'activation de NLRP6 induit la formation de deux complexes distincts mais impliquant la séparation de phase liquide-liquide (Shen et al., 2021). Premièrement, l'interaction de NLRP6 avec l'adaptateur ASC

induit la formation d'un inflammasome responsable de l'activation de la Caspase-1. D'autre part, l'activation de NLRP6 induit également son interaction avec l'hélicase DHX15 qui active le récepteur MAVS pour induire la production d'Interférons (Shen et al., 2021; Wang et al., 2015).

### 2.9. L'inflammasome NLRP9

Il existe un seul NLRP9 chez l'homme et trois isoformes chez la souris (NLRP9a, b et c). Le récepteur NLRP9b est fortement exprimé dans les cellules épithéliales intestinales (Mullins and Chen, 2021).

La capacité du récepteur NLRP9 à former un inflammasome avec la Caspase-1 et ASC n'a été découvert que très récemment. Chez la souris, l'inflammasome NLRP9b est activé au cours de l'infection des cellules épithéliales intestinales par les rotavirus (virus à ARN double brin). Cet inflammasome est activé en aval de la détection de l'ARN bicaténaire viral par l'hélicase DHX9 (Zhu et al., 2017). L'activation de l'inflammasome NLRP9b et l'induction de la pyroptose en aval sont cruciales pour contenir la réplication virale. Cependant, la sécrétion d'IL-18 ne semble pas être un élément important pour restreindre l'infection.

A ce jour, le rôle et la capacité à former un inflammasome du récepteur NLRP9 humain restent à déterminer.

### 2.10. L'inflammasome AIM2

L'inflammasome AIM2 détecte l'ADN double brin cytosolique (Bürckstümmer et al., 2009; Fernandes-Alnemri et al., 2009; Hornung et al., 2009; Roberts et al., 2009). A l'état inactif, AIM2 est auto-inhibé : le domaine PYD interagit avec le domaine HIN-200 (Figure 8). Lorsque le domaine HIN-200 détecte et lie directement l'ADN, cela libère le domaine PYD qui peut alors recruter la protéine adaptatrice ASC et permet de former un inflammasome (Jin et al., 2012).

L'inflammasome AIM2 détecte l'ADN microbien mais également l'ADN endogène lors d'un stress cellulaire engendrant une rupture de l'enveloppe nucléaire (Lugrin and Martinon, 2018).

IFI16-β chez l'homme et p202 chez la souris sont des protéines de la famille PYHIN qui possèdent un domaine HIN-200, le domaine PYD est absent. Il a été montré que ces deux protéines lient l'ADN double brin avec une plus grande affinité que AIM2 et entrent en compétition avec ce dernier pour la liaison à l'ADN (Roberts et al., 2009; Wang et al., 2018; Yin et al., 2013). Ce mécanisme permet une inhibition de l'activation de l'inflammasome AIM2. De façon intéressante, ces deux protéines n'inhibent pas l'activation de la voie cGAS-STING (Yin et al., 2013). Chez l'homme il existe la protéine POP3, qui a l'inverse, est composée d'un domaine PYD uniquement, et qui est codée par un gène inductible par les Interférons de type I. POP3 inhibe l'inflammasome AIM2 en entrant en compétition avec ASC pour interagir avec le domaine PYD du récepteur AIM2 (Khare et al., 2014).

L'inflammasome AIM2 est également régulé par dégradation du récepteur AIM2 par autophagie (Shi et al., 2012). En effet, lors de la détection d'ADN cytosolique, la protéine TRIM11 est activée et interagit avec AIM2. L'auto-ubiquitination de TRIM11 induit la dégradation du complexe TRIM11-AIM2 par autophagie (Liu et al., 2016a).

Une autre voie de signalisation permet la détection de l'ADN double brin cytosolique chez l'homme. La protéine cGAS détecte l'ADN et produit le second messager cGAMP (2'3'-cyclic GMP-AMP) qui est détecté par STING (Ablasser et al., 2013). STING recrute ensuite TBK1 qui phosphoryle le facteur de transcription IRF3 dont la translocation nucléaire permet l'expression des Interférons de type I. En 2017, une étude a remis en question le rôle de l'inflammasome AIM2 dans la détection de l'ADN cytosolique dans les monocytes humains. En effet, l'activation de la voie cGAS-STING provoquerait la rupture des lysosomes provoquant l'activation de l'inflammasome NLRP3 (Gaidt et al., 2017).

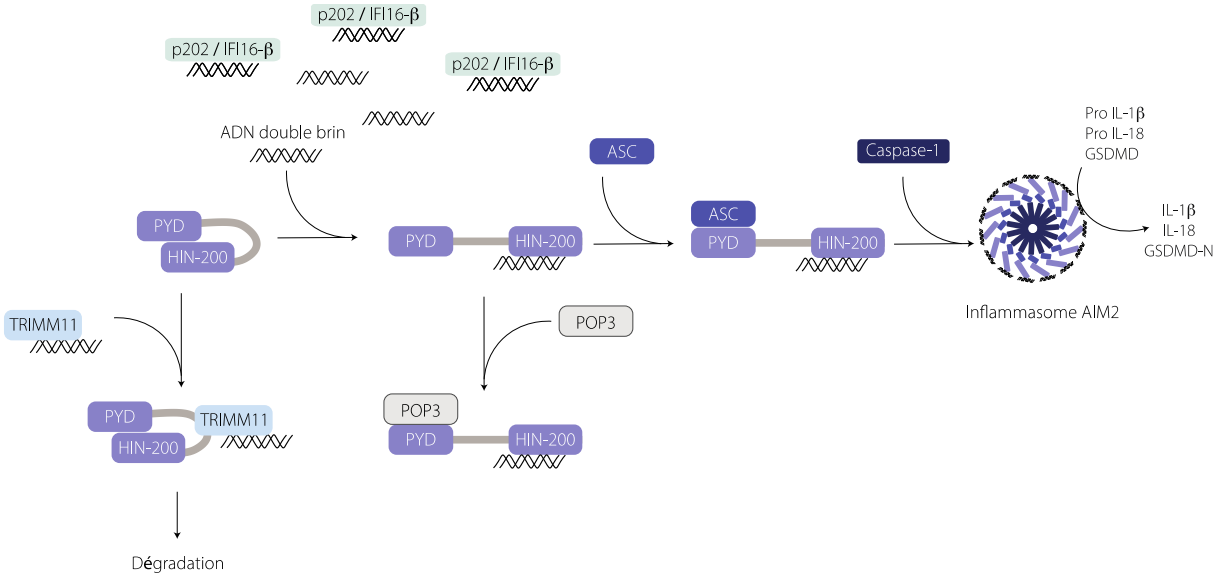


*Figure 8 : Activation de l'inflammasome AIM2*

### 2.11. L'inflammasome Pyrin

L'inflammasome Pyrin veille au maintien de l'homéostasie de la Rho-GTPase RhoA. Initialement, la fonction de Pyrin a été découverte dans le cadre de l'inactivation de RhoA par des toxines bactériennes (Xu et al., 2014). A l'état basal, RhoA est actif dans la cellule et active ces effecteurs dont les kinases PKN1 et PKN2 (Gao et al., 2016). Ces kinases phosphorylent Pyrin sur les Ser208 et Ser242 (Ser205 et Ser241 chez la souris) ce qui permet le recrutement des protéines chaperonnes 14-3-3 qui maintiennent Pyrin inactif (Jamilloux et al., 2018; Park et al., 2016) (Figure 9). Cette partie est développée dans la revue publiée dans *PLOS Pathogens*, en annexe (Dufies and Boyer, 2021).

Le Syndrome de fièvre périodique avec hyperimmunoglobulinémie D (HIDS) est caractérisé par un déficit en mévalonate kinase et se manifeste par des accès fébriles, une atteinte articulaire, une

adénopathie et des éruptions cutanées (Drenth et al., 1999). Cette maladie auto-inflammatoire est causée par l'activation de l'inflammasome Pyrin (Park et al., 2016). La mévalonate kinase est une enzyme impliquée dans la synthèse de géranylgéranyl nécessaire à la modification post-traductionnelle des Rho-GTPases et à leur ancrage membranaire. La déficience en mévalonate kinase provoque une dérégulation de l'activation des Rho-GTPases.

L'activation de l'inflammasome Pyrin semble être dépendante des microtubules, l'inhibition de polymérisation des microtubules par la colchicine bloque l'activation de l'inflammasome Pyrin (Gao et al., 2016). La dynamique des microtubules semble être importante en aval de la libération de Pyrin par les protéines 14-3-3 et en amont de l'oligomérisation de l'inflammasome et la formation de specks ASC. La colchicine, qui inhibe la polymérisation des microtubules, est le traitement préférentiel pour les patients FMF (Ozen et al., 2016). Étrangement, une étude a montré que les mutations associées à la FMF (fièvre familiale méditerranéenne) semblaient rendre l'activation de Pyrin par la toxine TcdA, inhibant RhoA, indépendante des microtubules (Van Gorp et al., 2016). Une récente étude a montré que l'inhibition, par des composés chimiques, de PKN1/2 chez les patients FMF est suffisante pour induire l'activation de Pyrin, et ce de manière dépendante des microtubules (Magnotti et al., 2019). Les mécanismes impliqués dans la dérégulation de l'inflammasome Pyrin par les mutations affectant le domaine B30.2 de Pyrin restent obscures.

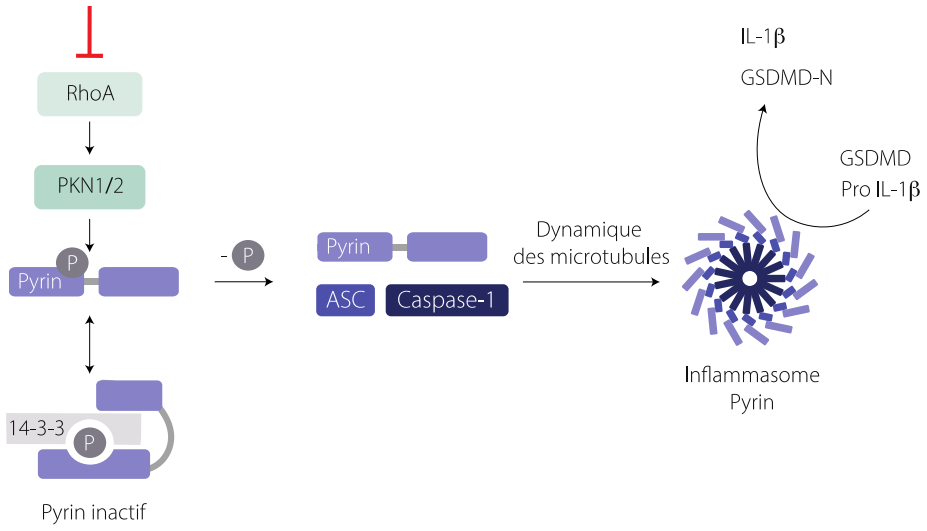


*Figure 9 : Activation de l'inflammasome Pyrin*

## 3. Détection des facteurs de virulence ciblant des Rho-GTPases

### 3.1. Les Rho-GTPases

Les Rho-GTPases (Guanosine triphosphatases de la famille Rho) appartiennent à la superfamille Ras des petites protéines G participant à la régulation d'un grand panel de fonctions cellulaires. Cette superfamille regroupe plus de 150 protéines classées en 5 sous-familles majeures : Ras, Arf, Rab, Ran et

Rho. Actuellement, les familles de Rho-GTPases les mieux caractérisées sont RhoA, Rac1/2 et Cdc42. Elles sont notamment impliquées dans la transcription des gènes, le cycle cellulaire, la morphologie, la migration, la prolifération, la différenciation cellulaire, l'endocytose, la polarisation et l'immunité (Wennerberg et al., 2005).

### 3.1.1. Cycle des Rho-GTPases

Les protéines Rho, Rac et Cdc42 sont des GTPases : elles hydrolysent le GTP (Guanosine Tri-Phosphate) en GDP (Guanosine Di-Phosphate). Les Rho-GTPases agissent à la manière d'un interrupteur moléculaire afin de contrôler la transduction du signal au sein d'une voie de signalisation (Bishop and Hall, 2000).

Les Rho-GTPases passent d'un état inactif lié au GDP à un état actif lié au GTP (Figure 10). L'échange du GDP en GTP se fait grâce à un facteur d'échange appelé GEF (Guanine Exchange Factor). La conformation des Rho-GTPases actives dévoile leur extrémité N-terminale isoprénylée permettant leur ancrage à la membrane, à proximité de leurs effecteurs. La GTPase de la famille Rho est alors capable d'interagir avec ses effecteurs et de les activer. Le retour à l'état inactif se fait à l'aide d'une GAP (GTPase Activating Protein) qui stimule l'activité intrinsèque de la GTPase et permet l'hydrolyse du phosphate γ du GTP. Les Rho-GTPases alors inactives sont séquestrées dans le cytosol par une protéine GDI (Guanine Nucleoside Dissociation Inhibitor) qui inhibe leur dissociation du GDP (Aspenström, 1999; Wennerberg et al., 2005).

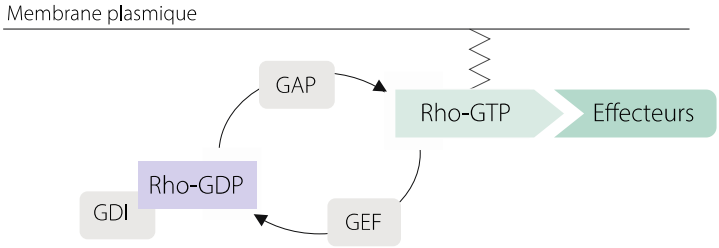


*Figure 10 : Cycle des Rho-GTPases*

### 3.1.2. Rôle et effecteurs des Rho-GTPases

#### 3.1.2.1. Régulation du cytosquelette

Les différents effets de l'activation de Rho, Rac et Cdc42 sur le cytosquelette ont d'abord été étudiés sur des fibroblastes (Ridley and Hall, 1992) puis ont été observés dans un grand nombre de types cellulaires : astrocytes, cellules endothéliales et épithéliales, macrophages ou encore plaquettes (Hall, 1998).

L'activation de chaque sous-famille de Rho-GTPases provoque des effets distincts via leur interaction avec des protéines régulant la polymérisation et la dépolymérisation des filaments d'actine, des microtubules et des filaments intermédiaires (Burridge and Wennerberg, 2004).

L'activation de Rac mène à l'activation de la famille de protéines WASp qui activent le complexe ARP2/3, induisant la nucléation et la polymérisation de réseaux d'actine branchée constituant les lamellipodes (Higgs and Pollard, 2001; Machesky and Insall, 1998). L'activation de Cdc42 mène, à partir du même mécanisme, à la formation de filopodes via l'élongation des filaments d'actine formant une protrusion membranaire. Les filopodes sont composés de filaments d'actine maintenus parallèles grâce à des protéines liant l'actine comme la Fascine (Kureishy et al., 2002). De plus, l'activation de la kinase Pak1 par Rac et Cdc42 induit la polymérisation des microtubules (Rane and Minden, 2014). Le cytosquelette d'actine est également contrôlé par Rho via des protéines de la famille des formines comme mDia1, responsable de la nucléation d'actine filamenteuse (Li and Higgs, 2003) et permettant la formation de câbles d'actines (ou fibres de stress).

La dynamique de l'actine (cycle polymérisation – dépolymérisation) est régulée par Rac et Rho en activant respectivement les kinases Pak et ROCK qui activent à leur tour la kinases LIM (LIMK) qui phosphoryle la cofiline (ou ADF) et l'inactive. Cette dernière est responsable de la rupture des filaments d'actine. De plus, Pak inhibe la kinase MLCK, une kinase responsable de la phosphorylation des chaines légères de myosines, tandis que ROCK inhibe la phosphatase MLCP ciblant également les chaines légères de myosines, impliquées dans la formation des fibres de stress. Les kinases Pak et ROCK ont donc un effet antagoniste : l'activation de ROCK par Rho favorise la formation de fibres de stress tandis que l'activation de Pak par Rac et Cdc42 induit la dépolymérisation des fibres de stress (Figure 11) (Qu et al., 2001; Sanders et al., 1999; Vicente-Manzanares and Sánchez-Madrid, 2004).

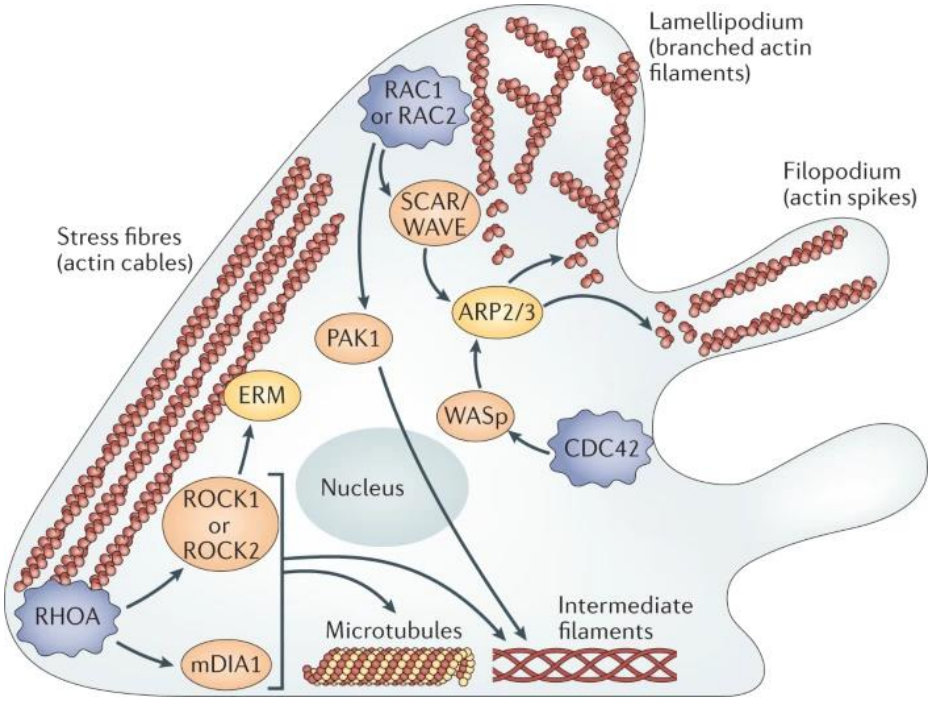


*Figure 11 : Différents types de structures impliquant le cytosquelette d'actine*

Issu de (El Masri and Delon, 2021).

#### 3.1.2.2. Immunité

Les Rho-GTPases régulent des processus immunitaires majeurs comme la phagocytose, la production d'espèces réactives de l'oxygène (ROS), la migration cellulaire ou encore la régulation de l'expression de gènes codant pour des cytokines.

La Rho-GTPase Rac2 est spécifiquement exprimée par les cellules de la lignée hématopoïétique (Reibel et al., 1991), elle est considérée comme la Rho-GTPase de l'immunité. En effet, elle a été démontrée nécessaire à la motilité chimiotactique des leucocytes et à l'activation de la NADPH oxydase au sein de ces cellules (Matono et al., 2014). La NADPH oxydase Nox2 permet la formation d'ions superoxydes et de ROS nécessaires à la dégradation des pathogènes (Bokoch and Knaus, 2003). Ces espèces réactives agissent au sein du phagosome en oxydant et en endommageant les protéines et l'ADN des pathogènes phagocytés (Imlay and Linn, 1988).

Des mutations associées aux Rho-GTPases sont responsables d'immunodéficience primaire ainsi que d'état auto-inflammatoires (El Masri and Delon, 2021).

Il a été rapporté que des patients portant la mutation de Rac2 Asp57Asn (qui rend la GTPase non fonctionnelle et fonctionne comme un dominant négatif) souffraient d'infections sévères et récurrentes dues à un défaut de migration des neutrophiles et d'activation de la NADPH oxydase (Ambruso et al., 2000; Williams et al., 2000). Plus récemment, les mutations Glu62Lys et Asn92Thr rendant Rac2 constitutivement actif ont été associées à des patients présentant un défaut des lignées lymphocytaires et myéloïdes et un excès de production de ROS par les neutrophiles. Ces patients présentaient des infections récidivantes (Hsu et al., 2019; Sharapova et al., 2019).

D'autre part, les mutations Arg186Cys et Cys188Tyr de Cdc42 sont responsables d'une auto-inflammation sévère chez les patients. Ceux-ci présentent des épisodes fébriles, des rash cutanés ainsi qu'une cytopénie (Gernez et al., 2019). Ces patients présentaient des taux plasmatiques élevés d'IL-18 et IL-1ß et l'administration d'anakinra (antagoniste de l'IL-1R) a permis d'améliorer leur tableau clinique (Gernez et al., 2019; Lam et al., 2019).

Des mutations associées à la mévalonate kinase, nécessaire à la prénylation des Rho-GTPases, est à l'origine du syndrome de fièvre périodique avec hyperimmunoglobulinémie D (HIDS) via la perte d'activation de RhoA et l'activation de l'inflammasome Pyrin (Park et al., 2016).

### 3.2. Facteurs de virulence ciblant les RhoGTPases

Les micro-organismes pathogènes produisent des facteurs de virulence ciblant de grandes voies de signalisation de la cellule cible. Parmi celles-ci, les Rho-GTPases, situées au carrefour de nombreuses voies de signalisation, sont la cible d'un grand nombre d'effecteurs bactériens (Aktories, 1997). Les

bactéries pathogènes ont développé un large panel de toxines et effecteurs modifiant les GTPases de la famille Rho afin de détourner ces voies de signalisation à leur avantage. Cette modification peut être activatrice ou inhibitrice et fait appel à différents modes d'action des toxines (Tableau 3).

### 3.2.1. La toxine CNF1 des *Escherichia coli* uropathogènes

La toxine CNF1 est exprimée par plus 30% des souches *Escherichia coli* (*E. coli*) uropathogènes retrouvées en clinique (Landraud et al., 2000).

Cette toxine de type AB est sécrétée par *E. coli* et se fixe aux récepteurs Lu/BCAM et LRP (Chung et al., 2003; Reppin et al., 2018). CNF1 est endocytée de façon récepteur-dépendante par la cellule cible (Chung et al., 2003). L'acidification de l'endosome permet l'ancrage du domaine de translocation de CNF1 dans la membrane de l'endosome afin de libérer le domaine catalytique dans le cytosol (Knust et al., 2009). CNF1 possède une activité dé-amidase ciblant les Gln61 de RhoA et Gln63 de Cdc42 et Rac, et provoquant leur « mutation » en acide glutamique (Flatau et al., 1997; Schmidt et al., 1997). Ces glutamines sont localisées dans le domaine switch II des Rho-GTPases, jouant un rôle primordial dans l'activité GTPase intrinsèque. Cette modification post-traductionnelle détruit l'activité GTPasique intrinsèque et stimulée par les GAP, avec pour conséquence l'activation constitutive des Rho-GTPases et de leurs effecteurs (Flatau et al., 1997).

L'activation constitutive des Rho-GTPases induit des ondulations membranaires ce qui promeut la macropinocytose et facilite l'invasion des cellules épithéliales par *E. coli* (Fiorentini et al., 2001). De plus, l'activité de CNF1 tend à désorganiser les jonctions intercellulaires et diminue ainsi l'effet barrière des épithéliums du système urinaire (Lemonnier et al., 2007). Ces changements au niveau cellulaire ont pour conséquence l'accélération de la dissémination des bactéries dans la circulation, provoquant des bactériémies (Moreno et al., 2005).

Lors de l'activation soutenue de Rac1 par CNF1, la kinase effectrice Pak1 phosphoryle l'E3-ligase HACE1 pour l'activer. HACE1 ubiquitine ensuite Rac1 pour induire sa dégradation par le protéasome, cela agit comme un rétrocontrôle négatif de l'activation de Rac1 par CNF1 (Acosta et al., 2018).

Le gène codant pour CNF1 est situé dans un opéron codant également pour l'hémolysine-$\alpha$, une toxine cytolytique et l'expression de CNF1 est systémiquement associée à celle de l'hémolysine-$\alpha$ (Landraud et al., 2003).

| | Pathogène | Cible | Modification | Réference |
|---|---|---|---|---|
| Toxines inhibant les Rho-GTPases | | | | |
| C3 | *C. botulinum*<br>*C. limosum*<br>*B. cereus*<br>*B. thuringiensis* | Rho | ADP-ribosylation | (Aktories et al., 1989; Just et al., 1992) |
| EDIN-A | *S. aureus* | Rho | ADP-ribosylation | (Sugai et al., 1992) |
| EDIN-B | *S. aureus* | Rho, Rnd3 | ADP-ribosylation | (Wilde et al., 2001) |
| TcdA, TcdB | *C. difficile* | Rho, Rac, Cdc42 | Glucosylation | (Just et al., 1995a)<br>(Just et al., 1995b) |
| TcsL | *C. sordellii* | Rac | Glucosylation | (Popoff et al., 1996) |
| VopS | *V. parahaemolyticus* | Rho, Rac, Cdc42 | AMPylation | (Yarbrough et al., 2009) |
| IbpA | *H. somni* | Rho, Rac, Cdc42 | AMPylation | (Worby et al., 2009) |
| TecA | *B. cenocepacia* | Rho, Rac, Cdc42 | Déamidation | (Aubert et al., 2016) |
| YopT | *Y. pestis*<br>*Y. pseudotuberculosis*<br>*Y. enterocolitica* | Rho, Rac, Cdc42 | Clivage du CAAX | (Shao et al., 2002; Zumbihl et al., 1999) |
| YopE | *Y. pestis*<br>*Y. pseudotuberculosis*<br>*Y. enterocolitica* | Rho, Rac, Cdc42 | GAP | (Pawel-Rammingen et al., 2000) |
| ExoS, ExoT | *P. aeruginosa* | Rho, Rac, Cdc42 | GAP | (Goehring et al., 1999; Krall et al., 2000) |
| SptP | *Salmonella spp.* | Rac, Cdc42 | GAP | (Fu and Galán, 1999) |
| YopO/YpkA | *Y. pestis*<br>*Y. pseudotuberculosis*<br>*Y. enterocolitica* | Rho, Rac | GDI | (Prehna et al., 2006) |
| Toxines activant les Rho-GTPases | | | | |
| CNF1, CNF2 | *E. coli* | Rho, Rac, Cdc42 | Déamidation | (Flatau et al., 1997) |
| CNF3 | *E. coli* | Rho, Rac, Cdc42 | Déamidation | (Stoll et al., 2009) |
| CNFY | *Y. pseudotuberculosis* | Rho, Rac, Cdc42 | Déamidation | (Hoffmann et al., 2004; Wolters et al., 2013) |
| DNT | *B. pertussis*<br>*B. parapertussis*<br>*B. bronchiseptica* | Rho, Rac, Cdc42 | Déamidation<br>Transglutamination | (Horiguchi et al., 1997; Masuda et al., 2000) |
| VopC | *V. parahaemolyticus*<br>*V. cholerae* | Rac, Cdc42 | Déamidation | (Zhang et al., 2012) |
| SopE | *Salmonella spp.* | Rho, Rac, Cdc42 | GEF | (Hardt et al., 1998) |
| SopE2 | *Salmonella spp.* | Cdc42 | GEF | (Friebel et al., 2001; Stender et al., 2000) |
| IpgB1 | *S. flexneri* | Rac, Cdc42 | GEF | (Alto et al., 2006; Ohya et al., 2005) |
| IpgB2 | *S. flexneri* | Rho | GEF | (Alto et al., 2006; Klink et al., 2010) |
| Map | *E. coli* | Cdc42 | GEF | (Alto et al., 2006) |
| EspT | *E. coli*<br>*C. rodentium* | Rac, Cdc42 | GEF | (Bulgin et al., 2009) |
| EspM1,2,3 | *E. coli*<br>*C. rodentium* | RhoA | GEF | (Arbeloa et al., 2010) |
| BopE | *B. pseudomallei* | Rac, Cdc42 | GEF | (Stevens et al., 2003) |
| SifA, SifB | *S. Typhimurium* | Non déterminé | GEF putative | (Alto et al., 2006) |

*Tableau 3 : Toxines modifiant les Rho-GTPases*

### 3.3. Réponse anti-virulence induite par l'activation des Rho-GTPases

L'activation des Rho-GTPases par des toxines bactériennes induit la transcription de gènes codant pour des cytokines et chimiokines pro-inflammatoires. Il a été démontré que l'effecteur SopE de *Salmonella* active différentes voies de signalisation menant à la transcription des gènes (Figure 12). D'une part, l'infection de cellules épithéliales par des salmonelles exprimant SopE et SopE2 induit l'activation des MAPK JNK, p38 et ERK, menant à l'activation du facteur de transcription NF-κB (Bruno et al., 2009). De plus, SopE a été montré pour activer NOD1 et RIP2, conduisant la production de cytokines (Keestra et al., 2013). Plus récemment, une étude a établi que SopE active l'axe Cdc42-Pak1 menant à l'activation de NF-κB de façon dépendante de TAK1 et TRAF6 (Sun et al., 2018). Des études complémentaires permettraient d'établir si ces trois voies de signalisation sont interconnectées ou si celles-ci sont séparées pendant l'infection. La toxine CNF1 est un exemple intéressant de réponse antimicrobienne déclenchée par l'activation des Rho-GTPases. La toxine CNF1 des *E. coli* uropathogènes a été montrée pour induire une réponse antimicrobienne protective en activant la Rho-GTPase Rac2 qui en retour active les voies IMD-Relish et RIP1/2-NF-κB chez les cellules de drosophile et mammifères respectivement (Boyer et al., 2011; Diabate et al., 2015) (Figure 12). Il a également été montré que l'activation des Rho-GTPases par CNF1 induit une réponse immunitaire au cours de la bactériémie de façon dépendante des Caspases-1/11 ainsi que de l'IL-1ß (Diabate et al., 2015). Ces données indiquent qu'un inflammasome est activé par la toxine CNF1. La clairance bactérienne en réponse à la détection de la toxine CNF1 est néanmoins contrecarrée par l'hémolysine-α (Diabate et al., 2015).

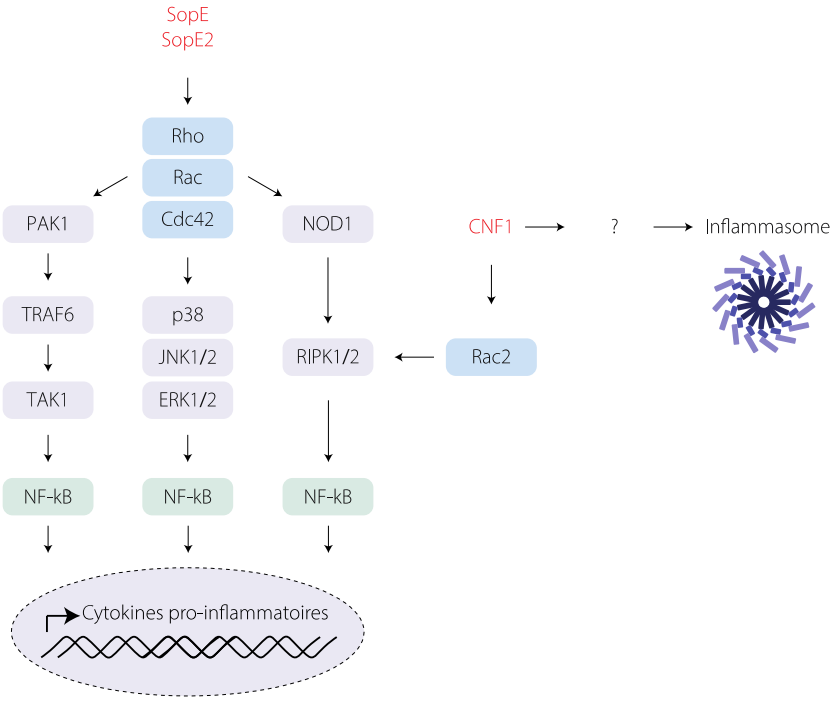


*Figure 12 : Détection des toxines activant les RhoGTPases*

### 3.4. Réponse anti-virulence induite par l'inhibition des Rho-GTPases

L'inflammasome Pyrin est historiquement associé à des pathologies auto-inflammatoires comme la FMF où des mutations de Pyrin sont retrouvées (Centola et al., 1998; Jamilloux et al., 2018), cependant, de récentes études ont associé à Pyrin une fonction protectrice au cours de l'infection. En effet, l'inflammasome Pyrin est capable de détecter l'inactivation des Rho-GTPases par des facteurs de virulence bactériens divers (Figure 13). En effet, l'inactivation des Rho-GTPases par TcdA et TcdB (de *Clostridium difficile*), VopS (de *Vibrio parahaemolyticus*), IbpA (de *Histophilus somni*) et TecA (de *Burkholderia cenocepacia*) est détectée par Pyrin. Il est important de noter que ces effecteurs bactériens inactivent RhoA par quatre mécanismes distincts : glycosylation, ADP-ribosylation, AMPylation et déamidation (Aubert et al., 2016; Gao et al., 2016; Park et al., 2016; Xu et al., 2014). De plus, il a été montré que le facteur de virulence de TcsL de *Clostridium serdellii* qui inhibe Rac et Cdc42 mais ne cible pas RhoA, n'est pas détecté par l'inflammasome Pyrin, suggérant que Pyrin détecte spécifiquement le statut d'activation de RhoA (Xu et al., 2014). L'inhibition de RhoA par des facteurs de virulence induit une perte de la phosphorylation de Pyrin par PKN1/2 et de l'interaction de Pyrin avec les protéines 14-3-3 ce qui a pour effet d'activer l'inflammasome Pyrin (Gao et al., 2016; Medici et al., 2019; Park et al., 2016).

La bactérie *Yersinia* est un exemple de co-évolution hôte-pathogène. En effet, pour contourner l'activation de l'inflammasome Pyrin induite par l'inhibition de RhoA (par YopE), *Yersinia* injecte l'effecteur YopM qui active les kinases PKN1/2 et RSK1/2/3 qui phosphorylent Pyrin pour le maintenir inactif (Chung et al., 2016; Ratner et al., 2016). Cela a mené à la sélection de mutations du domaine B30.2 de Pyrin rendant Pyrin insensible à YopM et permettant ainsi à ces individus d'être résistants à l'infection par *Yersinia pestis*, à l'origine de la peste (Park et al., 2020). Ces mutations sélectionnées au cours d'épidémies de peste, sont responsables, pour partie, de la maladie auto-inflammatoire FMF.

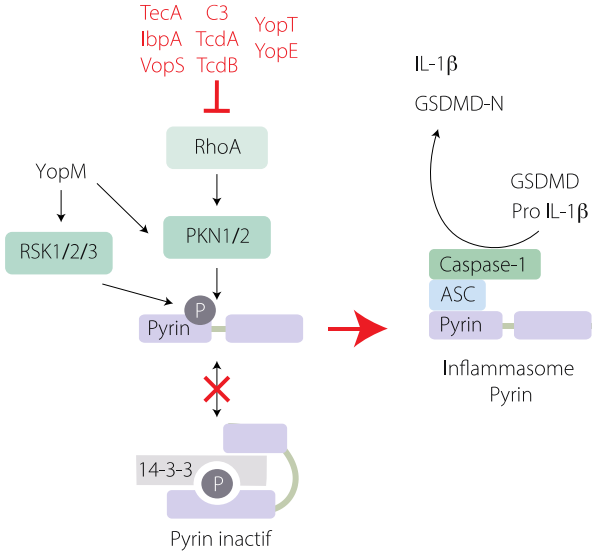


*Figure 13 : Détection par Pyrin des facteurs de virulence inhibant RhoA*

## 4. Rôle de l'inflammasome NLRP3 dans le sepsis

Le sepsis est défini comme une dysfonction des organes mettant en jeu la vie du patient et causée par une dérégulation de la réponse de l'hôte face à une infection (définition Sepsis-3) (Singer et al., 2016). Il est la conséquence d'une exacerbation de la réponse immunitaire face à une infection non résolue. Celle-ci mène à une production excessive de cytokines (IL-6, IL-1ß, TNF…) et à une libération de DAMPs (HMGB1, ATP, ADN mitochondrial et nucléaire…) en réponse à la présence d'un microbe. En plus d'une trop forte inflammation, le sepsis induit également une immunosuppression. La physiopathologie du sepsis est complexe et fait intervenir de nombreux mécanismes comme l'activation de la cascade du complément, une augmentation de la coagulation, un épuisement des lymphocytes ou encore la mort des neutrophiles par NETose (van der Poll et al., 2021). Le passage d'une réponse immunitaire protectrice au sepsis et au choc septique est vu comme la conséquence de l'absence de retour à l'homéostasie ou que celui-ci soit trop tardif (Singer et al., 2016).

Il semble y avoir une boucle amplificatrice de la réponse immunitaire impliquant les inflammasomes. En effet, parmi les évènements cités plus haut, de nombreux évènements peuvent être une cause ou une conséquence de l'activation d'un inflammasome. Pour une question de concision, je m'intéresserai ici exclusivement à l'implication de l'inflammasome NLRP3 dans le sepsis.

Les bactéries *Staphylococcus aureus* (*S. aureus*) et *Escherichia coli* (*E. coli*) sont l'étiologie la plus fréquente des bactériémies et sepsis bactériens (Kern and Rieg, 2020; Vincent et al., 2006). Au cours de la bactériémie à *E. coli*, la présence de LPS dans la circulation induit l'activation non canonique de l'inflammasome NLRP3 chez la souris (Kayagaki et al., 2015). L'ancrage membranaire de la GSDMD induit l'exposition de phosphatidylsérine qui mène à l'activation du facteur tissulaire, un acteur majeur de la cascade de coagulation (Yang et al., 2019a). Une coagulation intravasculaire disséminée est observée chez les patients en état de sepsis et prédispose à une défaillance des organes (Gando et al., 2019). De plus, l'activation d'un inflammasome et la pyroptose associée induit la libération de DAMPs tels que HMGB1 ou l'ATP. Ces DAMPs amplifient la réponse immunitaire. L'ATP va activer l'inflammasome NLRP3 présent dans les cellules voisines et HMGB1 est capable de se fixer à différents PRRs (RAGE, TLR2, TLR4) afin d'induire la production de cytokines pro-inflammatoires (Andersson et al., 2000; Park et al., 2004). Enfin, HMGB1 est capable de se lier au LPS et après son endocytose médiée par RAGE et la rupture de l'endolysosome, d'induire l'activation non-canonique de l'inflammasome NLRP3 (Deng et al., 2018).

L'émergence du COVID-19 a mis en lumière l'orage cytokinique ou « cytokine storm » dont certains paramètres immunitaires sont proches du sepsis notamment la présence d'IL-1ß circulant et une dérégulation de la formule sanguine.

## 5. Réponse immunitaire innée au cours du COVID-19

### 5.1. COVID-19 et SARS-CoV-2 : généralités

Le SARS-CoV-2 (severe acute respiratory syndrome coronavirus 2) a émergé à Wuhan (Chine) à la fin de l'année 2019 (Li et al., 2020b). Ce virus est à l'origine d'une maladie respiratoire nommée COVID-19 (coronavirus disease 2019). Le SARS-CoV-2 appartient au genre des betacoronavirus comme le SARS-CoV et le MERS-CoV (Middle East respiratory syndrome-related coronavirus). Le SARS-CoV-2 est un virus enveloppé à ARN simple brin à polarité positive. Le SARS-CoV-2 a un tropisme majoritairement respiratoire mais infecte également le tractus gastro-intestinal et le système nerveux central (Gomes et al., 2021; Liu et al., 2021). Bien que d'autres coronavirus, responsables de rhumes, circulent activement dans la population, la population générale était naïve des betacoronavirus lorsque le SARS-CoV-2 a émergé.

Chez une grande partie des sujets infectés, la maladie est asymptomatique ou pauci-symptomatique (fièvre, toux, céphalées, perte de goût et d'odorat…). Cependant, dans une proportion non négligeable de cas (estimée à 10-20%) le SARS-CoV-2 est responsable d'une pneumonie pouvant évoluer en syndrome de détresse respiratoire aigüe (SDRA) nécessitant l'hospitalisation. L'aggravation du COVID-19 survient une dizaine de jours après les premiers symptômes. Cette aggravation ne semble ni être liée au SARS-CoV-2 en lui-même ni à la charge virale détectée dans les échantillons nasopharyngés (Cocconcelli et al., 2021). La sévérité de ces patients semble impliquer différentes dérégulations immunitaires comme la tempête cytokinique ou encore un défaut de production d'Interférons (Figure 14) (Jamilloux et al., 2020; Schultze and Aschenbrenner, 2021).

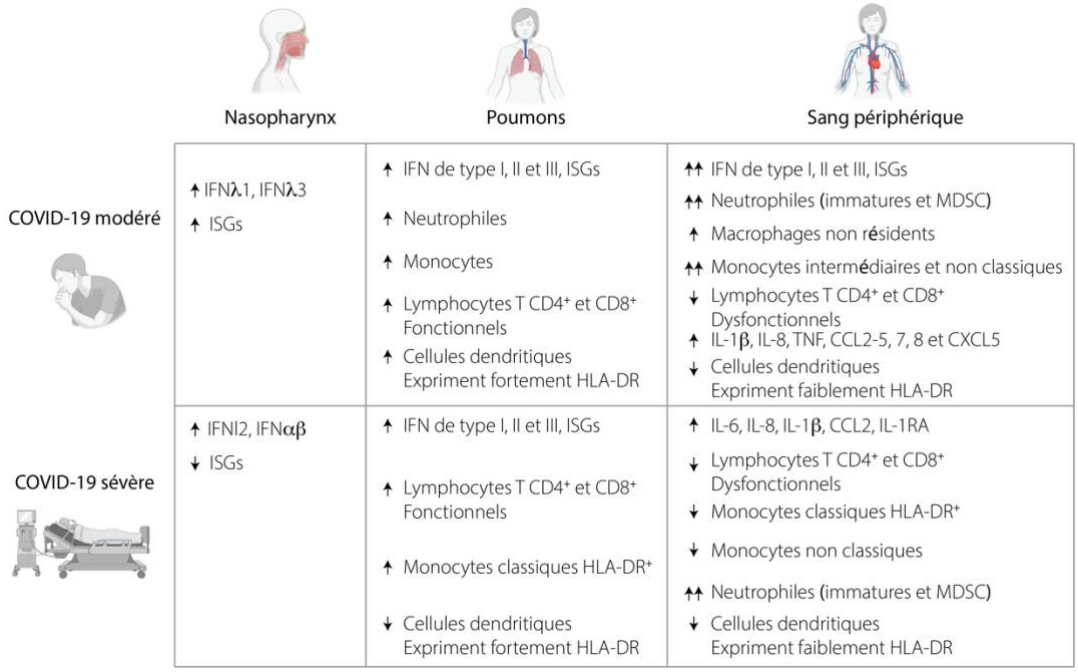


*Figure 14 : Dérégulation de la réponse immunitaire au cours du COVID-19 sévère*
ISGs : Gènes stimulés par les Interférons ; MDSC : Cellules myéloïdes suppressives

### 5.2. La réponse immunitaire au cours des formes sévères de COVID-19

L'infection des cellules par des virus à ARN simple brin active différents PRRs de la famille des TLRs (TLR3, 7 et 8) et des RLRs (RIG-I et MDA-5) (Saito and Gale, 2008). La détection de l'ARN viral par ces PRRs active les facteurs de transcription NF-kB et IRF3/7 responsables de la production de cytokines pro-inflammatoires (TNF, IL-6…) et antivirales (Interférons (IFN) de type I et III) respectivement. Le SARS-CoV-2 active ces différentes voies de signalisation (Salvi et al., 2021; Thorne et al., 2021; Yamada et al., 2021). Il a également été montré que la protéine d'enveloppe (E) du SARS-CoV-2 est détectée par le TLR2, induisant la production de cytokines pro-inflammatoires telles que l'IL-6, l'IFNγ ou encore l'IL-1ß (Zheng et al., 2021). De plus, les Lectines de type C sont activées par la protéine Spike du SARS-CoV-2, menant également à la synthèse de cytokines et chimiokines pro-inflammatoires (Lu et al., 2021).

Très rapidement, l'aggravation des patients COVID-19 a été associée à une production excessive de cytokines et chimiokines pro-inflammatoires comme l'IL-6, IL-8, IL-1ß, CCL2, ou CXCL8 (Huang et al., 2020; Lucas et al., 2020; McElvaney et al., 2020; Yang et al., 2020b). L'augmentation des cytokines telles que l'IL-1ß, l'IL-18 ou leur antagonistes (IL-1RA, IL-18BPa) semble indiquer l'implication d'un (ou plusieurs) inflammasome(s).

D'autre part, une immunoparalysie (épuisement des lymphocytes T et altération de la réponse antivirale liée aux IFNs) a également été observée chez les cas sévères (Blanco-Melo et al., 2020; Kaneko et al., 2020). Ces observations ont amené les cliniciens à considérer la sévérité des cas de COVID-19 comme étant liée au sepsis viral (Li et al., 2020a).

#### 5.2.1. Cytokines de la famille de l'IL-1 et inflammasomes

L'IL-1ß est une cytokine produite précocement et induit la production d'IL-6 par les cellules voisines et pourrait être à l'origine de la tempête cytokinique observée chez les patients COVID-19 sévères (Sironi et al., 1989; Tosato and Jones, 1990). Ces patients ont des taux plasmatiques élevés d'IL-18 et d'IL-1RA, l'antagoniste de l'IL-1R produit en aval de l'activation de ce récepteur comme rétrocontrôle négatif de la voie de l'IL-1 (Zhao et al., 2020b). Certaines études associent également une hausse plasmatique de l'IL-1ß avec la sévérité, tandis que d'autres ne dessellent que des taux faibles – voire absents – d'IL-1ß (Del Valle et al., 2020; Lucas et al., 2020; Rodrigues et al., 2021; Theobald et al., 2021; Vora et al., 2021). Cette disparité peut s'expliquer par la courte demi-vie de cette cytokine dans la circulation et donc par sa difficulté de détection (Kudo et al., 1990).

Cependant, les études portant sur la réponse immunitaire au niveau voies aériennes basses s'accordent pour affirmer que les cas sévères de COVID-19 sont caractérisés par une forte production d'IL-1ß qui serait associée aux macrophages dérivés de monocytes (Bost et al., 2020; Liao et al., 2020; Wauters et al., 2021; Xu et al., 2020). De plus, l'ATP extracellulaire mesuré dans des lavages broncho-alvéolaires est

plus élevé chez les patients atteints d'une forme sévère, dont les auteurs supposent que ce dernier est libéré lors de la mort des cellules épithéliales infectées par le SARS-CoV-2, comme lors d'autres infections virales pulmonaires (Wauters et al., 2021). L'ATP extracellulaire est un activateur connu de l'inflammasome NLRP3 (Mariathasan et al., 2006). Des specks contenant l'adaptateur ASC et le récepteur NLRP3 ont été observés sur des coupes histologiques de poumons de patients COVID-19 décédés, suggérant l'activation de cet inflammasome (Rodrigues et al., 2021; Xian et al., 2021). D'autre part, la forme clivée (active) de la GSDMD a été détectée sur des coupes histologiques de poumons (Zhang et al., 2021). De plus, l'infection de monocytes primaires humains par le SARS-CoV-2 (*ex vivo*) induit la sécrétion d'IL-1ß et l'analyse de monocytes circulants de patients COVID-19 montre une activation de la Caspase-1 ainsi que la présence de specks contenant NLRP3 et ASC (Ferreira et al., 2021; Rodrigues et al., 2021). Il a également été montré que la protéine de la nucléocapside (N) et l'ARN simple brin du SARS-CoV-2 activent l'inflammasome NLRP3 (Campbell et al., 2021; Pan et al., 2021). Ces éléments indiquent qu'un inflammasome est activé au sein de l'appareil respiratoire inférieur ainsi que dans les monocytes circulants au cours du COVID-19, cependant, ces études ne montrent pas de lien clair entre la sévérité des patients et l'activation d'un inflammasome.

Il a été montré qu'en activant le TLR2, la protéine Spike (S) du SARS-CoV-2 induit un priming transcriptionnel de l'inflammasome NLRP3 (Eisfeld et al., 2021; Theobald et al., 2021). De plus, il semble exister une immunité mémoire dirigée contre cette protéine S. En effet, la stimulation de macrophages dérivés de monocytes de patients ayant été infectés par le SARS-CoV-2 induit une réponse transcriptionnelle tandis que ceux issus de patients naïf vis-à-vis du SARS-CoV-2 ne sont que très peu répondeurs à la protéine S. Cette mémoire immunitaire portée par les monocytes semble subsister jusqu'à 7 semaines après le diagnostic du COVID-19 (Theobald et al., 2021).

Le SARS-CoV-2 a également été montré pour activer l'inflammasome NLRP1 au sein des cellules épithéliales humaines. En effet, la protéine NSP5 (protéase de type 3CL) clive NLRP1 au niveau du domaine NACHT ce qui induit la dégradation de NLRP1 par le protéasome et libère le fragment UPA-CARD qui s'oligomérise (Planès et al., 2021). En plus de cliver le récepteur NLRP1, les auteurs ont montré que la protéase NSP5 clive également la GSDMD pour l'inactiver. La protéine N du SARS-CoV-2 qui active l'inflammasome NLRP3 inhibe également l'activation de la GSDMD (Ma et al., 2021).

#### 5.2.2. Défaut de production et de réponse aux Interférons

Les IFNs jouent un rôle primordial pour contenir une infection. En se fixant à leurs récepteurs, les IFNs de type I (IFN-α/ß) et III (IFNλ) induisent l'expression des ISGs (gènes stimulés par l'IFN). La principale différence entre ces deux types d'IFNs réside dans l'expression de leur récepteur. Alors que le récepteur aux IFN de type I (IFNAR) est exprimé dans toutes les cellules, le récepteur aux IFN de type III (IFNLR)

est préférentiellement exprimé par les cellules épithéliales et certaines cellules immunitaires comme les cellules dendritiques plasmacytoïdes (Lazear et al., 2019). Cela suggère que les IFN de type III ont une activité anti-virale majoritairement au niveau des barrières épithéliales.

Les cas sévères de COVID-19 se distinguent par une diminution des IFN de type I plasmatiques et de l'induction des ISGs dans les cellules mononuclées circulantes (PBMCs) (Blanco-Melo et al., 2020; Combes et al., 2021; Hadjadj et al., 2020). Deux études ont montré que la production des Interférons de type I et III n'était en fait pas absente chez les patients présentant une forme sévère mais que celle-ci était retardée (Galani et al., 2021; Lucas et al., 2020).

Les premières études concernant la réponse immunitaire au cours de l'infection au SARS-CoV-2 ont été menées sur des PBMCs. Cependant, l'étude de la réponse immunitaire au niveau des voies respiratoires est essentielle puisqu'il s'agit du point d'entrée du SARS-CoV-2.

Chez les patients atteints de COVID-19 modéré, les cellules ciliées situées dans le nasopharynx produisent des ISGs en grande quantité tandis que cette production est faible chez les patients sévères (Sposito et al., 2021; Ziegler et al., 2021). Il a été observé que les patients sévères n'ont pas d'induction de l'expression des facteurs de transcription impliqués dans la réponse IFN (STAT1, STAT2, IRF1, et IRF9) dans les cellules ciliées (Ziegler et al., 2021). Il apparaît également une diversité dans le type d'IFN produit dans les voies aérienne supérieures des patients COVID-19 modérés et sévères. Les patients modérés ont une production d'IFN λ1 et λ3 tandis que les patients sévères ont une production d'Interféron λ2 et α/ß (Sposito et al., 2021).

L'étude des lavages broncho-alvéolaires permet d'étudier la réponse immunitaire au niveau des voies respiratoires basses. Au contraire des voies aérienne haute, il a été observé une forte production des IFN de type I, II et III ainsi qu'une induction des ISGs dans les lavages broncho-alvéolaires des patients atteints de COVID-19 sévères (Desai et al., 2020; Sposito et al., 2021; Zhou et al., 2020). La réponse IFN chez les patients modérés est moins importante. Cela pourrait être dû à une plus forte charge virale au niveau du voies respiratoires basses chez les patients les plus sévères (Chen et al., 2021; Zheng et al., 2020).

Les voies de signalisation menant à la production d'IFNs sont dérégulées (mutations, auto-anticorps) chez certains patients atteints de formes sévères du COVID-19. Des mutations « perte de fonction » sur les gènes *TLR3*, *TLR7* et *IRF7* sont enrichies dans le groupe de patients présentant une forme sévère (Asano et al., 2021; van der Made et al., 2020; Zhang et al., 2020b). De plus, des anticorps auto-réactifs dirigés contre l'IFN$\alpha_2$ et ß ainsi que l'IFNω ont été spécifiquement retrouvés dans les groupes de patients COVID-19 sévères et seraient associés à 20% de la mortalité des patients COVID-19 (Bastard et al., 2020, 2021; Lopez et al., 2021).

La réponse immunitaire médiée par les IFNs est donc primordiale pour résoudre l'infection rapidement. Le SARS-CoV-2 bloque cette réponse immunitaire en inhibant diverses protéines impliquées dans la réponse IFN (Beyer and Forero, 2021).

### 5.2.3. Dérégulation des cellules immunitaires

Les cas de COVID-19 sévères ont été rapidement associés à une dérégulation des cellules immunitaires. La sévérité est en effet associée à une perte des éosinophiles et des lymphocytes T ainsi qu'une augmentation des monocytes classiques et des neutrophiles immatures. En plus d'une proportion de cellules déséquilibrée, les leucocytes présentaient également un phénotype altéré chez les patients sévères.

- *Lymphocytes*

L'analyse de la formule sanguine des patients COVID-19 a révélé une lymphopénie chez les patients atteints de formes sévères ou décédés suite à l'infection (Huang et al., 2020; Ruan et al., 2020; Yang et al., 2020a). Des études plus poussées ont montré que les patients sévères présentent une diminution des lymphocytes T $CD4^+$ et $CD8^+$ circulants (Carissimo et al., 2020; Chen et al., 2020; Silvin et al., 2020; Wang et al., 2020). De plus, au cours du COVID-19, les lymphocytes T circulants présentent des marqueurs de dysfonctionnement mitochondrial et d'apoptose associés à un profil métabolique dérégulé (Thompson et al., 2021).

Dans les voies aériennes inférieures des patients atteints de COVID-19 modéré, il a été observé une expansion clonale et une augmentation des fonctions effectrices des lymphocytes T $CD8^+$ , et $CD4^+$ de type Th1 et Th17 (Liao et al., 2020; Wauters et al., 2021). Les lymphocytes présents au niveau des voies aériennes basses des patients sévères ont un phénotype dérégulé, sont peu différenciés et leur réponse aux IFN de type I et II est faible (Liao et al., 2020; Wauters et al., 2021).

- *Granulocytes*

Les cas sévères de COVID-19 sont caractérisés par une réduction du nombre d'éosinophiles et une augmentation du nombre de neutrophiles circulants (Lourda et al., 2021). Tandis que les neutrophiles circulants des patients atteints de COVID-19 modéré sont caractérisés par une réponse de type IFN de type I/II, chez les patients sévères ces cellules ont une signature pro-inflammatoire (production de ROS, activation de la voie NF-κB et réponse à l'IL-1) et promouvant la coagulation (Facteurs VII, VIII et IX) (Lourda et al., 2021; Silvin et al., 2020). Cependant, une autre étude a montré que les neutrophiles isolés de patients COVID-19 sévères ont un défaut de production de ROS en réponse à une infection par *E. coli* (Schulte-Schrepping et al., 2020).

Parmi les neutrophiles, plusieurs études ont observé une expansion des neutrophiles immatures et de neutrophiles matures de type MDSC (cellules myéloïdes suppressives) chez les patients sévères (Carissimo et al., 2020; Combadière et al., 2021; Lourda et al., 2021; Schulte-Schrepping et al., 2020; Silvin et al., 2020; Wilk et al., 2020). Les neutrophiles immatures, caractérisés par le marqueur LOX-1 et l'absence d'expression du marqueur CD10, sont décrits pour résulter d'une hématopoïèse d'urgence au cours du sepsis (Evrard et al., 2018). Les neutrophiles de type MDSC sont caractérisés par l'expression de PD-L1 et leur émergence a également été observée au cours du sepsis bactérien. Les neutrophiles de type MDSC inhibent l'activation les lymphocytes T et induisent l'apoptose de ces cellules (Langereis et al., 2017; Qi et al., 2021).

Au cours COVID-19 modéré, les neutrophiles infiltrent les poumons et cette infiltration est exacerbée chez les patients sévères (Chua et al., 2020; Liao et al., 2020). Il a été observé que les neutrophiles immatures et MDSC migrent vers les poumons chez les patients sévères (Combadière et al., 2021; Silvin et al., 2020).

- *Monocytes et cellules dendritiques*

Chez les patients atteints de COVID-19 sévère, la proportion des différents types de monocytes (classiques, intermédiaires et non classiques) au niveau périphérique est déséquilibrée en faveur des monocytes classiques avec une perte des monocytes non classiques (Sánchez-Cerrillo et al., 2020; Schulte-Schrepping et al., 2020; Silvin et al., 2020). En plus de ce déséquilibre, les monocytes classiques ont un phénotype immunosuppresseur. En effet, chez les patients sévères, l'expression de la molécule HLA-DR du CMH de classe II est fortement diminuée, illustrant une diminution de la présentation d'antigènes et indiquant un phénotype MDSC (Carissimo et al., 2020; Schulte-Schrepping et al., 2020; Silvin et al., 2020; Wilk et al., 2020). Cette diminution a été observée aussi bien chez les monocytes circulants que chez les macrophages pulmonaires. L'analyse transcriptionnelle des monocytes exprimant faiblement HLA-DR montre une activation de la voie NF-κB alors que les monocytes ayant une forte expression de HLA-DR ont une signature correspondant à un programme transcriptionnel médié par les IFN de type I (Schulte-Schrepping et al., 2020; Silvin et al., 2020).

Au niveau pulmonaire, la proportion de macrophages alvéolaires est diminuée au profit d'une infiltration de monocytes chez les patients sévères (Bost et al., 2020; Chua et al., 2020; Silvin et al., 2020; Wauters et al., 2021). Les macrophages dérivés de monocytes expriment des cytokines pro-inflammatoires (IL-1ß, IL-8, TNF) et des chimiokines (CCL2, 3, 4, 5, 7, 8, et CXCL5) (Chua et al., 2020; Liao et al., 2020; Wauters et al., 2021). Dans le contexte du syndrome respiratoire aigu, ces chimiokines sont responsables du recrutement des monocytes et neutrophiles au niveau des poumons (Luster, 2009; Reutershan and Ley, 2004). Une étude montre que les monocytes intermédiaires et non classiques sont

les deux sous-type de monocytes qui infiltrent les poumons des patients atteints de COVID-19 sévère (Sánchez-Cerrillo et al., 2020).

Les cellules dendritiques sont également affectées au cours du COVID-19. Les patients atteints de COVID-19 présentent une diminution des cellules dendritiques circulante et cette différence est amplifiée chez les patients atteints de forme grave (Carissimo et al., 2020; Kvedaraite et al., 2021; Winheim et al., 2021). En plus de cette diminution, les cellules dendritiques circulantes des patients sévères expriment faiblement la molécule HLA-DR du CMH de classe II et ont une capacité moindre à stimuler les lymphocytes $CD4^+$ naïfs, indiquant un phénotype MDSC (Kvedaraite et al., 2021; Winheim et al., 2021).

Les cellules dendritiques sont recrutées au niveau des poumons des patients atteints de COVID-19 modéré. Cependant, ce recrutement est moindre chez les patients atteints de formes sévères (Bost et al., 2020; Chua et al., 2020; Liao et al., 2020; Sánchez-Cerrillo et al., 2020).

# Résultats

## 1. Détection de l'activité de la toxine CNF1 par l'axe Pak1/2-inflammasome NLRP3

### *Contexte et objectifs de recherche*

La détection quantitative et qualitative des micro-organismes est essentielle pour permettre à l'hôte de mettre en place une réponse immunitaire efficace mais également proportionnée. Les bactéries pathogènes expriment spécifiquement des facteurs de virulence ciblant les voies de signalisation de l'hôte et qui leur permettent d'infecter l'hôte, de se disséminer ou encore de contourner la réponse immunitaire. Cependant, au cours de l'évolution hôte-pathogène, l'hôte a mis en place une réponse dirigée contre ces facteurs de virulence (Effector-triggered immunity).

La toxine CNF1 des *E. coli* uropathogènes active constitutivement les Rho-GTPases. Cette toxine améliore la dissémination des bactéries, notamment dans la circulation sanguine, provoquant une bactériémie. L'équipe du Dr Laurent Boyer a précédemment montré que la toxine CNF1 induit une réponse immunitaire menant à l'élimination des bactéries au cours de la bactériémie chez la souris et l'infection systémique chez la drosophile. La toxine CNF1 induit deux réponses : une première réponse transcriptionnelle via l'activation de la voie NF-κB et la production de cytokines pro-inflammatoires. En parallèle de celle-ci, CNF1 induit également l'activation de la Caspase-1 et la maturation de l'IL-1ß. L'équipe a également montré que l'élimination bactérienne au cours de la bactériémie dépend de la voie de l'IL-1. Ces données suggèrent qu'un inflammasome est activé à la suite de la détection de la toxine CNF1. Le but de ce travail était de déterminer quel inflammasome est responsable de la détection de l'activité de cette toxine et de caractériser la voie de signalisation en amont de l'activation de cet inflammasome.

nature microbiology

ARTICLES

https://doi.org/10.1038/s41564-020-00832-5

Check for updates

# *Escherichia coli* Rho GTPase-activating toxin CNF1 mediates NLRP3 inflammasome activation via p21-activated kinases-1/2 during bacteraemia in mice

Océane Dufies[1], Anne Doye[1], Johan Courjon[1,2], Cédric Torre[1], Gregory Michel[1], Celine Loubatier[1], Arnaud Jacquel[1], Paul Chaintreuil[1], Alissa Majoor[1], Rodolphe R. Guinamard[1], Alexandre Gallerand[1], Pedro H. V. Saavedra[3], Els Verhoeyen[1,4], Amaury Rey[4], Sandrine Marchetti[1], Raymond Ruimy[1,2], Dorota Czerucka[5,6], Mohamed Lamkanfi[3], Bénédicte F. Py[4], Patrick Munro[1], Orane Visvikis[1] and Laurent Boyer[1,6]✉

**Inflammasomes are signalling platforms that are assembled in response to infection or sterile inflammation by cytosolic pattern recognition receptors. The consequent inflammasome-triggered caspase-1 activation is critical for the host defence against pathogens. During infection, NLRP3, which is a pattern recognition receptor that is also known as cryopyrin, triggers the assembly of the inflammasome-activating caspase-1 through the recruitment of ASC and Nek7. The activation of the NLRP3 inflammasome is tightly controlled both transcriptionally and post-translationally. Despite the importance of the NLRP3 inflammasome regulation in autoinflammatory and infectious diseases, little is known about the mechanism controlling the activation of NLRP3 and the upstream signalling that regulates the NLRP3 inflammasome assembly. We have previously shown that the Rho-GTPase-activating toxin from *Escherichia coli* cytotoxic necrotizing factor-1 (CNF1) activates caspase-1, but the upstream mechanism is unclear. Here, we provide evidence of the role of the NLRP3 inflammasome in sensing the activity of bacterial toxins and virulence factors that activate host Rho GTPases. We demonstrate that this activation relies on the monitoring of the toxin's activity on the Rho GTPase Rac2. We also show that the NLRP3 inflammasome is activated by a signalling cascade that involves the p21-activated kinases 1 and 2 (Pak1/2) and the Pak1-mediated phosphorylation of Thr 659 of NLRP3, which is necessary for the NLRP3–Nek7 interaction, inflammasome activation and IL-1β cytokine maturation. Furthermore, inhibition of the Pak–NLRP3 axis decreases the bacterial clearance of CNF1-expressing UTI89 *E. coli* during bacteraemia in mice. Taken together, our results establish that Pak1 and Pak2 are critical regulators of the NLRP3 inflammasome and reveal the role of the Pak–NLRP3 signalling axis in vivo during bacteraemia in mice.**

Uropathogenic *E. coli* is the leading causative agent of bacteraemia[1]. It is therefore fundamental to decipher the mechanisms that determine the fate of this pathogen in the blood. The innate immune sensing of *E. coli* is mediated by pattern recognition receptors (PRRs), mainly by Toll-like receptor-4 (TLR4), which detects bacterial lipopolysaccharides (LPS). LPS are the principal component of the external membrane of both pathogenic and non-pathogenic *E. coli* and, therefore, pattern-triggered immunity does not seem to be sufficient to gauge the pathogenic potential of microorganisms. As TLR4 is activated by both live and dead bacteria, pattern-triggered immunity is certainly important for monitoring the quantity of bacteria, but is not sufficient to determine their quality[2]. One strategy to determine microbial pathogenicity is the detection of virulence factor activities that are specific to pathogens[3]. Virulence factors of uropathogenic *E. coli* include CNF1, which is a Rho-GTPase-targeting toxin. The CNF1 toxin bears enzymatic activity that is responsible for the post-translational deamidation of a specific glutamine residue on a subset of Rho GTPases, namely Rac, Cdc42 and RhoA[4–6]. This modification destroys the intrinsic and GTPase-activating-protein- (GAP)-regulated ability of these Rho GTPases to hydrolyse GTP, conferring dominant positive mutant characteristics to Rho proteins[4–6]. This modification increases GTP-bound activated Rho proteins and the activation of their downstream signalling pathways[6]. By modulating the host cytoskeleton, these virulence factors confer to bacteria invasion properties and the ability to modulate inflammatory responses[7–10]. Among the virulence factors, there are more than 30 that target Rho GTPases. They are either activators or inhibitors of Rho GTPases, both of which activate caspase-1 (refs. [11,12]).

Inflammasomes are signalling platforms that are assembled by cytosolic PRRs that activate caspase-1. NLRP3 oligomerizes on infection or cellular damage, and recruits ASC, Nek7 and caspase-1 to form the NLRP3 inflammasome. This assembly results in ASC speck formation, cleavage of pro-caspase-1 into active caspase-1 and

[1]Université Côte d'Azur, Inserm, C3M, Nice, France. [2]Université Côte d'Azur, CHU Nice, Nice, France. [3]Department of Internal Medicine and Pediatrics, Ghent University, Ghent, Belgium. [4]CIRI, Centre International de Recherche en Infectiologie, Université de Lyon, Inserm U1111, Université Claude Bernard Lyon 1, CNRS UMR5308, ENS de Lyon, Lyon, France. [5]Centre Scientifique de Monaco, Monaco, Monaco. [6]LIA ROPSE, Laboratoire International Associé Université Côte d'Azur, Centre Scientifique de Monaco, Nice, France. ✉e-mail: laurent.boyer@univ-cotedazur.fr

the maturation of pro-IL-1β into IL-1β. The NLRP3 inflammasome assembly is controlled by both the priming by TLR ligands and activation signals. Furthermore, the NLRP3 inflammasome assembly is regulated by phosphorylation and ubiquitination events[13,14]. Despite a variety of identified NLRP3 activators, the upstream signalling pathways that control NLRP3 post-translational modifications and activation mechanisms remain unclear[14]. Interestingly, toxins that inactivate Rho GTPases activate the Pyrin inflammasome through the modification of its phosphorylation status by the PKN1/2 kinases. The Pyrin inflammasome has been shown to detect toxins that inhibit Rho GTPases, but information about the sensing of toxins that activate Rho GTPases through inflammasomes is lacking[15,16]. In this Article, we used the CNF1 toxin as a model of the Rho-GTPase-activating virulence factor to demonstrate the role of the Pak–NLRP3 axis in sensing CNF1 activity and controlling the clearance of bacteria during bacteraemia.

## Results

**CNF1-triggered immunity requires NLRP3.** We set up an assay to monitor the CNF1-triggered activation of caspase-1 using a FAM-YVAD-FMK (FAM-FLICA) probe. Primary bone-marrow-derived macrophages (BMDMs) isolated from BALB/c mice were treated with CNF1 and analysed using confocal microscopy. Cells with dots of FAM-FLICA staining corresponding to ASC specks were counted (Extended Data Fig. 1a). This unbiased screen revealed that NLRP3 is the major NLR involved in CNF1-triggered caspase-1 activation (Fig. 1a). The role of NLRP3 in this pathway was confirmed in BMDMs isolated from C57BL/6J mice bearing ASC–citrine knockin using flow cytometry (Extended Data Fig. 1b,c). In this assay, we quantified the percentage of cells with ASC specks as previously described[17,18]. These data revealed the conserved role of NLRP3 in the response to CNF1 in macrophages isolated from both BALB/c and C57BL/6J background.

Next, we investigated the role of NLRP3 in CNF1-triggered immunity. Co-treatment of BMDMs isolated from wild-type (WT) mice with the CNF1 toxin together with the NLRP3 inhibitor MCC950 was sufficient to block caspase-1 activity, demonstrating that the CNF1 toxin is an NLRP3 activator (Fig. 1b,c). Importantly, the number of FAM-FLICA$^+$ cells was substantially reduced in BMDMs that were treated with catalytically inactive mutant CNF1$^{C866S}$. This result provided evidence that CNF1 toxin activity is monitored by NLRP3, rather than the pattern of the toxin[3]. Furthermore, CNF1-triggered maturation and secretion of IL-1β and activation of caspase-1 was impaired in NLRP3-knockout BMDMs (Fig. 1d and Supplementary Fig. 1). By contrast, CNF1 treatment did not affect the secretion of IL-6 or TNF-α, two cytokines that are not regulated by inflammasomes (Fig. 1d and Supplementary Fig. 1). Activation of the NLRP3 inflammasome is often associated with pyroptosis[19]. To investigate whether CNF1 triggered pyroptosis, we measured propidium iodide incorporation (Extended Data Fig. 2a), lactate dehydrogenase (LDH) release (Extended Data Fig. 2b) and gasdermin D (GSDMD) cleavage (Extended Data Fig. 2c). In contrast to nigericin, we did not observe any of these pyroptosis markers after CNF1 treatment and we observed a similar level of CNF1-triggered caspase-1 activation and IL-1β maturation/secretion in WT and GSDMD-knockout macrophages (Extended Data Fig. 2d,e). We subsequently tested the role of the NLRP3 inflammasome regulator Nek7 in CNF1-triggered immunity. Transfection of *Nlrp3* or *Nek7* short interfering RNA (siRNA) in BMDMs inhibited CNF1-triggered IL-1β maturation (Extended Data Fig. 3a,b). $K^+$ efflux is an upstream event for NLRP3 inflammasome activation and Nek7 requires $K^+$ efflux for NLRP3 inflammasome assembly[14,20]. We observed that KCl treatment was sufficient to inhibit CNF1-triggered caspase-1 cleavage (Extended Data Fig. 3c). Importantly, we confirmed that the KCl treatment did not inhibit CNF1 toxin activity towards Rho GTPase activation using a glutathione S-transferase (GST)–Pak-Rac-binding domain (RBD) pull-down assay (Extended Data Fig. 3d). We next investigated whether other toxins that target Rho GTPases have the ability to activate the NLRP3 inflammasome. Dermonecrotic toxin (DNT) from *Bordetella* has transglutaminase activity towards Rho GTPases that enables the constitutive activation of Rho GTPases[6,10]. We observed that purified recombinant DNT triggered the activation of caspase-1 in WT macrophages, but not in NLRP3-knockout macrophages (Extended Data Fig. 4a). We next tested whether the NLRP3 activation was triggered specifically by virulence factors activating Rho GTPases using NLRP3 inflammasome reconstitution in HEK293T cells[21]. Cells were transfected with plasmids encoding the DNT toxin or the injected bacterial virulence factors YopE from *Yersinia* containing a GAP domain that enables inactivation of the Rho GTPases[6]. We observed NLRP3-dependent IL-1β maturation when cells were transfected with the Rho-GTPase-activating toxin DNT, but not when cells were transfected with the Rho GTPase inhibitor YopE (Extended Data Fig. 4b). The expression of the virulence factor SopE from *Salmonella* containing a guanine nucleotide exchange factor (GEF) domain activating Rac and Cdc42 (refs. [6,22]) or the expression of the GEF domain of the Dbl exchange factor (Dbl$^{495–826}$)[23] were sufficient to trigger NLRP3-dependent IL-1β maturation (Extended Data Fig. 4b,c). Taken together, we showed that the activation of Rho GTPases by toxins and virulence factors triggered the activation of the NLRP3 inflammasome and that Rac has a major role in this pathway.

**Activation of the NLRP3 inflammasome by CNF1 relies on Rac2 and the Pak serine–threonine kinases.** Although the CNF1 toxin is a Rho GTPases activator and Rac2 is a haematopoietic-specific Rho GTPase that is involved in the innate immune response to the CNF1 toxin[24], the contribution of Rac1 and Rac2 in this process is still unknown. To investigate the role of Rac in the CNF1-triggered NLRP3 inflammasome activation, we knocked down *Rac1* and/or *Rac2* using siRNA in BMDMs. Interestingly, *Rac1* knockdown resulted in an increase in the level of CNF1-triggered IL-1β maturation whereas *Rac2* knockdown was sufficient to block it (Fig. 2a). We tested whether activated GTP-bound Rac2 levels would increase when *Rac1* was targeted by siRNA. The GST–Pak-RBD pull-down analysis showed an increase in activated Rac2 when *Rac1* was knocked-down using siRNA (Fig. 2b). These data demonstrate the critical role of Rac2 in CNF1-triggered IL-1β maturation (Fig. 2a,b). To determine the molecular mechanism of the caspase-1 activation, we used a system of NLRP3 inflammasome reconstitution in HEK293T cells. This analysis showed that CNF1 is sufficient for the NLRP3 inflammasome activation-triggered caspase-1 cleavage and that the co-treatment of CNF1 with MCC950 inhibited this caspase-1 activation (Fig. 2c). The transfection of Rac2 GTPase or activated mutant forms of Rac2 (including Q61E mimicking the CNF1 modification or Q61L and G12V) were sufficient to activate caspase-1, in contrast to the inactive mutant Rac2$^{T17N}$ (Fig. 2d). Interestingly, the strength of caspase-1 activation observed using the activated forms of Rac2 GTPase was correlated with the amount of Rho GTPases that were bound to GST–Pak-RBD (Fig. 2e). These data indicate that NLRP3 senses the activation level of the Rho GTPase Rac2 proportionally to the strength of activation rather than by detecting the structural modification made by the toxin as it would be predicted for a classical PRR.

The correlation between caspase-1 activation and the amount of Rac2 bound to GST–Pak-RBD suggested a potential role of Pak kinases in CNF1-triggered NLRP3 inflammasome activation. We therefore knocked-down Pak1 and/or Pak2 in BMDMs by transfecting siRNA (Pak3 is predominantly expressed in the brain[25,26]). We observed a major decrease in caspase-1 cleavage in cells treated with *Pak1* siRNA but a moderate impact when using siRNA targeting *Pak2*, indicating that Pak1 has a main role (Fig. 3a). However, we could not exclude the possibility that the total inhibition of

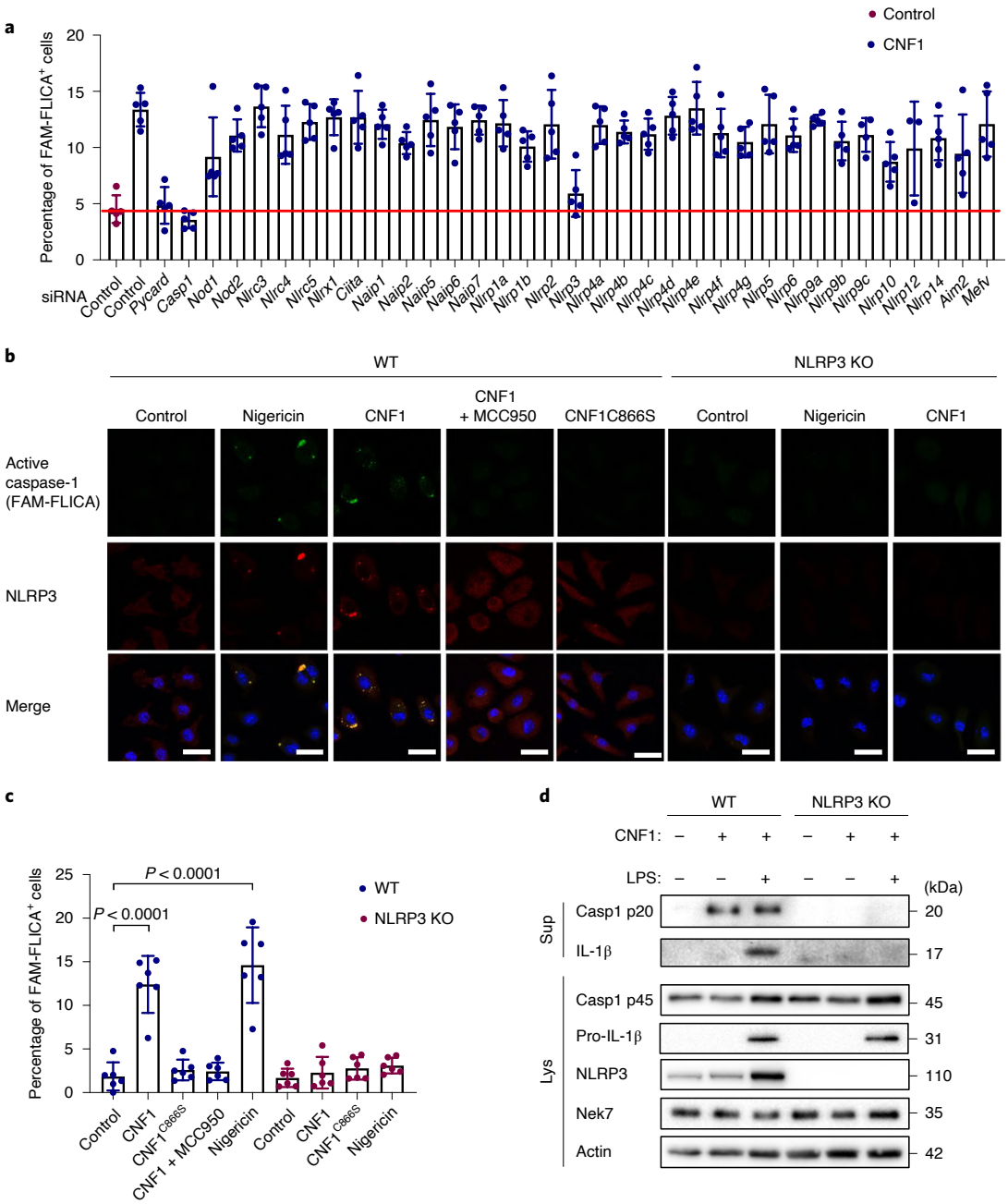


**Fig. 1 | CNF1-triggered caspase-1 activation and IL-1β maturation requires NLRP3. a**, BMDMs isolated from BALB/c mice were transfected with the indicated siRNA for 72 h before treatment for 6 h with CNF1 (500 ng ml$^{-1}$). Active caspase-1 was detected using the FAM-FLICA probe. Cells harbouring FAM-FLICA dots were counted as positive using Fiji. The red horizontal line indicates the mean percentage of FAM-FLICA$^+$ cells in the untreated control. Each dot represents 200 cells. $n = 1{,}800$ cells. Data are mean ± s.e.m. **b**,**c**, BMDMs extracted from WT or NLRP3-knockout C57BL/6J mice were or were not pretreated for 45 min with MCC950 (1 μM) before treatment for 6 h with CNF1 (500 ng ml$^{-1}$), or the CNF1 catalytic inactive mutant CNF1$^{C866S}$ (500 ng ml$^{-1}$) or nigericin (5 μM). **b**, Cells were analysed using immunofluorescence and confocal imaging. Active caspase-1 (FAM-FLICA) is shown in green, NLRP3 in red and nuclei in blue. Scale bars, 20 μm. **c**, Quantification of FAM-FLICA$^+$ cells in WT (blue) or NLRP3-knockout BMDMs (red). Each dot represents 100 cells. $n = 600$ cells. Data are mean ± s.e.m. Statistical analyses were performed using two-tailed unpaired Student's *t*-tests. **d**, WT or NLRP3-knockout BMDMs were treated with CNF1 (500 ng ml$^{-1}$) and/or LPS (100 ng ml$^{-1}$) for 8 h before the supernatants (Sup) and cell lysates (Lys) were collected and analysed using immunoblotting. Experiments were repeated at least three times, and representative data are shown.

caspase-1 cleavage observed with the *Pak1* siRNA treatment might be due to a limit in the detection level of cleaved caspase-1, or to *Pak1* siRNA that may affect *Pak2*, suggesting that there is a partial Pak1/2 redundancy. The treatment with Pak1 inhibitors (IPA-3 or FRAX597) was sufficient to block the CNF1-triggered IL-1β maturation that was observed in macrophages treated with LPS, and was also sufficient to block caspase-1 activation (Fig. 3b,c). The inhibition of the caspase-1 cleavage after IPA-3 treatment was similarly observed in macrophages treated with DNT (Extended Data Fig. 4d). Interestingly, IPA-3 was shown to inhibit the binding of activated forms of Rac and Cdc42 to Pak1, thereby inhibiting the autophosphorylation of Thr 423, whereas the FRAX597

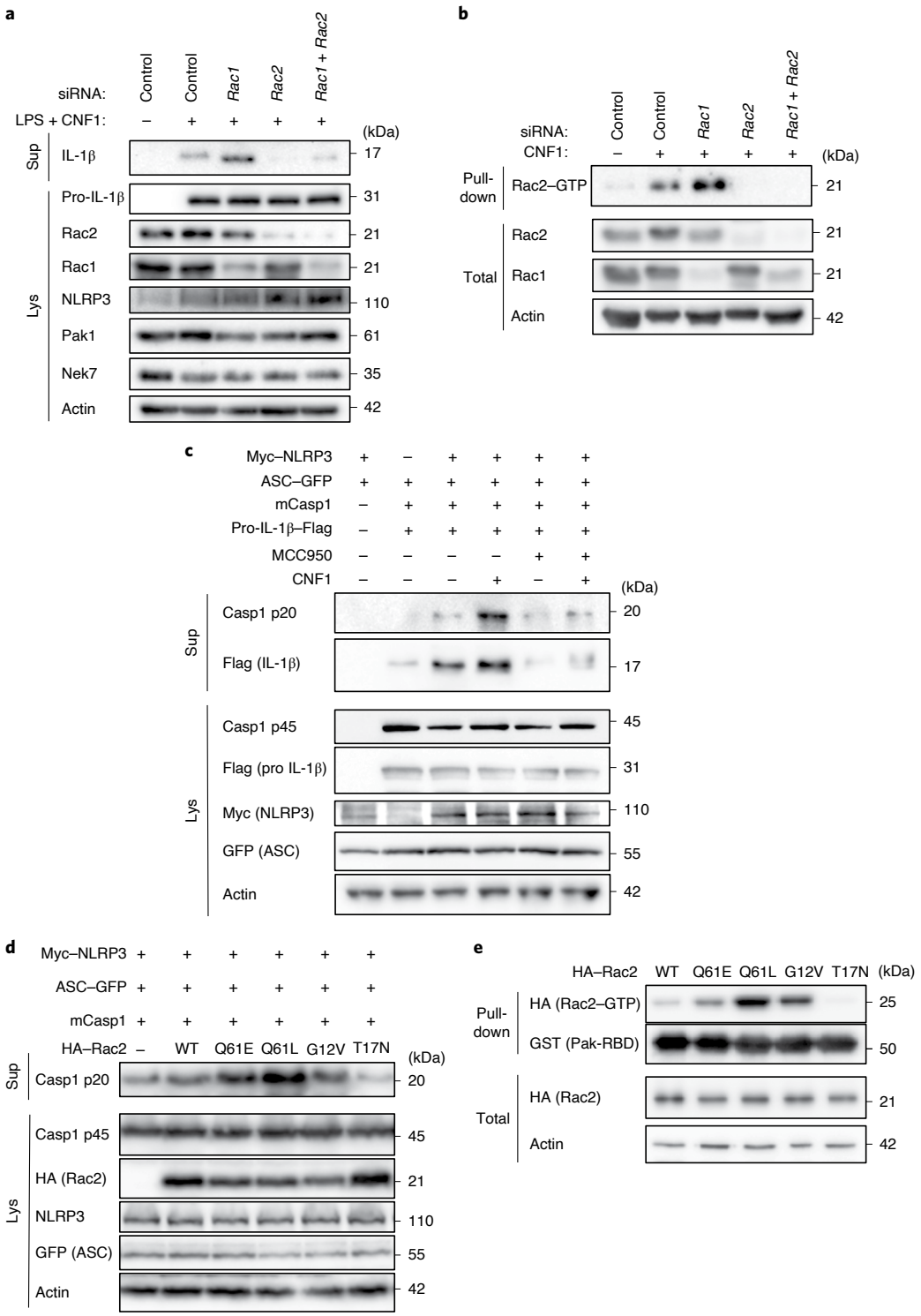


**Fig. 2 | Rac2 activation triggers NLRP3 inflammasome activation. a**, BMDMs extracted from BALB/c mice were transfected with siRNA targeting the indicated isoform of Rac GTPase for 72 h and treated with CNF1 (500 ng ml$^{-1}$) and LPS (100 ng ml$^{-1}$) for 8 h. Supernatants and cell lysates were analysed using immunoblotting. **b**, Immortalized BMDMs (iBMDMs) were transfected with the indicated siRNA for 72 h before being treated or not treated with CNF1 (500 ng ml$^{-1}$) for 6 h before analysis using a GST–Pak-RBD pull-down assay. The Rac2 associated with the GST–Pak-RBD beads is indicated as Rac2–GTP. **c**,**d**, HEK293T cells were transfected for 16 h with plasmids encoding NLRP3 inflammasome components: Myc–NLRP3, green fluorescent protein (GFP)-tagged ASC, mouse caspase-1 (mCasp1) and pro-IL-1β–Flag as indicated, before analysing caspase-1 cleavage or pro-IL-1β maturation using immunoblotting. **c**, Cells were pretreated or not with 1 μM MCC950 for 45 min before treatment for 6 h with CNF1 (500 ng ml$^{-1}$). **d**, Cells were transfected with the following haemagglutinin (HA)-tagged mutants of Rac2: the constitutively active mutant mimicking CNF1-induced deamidation Rac2$^{Q61E}$ (Q61E), the constitutively active mutants Rac2$^{Q61L}$ (Q61L) or Rac2$^{G12V}$ (G12V), or the dominant negative mutant Rac2$^{T17N}$ (T17N). Supernatants and cell lysates were analysed using immunoblotting. **e**, HEK293T cells were transfected for 16 h with HA-tagged active mutants Rac2$^{Q61E}$, Rac2$^{Q61L}$ or Rac2$^{G12V}$, or the dominant negative mutant Rac2$^{T17N}$ before analysis using a GST–Pak-RBD pull-down assay. HA–Rac2 associated with the GST–Pak-RBD beads is indicated as Rac2–GTP. Experiments were repeated at least three times, and representative data are shown.

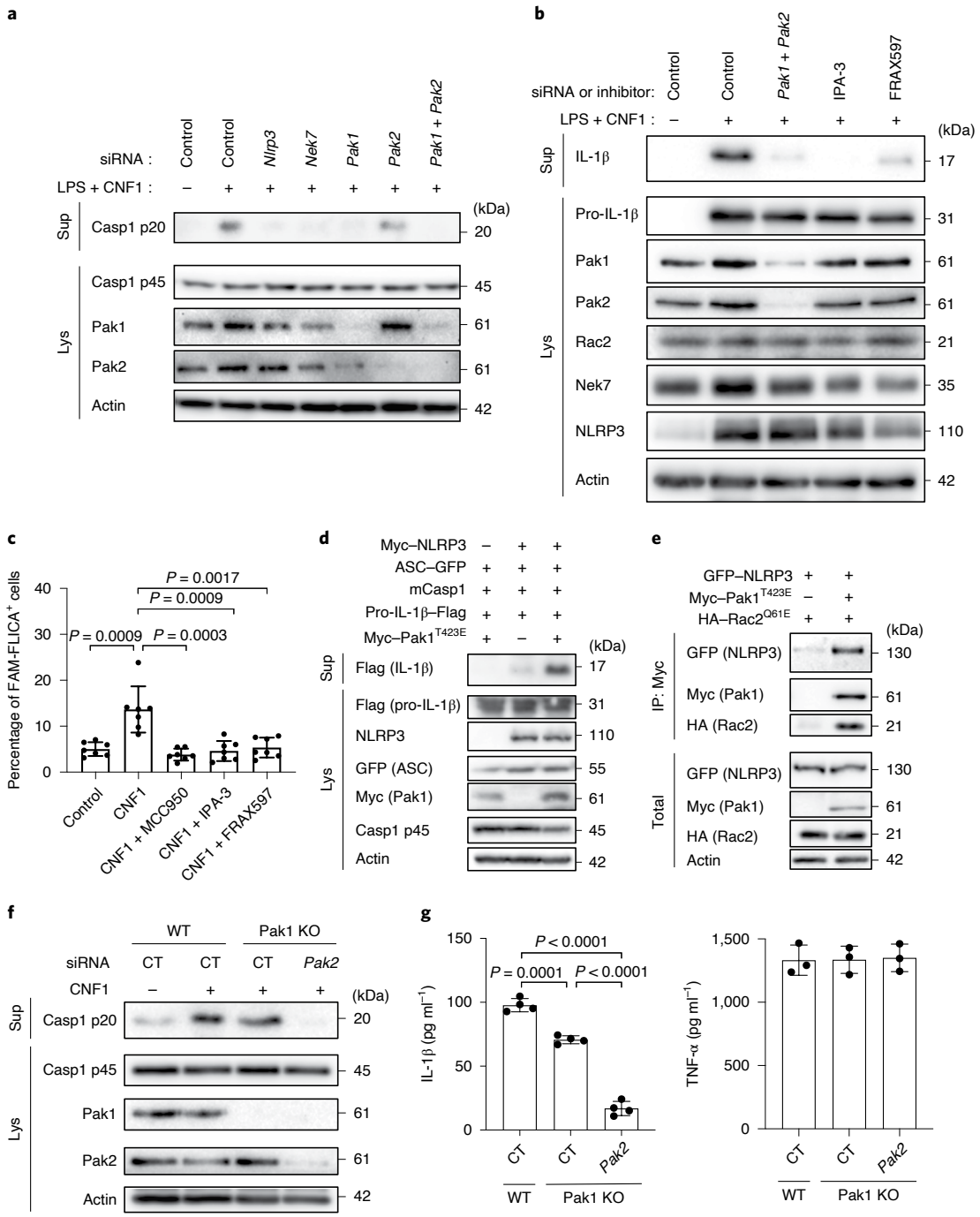


**Fig. 3 | Rac2–NLRP3 signalling is dependent on Pak1 kinase. a**, BMDMs isolated from BALB/c mice were transfected for 72 h with siRNA targeting *Nlrp3*, *Nek7*, *Pak1* or *Pak2* as indicated; non-targeting siRNA was used as a control. Cells were treated with CNF1 (500 ng ml$^{-1}$) and LPS (100 ng ml$^{-1}$) for 8 h, as indicated. Supernatants and cell lysates were analysed using immunoblotting. **b**, BMDMs isolated from BALB/c mice were transfected with *Pak1*- and *Pak2*-targeting siRNA or with non-targeting siRNA for 72 h, and treated with 5 μM IPA-3, 1 μM FRAX597 or vehicle for 45 min before treatment with CNF1 (500 ng ml$^{-1}$) and LPS (100 ng ml$^{-1}$) for 8 h. Supernatants and cell lysates were analysed using immunoblotting. **c**, BMDMs isolated from BALB/c mice were treated with vehicle (control), or treated either with 1 μM MCC950, 5 μM IPA-3 or 1 μM FRAX597 for 45 min before treatment with CNF1 (500 ng ml$^{-1}$) for 6 h. Active caspase-1 was stained with FAM-FLICA, analysed using microscopy and FAM-FLICA$^+$ cells were counted. Each dot represents 100 cells. $n = 800$ cells. Data are mean ± s.e.m. Statistical analyses were performed using two-tailed unpaired Student's *t*-tests. **d**, HEK293T cells were transfected as indicated with plasmids encoding components of the NLRP3 inflammasome (Myc-NLRP3, ASC-GFP, mouse caspase-1) and pro-IL-1β-Flag together with Myc-Pak1$^{T423E}$, and pro-IL-1β-Flag cleavage was analysed using immunoblotting. **e**, HEK293T cells were transfected with plasmids encoding GFP-NLRP3, Myc-Pak1$^{T423E}$ and HA-Rac2$^{Q61E}$. Cell lysates were processed for anti-Myc immunoprecipitation (IP). **f**, BMDMs isolated from WT or Pak1-knockout C57BL/6J mice were transfected 72 h with non-targeting or *Pak2*-targeting siRNA before treatment with CNF1 (500 ng ml$^{-1}$) for 8 h. Supernatants and cell lysates were analysed using immunoblotting. CT, control. **g**, BMDMs isolated from WT or Pak1-knockout C57BL/6J mice were transfected for 72 h with non-targeting or *Pak2*-targeting siRNA before treatment with CNF1 (500 ng ml$^{-1}$) and LPS (100 ng ml$^{-1}$) for 8 h. Supernatants were analysed using enzyme-linked immunosorbent assay (ELISA) for IL-1β ($n = 4$ biologically independent samples) and TNF-α ($n = 3$ biologically independent samples). Data are mean ± s.e.m. Statistical analyses were performed using two-tailed unpaired Student's *t*-tests. Experiments were repeated at least three times, and representative data are shown.

is an ATP-competitive inhibitor[27]. In the inflammasome reconstitution system in HEK293T, we expressed the activated form of Pak1 (T423E) together with caspase-1, ASC and pro-IL-1β, and we observed no IL-1β maturation. By contrast, when NLRP3 was transfected together with ASC and caspase-1, the expression of the activated form of Pak1 was sufficient to trigger maturation of IL-1β (Fig. 3d). Furthermore, phosphorylated forms of Pak colocalized in dot-like structures with NLRP3 and active caspase-1 (Supplementary Fig. 2). We next investigated whether Rac2, Pak1 and NLRP3 proteins formed a complex. We found NLRP3 interacting with activated Rac2 when activated Pak1 was expressed (Fig. 3e). We next investigated whether Pak1 was involved in the nigericin-triggered activation of the NLRP3 inflammasome and observed that IPA-3 treatment was sufficient to inhibit both caspase-1 cleavage and the release of LDH (Extended Data Fig. 5a,b). Furthermore, siRNA targeting of *Pak1* was found to decrease nigericin-triggered caspase-1 maturation (Extended Data Fig. 5c).

To genetically prove the involvement of Pak1 in NLRP3 inflammasome activation, we used Pak1-knockout mice. We observed a reduction in caspase-1 cleavage triggered by CNF1 in Pak1-knockout macrophages and a reduction in IL-1β secretion (Fig. 3f,g). By contrast, the secretion of TNF-α was unaffected (Fig. 3g). Both caspase-1 cleavage and IL-1β secretion triggered by CNF1 were substantially reduced when the Pak1-knockout macrophages were treated with the *Pak2* siRNA, suggesting that there is a partial compensation in Pak1-knockout macrophages (Fig. 3f,g).

**Pak1 phosphorylates NLRP3 and triggers inflammasome activation.** To further investigate whether NLRP3 is a substrate for the Pak1 serine–threonine kinase, we set-up an in vitro kinase assay. When both Pak1 and NLRP3 proteins were incubated with ATPγ$^{32P}$, we observed a band at the size of NLRP3, indicating that NLRP3 is directly phosphorylated by Pak1 in vitro (Fig. 4a). The in vitro kinase assay was then used to identify the phosphorylated sites of NLRP3 by analysing the band corresponding to NLRP3 using mass spectrometry. The analysis revealed that Pak1 phosphorylates NLRP3 at three independent positions that correspond to Ser 163, Ser 198 and Thr 659 in the human NLRP3 (Extended Data Fig. 6a,c and Supplementary Table 1). Interestingly, the Ser 163 and Ser 198 residues were previously reported to be phosphorylated, and Ser 198 was reported to be important for NLRP3 priming[28]. NLRP3 Thr 659 was not reported to be phosphorylated and, interestingly, the identified peptide appears to be conserved between humans and mice (Extended Data Fig. 6d). Reinforcing the potential conservation of the Pak–NLRP3 axis, CNF1-triggered caspase-1 activation was observed in primary human macrophages and was inhibited by treatment with NLRP3 inhibitor or Pak1 inhibitor (Extended Data Fig. 7a,b). In the inflammasome reconstitution system, we next expressed the activated Pak1$^{T423E}$ and compared the effect of the expression of NLRP3 WT with the triple-mutant NLRP3$^{S163A\,S198A\,T659A}$ or single mutants NLRP3$^{S163A}$, NLRP3$^{S198A}$ and NLRP3$^{T659A}$ in which the phosphorylated residues were replaced with alanine residues, which are not sensitive to phosphorylation. The results show that the triple-mutant NLRP3$^{S163A\,S198A\,T659A}$ and the single mutant NLRP3$^{T659A}$ is impaired in IL-1β maturation triggered by the activated Pak1$^{T423E}$, indicating that the NLRP3 Thr 659 residue has an important role in Pak1-triggered NLRP3 inflammasome activation (Fig. 4b). Furthermore, we generated a T659D phosphomimetic NLRP3 mutant and observed that, compared with NLRP3$^{T659A}$, the NLRP3$^{T659D}$ mutant had an increased ability to trigger pro-IL-1β maturation (Fig. 4c). Importantly, similar results were obtained when the Rho-GTPase-activating virulence factor SopE was transfected to activate the pathway, highlighting the involvement of this NLRP3 post-translational regulation for the sensing of other virulence factors activating Rho GTPases (Extended Data Fig. 8a). We next stably reconstituted immortalized macrophages knocked-out for NLRP3 with plasmids encoding either NLRP3 or NLRP3$^{T659A}$. Confirming our results, we observed impaired CNF1-triggered IL-1β maturation/secretion in macrophages expressing NLRP3$^{T659A}$ compared with macrophages expressing WT NLRP3 (Fig. 4d,e). By contrast, TNF-α was similarly secreted by macrophages expressing either NLRP3 or NLRP3$^{T659A}$ (Fig. 4e). After treatment with the DNT toxin, we also observed an impairment in CNF1-triggered IL-1β maturation in macrophages expressing the NLRP3$^{T659A}$ mutant compared with macrophages expressing WT NLRP3 (Extended Data Fig. 8b). Reinforcing the importance of this NLRP3 phosphorylation site in the inflammasome activation process, nigericin-triggered IL-1β maturation and secretion were reduced in macrophages expressing the NLRP3$^{T659A}$ compared with the macrophages expressing NLRP3, whereas TNF-α secretion was unaffected (Extended Data Fig. 9). Taken together, these results show that phosphorylation of NLRP3 at Thr 659 has a functional role, and that Pak1 is a regulator of the NLRP3 inflammasome. Structural analysis of the NLRP3–Nek7 interaction revealed a putative interaction domain at the level of the Thr 659 of NLRP3 (ref. [29]). Using co-immunoprecipitation experiments, we tested whether the NLRP3$^{S163A\,S198A\,T659A}$ triple mutant or NLRP3$^{S163A}$, NLRP3$^{S198A}$ and NLRP3$^{T659A}$ single mutants affected the interaction with endogenous Nek7. The interaction between NLRP3 and Nek7 was impaired in the NLRP3$^{S163A\,S198A\,T659A}$ triple mutant and in the NLRP3$^{T659A}$ mutant, indicating that Thr 659 is a critical site for NLRP3–Nek7 interaction and suggesting that the phosphorylation of NLRP3 at Thr 659 is important for the NLRP3–Nek7 interaction (Fig. 4f). This observation was confirmed using anti-Nek7 immunoprecipitation in macrophages in which we found a decrease in NLRP3$^{T659A}$ binding to Nek7 compared with WT NLRP3 (Fig. 4g).

**Clearance of CNF1-expressing *E. coli* during bacteraemia requires the Pak–NLRP3 signalling axis.** We next addressed the relevance of the CNF1-triggered Pak–NLRP3 signalling axis during infection. We observed an increase in caspase-1 maturation when macrophages were infected with CNF1-expressing *E. coli* compared

**Fig. 4 | Pak1 phosphorylates NLRP3 to promote inflammasome activation. a**, In vitro [γ-32P]ATP kinase assay using human recombinant NLRP3 (arrows) and human recombinant Pak1 (arrowheads) analysed using autoradiography and Coomassie brilliant blue (CBB) staining. **b**, HEK293T cells were transfected with plasmids encoding components of the NLRP3 inflammasome (ASC–GFP, mouse caspase-1), pro-IL-1β–Flag, Myc–Pak1$^{T423E}$, with Myc–NLRP3, Myc–NLRP3$^{S163A}$, Myc–NLRP3$^{S198A}$, Myc–NLRP3$^{T659A}$ or Myc–NLRP3$^{S163A\,S198A\,T659A}$, and IL-1β maturation was analysed using immunoblotting. **c**, HEK293T cells were transfected with plasmids encoding components of the NLRP3 inflammasome (ASC–GFP, mouse caspase-1) and Myc–Pak1$^{T423E}$, with Myc–NLRP3, Myc–NLRP3$^{T659A}$ or Myc–NLRP3$^{T659D}$, and IL-1β maturation was analysed using immunoblotting. **d**,**e**, NLRP3-knockout iBMDMs that were reconstituted with either NLRP3 or NLRP3$^{T659A}$ were treated with vehicle or LPS (100 ng ml$^{-1}$) and CNF1 (500 ng ml$^{-1}$) for 8 h. **d**, Supernatants and cell lysates were analysed using immunoblotting. **e**, Supernatants were analysed using ELISA for IL-1β ($n=4$ biologically independent samples) and TNF-α ($n=3$ biologically independent samples). Data are mean ± s.e.m. Statistical analyses were performed using two-tailed unpaired Student's *t*-tests. **f**, HEK293T cells were transfected with plasmids encoding Myc–NLRP3, Myc–NLRP3$^{S163A}$, Myc–NLRP3$^{S198A}$, Myc–NLRP3$^{T659A}$ or Myc–NLRP3$^{S163A\,S198A\,T659A}$. Cell lysates were processed for anti-Myc immunoprecipitation and endogenous Nek7 was revealed using anti-Nek7 antibodies. **g**, NLRP3-knockout iBMDMs that were reconstituted with either NLRP3 or NLRP3$^{T659A}$ were treated with CNF1 (500 ng ml$^{-1}$) for 6 h. Cell lysates were analysed using immunoprecipitation with anti-Nek7 antibodies or isotypic IgG. Experiments were repeated at least three times, and representative data are shown.

with the isogenic *E. coli* CNF1-knockout strain, and treatment with NLRP3 or Pak1 inhibitors decreased the caspase-1 cleavage triggered by the *E. coli* expressing CNF1 (Fig. 5a). Furthermore, IL-1β secretion triggered by the CNF1-expressing *E. coli* was reduced when bacteria were added to NLRP3-knockout macrophages (Fig. 5b). Furthermore, the secretion of IL-1β triggered by CNF1-expressing *E. coli* in macrophages complemented with the NLRP3$^{T659A}$ mutant was decreased compared with control macrophages expressing

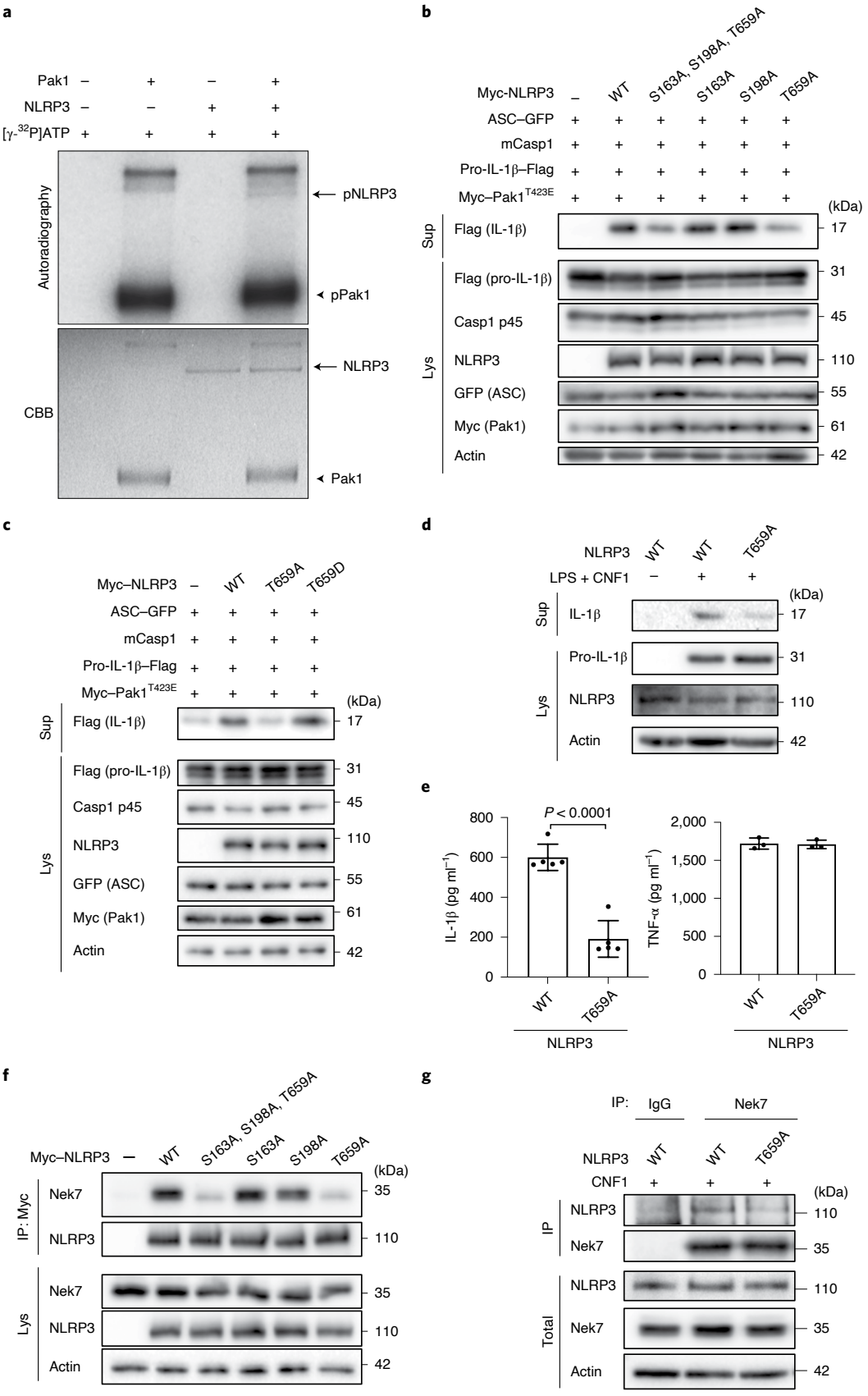

NLRP3 (Fig. 5c). TNF-α secretion measured during infection with CNF1-expressing *E. coli* was not affected in macrophages that were isolated from NLRP3-knockout mice or macrophages expressing the NLRP3$^{T659A}$ mutant (Fig. 5b,c). We previously demonstrated that the CNF1 toxin expressed by *E. coli* triggered both an immune response in vivo and bacterial clearance during bacteraemia[11]. To investigate the role of Pak1 during CNF1-expressing *E. coli* bacteraemia, we used the Pak1 inhibitor AZ13711265, which blocks CNF1-triggered IL-1β maturation (Supplementary Fig. 3) and is associated with good in vivo pharmacokinetic properties[27]. We monitored the bacterial burden during bacteraemia in control mice or mice injected with AZ13711265. Mice bacteraemia was measured for each mouse at 4 h, 24 h and 48 h after infection (Fig. 5d). The bacterial clearance of CNF1-expressing *E. coli* was observed; no bacteria were detectable at 48 h in all of the control animals (Fig. 5d). We measured a statistically significant higher bacterial load at 48 h and 77% of the animals were found to be positive for bacteraemia in the mice that were injected with the Pak1 inhibitor, indicating that in vivo the inhibition of Pak1 is sufficient to inhibit the CNF1-expressing *E. coli* clearance (Fig. 5d). We next used an NLRP3 inhibitor, MCC950, which has been shown to be efficient in vivo[30]. We monitored bacteraemia in mice injected with MCC950 compared with the controls. The bacterial clearance of CNF1-expressing *E. coli* in mice injected with the NLRP3 inhibitor was significantly higher at 48 h, and 70% of the animals were found to be positive for bacteraemia (Fig. 5d). Consistent with our model, we observed no significant effect of both AZ13711265 and MCC950 towards the bacterial clearance when we infected mice with the isogenic *E. coli* CNF1-knockout strain (Extended Data Fig. 10a). To genetically prove this point, we infected WT mice, NLRP3-knockout mice or Pak1-knockout mice, and compared the CNF1-expressing *E. coli* burden. Consistent with the results obtained with the NLRP3 and Pak1 inhibitors, we did not detect any bacteria in the blood of infected WT mice at 48 h, whereas we measured a mean of $1.5\times10^4$ and $2.5\times10^2$ bacteria per mouse in the blood of NLRP3-knockout and Pak1-knockout mice, respectively (Fig. 5e,f). The smaller effect observed in Pak1-knockout mice compared with NLRP3-knockout mice could be explained by the redundancy observed between Pak1 and Pak2 at the cellular level. The difference in the clearance of CNF1-expressing *E. coli* measured at 48 h between WT and NLRP3-knockout mice was still observable at later time points and was not observed when mice were infected with the isogenic *E. coli* CNF1-knockout strain, indicating the specificity of the CNF1 response towards the NLRP3 pathway in vivo (Extended Data Fig. 10b,c). Furthermore, we measured a similar trend in the clearance of the CNF1-expressing *E. coli* strain in WT and GSDMD-knockout mice (Extended Data Fig. 10d). We next monitored the bacterial burden in mice that were infected with CNF1-expressing *E. coli* and treated with AZ13711265, MCC950 or both. We observed no differences in the bacterial clearance between the three groups (Fig. 5d). NLRP3-knockout mice that were injected with vehicle or with AZ13711265 demonstrated no differences in bacterial clearance, suggesting that Pak1 and NLRP3 act within the same signalling pathway during bacteraemia (Fig. 5g). Together, these results unravel the critical role of Pak1 and NLRP3 in the clearance of CNF1-expressing bacteria and their importance in the innate immune response during bacteraemia.

## Discussion

Our results shed light on a regulatory mechanism for NLRP3 after the activation of Rac2 by the bacterial toxin CNF1. The level of NLRP3 inflammasome activation is correlated with the strength of the interaction between activated Rac2 and Pak1-RBD, indicating that the innate immune system can adapt its response to the level of Rac2 activity. This seems to be an elegant strategy to deliver a commensurate response to the level of CNF1 toxin activity. Notably, the phosphorylated peptide containing Thr 659 of human NLRP3 isolated by mass spectrometry is highly conserved between species, and the Pak–NLRP3 axis is conserved in human macrophages and is involved in the nigericin-triggered NLRP3 inflammasome activation. Complementary studies will be necessary to determine the precise molecular mechanism in other species or in other contexts as well as to determine whether the phosphorylation of NLRP3 at Thr 659 is a consensus site used by other kinases. Nevertheless, our results show that phosphorylation of NLRP3 at Thr 659 is important for NLRP3 inflammasome activation and suggest that it is implicated in NLRP3-related inflammatory disorders or susceptibility to infection.

Our results suggest that there is redundancy between Pak1 and Pak2, as shown by a partial compensation by Pak2 in Pak1-knockout macrophages and mice. Further studies are required to clarify the importance of each of the group-1 Pak proteins in the activation of the NLRP3 inflammasome. Unfortunately, the Pak2-knockout mutations in mice are embryonically lethal (at embryonic day 8.0) and these studies would require the generation of conditional transgenic mice[31].

We unravelled a CNF1-triggered secretion of IL-1β that is not linked to an increase in cell death and is independent of GSDMD. Studies of NLRP3 inflammasome canonical triggers have demonstrated different IL-1β secretion scenarios. In the conventional scenario, caspase-1 cleaves the inflammasome-related cytokines and GSDMD to generate active N-GSDMD[32,33]. N-GSDMD relocates in the plasma membrane to form pores, enabling IL-1β secretion[32,33]. GSDMD pores are associated with pyroptosis in the case of classical inflammasome activation or are controlled during inflammasome hyperactivation, leading to secretion without pyroptosis[34–36]. The CNF1-triggered IL-1β secretion seems to fall into another category, independent of both GSDMD cleavage and cell death, that may share similarities with the unconventional IL-1β secretion[37]. This unconventional secretion relies on the affinity of IL-1β to the plasma membrane ruffles that are characteristic of the CNF1-triggered Rac GTPase activation. The mechanism explaining how CNF1 triggered caspase-1 activation without GSDMD cleavage remains to be elucidated and may be unique to toxins activating Rho GTPases. One hypothesis is that the activation of Rac2, in parallel to the

**Fig. 5 | Pak1 and NLRP3 control the burden of CNF1-expressing *E. coli* during bacteraemia. a**, BMDMs isolated from C57BL/6 mice were pretreated for 45 min with 1 μM MCC950 or 5 μM IPA-3 and were infected or not (multiplicity of infection (m.o.i.) = 5) with either *E. coli*$^{CNF1+}$ or isogenic CNF1-deleted mutant *E. coli*$^{CNF1-}$. Supernatants and cell lysates were analysed using immunoblotting. **b**,**c**, BMDMs isolated from C57BL/6 or C57BL/6 NLRP3-knockout mice (**b**) or iBMDMs expressing NLRP3 or NLRP3$^{T659A}$ (**c**) were infected (m.o.i. = 5) with *E. coli*$^{CNF1+}$. The supernatants were analysed using ELISA. $n = 4$ biologically independent samples per group. Data are mean ± s.e.m. Statistical analyses were performed using two-tailed unpaired Student's *t*-tests. **d**–**g**, Mice were intravenously infected with $10^7$ colony-forming units (c.f.u.) of *E. coli*$^{CNF1+}$, before collecting peripheral blood at 4 h, 24 h and 48 h for the measurement of bacteraemia. **d**, C57BL/6J mice were injected intraperitoneally with vehicle, or with 50 mg kg$^{-1}$ MCC950 ($n = 10$ mice), 10 mg kg$^{-1}$ AZ13711265 ($n = 10$ mice) or both once a day ($n = 9$ mice). $^{**}P < 0.01$ (each individual inhibitor-treated group compared with the group injected with vehicle). **e**, WT ($n = 7$ mice) or NLRP3-knockout C57BL/6J mice ($n = 6$ mice) were analysed. $^{***}P < 0.001$. **f**, WT ($n = 4$ mice) or Pak1-knockout C57BL/6J mice were analysed ($n = 4$ mice). $^{*}P < 0.05$. **g**, NLRP3-knockout C57BL/6J mice were injected intraperitoneally with 10 mg kg$^{-1}$ AZ13711265 ($n = 7$ mice) or vehicle ($n = 9$ mice) once each day. Experiments were repeated at least two times, and representative data are shown. Data are the geometric mean ± 95% confidence interval. Statistical analyses were performed using two-tailed nonparametric Mann–Whitney *U*-tests. $^{*}P < 0.05$, $^{**}P < 0.01$, $^{***}P < 0.001$.

Pak1–NLRP3 pathway activation, inhibits the cleavage of GSDMD. Similar to *Toxoplasma gondii*, the NF-κB activation triggered by Rac2 might be another mechanism explaining the IL-1β secretion independent of cell death and GSDMD[38]. Rac2 signalling may also regulate a potassium channel explaining the inhibition by KCl of the CNF1-triggered IL-1β secretion. Favouring this hypothesis, Rac GTPases have been found to modulate Kir2.1, a Kir-family potassium channel[39].

Our study shows that NLRP3 is a major sensor of toxins that activate Rho GTPases, whereas previous research has shown the sensing of Rho-GTPase-inactivating toxins by Pyrin[12]. These studies highlight that the mammalian innate immune system has evolved strategies that share similarities with the effector-triggered immunity to detect abnormal activation of Rho GTPases[3,40,41]. Interestingly, both inactivation of RhoA and activation of Rac2 by bacterial toxins are monitored by Pyrin and NLRP3, respectively. More precisely,

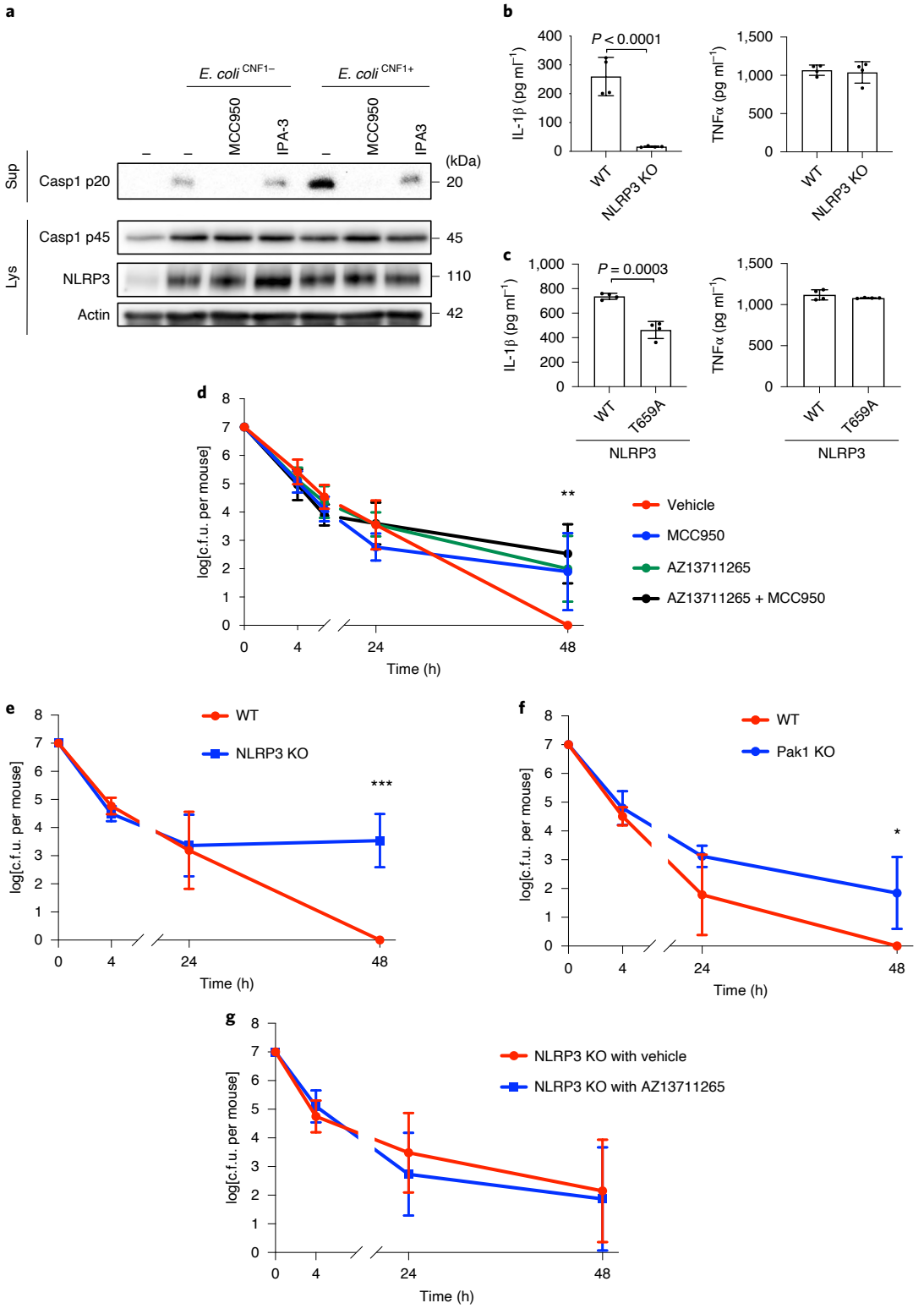

here we show that Rac GTPases that activate bacterial factors are sensed by NLRP3 independently of the type of modification made. Similarly, bacterial factors that inactivate RhoA activate Pyrin independently of the type of modifications[12,42,43]. These results suggest that the host guarding of Rho GTPase signalling integrity relies on two sensors that monitor the abnormal Rho GTPase cycling rather than toxin-triggered post-translational modifications of host proteins or virulence factor enzymatic activities. Interestingly, both Pyrin and NLRP3 require regulation by the serine–threonine kinases PKN1/2 and Pak1/2, respectively. The fact that two different inflammasomes have been evolutionarily selected to detect bacterial toxins that modify Rho GTPases highlights the importance of Rho GTPases in innate immunity.

Further studies are necessary to determine the in vivo conservation of the Pak–NLRP3 axis and whether the sensing of other Rho-GTPase-activating virulence factors by the NLRP3 inflammasome impacts the bacterial burden during infection. Similarly, we expect that further studies will determine the importance of other inflammasomes in detecting bacterial virulence factors that are endowed with enzymatic activities.

Our results reveal the importance of Pak1 and NLRP3 in controlling the bacterial burden during bacteraemia in mice. Even though further studies will be required to determine the role of the Pak–NLRP3 signalling axis in patients with bacteraemia, our results showing an increase in bacterial burden in MCC950-treated mice suggest that caution will be necessary for the use of NLRP3 inhibitors in the clinical setting. This is consistent with clinical data showing that there is an increased risk of infections associated with IL-1 signalling inhibition[44,45]. One option would be to consider combining inflammasome inhibitors with antibiotherapies or with an enhanced surveillance for a potential for bacteraemia risk.

## Methods

**Ethics statement.** This study was carried out in strict accordance with the guidelines of the Council of the European Union (Directive 86/609/EEC) regarding the protection of animals used for experimental and other scientific purposes. The protocol was approved by the Institutional Animal Care and Use Committee on the Ethics of Animal Experiments of Nice, France (APAFIS#18322-20181218099427035 v2 and APAFIS#24906-2020031614223228 v2).

**Bacterial strains and toxins.** The *E. coli* UTI89 clinical isolate was originally obtained from a patient with cystitis[46] and the isogenic UTI89 CNF1$^{+}$ (*E. coli*$^{CNF1+}$) or UTI89 CNF1$^{-}$ (*E. coli*$^{CNF1-}$) streptomycin-resistant strain generation and culture conditions were previously described[11]. For the infections, a 1/100 dilution of an overnight culture was inoculated and grown up to an optical density at 600 nm of 1.2 using a Luria–Bertani (LB) medium supplemented with streptomycin (200 μg ml$^{-1}$). Bacteria were collected by centrifugation and washed twice in PBS before dilution in PBS to obtain the desired bacterial concentrations for the mouse infection experiments. Recombinant WT CNF1 and its catalytically inactive form (CNF1$^{C866S}$) were produced and purified as previously reported[47,48]. The recombinant DNT toxin was purified from pQEDNTwt using the same protocol[49]. The recombinant proteins were passed through a polymyxin B column (Affinity Detoxi-Gel, Pierce). The removal of endotoxin was verified using a colorimetric limulus amebocyte lysate (LAL) assay (LAL QCL-1000, Cambrex). Each stock of the CNF1 preparation (2 mg ml$^{-1}$) was shown to contain less than 0.5 endotoxin units per ml. Plasmid expressing the virulence factor pCMV-SopE-HA was previously reported[22] and SopE expression was stabilized by adding MG132 (10 μM) to the cells to block its proteasomal degradation as previously described[50]. Plasmids expressing the pRK5-Myc-DNT were obtained by PCR amplification of pQEDNTwt, and pCMV-HA-YopE was obtained by PCR amplification and subcloning from pACY184-YopE-GSK (gift from I. Brodsky). All of the plasmids were verified by sequencing (Eurofins).

**Cell culture, transfection and inhibitors.** HEK293T cells were obtained from ATCC (CRL-3216) and maintained according to the ATCC instructions. BMDMs were extracted from the femurs of BALB/c, C57BL/6J, C57BL/6J knockin or C57BL/6J knockout mice (aged 6–10 weeks) as indicated in the legends and were cultured in RPMI GlutaMax medium (Life Technologies) supplemented with 100 ng ml$^{-1}$ M-CSF (premium grade, Miltenyi Biotec), 10% heat-inactivated FBS (Biowest) and 50 μg ml$^{-1}$ gentamycin (Life Technologies) at 37 °C in an atmosphere containing 5% $CO_2$. The cells were seeded at a concentration of $10^6$ cells per well in a six-well plate. After 6 d of differentiation, BMDMs were used for experiments. HEK293T cells were transfected with plasmids using Lipofectamine 2000 (Life Technologies) according to the manufacturer's instructions. siRNAs were transfected in BMDMs for 72 h using Lipofectamine RNAiMAX Reagent (Thermo Fisher Scientific) according to the manufacturer's instructions. Cells were transfected as indicated in the figure legends with siRNAs (Dharmacon) targeting *Nlrp3* (L-053455-00), *Rac1* (L-041170-00), *Rac2* (L-041171-01), *Nek7* (J-063266-09), *Pak1* (L-048101-00), *Pak2* (L-040615-00) or non-targeting control siRNA (D-001810-10). For the siRNA screen, the BMDMs were transfected with siRNA (Dharmacon) targeting *Nod1* (L-055182-00), *Nod2* (L-052735-00), *Nlrc3* (L-052823-01), *Nlrc4* (L-055000-00), *Nlrc5* (L-067620-01), *Nlrx1* (L-057712-01), *Ciita* (L-043166-02), *Naip1* (L-047682-00), *Naip2* (L-044151-01), *Naip5* (L-044142-01), *Naip6* (L-044145-01), *Naip7* (L-065757-00), *Nlrp1a* (L-066229-00), *Nlrp1b* (L-161107-01), *Nlrp2* (L-053528-01), *Nlrp3* (L-053455-01), *Nlrp4a* (L-052395-01), *Nlrp4b* (L-058181-01), *Nlrp4c* (L-049416-01), *Nlrp4d* (L-067051-01), *Nlrp4e* (L-068064-01), *Nlrp4f* (L-052668-01), *Nlrp4g* (L-066364-01), *Nlrp5* (L-045315-01), *Nlrp6* (L-066157-01), *Nlrp9a* (L-058269-01), *Nlrp9b* (L-066417-01), *Nlrp9c* (L-057344-01), *Nlrp10* (L-056559-01), *Nlrp12* (L-060234-01), *Nlrp14* (L-066093-01), *Pycard* (L-051439-01), *Mefv* (L-048693-01) and *Aim2* (L-044968-01). BMDMs were pretreated with the following inhibitors for 45 min: 1 μM CP-456773 or MCC950 (Sigma-Aldrich), 5 μM IPA-3 (Tocris), 1 μM FRAX597 (Tocris) or the indicated concentration of AZ13711265 (AGV Discovery) in 2% FBS containing RPMI followed by the addition of CNF1 500 ng ml$^{-1}$ and/or ultrapure LPS 100 ng ml$^{-1}$ (Invivogen) as indicated in the figure legends. Cells treated with nigericin 5 μM (Invivogen) or ATP 5 mM (Invivogen) for 30 min were used as positive control for NLRP3 inflammasome activation. For $K^+$-efflux-preventing experiments, BMDMs were treated with 10 mM, 20 mM or 40 mM KCl. Primary macrophages were infected with *E. coli*$^{CNF1+}$ or the isogenic *E. coli*$^{CNF1-}$ (m.o.i. = 5) for 16 h. Immortalized NLRP3-knockout BMDMs were stably complemented with pINDUCER21 plasmids encoding human NLPR3 WT or NLRP3$^{T659A}$ under a doxycycline-inducible promoter as previously described[51]. NLRP3 expression was induced by adding 2 μg ml$^{-1}$ doxycycline for 16 h (Takara Bio). All of the cell lines were authenticated using PCR assays with species-specific primers. Mycoplasma testing was negative.

**Mouse model of infection.** Female C57BL/6J mice (aged 7 weeks; Charles River Laboratory) were injected intraperitoneally with MCC950 (Sigma-Aldrich) at 50 mg kg$^{-1}$ every 24 h or AZ13711265 (AGV Discovery) at 10 mg kg$^{-1}$ every 24 h or both. NLRP3-knockout mice were provided by V. Petrilli and were described previously[52]. The Pak1-knockout, GSDMD-knockout and ASC–citrine-knockin mice used in this study were reported previously[17,32,53]. Female NLRP3-knockout or Pak1-knockout and female congenic WT C57BL/6J littermate mice were injected intravenously with $10^7$ colony-forming units of *E. coli* and the determination of bacteraemia was monitored as previously described[11]. Mice were housed with their littermates and kept under a regular 12 h–12 h light–dark cycle at room temperature (20–25 °C) and a relative humidity of 50–70%. Food and water were available ad libitum. Experiments were performed under pathogen-free conditions with randomly chosen animals (same sex, matched by age and body weight). Investigators were blinded for in vivo experiments. Sample size was determined on the basis of our previous research[11] and using G*Power software.

**Reconstituted NLRP3 inflammasome in HEK293T cells.** HEK293T cells were transfected with plasmids encoding the NLRP3 inflammasome components as previously described[21,28]. HEK293T cells were transfected with plasmids encoding Myc–NLRP3 or NLRP3 mutants, ASC–GFP, mpro-caspase1 and pro-IL-1β–Flag. Where indicated in the legend, cells were cotransfected with HA–Rac2, the constitutively active mutant of Rac2 mimicking CNF1-induced deamidation Rac2$^{Q61E}$, Rac2$^{Q61L}$, Rac2$^{G12V}$ or Rac2$^{T17N}$, a dominant negative mutant of Rac2 for 16 h. The monitoring of caspase-1 or IL-1β cleavage was performed using supernatant immunoblotting.

**Immunoprecipitation.** HEK293T cells were transfected with plasmids encoding Myc–NLRP3, Myc–NLRP3$^{S163A\,S198A\,T659A}$, Myc–NLRP3$^{S163A}$ and Myc–NLRP3$^{T659A}$, GFP–NLRP3, Myc–Pak1$^{T423E}$ and HA–Rac2$^{Q61E}$, or NLRP3 expression was induced by adding 2 μg ml$^{-1}$ doxycycline for 16 h to iBMDMs stably expressing NLPR3 or NLRP3$^{T659A}$. Cells were lysed and processed for immunoprecipitation using 2 μg of anti-Myc or 3 μg of anti-Nek7 antibodies according to previously described conditions[54]. The expression of NLRP3 and endogenous levels of Nek7 were monitored in the cell lysate as well as in the immunoprecipitated fraction.

**LDH release.** The supernatant of stimulated macrophages was collected and centrifuged at 300*g* for 5 min to remove cellular debris. LDH measurement was performed using the LDH Cytotoxicity Assay Kit (Thermo Fisher Scientific) according to the manufacturer's instructions, in samples diluted 1:5 in PBS. Data were plotted as the percentage of LDH release considering a Triton X-100 treated well as 100%.

**Cell permeabilization kinetics.** BMDMs were plated and stimulated in a 96-well plate in medium containing propidium iodide (0.1 μg ml$^{-1}$) and data were acquired with a ×10 objective using the IncuCyte Zoom system v.6.2.9200.0

(Essen BioScience) under a $CO_2$- and temperature-controlled environment. Each condition was run in quadruplicate. The number of fluorescent objects was counted using Incucyte Zoom (Essen BioScience).

**In vitro kinase assay.** Recombinant purified Pak1 (500 ng) was incubated with 1 µg of recombinant human NLRP3 protein (Abcam, ab165022), and with 50 µM ATP and 4 µCi of [γ 32 P]ATP in kinase buffer (50 mM HEPES pH 7.3, 50 mM NaCl, 0.05% Triton X-100, 10 mM β-glycerophosphate, 5 mM NaF, 10 mM $MgCl_2$ and 0.2 mM $MnCl_2$) at 30 °C for 30 min in a final volume of 39 µl. The reaction was stopped by adding 15 µl of LDS (Thermo Fisher Scientific) and 6 µl of dithiothreitol 500 mM. Samples were analysed by electrophoresis using Bolt 4–12% Bis-Tris Plus gels (Thermo Fisher Scientific) followed by Coomassie blue staining and autoradiography.

**Immunofluorescence staining, antibodies and ELISA assays.** Caspase-1 activation was detected using the fluorescent probe FAM-FLICA (ImmunoChemistry Technologies) after 6 h of treatment, according to the manufacturer's instructions. After labelling, cells were fixed in 4% paraformaldehyde for 15 min, PFA was neutralized with 50 mM $NH_4Cl$ for 15 min, cells were permeabilized with 0.5% Triton X-100 for 5 min and blocked with 2% TBS-BSA. Cells were incubated with mouse anti-NLRP3 (clone Cryo-2, Adipogen) and/or rabbit anti-ASC (AG-25B-0006, Adipogen) or rabbit anti-phosphorylated-Pak (ab40795, Abcam) antibodies for 1 h followed by incubation with the secondary antibodies TexasRed anti-mouse IgG (TI-2000, Vector Laboratories) or Cy5 anti-mouse IgG (715-175-151, Jackson Immunoresearch) and/or TexasRed anti-rabbit IgG (711-075-152, Jackson Immunoresearch) and/or phalloidin Alexa Fluor 647 (ab176759, Abcam) and Hoechst 33342 (H1399, Thermo Fisher Scientific) for 30 min. Cells were imaged using a Nikon A1R confocal microscope. The following antibodies were used in this study: rabbit anti-IL-1β (GTX74034, Genetex), mouse anti-caspase-1 (clone Casper-1, Adipogen), mouse anti-Rac (clone 102/Rac1, BD Biosciences), goat anti-Rac2 (ab2244, Abcam), mouse anti-NLRP3 (clone Cryo-2, Adipogen), rabbit anti-Nek7 (ab133514, Abcam), rabbit anti-Pak1 (2602, CST), rabbit anti-Pak2 (2608, CST), rabbit monoclonal anti-GSDMD (ab209845), mouse anti-β-actin (AC-74, Sigma-Aldrich), mouse anti-Myc (9E10, Roche), mouse anti-HA (16B12, Covance), mouse anti-Flag (clone M2, Sigma-Aldrich), mouse anti-GFP (clone 7.1, 13.1, Roche). Cytokine secretion was determined by ELISA using the mouse Quantikine ELISA kits for mouse IL-6, IL-18, TNF-α and IL-1β (R&D Systems) according to the manufacturer's instructions.

**Flow cytometry analysis.** BMDMs isolated from C57BL/6J mice constitutively expressing ASC–citrine fusion protein (R26-CAG-ASC-citrine) were treated with LPS (100 ng ml$^{-1}$) for 16 h before 6 h of treatment with vehicle or CNF1 (500 ng ml$^{-1}$) or 30 min with nigericin (5 µM). Cells were collected and analysed by flow cytometry using a BD FACSCanto II cytometer (BD Biosciences). Cytometry data were analysed using FlowJo v.10.6.2. Doublets were excluded using a side scatter (SSC)-A (area) and SSC-H (height) plot; cells with a high expression of ASC–citrine were gated and then analysed for ASC–citrine signal area (ASC–citrine-A) and ASC–citrine signal height (ASC–citrine-H). Cells with ASC specks were defined with a higher ASC-H:ASC-A ratio.

**Statistical analyses.** Statistical analyses were performed using GraphPad Prism v.8.2.1. Comparisons of the bacterial load of mice were performed using nonparametric Mann–Whitney *U*-tests. Statistical analyses of FAM-FLICA$^+$ cells, cytokine secretion and LDH release were performed using unpaired two-tailed Student's *t*-tests.

**Reporting Summary.** Further information on research design is available in the Nature Research Reporting Summary linked to this article.

## Data availability

All data supporting the findings of this study are available within the Article and its Supplementary Information or from the corresponding author on reasonable request. Source data are provided with this paper.

Received: 21 August 2019; Accepted: 13 November 2020;

## References


1. Martin, G. S., Mannino, D. M., Eaton, S. & Moss, M. The epidemiology of sepsis in the United States from 1979 through 2000. *N. Engl. J. Med.* **348**, 1546–1554 (2003).
2. Vance, R. E., Isberg, R. R. & Portnoy, D. A. Patterns of pathogenesis: discrimination of pathogenic and nonpathogenic microbes by the innate immune system. *Cell Host Microbe* **6**, 10–21 (2009).
3. Stuart, L. M., Paquette, N. & Boyer, L. Effector-triggered versus pattern-triggered immunity: how animals sense pathogens. *Nat. Rev. Immunol.* **13**, 199–206 (2013).
4. Flatau, G. et al. Toxin-induced activation of the G protein p21 Rho by deamidation of glutamine. *Nature* **387**, 729–733 (1997).
5. Schmidt, G. et al. Gln 63 of Rho is deamidated by *Escherichia coli* cytotoxic necrotizing factor-1. *Nature* **387**, 725–729 (1997).
6. Aktories, K. & Barbieri, J. Bacterial cytotoxins: targeting eukaryotic switches. *Nat. Rev. Microbiol.* **3**, 397–410 (2005).
7. Galán, J. E. Common themes in the design and function of bacterial effectors. *Cell Host Microbe* **5**, 571–579 (2009).
8. Bruno, V. M. et al. *Salmonella* Typhimurium type III secretion effectors stimulate innate immune responses in cultured epithelial cells. *PLoS Pathog.* **5**, e1000538 (2009).
9. Munro, P. et al. Activation and proteasomal degradation of Rho GTPases by cytotoxic necrotizing factor-1 elicit a controlled inflammatory response. *J. Biol. Chem.* **279**, 35849–35857 (2004).
10. Boquet, P. & Lemichez, E. Bacterial virulence factors targeting Rho GTPases: parasitism or symbiosis? *Trends Cell Biol.* **13**, 238–246 (2003).
11. Diabate, M. et al. *Escherichia coli* α-hemolysin counteracts the anti-virulence innate immune response triggered by the Rho GTPase activating toxin CNF1 during bacteremia. *PLoS Pathog.* **11**, e1004732 (2015).
12. Xu, H. et al. Innate immune sensing of bacterial modifications of Rho GTPases by the pyrin inflammasome. *Nature* **513**, 237–241 (2014).
13. Groslambert, M. & Py, B. F. Spotlight on the NLRP3 inflammasome pathway. *J. Inflamm. Res.* **11**, 359–374 (2018).
14. Yang, Y., Wang, H., Kouadir, M., Song, H. & Shi, F. Recent advances in the mechanisms of NLRP3 inflammasome activation and its inhibitors. *Cell Death Dis.* **10**, 128 (2019).
15. Gao, W., Yang, J., Liu, W., Wang, Y. & Shao, F. Site-specific phosphorylation and microtubule dynamics control pyrin inflammasome activation. *Proc. Natl Acad. Sci. USA* **113**, E4857–E4866 (2016).
16. Park, Y. H., Wood, G., Kastner, D. L. & Chae, J. J. Pyrin inflammasome activation and RhoA signaling in the autoinflammatory diseases FMF and HIDS. *Nat. Immunol.* **17**, 914–921 (2016).
17. Tzeng, T. C. et al. A fluorescent reporter mouse for inflammasome assembly demonstrates an important role for cell-bound and free ASC specks during in vivo Infection. *Cell Rep.* **16**, 571–582 (2016).
18. Sester, D. P. et al. Assessment of inflammasome formation by flow cytometry. *Curr. Protoc. Immunol.* **114**, 14.40.1–14.40.29 (2016).
19. Lamkanfi, M. & Dixit, V. M. In retrospect: the inflammasome turns 15. *Nature* **548**, 534–535 (2017).
20. He, Y., Hara, H. & Núñez, G. Mechanism and regulation of NLRP3 inflammasome activation. *Trends Biochem. Sci.* **41**, 1012–1021 (2016).
21. Shi, H., Murray, A. & Beutler, B. Reconstruction of the mouse inflammasome system in HEK293T cells. *Bio. Protoc.* **6**, e1986 (2016).
22. Keestra, A. M. et al. Manipulation of small Rho GTPases is a pathogen-induced process detected by NOD1. *Nature* **496**, 233–237 (2013).
23. Doye, A. et al. CNF1 exploits the ubiquitin-proteasome machinery to restrict Rho GTPase activation for bacterial host cell invasion. *Cell* **111**, 553–564 (2002).
24. Boyer, L. et al. Pathogen-derived effectors trigger protective immunity via activation of the Rac2 enzyme and the IMD or Rip kinase signaling pathway. *Immunity* **35**, 536–549 (2011).
25. Manser, E., Leung, T., Salihuddin, H., Zhao, Z. S. & Lim, L. A brain serine/threonine protein kinase activated by Cdc42 and Rac1. *Nature* **367**, 40–46 (1994).
26. Wells, C. M. & Jones, G. E. The emerging importance of group II PAKs. *Biochem. J.* **425**, 465–473 (2010).
27. Semenova, G. & Chernoff, J. Targeting PAK1. *Biochem. Soc. Trans.* **45**, 79–88 (2017).
28. Song, N. et al. NLRP3 phosphorylation is an essential priming event for inflammasome activation. *Mol. Cell* **68**, 185–197 (2017).
29. Sharif, H. et al. Structural mechanism for NEK7-licensed activation of NLRP3 inflammasome. *Nature* **570**, 338–343 (2019).
30. Coll, R. C. et al. A small-molecule inhibitor of the NLRP3 inflammasome for the treatment of inflammatory diseases. *Nat. Med.* **21**, 248–255 (2015).
31. Kelly, M. L. & Chernoff, J. Mouse models of PAK function. *Cell Logist.* **2**, 84–88 (2012).
32. Shi, J. et al. Cleavage of GSDMD by inflammatory caspases determines pyroptotic cell death. *Nature* **526**, 660–665 (2015).
33. He, W. T. et al. Gasdermin D is an executor of pyroptosis and required for interleukin-1β secretion. *Cell Res.* **25**, 1285–1298 (2015).
34. Broz, P., Pelegrín, P. & Shao, F. The gasdermins, a protein family executing cell death and inflammation. *Nat. Rev. Immunol.* **20**, 143–157 (2020).
35. Rühl, S. et al. ESCRT-dependent membrane repair negatively regulates pyroptosis downstream of GSDMD activation. *Science* **362**, 956–960 (2018).
36. Evavold, C. L. et al. The pore-forming protein gasdermin D regulates interleukin-1 secretion from living macrophages. *Immunity* **48**, 35–44 (2018).
37. Monteleone, M. et al. Interleukin-1β maturation triggers its relocation to the plasma membrane for gasdermin-D-dependent and -independent secretion. *Cell Rep.* **24**, 1425–1433 (2018).

38. Pandori, W. J. et al. *Toxoplasma gondii* activates a Syk-CARD9-NF-κB signaling axis and gasdermin D-independent release of IL-1β during infection of primary human monocytes. *PLoS Pathog.* **15**, e1007923 (2019).
39. Muessel, M. J., Harry, G. J., Armstrong, D. L. & Storey, N. M. SDF-1α and LPA modulate microglia potassium channels through rho GTPases to regulate cell morphology. *Glia* **61**, 1620–1628 (2013).
40. Jones, J. D. & Dangl, J. L. The plant immune system. *Nature* **444**, 323–329 (2006).
41. Lopes Fischer, N., Naseer, N., Shin, S. & Brodsky, I. E. Effector-triggered immunity and pathogen sensing in metazoans. *Nat. Microbiol.* **5**, 14–26 (2020).
42. Aubert, D. F. et al. A *Burkholderia* type VI effector deamidates Rho GTPases to activate the pyrin inflammasome and trigger inflammation. *Cell Host Microbe* **19**, 664–674 (2016).
43. Medici, N. P., Rashid, M. & Bliska, J. B. Characterization of pyrin dephosphorylation and inflammasome activation in macrophages as triggered by the yersinia effectors YopE and YopT. *Infect. Immun.* **87**, e00822-18 (2019).
44. Cabral, V. P., Andrade, C. A., Passos, S. R., Martins, M. F. & Hökerberg, Y. H. Severe infection in patients with rheumatoid arthritis taking anakinra, rituximab, or abatacept: a systematic review of observational studies. *Rev. Bras. Reumatol. Engl. Ed.* **56**, 543–550 (2016).
45. Ridker, P. M. et al. Antiinflammatory therapy with canakinumab for atherosclerotic disease. *N. Engl. J. Med.* **377**, 1119–1131 (2017).
46. Mulvey, M. A., Schilling, J. D. & Hultgren, S. J. Establishment of a persistent *Escherichia coli* reservoir during the acute phase of a bladder infection. *Infect. Immun.* **69**, 4572–4579 (2001).
47. Buetow, L., Flatau, G., Chiu, K., Boquet, P. & Ghosh, P. Structure of the Rho-activating domain of *Escherichia coli* cytotoxic necrotizing factor 1. *Nat. Struct. Biol.* **8**, 584–588 (2001).
48. Doye, A., Boyer, L., Mettouchi, A. & Lemichez, E. Ubiquitin-mediated proteasomal degradation of Rho proteins by the CNF1 toxin. *Methods Enzymol.* **406**, 447–456 (2006).
49. Matsuzawa, T., Kashimoto, T., Katahira, J. & Horiguchi, Y. Identification of a receptor-binding domain of *Bordetella* dermonecrotic toxin. *Infect. Immun.* **70**, 3427–3432 (2002).
50. Kubori, T. & Galán, J. E. Temporal regulation of salmonella virulence effector function by proteasome-dependent protein degradation. *Cell* **115**, 333–342 (2003).
51. Lagrange, B. et al. Human caspase-4 detects tetra-acylated LPS and cytosolic *Francisella* and functions differently from murine caspase-11. *Nat. Commun.* **9**, 242 (2018).
52. Martinon, F., Pétrilli, V., Mayor, A., Tardivel, A. & Tschopp, J. Gout-associated uric acid crystals activate the NALP3 inflammasome. *Nature* **440**, 237–241 (2006).
53. McDaniel, A. S. et al. *Pak1* regulates multiple c-Kit mediated Ras-MAPK gain-in-function phenotypes in *Nf1*$^{+/-}$ mast cells. *Blood* **112**, 4646–4654 (2008).
54. Stutz, A. et al. NLRP3 inflammasome assembly is regulated by phosphorylation of the pyrin domain. *J. Exp. Med.* **214**, 1725–1736 (2017).


## Acknowledgements

We thank P. Auberger, A. Baumler, I. Brodsky, J. Chernoff, D. Golenbock, T. Henry, M. Keestra-Gounder, E. Lemichez, E. Manser, E. Meunier, V. Petrilli, D. Pisani, J.-E. Ricci, G. Robert, P.-M. Roger, L. Stuart, P. Vandenabeele, S. Ivanov and L. Yvan-Charvet for sharing materials or discussions; A.-S. Dufour, E. Garcia, M. Irondelle and J. Murdaca for technical assistance; members of the Innate Sensors Community (InnaSCo) for sharing tools; A. Cuttriss and staff at the Office of International Scientific Visibility of Université Côte d'Azur for professional language editing; staff at the Etablissement Français du Sang of Marseille for providing human blood from human healthy donors; and staff at the C3M facilities (animal, genomic, cytometry and imaging) and the Harvard Taplin mass spectrometry core. The mouse strain used for this research project, B6.129S2-Pak1tm1Cher/Mmnc (RRID, MMRRC_031838-UNC) was obtained from the Mutant Mouse Resource and Research Center (MMRRC) at University of North Carolina at Chapel Hill, an NIH-funded strain repository, and was donated to the MMRRC by J. Chernoff, Fox Chase Cancer Center. This work was supported by grants from the ANR (ANR-17-CE15-0001), Investments for the Future programs LABEX SIGNALIFE ANR-11-LABX-0028-01, IDEX UCA$^{JEDI}$ ANR-15-IDEX-01, ARC (RAC15014AAA), Université Côte d'Azur, Infectiopole sud and REDPIT. B.F.P. is supported by ERC (ERC-2013-CoG_616986). A.M. is supported by a fellowship from FRM; C.T. by a fellowship from Ville de Nice; and O.D. by a fellowship from INSERM and Université Côte d'Azur.

## Author contributions

O.D. and A.D. designed, performed and analysed most of the experiments with input from C.T., C.L., A.J., A.G., A.M., P.C., A.R. and S.M.; J.C. and R.R. provided advice on the mice infection model. E.V., R.R.G., D.C., B.F.P., A.R., P.H.V.S. and M.L. provided tools and advice on NLRP3 inflammasome regulation. P.M. generated NLRP3 mutants and, with G.M. and O.D., performed and analysed most of the in vivo experiments. O.V. performed virulence factor and toxin subcloning, protein purifications, the in vitro kinase assay and analysed the mass spectrometry results. L.B. conceived the project, designed experiments and wrote the manuscript.

## Competing interests

The authors declare no competing interests.

## Additional information

**Extended data** is available for this paper at https://doi.org/10.1038/s41564-020-00832-5.

**Supplementary information** is available for this paper at https://doi.org/10.1038/s41564-020-00832-5.

**Correspondence and requests for materials** should be addressed to L.B.

**Peer review information** *Nature Microbiology* thanks Igor Brodsky, Gad Frankel and the other, anonymous, reviewer(s) for their contribution to the peer review of this work.

**Reprints and permissions information** is available at www.nature.com/reprints.

**Publisher's note** Springer Nature remains neutral with regard to jurisdictional claims in published maps and institutional affiliations.

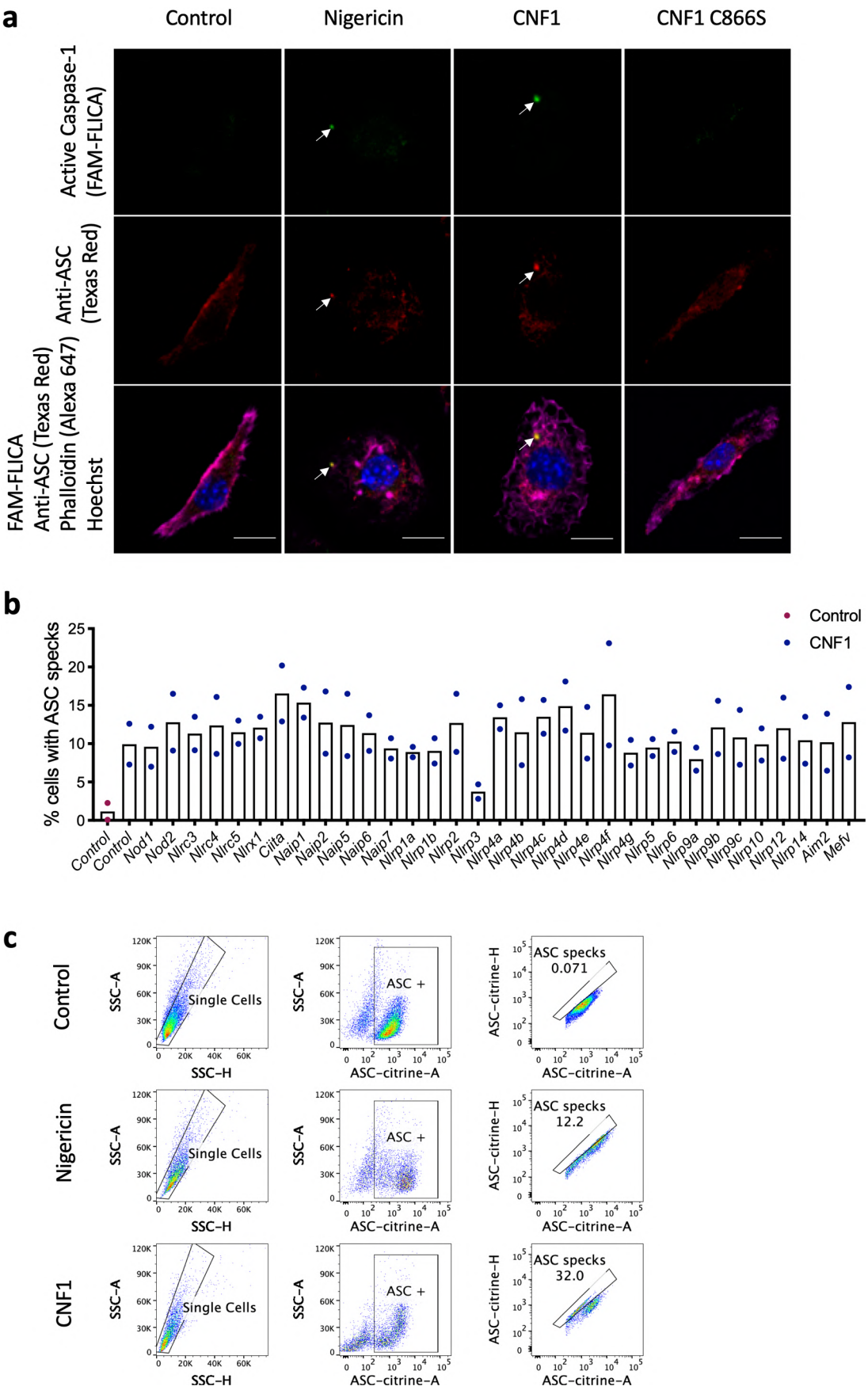


**Extended Data Fig. 1 | See next page for caption.**

**Extended Data Fig. 1 | CNF1 triggers Caspase-1 activation and ASC specks formation. a**, BMDMs isolated from BALB/c mice were either treated with vehicle (control) or CNF1 (500 ng $ml^{-1}$), inactive catalytic mutant CNF1 C866S (500 ng/mL) for 6 h, or Nigericin (5 µM) for 30 min. Active Caspase-1 was revealed with FAM-FLICA (green), ASC was stained using an anti-ASC antibody (Texas Red), nuclei and actin filament were stained with Hoechst and phalloidin-Alexa 647 respectively. Cells were analyzed by confocal microscopy. Arrows indicates FAM-FLICA dots that colocalize with the ASC staining. Scale bar: 10µm. **b**, BMDM isolated from C57BL/6 J mice constitutively expressing ASC-citrine fusion protein (R26-CAG-ASC-citrine) were transfected with the indicated siRNA for 72 h prior to 6 h of CNF1 treatment (500 ng/mL) or treated with vehicle (control). Percent of cells with ASC specks. Data are expressed as the mean ± SEM. Each dot represents $10^5$ cells (n = 2 biologically independent samples). **c**, BMDM isolated from C57BL/6 J mice constitutively expressing ASC-citrine fusion protein (R26-CAG-ASC-citrine) were treated 6 h with CNF1 (500 ng/mL) or Nigericin (5 µM) for 30 min or vehicle (control). Cells were analyzed for ASC speck formation by flow cytometry as indicated, doublets were excluded using SSC-A and SSC-H plot, cells with a high expression of ASC-citrine were gated and then analyzed for ASC-citrine area (ASC-citrine-A) and ASC-citrine height (ASC-citrine-H). Cells with ASC specks are defined with a higher ASC-H:ASC-A ratio. Experiments were repeated at least three times, and representative data are shown.

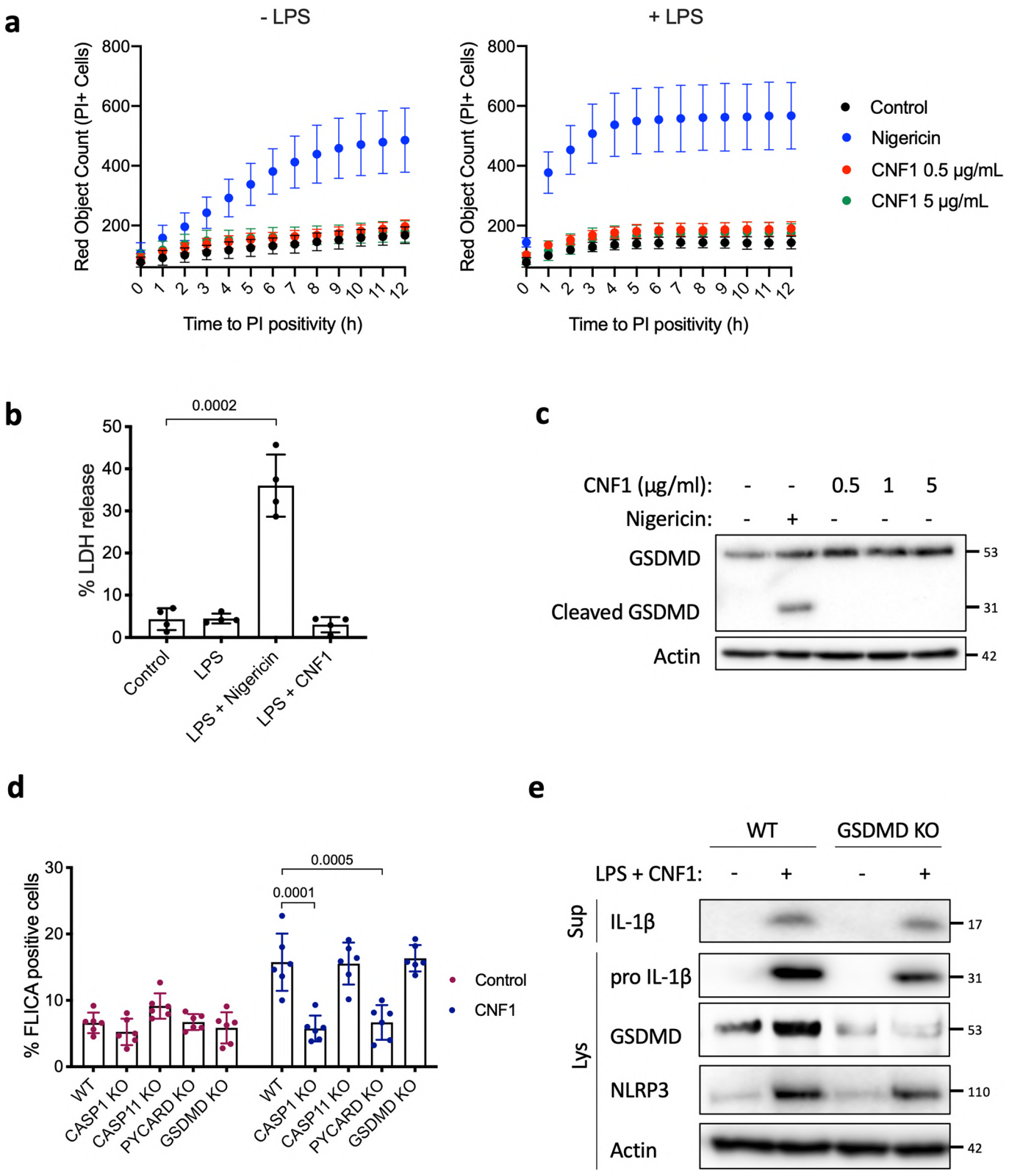


**Extended Data Fig. 2 | See next page for caption.**

**Extended Data Fig. 2 | NLRP3 inflammasome activation by CNF1 does not induce pyroptosis. a**, BMDMs isolated from C57BL/6 J mice were treated with vehicle (control), Nigericin (5 μM) or CNF1 (500 ng/mL or 5 μg/mL) with or without LPS (100 ng/mL). Propidium iodide (PI) uptake was monitored over time (red object count) by real time imaging. Data are expressed as mean ± SD. $10^4$ cells were analyzed for each replicate (n = 4 independent wells). **b**, BMDMs isolated from C57BL/6 J mice were treated with vehicle (control, n = 6 independent experiments), LPS (100 ng/mL, n = 4 independent experiments), LPS and CNF1 (500 ng/mL, n = 6 independent experiments) or LPS and Nigericin (5 μM, n = 4 independent experiments), and LDH release was assessed. Data are expressed as the mean ± SEM. Statistical analyses were performed using a two-tailed nonparametric Mann Whitney test. **c**, BMDMs isolated from C57BL/6 J mice were treated either with Nigericin (5 μM) for 30 min or CNF1 (0.5, 1 or 5 μg/mL) for 8 h and GSDMD cleavage in cell lysates is shown. **d**, BMDMs isolated from C57BL/6 J wild-type or CASP1, CASP11, PYCARD (coding for ASC) or GSDMD knock-out mice were untreated or treated with CNF1 (500 ng/mL) for 6 h and were analyzed for Caspase-1 activation using the FAM-FLICA probe. Data are expressed as the mean ± SEM. Statistical analyses were performed using a two-tailed unpaired Student's t-test. Each dot represents 100 cells (n = 700 cells). **e**, BMDMs isolated from wild-type or GSDMD knock-out mice were treated with CNF1 (500 ng/mL) and LPS (100 ng/mL) for 8 h as indicated. Supernatants and cell lysates were analyzed by immunoblot. The numbers on the side of the immunoblots indicate molecular weight (kDa). Experiments were repeated at least three times, and representative data are shown.

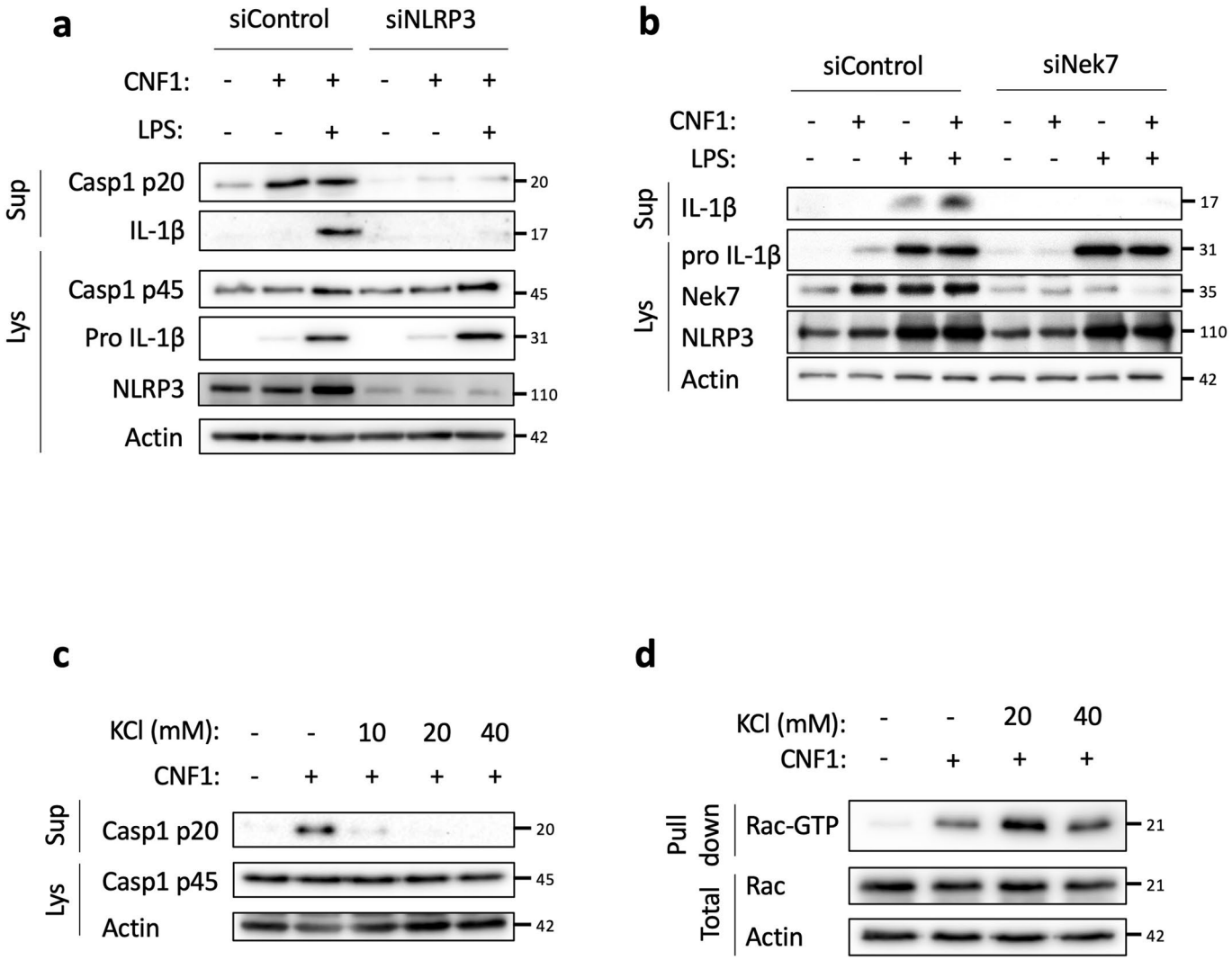


**Extended Data Fig. 3 | CNF1-triggered inflammasome activation depends on NLRP3, Nek7 and $K^+$ efflux. a**,**b**, BMDMs isolated from C57BL/6 J mice were transfected with siRNA-targeting NLRP3 (**a**), siRNA-targeting Nek7 (**b**), or control non-targeting siRNA for 72 h before treatment with CNF1 (500 ng/mL) and/or LPS (100 ng/mL) for 8 h. Supernatants and cell lysates were analyzed by immunoblot. **c**,**d**, BMDMs isolated from C57BL/6 J mice (**c**) or iBMDMs (**d**) were treated with the indicated KCl concentration and CNF1 (500 ng/mL) for 8 h. **c**, Supernatants and cell lysates were analyzed by immunoblot, or (d) cell lysates were analyzed using a GST–Pak-RBD pull-down assay. The Rac associated with the GST-Pak-RBD beads is indicated as Rac-GTP. The numbers on the side of the immunoblots indicate molecular weight (kDa). Experiments were repeated at least three times, and representative data are shown.

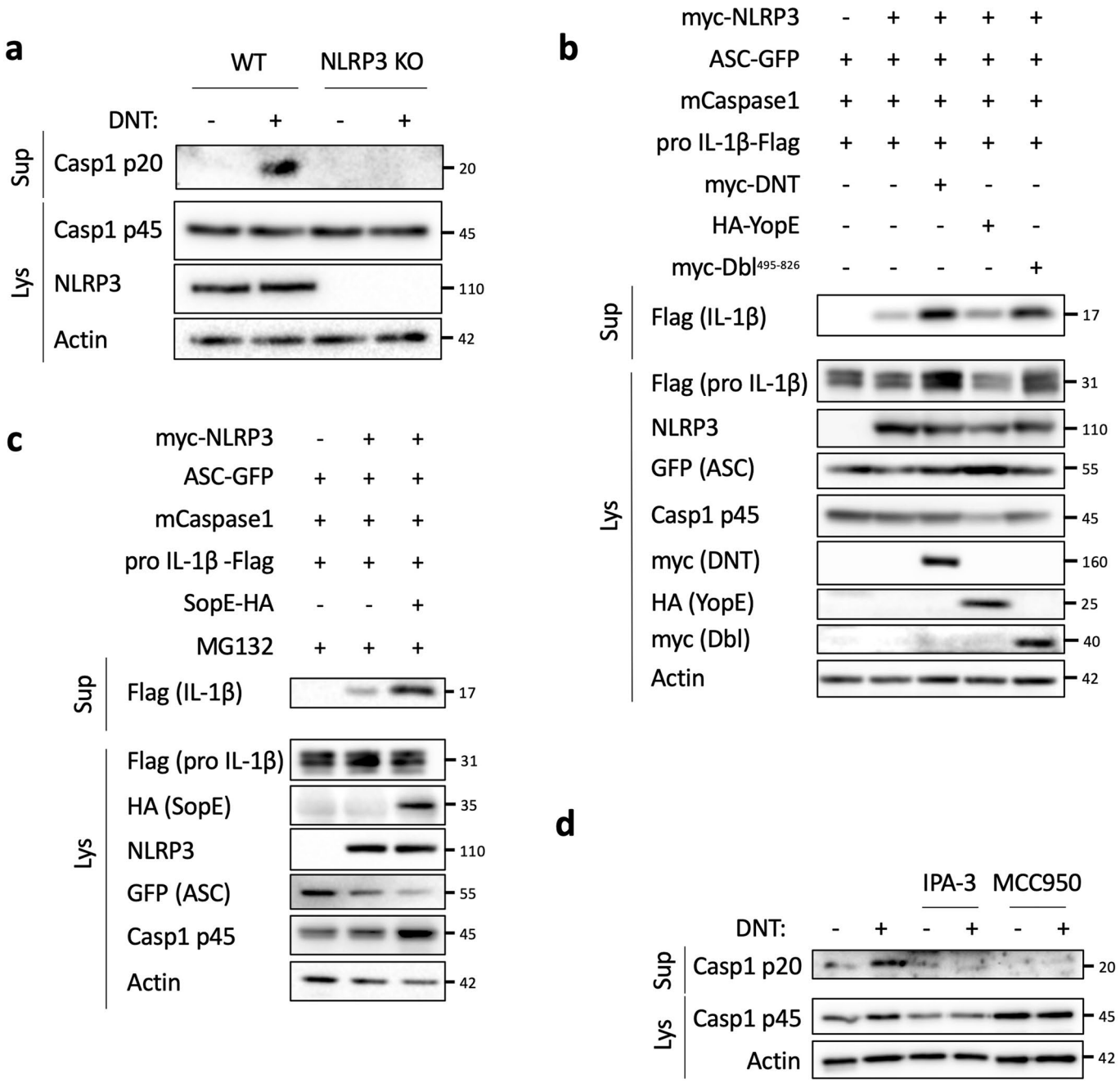


**Extended Data Fig. 4 | Toxins mediated Rho GTPases activation but not inhibition trigger the NLRP3 inflammasome. a**, BMDMs isolated from wild-type or NLRP3 knock out C57BL/6 J mice were treated with DNT (1 μg/mL) for 8 h. Supernatants and cell lysates were analyzed by immunoblot. **b-c**, HEK293T cells were transfected as indicated with plasmids encoding NLRP3 inflammasome components (myc-NLRP3, ASC-GFP, mCaspase-1) and pro-IL-1β-Flag together with (**b**) myc-DNT, HA-YopE or myc-Dbl$^{495-826}$ or (**c**) transfected with SopE-HA and treated with MG132 to block SopE degradation (10 μM). Supernatants and cell lysates were analyzed by immunoblot. **d**, BMDMs isolated from C57BL/6 J mice were treated with IPA-3 (5 μM) or MCC950 (1 μM) for 45 min prior to 8 h of DNT treatment (1 μg/mL). Supernatants and cell lysates were analyzed by immunoblot. The numbers on the side of the immunoblots indicate molecular weight (kDa). Experiments were repeated at least three times, and representative data are shown.

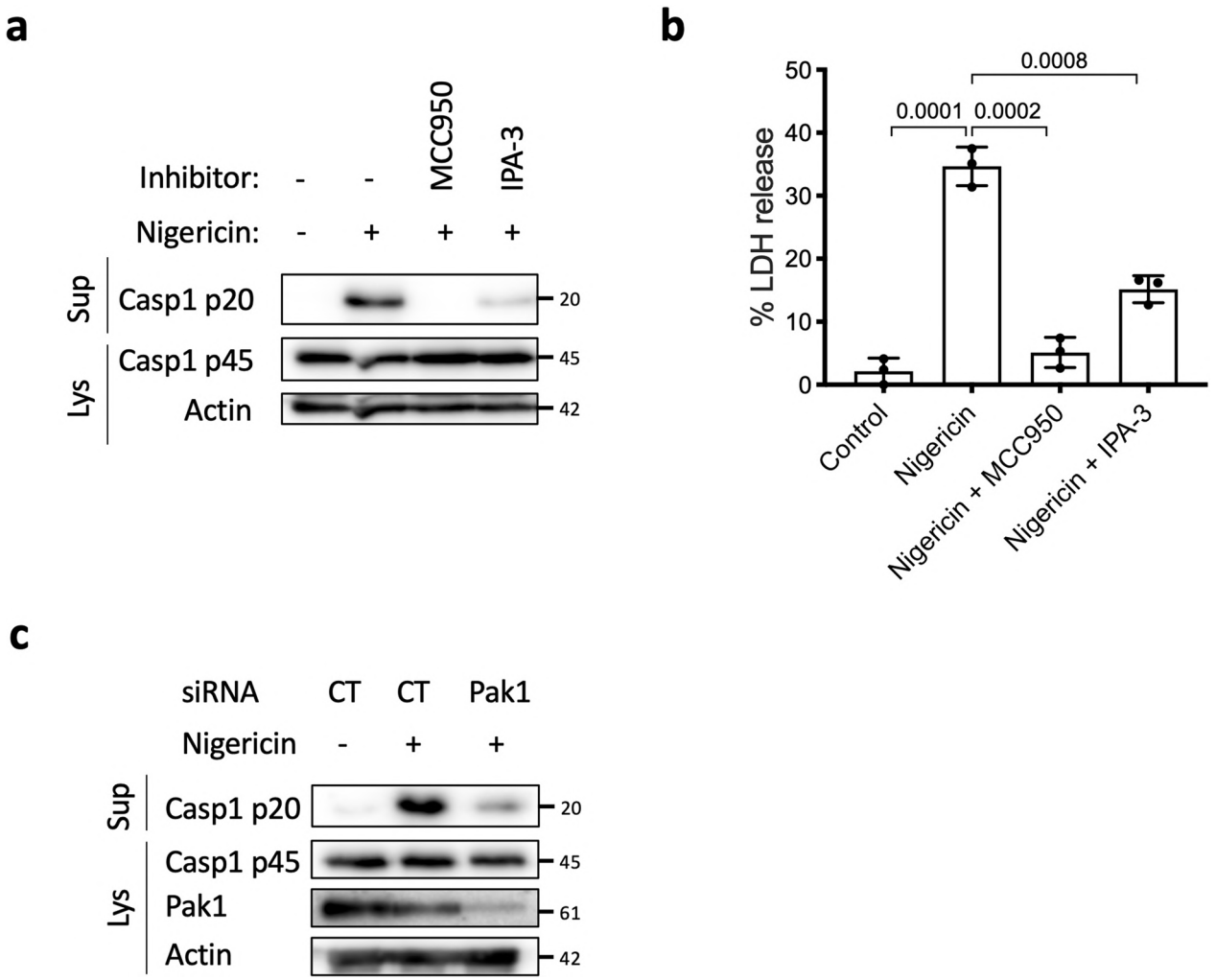


**Extended Data Fig. 5 | Inhibition of Pak1 diminishes NLRP3 activation by Nigericin. a**,**b**, BMDMs isolated from C57BL/6 J mice were treated with MCC950 (1 μM) or IPA-3 (5 μM) for 45 min prior to Nigericin (5 μM) treatment for 30 min. Supernatants and cell lysates were analyzed by (**a**) immunoblot and (**b**) supernatants were analyzed for LDH release (n = 3 biologically independent experiments). Statistical analyses were performed using a two-tailed nonparametric Mann Whitney test. n = 3 biologically independent samples were analyzed. **c**, BMDMs isolated from C57BL/6 J mice were treated for 72 h with non-targeting (CT) or Pak1-targeting siRNA before treatment with Nigericin (5 μM) for 30 min. Supernatants and cell lysates were analyzed by immunoblot. The numbers on the side of the immunoblots indicate molecular weight (kDa). Experiments were repeated at least three times, and representative data are shown. Data are expressed as the mean ± SEM.

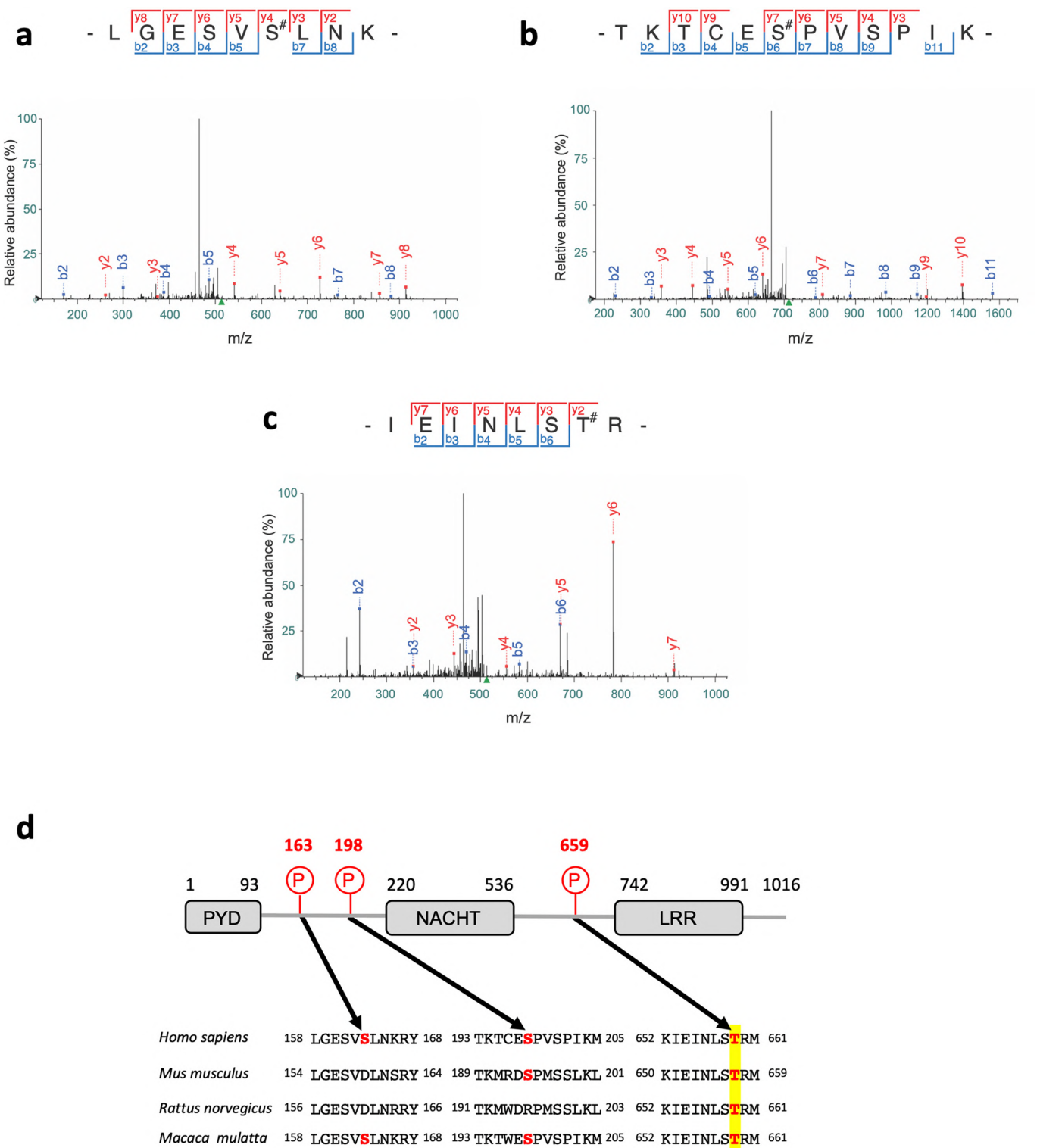


**Extended Data Fig. 6 | Mass spectrometry analysis of Pak1 triggered NLRP3 phosphorylation. a-c**, Fragmentation spectra of human NLRP3 peptides showing phosphorylation of Ser-163, Ser-198 and Thr-659. **d**, Representation of NLRP3 domain structure and sequence alignment of NLRP3 ortholog peptides surrounding phosphorylated residues identified by mass spectrometry. The phosphorylated residues are in bold red.

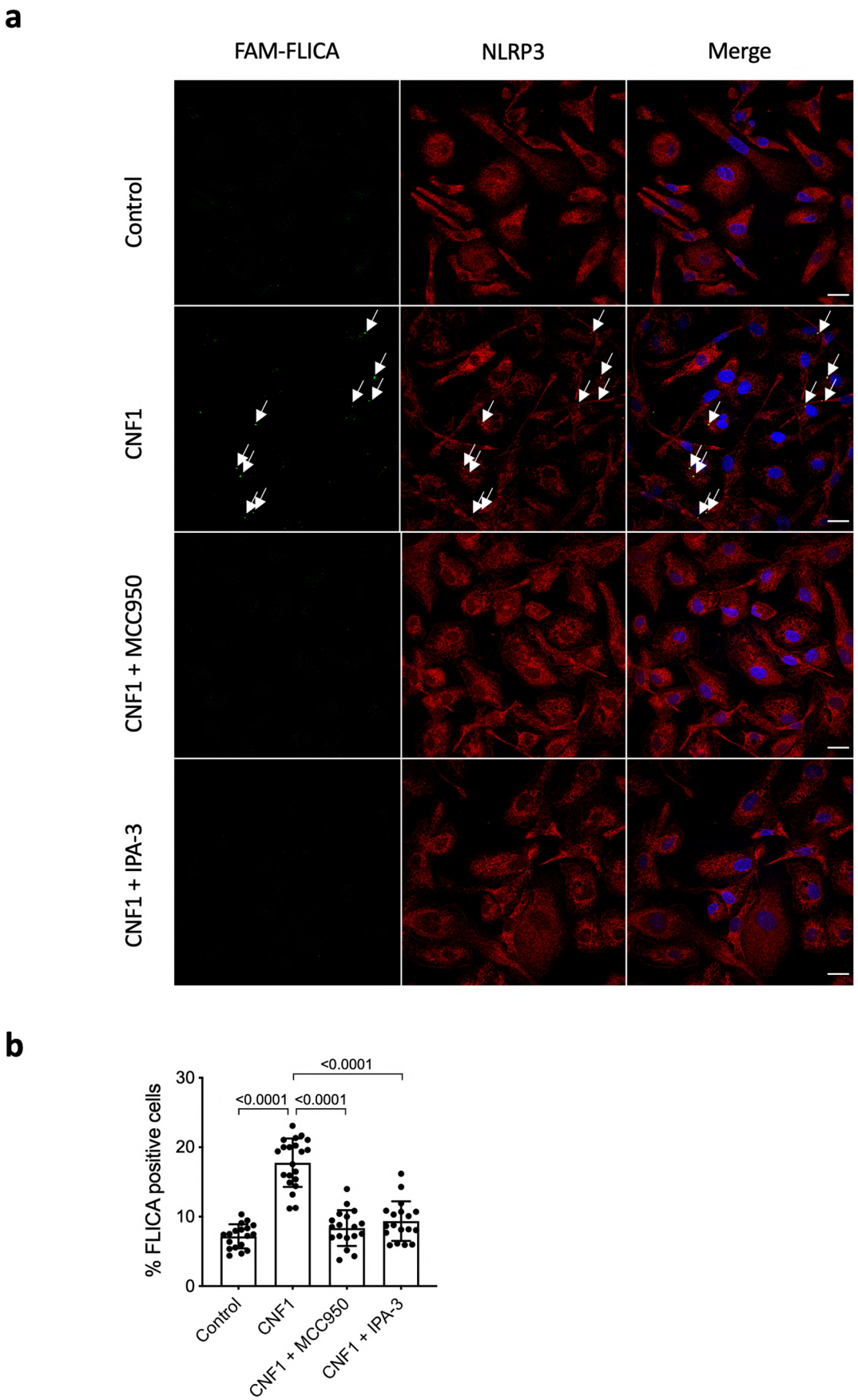


**Extended Data Fig. 7 | See next page for caption.**

**Extended Data Fig. 7 | Conservation of the Pak-NLRP3 axis in Human monocyte-derived macrophages. a-b**, Human monocyte-derived macrophages (hMDMs) were pretreated with vehicle, MCC950 (1 μM) or IPA-3 (5 μM) for 45 min before CNF1 (500 ng/mL) treatment for 6 h. Active Caspase-1 was stained with FAM-FLICA (green), NLRP3 (red) and nuclei (blue) were stained for immunofluorescence and confocal microscopy imaging. Arrows indicates FAM-FLICA dots that colocalize with NLRP3. Scale bar: 20 μm. **b**, quantification of FAM-FLICA positive cells. Data are expressed as the mean ± SEM. Statistical analyses were performed using a two-tailed unpaired Student's t-test. Each dot represents 100 cells (n = 1800 cells). Experiments were repeated at least three times, and representative data are shown.

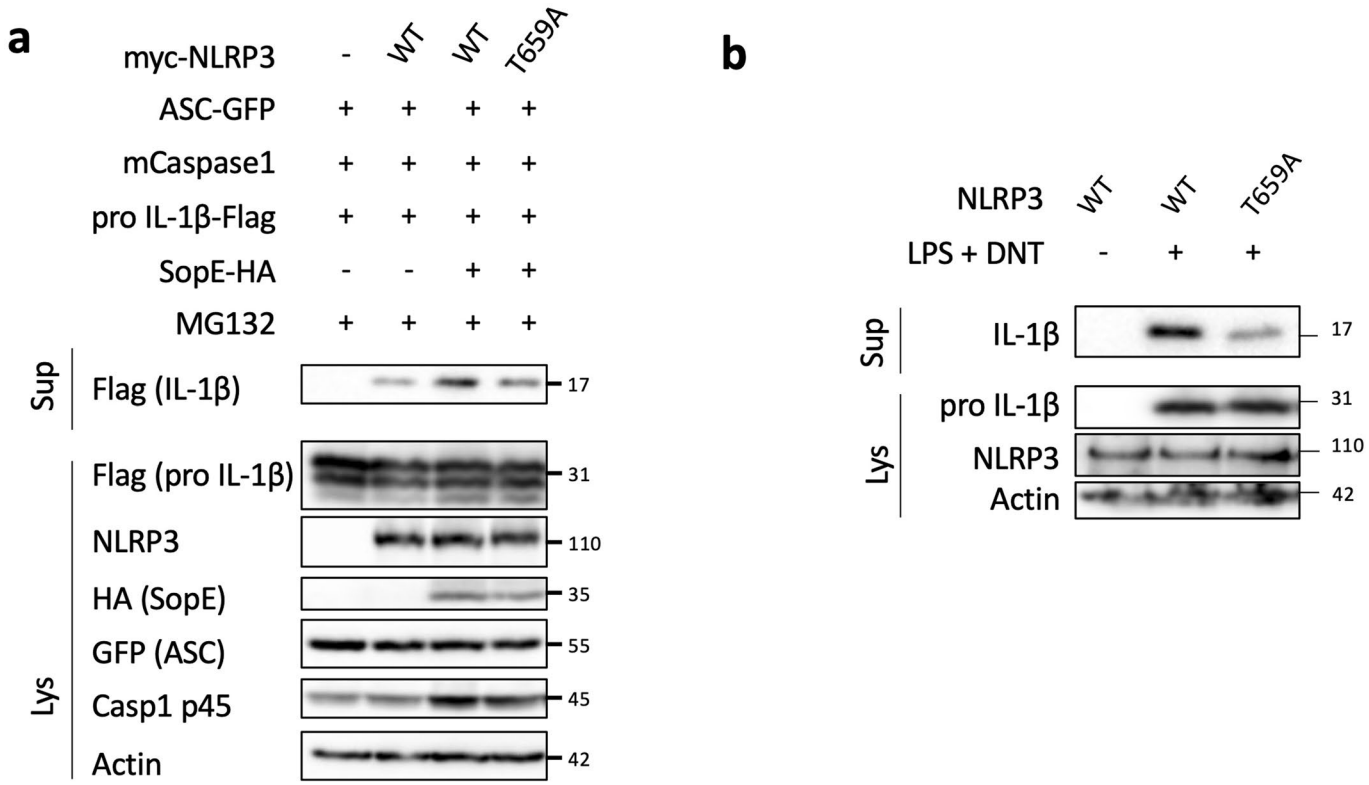


**Extended Data Fig. 8 | The NLRP3 T659A mutant inhibit the IL-1β maturation triggered by SopE and DNT. a**, HEK293T cells were transfected with plasmids encoding NLRP3 inflammasome components (ASC-GFP, mCaspase-1) and pro-IL-1β-Flag and either myc-NLRP3 (WT) or myc-NLRP3 T659A together with SopE-HA and treated with MG132 (10 μM) to block SopE degradation. Supernatants and cell lysates were analyzed by immunoblot. **b**, NLRP3 knock-out iBMDMs reconstituted either with NLRP3 or NLRP3 T659A were treated with vehicle or LPS (100 ng/mL) and DNT (1 μg/mL) for 8 h. The numbers on the side of the immunoblots indicate molecular weight (kDa). Experiments were repeated at least three times, and representative data are shown.

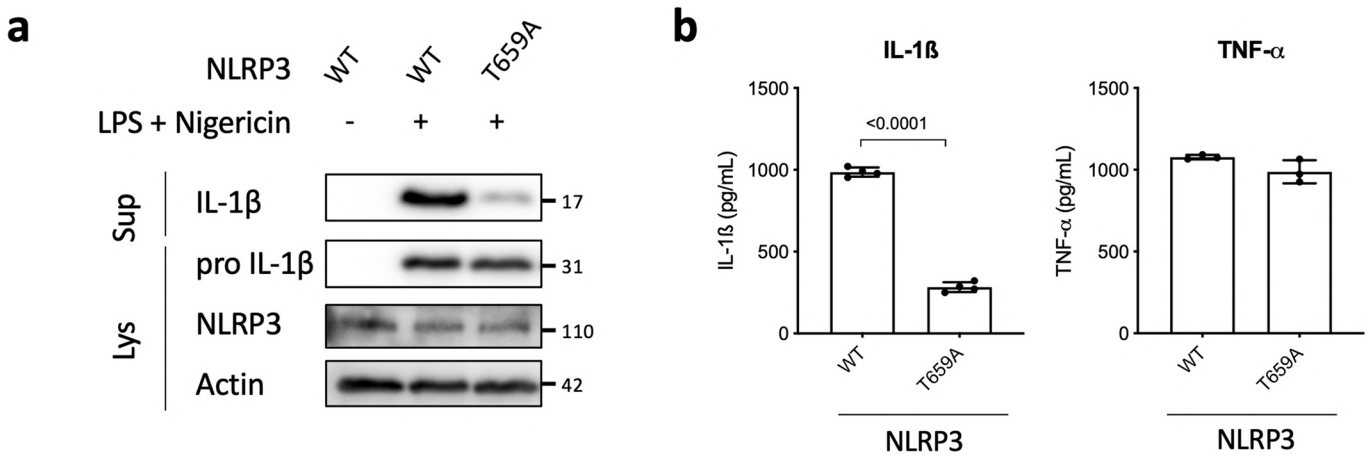


**Extended Data Fig. 9 | Macrophages expressing the NLRP3 T659A mutant have an impaired Nigericin- triggered IL-1β maturation. a-b**, iBMDMs stably expressing either NLRP3 or NLRP3 T659A were treated with Nigericin (5 μM) for 30 min. Supernatants and cell lysates were analyzed by immunoblot and by ELISA for IL-1β (n = 4 biologically independent samples) and TNF-α (n = 3 biologically independent samples). Data are expressed as the mean ± SEM. Statistical analyses were performed using a two-tailed unpaired Student's t-test. The numbers on the side of the immunoblots indicate molecular weight (kDa). Experiments were repeated at least three times, and representative data are shown.

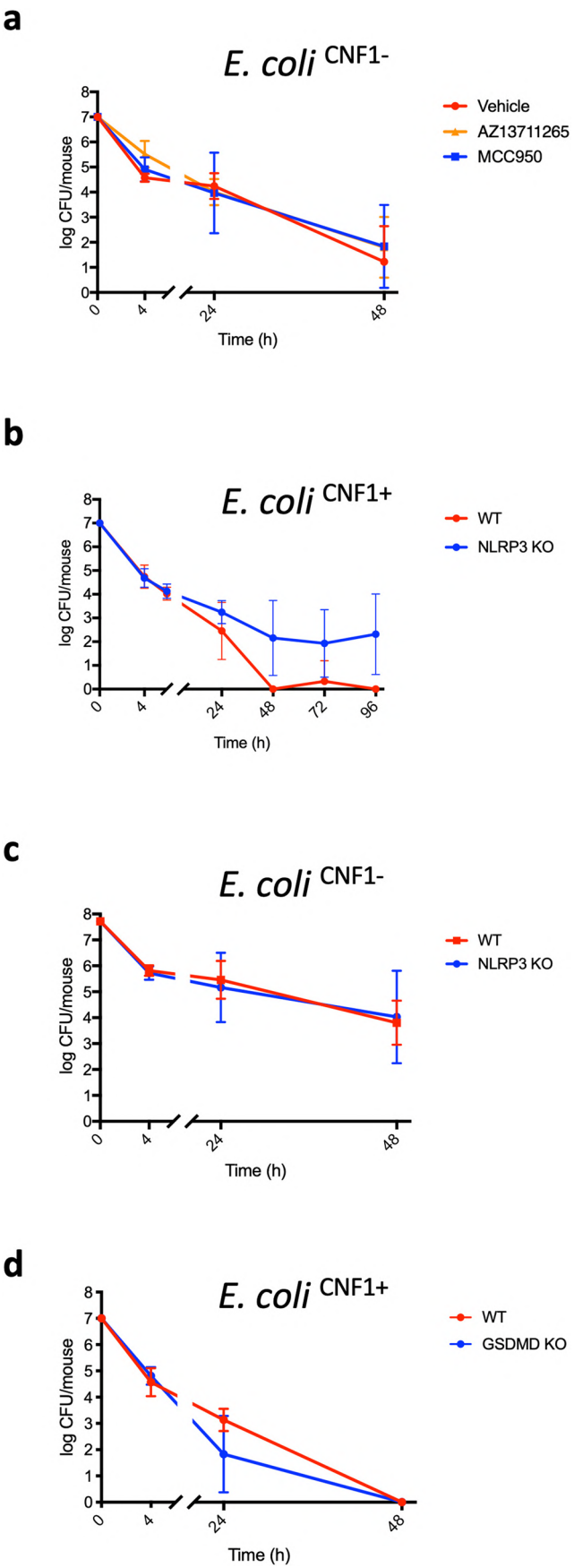


**Extended Data Fig. 10 | See next page for caption.**

**Extended Data Fig. 10 | *E. coli* $^{CNF1-}$ clearing is not affected by Pak1 or NLRP3 inhibition and *E. coli* $^{CNF1+}$ clearing does not rely on GSDMD. a-d**, Wild-type or knock-out mice were infected intravenously with isogenic CNF1-deleted *E. coli* (*E. coli* $^{CNF1-}$) or CNF1 expressing *E. coli* (*E. coli* $^{CNF1+}$). **a**, Wild-type mice were injected intraperitoneally with 10 mg/kg AZ13711265 or 50 mg/kg MCC950 or vehicle once a day and were infected intravenously with isogenic CNF1-deleted *E. coli* (*E. coli* $^{CNF1-}$) prior to the collection of peripheral blood at 4 h, 24 h and 48 h for measurement of bacteraemia (n = 5 mice per group). **b**, Wild-type or NLRP3 knock-out C57BL/6 J mice were infected intravenously with CNF1 expressing *E. coli* (*E. coli* $^{CNF1+}$) prior to the collection of peripheral blood at 4 h, 24 h, 48 h, 72 h and 96 h for measurement of bacteraemia (n = 6 per group). **c**, Wild-type (n = 6 mice) or NLRP3 knock-out C57BL/6 J mice (n = 4 mice) were infected intravenously with isogenic CNF1-deleted *E. coli* (*E. coli* $^{CNF1-}$) prior to the collection of peripheral blood at 4 h, 24 h and 48 h for measurement of bacteraemia (n = 6 per group). **d**, Wild-type (n = 6 mice) or GSDMD knock-out C57BL/6 J mice (n = 6 mice) were infected intravenously with *E. coli* $^{CNF1+}$ prior to the collection of peripheral blood at 4 h, 24 h and 48 h for measurement of bacteraemia. Experiments were repeated two times and representative data are shown. Data are expressed as the geometric mean ± 95 CI.

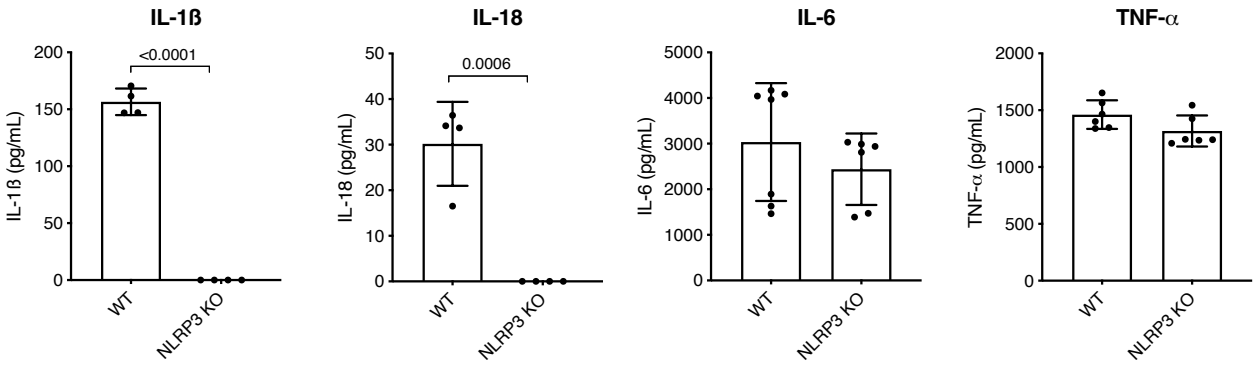


**Supplementary figure 1: CNF1-triggered IL-1β secretion depends on NLRP3.** BMDMs isolated from wild type or NLRP3 knock-out C57BL/6J mice were treated with LPS (100 ng/mL) and with CNF1 (500 ng/mL) for 8 h. Supernatants were analyzed for cytokine secretion by ELISA for IL-1ß, IL-18 (n=4 biologically independent samples) and IL-6 and TNF-α (n=6 biologically independent samples). Data are expressed as the mean ± SEM. Statistical analyses were performed using a two-tailed unpaired Student's t-test. Experiments were repeated at least four times, and representative data are shown.

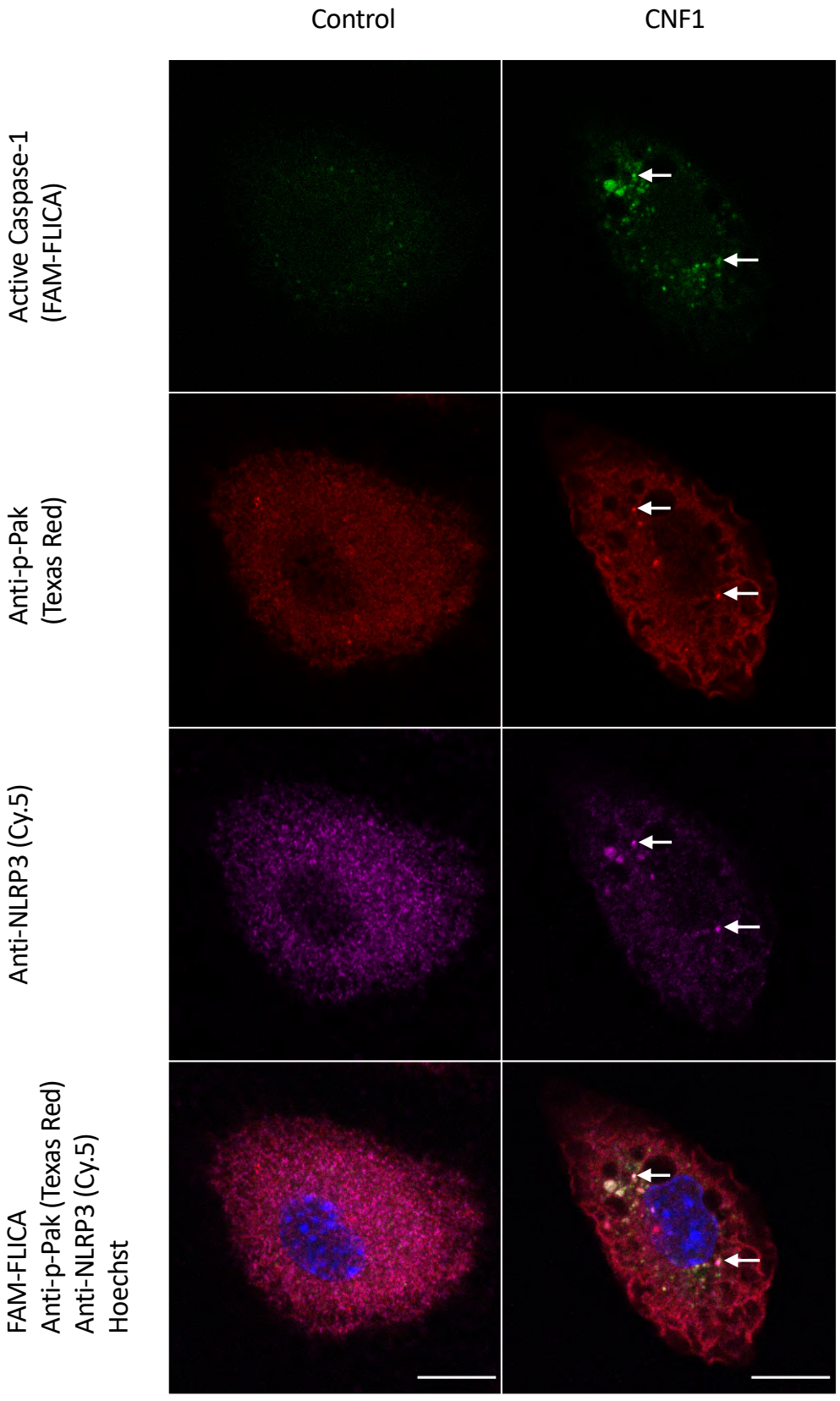


**Supplementary figure 2: NLRP3 and active Caspase-1 colocalize with phosphorylated Pak.** BMDMs isolated from BALB/c mice were treated or not with CNF1 (500 ng/mL) for 6 h. Active Caspase-1 was stained with FAM-FLICA (green), NLRP3 (purple) and phospho-Pak (red) were stained for immunofluorescence microscopy analysis. Scale bar: 10µm. Experiments were repeated at least three times, and representative data are shown.

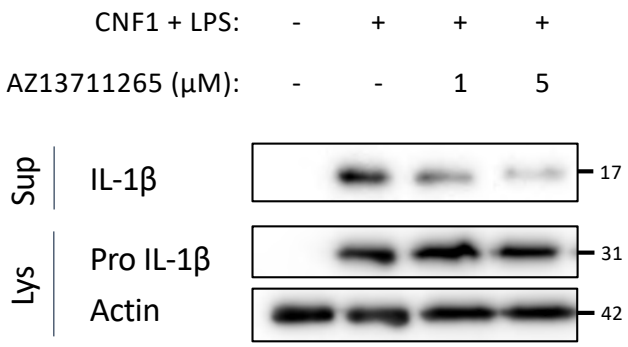


**Supplementary figure 3: CNF1-triggered IL-1β maturation is inhibited by the Pak1 inhibitor AZ13711265.** BMDMs isolated from BALB/c mice were treated or not with AZ13711265 (1 or 5 μM as indicated) for 45 min before treatment with CNF1 (500 ng/mL) and LPS (100 ng/mL) for 8 h. Supernatants and cell lysates were analyzed by immunoblot. The numbers on the side of the immunoblots indicate molecular weight (kDa). Experiments were repeated at least three times, and representative data are shown.

| Peptide sequence | Position | Modscore A | Modscore B |
|---|---|---|---|
| R.LGESVS#LNK.R | 163 | 48,9 | 60,9 |
| K.TKTCES#PVSPIK.M | 198 | 5,1 | 7,8 |
| K.IEINLST#R.M | 659 | 24,4 | 30,5 |

**Supplementary Table 1: Phosphorylated peptide sequence, assigned position and Modscore A and B values for each phosphorylation site assignment.** Phosphorylation site is considered confidently assigned to a residue when both Modscore A and B are above 19 (red). In peptide sequence, dots indicate the trypsin cleavage sites and the hashtag follows the phosphorylation sites of human NLRP3.

## 2. Activation de l'inflammasome NLRP3 au cours du COVID-19 et évolution des patients

### *Contexte et objectifs de recherche*

Les premiers cas de COVID-19 sont détectés début décembre 2019 à Wuhan (Chine) et le 11 mars 2020, l'OMS considère le COVID-19 comme une pandémie. Si une grande partie des sujets infectés par le SARS-CoV-2 présentent un syndrome pseudo-grippal ou sont asymptomatiques, environ 10% développent une forme sévère caractérisée par une atteinte pulmonaire et un syndrome respiratoire aigu sévère (SRAS). Très rapidement, des études font un lien entre la sévérité des patients et des taux plasmatiques élevés de cytokines pro-inflammatoires. Parmi ces cytokines figurent l'IL-1ß, l'IL-18 ainsi que l'IL-1RA. Ces cytokines semblent indiquer qu'un inflammasome pourrait jouer un rôle dans la tempête cytokinique associée aux formes sévères de COVID-19. Nous avons utilisé l'expertise que nous avons au laboratoire dans le suivi de l'activation de la Caspase-1 (grâce à la détection de l'activation de cette dernière par la sonde fluorescente FAM-YVAD-fmk) au cours de la bactériémie chez la souris et l'homme pour évaluer l'état d'activation des inflammasomes dans les cellules myéloïdes circulantes des patients COVID-19. De plus, nous avons utilisé nos observations pour mettre au point le score basé sur la détection d'activation de la Caspase-1 (C1B) permettant de prédire l'amélioration ou la détérioration de l'état clinique des patients atteints COVID-19 dans les 48 heures suivant le test.

REGULAR ARTICLE

blood advances



# Heterogeneous NLRP3 inflammasome signature in circulating myeloid cells as a biomarker of COVID-19 severity

Johan Courjon,[1,2,*] Océane Dufies,[1,*] Alexandre Robert,[1,3] Laurent Bailly,[2,4] Cédric Torre,[1] David Chirio,[2] Julie Contenti,[2] Sébastien Vitale,[1,2] Céline Loubatier,[1] Anne Doye,[1] Christelle Pomares-Estran,[1,2] Géraldine Gonfrier,[2] Romain Lotte,[1,2] Patrick Munro,[1] Orane Visvikis,[1] Jean Dellamonica,[2] Valérie Giordanengo,[1,2] Michel Carles,[2] Laurent Yvan-Charvet,[1] Stoyan Ivanov,[1] Patrick Auberger,[1] Arnaud Jacquel,[1,*] and Laurent Boyer[1,*]

[1]Université Côte d'Azur, Inserm, C3M, Nice, France; [2]Université Côte d'Azur, CHU Nice, Nice, France; [3]Service de Médecine Intensive Réanimation, Centre Hospitalier de Cannes, Cannes, France; and [4]Public Health Department, University Hospital of Nice, Université Côte d'Azur, Nice, France



**Key Points**

- Measurement of NLRP3 inflammasome activation in the blood of patients reveals an impaired immature neutrophil response in severe COVID-19.
- Inflammasome signature analysis in circulating myeloid cells allows COVID-19 patients to be stratified and predicts evolution.

Dysregulated immune response is the key factor leading to unfavorable coronavirus disease 2019 (COVID-19) outcome. Depending on the pathogen-associated molecular pattern, the NLRP3 inflammasome can play a crucial role during innate immunity activation. To date, studies describing the NLRP3 response during severe acute respiratory syndrome coronavirus 2 infection in patients are lacking. We prospectively monitored caspase-1 activation levels in peripheral myeloid cells from healthy donors and patients with mild to critical COVID-19. The caspase-1 activation potential in response to NLRP3 inflammasome stimulation was opposed between nonclassical monocytes and $CD66b^{+}CD16^{dim}$ granulocytes in severe and critical COVID-19 patients. Unexpectedly, the $CD66b^{+}CD16^{dim}$ granulocytes had decreased nigericin-triggered caspase-1 activation potential associated with an increased percentage of NLRP3 inflammasome impaired immature neutrophils and a loss of eosinophils in the blood. In patients who recovered from COVID-19, nigericin-triggered caspase-1 activation potential in $CD66b^{+}CD16^{dim}$ cells was restored and the proportion of immature neutrophils was similar to control. Here, we reveal that NLRP3 inflammasome activation potential differs among myeloid cells and could be used as a biomarker of a COVID-19 patient's evolution. This assay could be a useful tool to predict patient outcome. This trial was registered at www.clinicaltrials.gov as #NCT04385017.

## Introduction

Severe acute respiratory syndrome (SARS) coronavirus 2 (SARS-CoV-2) is a novel human coronavirus that emerged in December 2019 in Wuhan, China.[1] The virus is responsible for a contagious respiratory illness named coronavirus disease 2019 (COVID-19), which can evolve into life-threatening SARS in some cases.[2] However, some patients infected by SARS-CoV-2 suffer from mild COVID-19 conditions, reporting only slight cough and low-grade fever, and cases of even asymptomatic carriers have been reported.[2] As for most viral infections, it is very likely that the outcome of the infection is mainly governed by the interplay between virus and host antiviral immunity.[3,4] Innate immunity is the first line of defense against pathogen invasion in naive patients. It plays an essential role in restricting viral replication and activating adaptive immunity during the first stages of infection. Innate immune defects have been involved in susceptibility to infection whereas activating mutations can cause autoinflammatory diseases.[5] Both innate and adaptive immunity work as a continuum that starts by an efficient detection of the pathogen by the innate immune system.[6] The innate immune detection system of viruses relies on

Submitted 30 November 2020; accepted 3 February 2021; published online 8 March 2021. DOI 10.1182/bloodadvances.2020003918.

*J. Courjon, O.D., A.J., and L. Boyer contributed equally to this work.

Requests for data may be e-mailed to the corresponding author, Laurent Boyer, at laurent.boyer@univ-cotedazur.fr.

The full-text version of this article contains a data supplement.

pattern recognition receptors (PRRs). PRRs are conserved proteins able to sense pathogen-associated molecular patterns specific to microbes.[7] Viral nucleic acids as well as viral proteins have been shown to interplay with PRRs.[8] Among the PRRs, inflammasomes control the maturation of interleukin-1β (IL-1β) and IL-18 cytokines.[9] The NLRP3 inflammasome is the most extensively studied and is activated by either pathogen-associated molecular patterns or damage-associated molecular patterns. Among these triggers, nigericin is a bacterial pore–forming toxin widely used as a specific activator of the NLRP3 inflammasome. The stimulation of NLRP3 by nigericin results in assembly of the inflammasome through recruitment of the adaptor protein apoptosis-associated speck-like protein containing a C-terminal caspase recruitment domain (ASC) and the recruitment and activation of caspase-1, which has proteolytic activity and allows the maturation of pro–IL-1β into active IL-1β.

Recent studies suggest that the death of COVID-19 patients with no medical history can be attributed to a cytokine storm that is similar to what is observed during sepsis with excessive plasma IL-6 and IL-1β levels.[10-12] Recent reports have suggested a potential role of NLRP3 inflammasome during the COVID-19 cytokine storm, and clinical evidence of NLRP3 inflammasome involvement during COVID-19 is emerging.[13-20] Furthermore, clinical trials have been designed to dampen either the NLRP3 inflammasome or IL-1β cytokine-dependent inflammation, but the knowledge concerning NLRP3 inflammasome activation in COVID-19 patients is still limited.

To address this point, we designed an assay to monitor NLRP3-triggered caspase-1 activation in the whole blood of COVID-19 patients. Here, we used this assay to determine the innate immune status of patients by identifying myeloid cell activation profiles and propose these biomarkers as a tool to predict COVID-19 severity.

## Methods

### Study design and ethics

This prospective study was performed in the Emergency Department, Infectious Diseases Department, and intensive care unit (ICU) of the University Hospital of Nice (Nice, France) as well as in the ICU of Cannes Hospital (Cannes, France) between May and October 2020. A French ethics committee (Comité de Protection des Personnes NORD OUEST-1) approved the study (national registration number 2020-00959-30). The study design is summarized next.

All adult patients managed for COVID-19 in either institution were eligible. COVID-19 diagnosis was confirmed by positive SARS-CoV-2 reverse transcription–polymerase chain reaction on nasopharyngeal swab specimen. The exclusion criteria included pregnancy, breastfeeding, bone marrow aplasia, or HIV infection with a CD4 T-cell count $<200/\mu L$. Eligible participants provided written informed consent. When required during ICU management, written informed consent was provided by the surrogate decision-maker and confirmed later by patients themselves. The following characteristics of patients were collected: sex, age, and comorbidities; acquired, drug-induced, or congenital immunosuppression; oxygen supply or mechanical ventilation; COVID-19 symptoms; and complete blood cell count for hospitalized patients. COVID-19 disease severity was classified according to World Health Organization (WHO) guidelines.[21] As daily arterial blood gas is not performed outside of the ICU, we used the pulse oximetric saturation in oxygen ($Spo_2$)/fraction of inspired oxygen ($Fio_2$) ratio ($Spo_2/Fio_2$) to monitor respiratory dysfunction on the day of inclusion and 48 hours later. When $Fio_2$ could not be measured, it was calculated as follows: (oxygen flows in liters per minute) $\times$ 0.03 + 0.21.[22] Unfavorable outcome was defined as death, ICU transfer, or requirement of mechanical ventilation for patients directedly admitted to the ICU. Blood samples from healthy donors were used for comparison and characterization purposes. The recovered COVID-19 patients analyzed were clinically cured and were reanalyzed at a minimum of 29 days after inclusion (mean, 39 days). Blood samples from recovered patients followed the same protocol. Informed consent was provided according to the Declaration of Helsinki following the recommendations of an independent scientific review board. The project has been validated by the Etablissement Français du Sang, the French National Agency for Blood Collection (13-PP-11/CCTIRS no. 14.266).

### Statistical analysis

Statistical analysis of flow cytometry data was performed with a Mann-Whitney nonparametric *U* test. Patient characteristics were analyzed using the Fisher's exact test, the $\chi^2$ test, the unpaired Student *t* test, or 1-way analysis of variance where appropriate. Single correlations among $Spo_2/Fio_2$ ratio and flow cytometry data were evaluated with the Spearman coefficient of correlation. The relationship between $Spo_2/Fio_2$ ratio and flow cytometry data were checked by visual inspection of scatterplots and outliers were controlled before the analyses.

### ELISAs

Plasma from healthy donors or COVID-19 patients was obtained from the sodium citrate collection tubes used for flow cytometry analysis and stored at −80°C so that all samples could be analyzed simultaneously. The cytokine levels in the plasma were determined by enzyme-linked immunosorbent assay (ELISA) using human Quantikine ELISA kits for IL-1β, IL-1RA, IL-18, and IL-18BPa (R&D Systems) according to the manufacturer's instructions.

### Ex vivo stimulation of whole blood and flow cytometry

Whole-blood samples were obtained using sodium citrate collection tubes and analyzed 24 hours later. Peripheral blood was diluted 1/1 with RPMI 1640 medium and treated with 5 μM nigericin (Invivogen) or vehicle for 30 minutes at 37°C under agitation (500 rpm on Eppendorf ThermoMixer). Caspase-1 activation was detected using the FAM-FLICA Caspase-1 Assay kit (ImmunoChemistry Technologies) according to the manufacturer's instructions. Briefly, cells were incubated with the FAM-FLICA probe for 30 minutes at 37°C before being washed: 1 mL of RPMI 1640 was added to dilute the nonbounded probe. Cell-surface markers were stained for 10 minutes in the dark at room temperature using the following recombinant antibodies (1/100; Miltenyi Biotec): CD45-VioGreen (clone REA747), CD14–allophycocyanin (APC)–Vio770 (clone REA599), CD66b–phycoerythrin (PE)–Vio770 (clone REA306), CD16-PE (clone REA423), CD15-APC (clone VIMC6), CD10 APC-Vio770 (clone REA877), and Siglec-8 PE-Vio615 (clone REA1045). Red blood cells were lysed using BD Pharm Lyse buffer (BD Biosciences) according to the manufacturer's instructions. Cells were fixed with 4% paraformaldehyde for 10 minutes. A minimum of $10^5$ leukocytes ($CD45^+$) were recorded per condition. Cells were analyzed using a MACSQuant 10 flow

cytometer from Miltenyi Biotec. Data were analyzed with FlowJo and GraphPad Prism software. After single cells were gated and debris excluded, peripheral blood mononuclear cells were identified as $CD45^+$ cells. Monocytes and granulocytes were then gated as $CD14^+$ and $CD66b^+$ cells, respectively. The gating strategy used in this study is represented in supplemental Figures 1 and 2.

## Results

### Patient recruitment

Sixty-six COVID-19 patients and 24 healthy donors were included during the study period; their main clinical characteristics are presented in supplemental Table 1. COVID-19 patients were recruited upon SARS-CoV-$2^+$ reverse transcription–polymerase chain reaction; healthy donors were negative for SARS-CoV-2 serological assays. Patients were classified into 4 groups (mild, moderate, severe, and critical) in accordance with WHO guidelines.[21] None had any acquired, baseline drug-induced, or congenital immunosuppression. Blood from 24 healthy donors with a mean age of 62 years underwent the same assay at the same time, parallel to COVID-19 patients. Eight patients were included during their ICU stay whereas 4 patients included during their management in our Infectious Diseases Ward were subsequently admitted in ICU.

### Steady-state caspase-1 activity in circulating myeloid cells

The FAM-FLICA probe (FAM-YVAD-FMK) was previously shown to be a powerful tool for monitoring inflammatory caspase-1 activation in monocytes during bacterial infection.[23] To determine caspase-1 activation levels in multiple blood myeloid cells of COVID-19 patients, we used the FAM-FLICA probe together with specific extracellular immune cell markers (CD45, CD14, CD66b, and CD16) in the blood of patients; analyses were performed by flow cytometry (Figure 1; supplemental Figure 1).

Peripheral blood cells of healthy donors or COVID-19 patients were analyzed for the expression of monocyte and granulocyte surface markers and FAM-FLICA. To monitor caspase-1 activity in monocytes from healthy donors or COVID-19 patients, we first gated the $CD45^+CD14^+$ monocyte population, which was subsequently subdivided into 3 subpopulations: classical monocytes ($CD45^+CD14^{high}CD16^-$), intermediate monocytes ($CD45^+CD14^{high}CD16^+$), and nonclassical monocytes ($CD45^+CD14^{dim}CD16^+$) (Figure 1A; supplemental Figure 1). At steady state, we did not observe a statistical difference in the level of caspase-1 activation in any of these monocyte subsets in COVID-19 patients compared with healthy donors (Figure 1B-D).

We next focused our analysis on 2 subpopulations of granulocytes: $CD66b^+CD16^{high}$ and $CD66b^+CD16^{dim}$ (Figure 1E). $CD66b^+CD16^{high}$ cells of mild to moderate COVID-19 patients as well as severe to critical COVID-19 patients showed decreased caspase-1 activation compared with healthy controls (Figure 1F). We measured lower caspase-1 activation in $CD66b^+CD16^{dim}$ granulocytes in the severe and critical forms of COVID-19 that was not observed in mild cases (Figure 1G). $CD66b^+CD16^{dim}$ granulocytes of critical patients showed a twofold decrease in basal caspase-1 activation relative to healthy controls (Figure 1G). Consistent with previous reports and validating our cohort,[10,24] we measured an increase of inflammasome-related cytokines IL-1β, IL-1RA, IL-18, and IL-18BPa in the serum of COVID-19 patients, which correlated with the severity (supplemental Figure 3). Thus, our assay revealed specific regulations of caspase-1 activation in different myeloid cell populations depending on the clinical severity of COVID-19 patients.

### Nigericin-triggered caspase-1 activation in circulating myeloid cells

NLRP3 priming is critical for the activation of the inflammasome.[25] To investigate whether myeloid cells could be primed to respond to the SARS-CoV2 infection, we evaluated the activation potential of the NLRP3 inflammasome in COVID-19 patients. To this aim, we incubated 100 μL of blood samples with the NLRP3 trigger nigericin without lipopolysaccharide, and caspase-1 activation was monitored in myeloid innate immune cells of healthy donors and COVID-19 patients. Monocytes are known to be important innate immune effectors and thought to be key players during COVID-19.[15] We first investigated whether we could monitor the monocyte-priming state by analyzing nigericin-triggered NLRP3 activation in monocytes (Figure 2). We observed increased activation specifically in $CD14^{dim}CD16^+$ nonclassical monocytes isolated from severe to critical COVID-19 patients (Figure 2A-B). Interestingly, this effect was inversely correlated with the decreased number of these cells in severe to critical COVID-19 patients (Figure 2C). In contrast, the nigericin-triggered NLRP3 activation in intermediate and classical monocytes was found to be similar to healthy donors and their number remained unchanged (Figure 2D-I). These data reveal differences in the NLRP3 inflammasome–priming state not only between healthy controls vs COVID-19 patients but also depending on the subpopulation and the severity of COVID-19. Next, we investigated nigericin-triggered NLRP3 activation in granulocytes (Figure 3). In contrast to $CD66b^+CD16^{high}$ granulocytes in which we observed increased caspase-1 activation, we measured impaired response to the NLRP3 inflammasome trigger in $CD66b^+CD16^{dim}$ cells, which is associated with the severity of symptoms (Figure 3A-E). The proportion of $CD66b^+CD16^{high}$ granulocytes was found to be increased in correlation with the severity whereas the number of $CD66b^+CD16^{dim}$ granulocytes stayed similar in COVID-19 patients and in heathy donors. Importantly, $CD66b^+CD16^{dim}$ cells were found to exhibit a higher response to nigericin treatment in both healthy donors and mild COVID-19 patients (Figure 3B,D,E). Interestingly, $CD66b^+CD16^{dim}$ granulocytes from healthy donors displayed a fourfold increase in nigericin-triggered caspase-1 activation compared with those who were untreated (Figure 3D). In contrast, we observed that the $CD66b^+CD16^{dim}$ cell response to nigericin was lost in severe and critical COVID-19 patients (Figure 3B,D,E). We here identified different priming levels or tolerance states of the NLRP3 inflammasome in myeloid cell subpopulations that were specific to severe COVID-19 forms, suggesting that this priming is a consequence of the viral infection. The NLRP3 signature of $CD66b^+CD16^{dim}$ was noteworthy due to its potential value as a biomarker to stratify patients.

### Caspase-1 activation in $CD66b^+CD16^{dim}$ cells after recovery

Next, we wondered whether the impaired response to nigericin in $CD66b^+CD16^{dim}$ cells was due to a preexisting susceptibility that could be the cause of the symptom's severity or rather a consequence

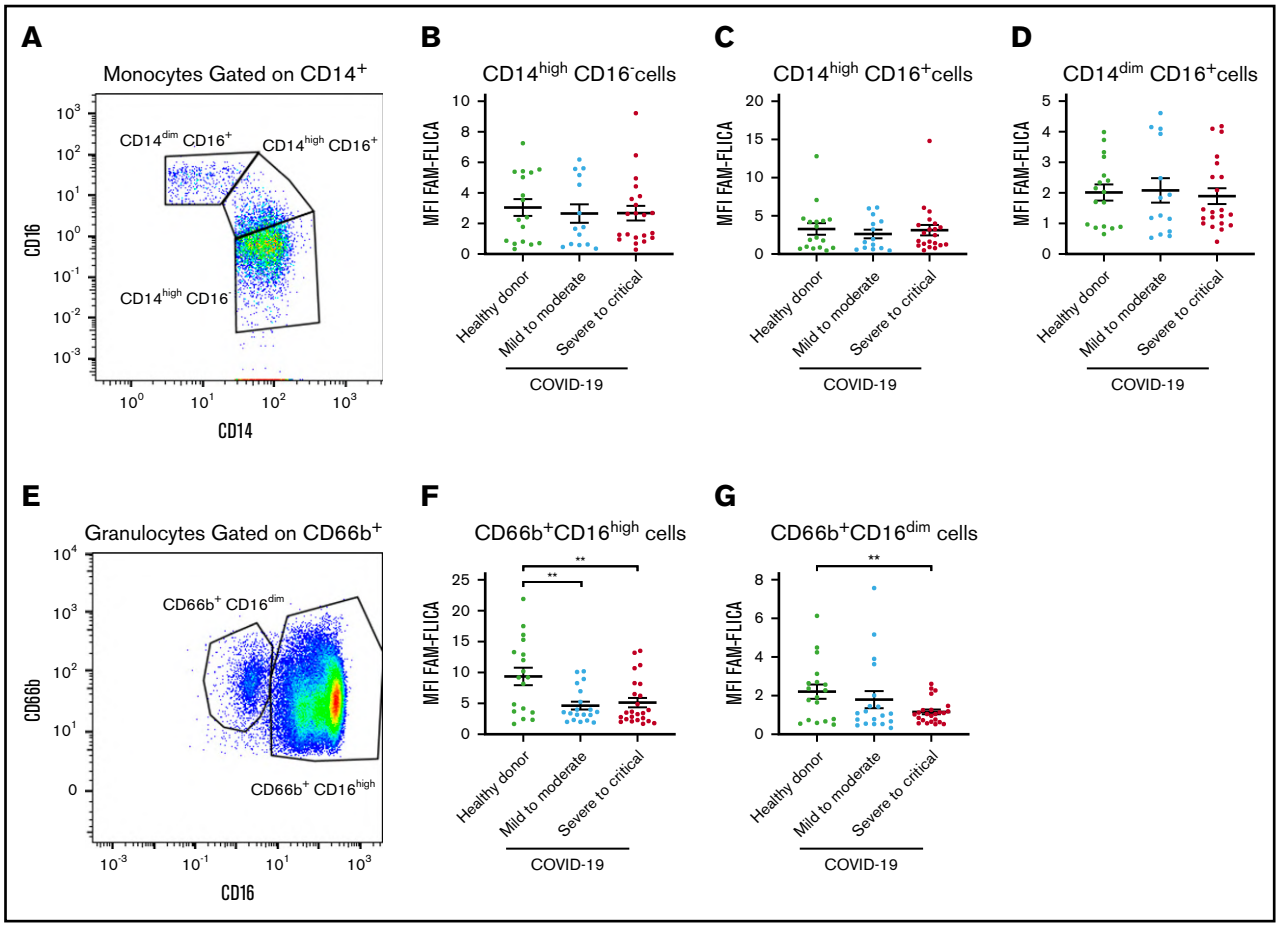


**Figure 1. Caspase-1 activation level in myeloid cells in the blood of COVID-19 patients.** Whole peripheral blood cells of healthy donors or COVID-19 patients with mild to critical symptoms were stained for active caspase-1 (detected using the FAM-FLICA probe) and for CD45, CD14, CD16, and CD66b markers. Cells were immunophenotyped by flow cytometry. Leukocytes were defined as $CD45^+$ and were analyzed for monocyte and granulocyte surface markers. (A-D) Monocytes were defined as $CD14^+$ and subpopulations were gated as indicated in panel A using CD14 and CD16 markers. The indicated monocyte subsets were analyzed for the mean fluorescence intensity (MFI) of FAM-FLICA corresponding to the activation of caspase-1 (B-D). (E-G) Granulocytes were defined as $CD66b^+$ and the different subsets were gated as indicated using CD66b and CD16 markers (E). (F-G) The indicated granulocyte subsets were analyzed for the FAM-FLICA MFI. $^{**}P \leq .01$.

of the infection. To address this question, after recovery, we reanalyzed the blood of patients after a mean time of 39 days following inclusion using the same settings (Figure 4). Our data revealed that the $CD66b^+CD16^{dim}$ cells of recovered patients had a restored nigericin-triggered caspase-1 activation potential (Figure 4A-B). Although 1 patient (number 12) still presented low nigericin-triggered caspase-1 activation (Figure 4B), both severe and critical patients tested had recovered the capacity to respond to nigericin treatment (Figure 4A-B). In addition, nonclassical $CD14^{dim}CD16^+$ monocytes isolated from recovered severe to critical COVID-19 patients showed a capacity to respond to nigericin treatment that was similar to controls (Figure 4C). The reversibility of nigericin-triggered caspase-1 activation in $CD66b^+CD16^{dim}$ granulocytes and $CD14^{dim}CD16^+$ monocytes of recovered patients reinforced our interest of this value as a biomarker of COVID-19 severity.

## Identification of immature neutrophils as a severity marker of COVID-19 patients

We further attempted to characterize the $CD66b^+CD16^{dim}$ cells impaired in the NLRP3 inflammasome response in the most severe forms of COVID-19. We observed that these cells showed differential CD45-expression levels, suggesting the presence of 2 different populations with a respective proportion depending on the severity of COVID-19 (Figure 5A). Indeed, we found that CD45 is highly expressed in the $CD66b^+CD16^{dim}$ cells of healthy donors and patients with mild cases of COVID-19 whereas, in patients with severe and critical COVID-19, we observed low CD45 expression (Figure 5A). $CD66b^+CD16^{dim}$ cells could be either eosinophils or immature neutrophils depending on their CD45-expression pattern. To discriminate between these populations, we introduced the CD15, Siglec-8, and CD10 markers in our immunophenotyping panel (supplemental Figures 1 and 2). Siglec-8 was used to identify eosinophils, and CD15 and CD10 were used as markers of mature neutrophils.[26] In accordance with the $CD66b^+CD16^{dim}CD45^{high}$ cell profile, we observed that the majority of Siglec-8–expressing cells in healthy donors and their proportion decreased in severe forms of COVID-19 (Figure 5B). In the same severe patients, we observed an increased number of $CD66b^+CD16^{dim}CD15^+CD10^-$ immature neutrophils in accordance with the $CD66b^+CD16^{dim}CD45^{dim}$ profile that we found increased in the severe forms (Figure 5C).

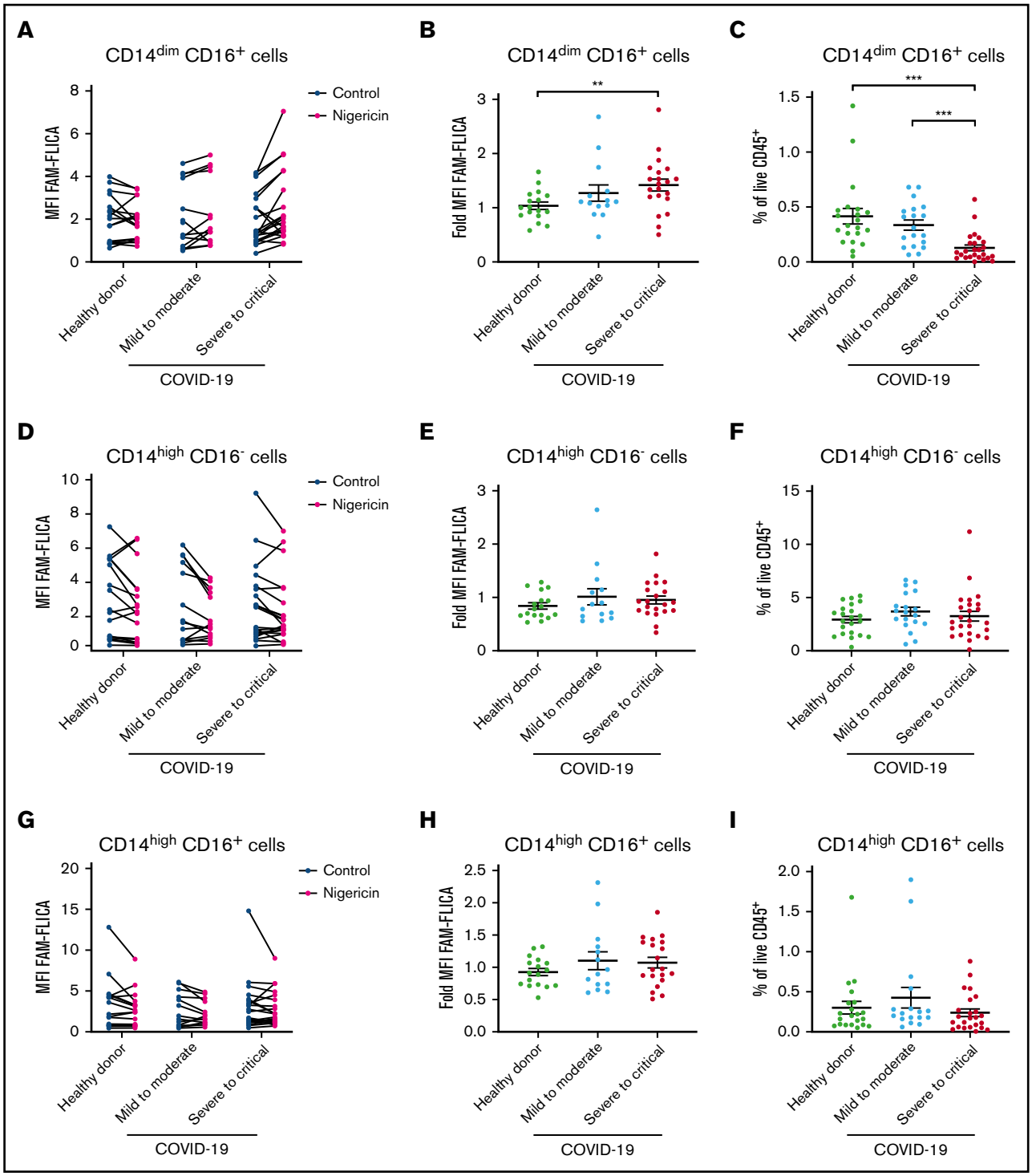


**Figure 2. Nonclassical monocyte disappearance and increased nigericin-triggered caspase-1 activation in nonclassical monocytes are associated with COVID-19 severity.** Whole peripheral blood cells of healthy donors or COVID-19 patients were analyzed by flow cytometry using CD45, CD14, and CD16 markers. Whole peripheral blood was treated with vehicle (control) or nigericin (5 μM) for 30 minutes and monocyte subsets were analyzed for FAM-FLICA MFI (caspase-1 activation) (A,D,G) and nigericin-induced fold of FAM-FLICA MFI compared with control (B,E,H). Leukocytes were defined as $CD45^+$ (C,F,I) and the frequency of monocyte subsets among leukocytes was analyzed: $CD14^{dim}CD16^+$ nonclassical monocytes (C) $CD14^{high}CD16^-$ classical monocytes (F) and $CD14^{high}CD16^+$ intermediate monocytes (I). $^{**}P \leq .01$; $^{***}P \leq .001$.

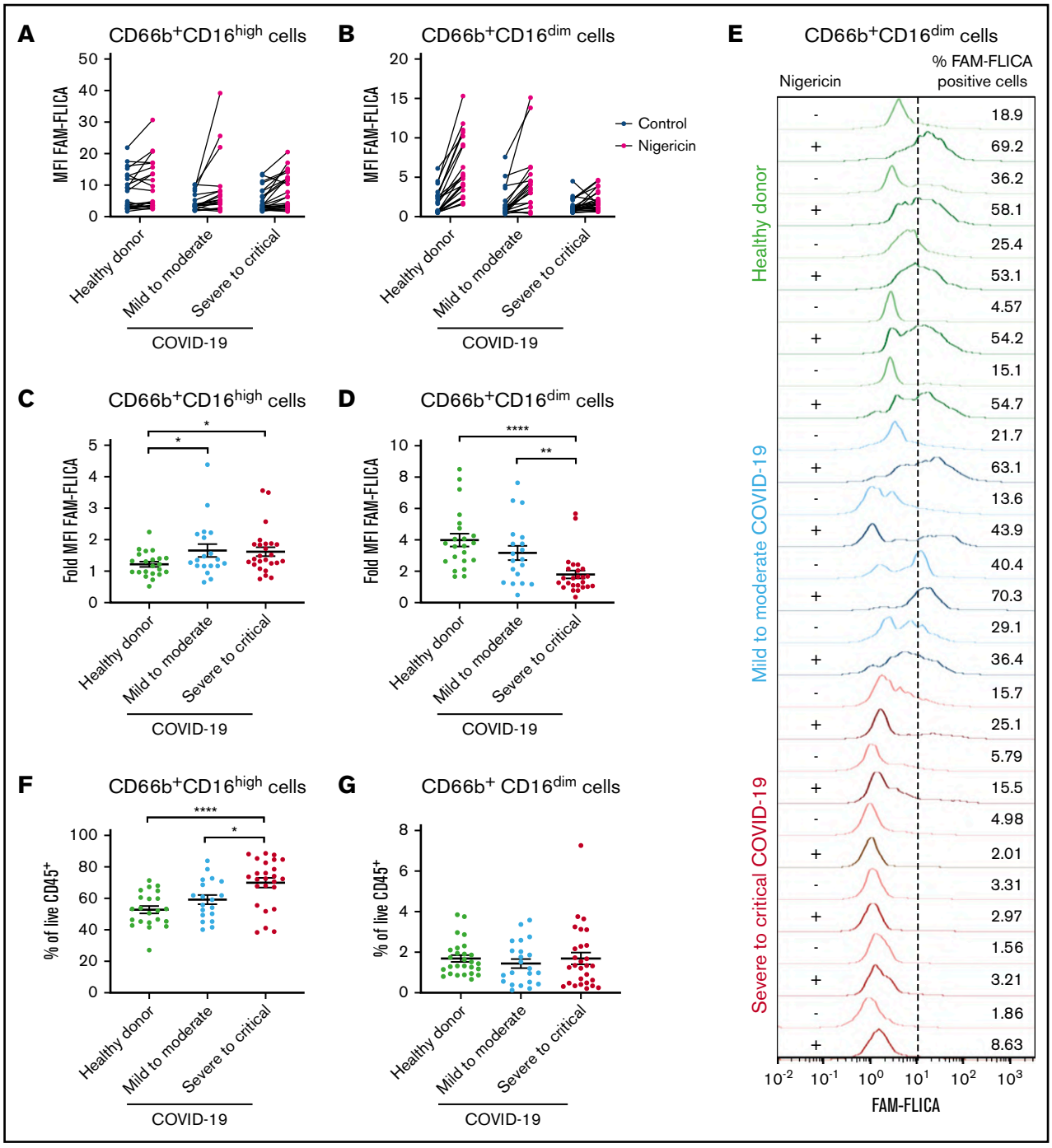


**Figure 3. CD66b$^+$ CD16$^{high}$ granulocytes display increased nigericin-triggered caspase-1 activation in severe COVID-19 whereas CD66b$^+$ CD16$^{dim}$ granulocytes of severe COVID-19 lost their capacity to respond to the NLRP3 stimulation.** Whole peripheral blood cells of healthy donors or COVID-19 patients were analyzed by flow cytometry using CD45, CD66b, and CD16 markers. (A-E) Whole peripheral blood was treated with vehicle (control) or nigericin (5 μM) for 30 minutes and granulocyte subsets were analyzed for FAM-FLICA MFI (caspase-1 activation) (A-B) and nigericin-induced fold of FAM-FLICA MFI compared with control (C-D). (E) Histogram of FAM-FLICA signal in CD66b$^+$CD16$^{dim}$ cells. Light colors, FAM-FLICA in the control condition; dark colors, FAM-FLICA in the nigericin-treated condition. The dotted line represents the gate used to determine the percentage of FAM-FLICA$^+$ cells. (F-G) Leukocytes were defined as CD45$^+$ and the frequency of granulocyte subsets among leukocytes was analyzed. *$P \leq .05$; **$P \leq .01$; ****$P < .0001$.

Importantly, both eosinophils and immature neutrophils were found to have impaired inflammasome activation in severe and critical forms (Figure 5D-G). Critical patients who recovered from COVID-19 showed a restored CD45 profile with a marked disappearance of CD66b$^+$CD16$^{dim}$CD45$^{dim}$ cells (Figure 5H). Interestingly, patient 12, found to have a low recovery rate in the

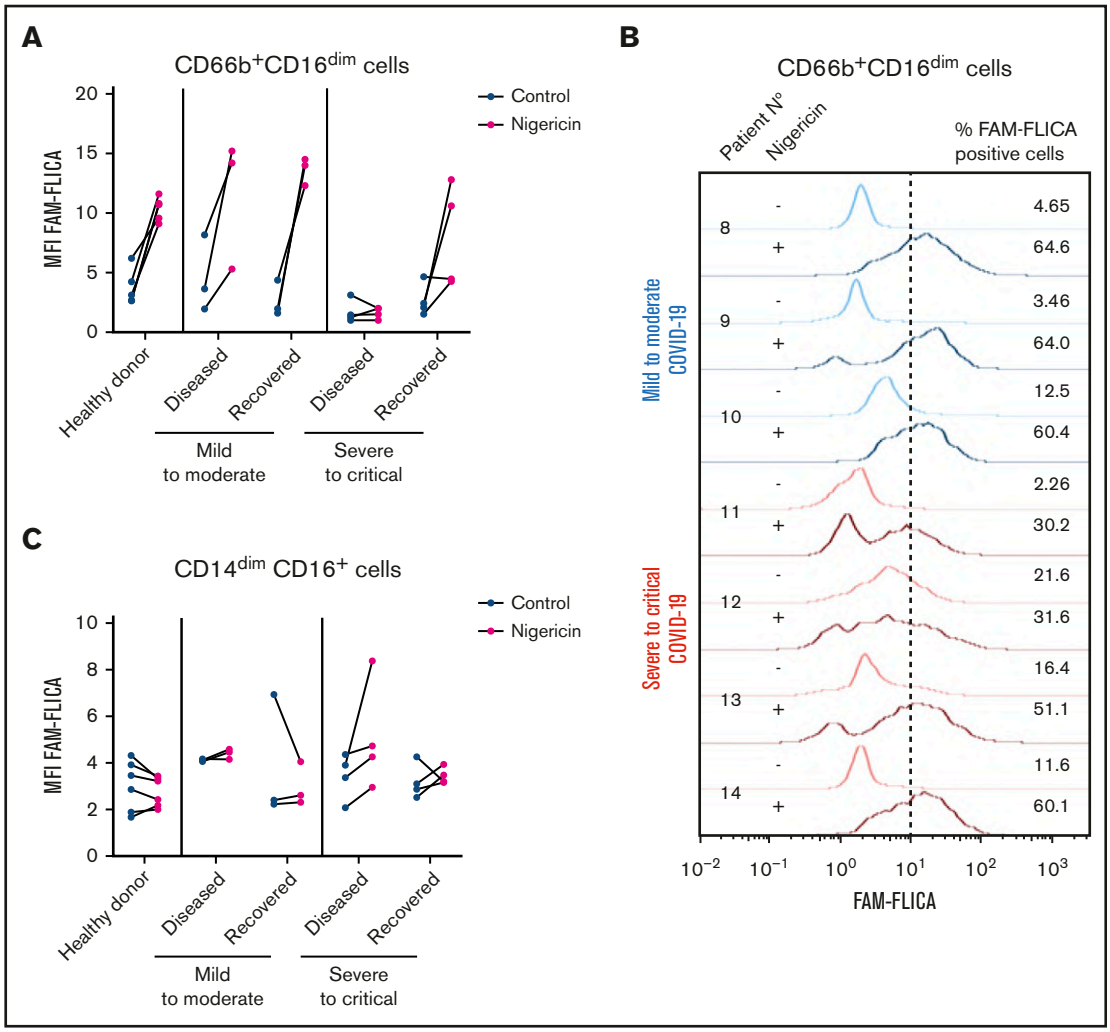


**Figure 4. Myeloid cell response to NLRP3 inflammasome stimulation in recovered COVID-19 patients.** Peripheral blood cells of recovered COVID-19 patients were collected 30 to 50 days after the first analysis. Whole peripheral blood cells of recovered COVID-19 patients were analyzed by flow cytometry using CD45, CD16, and CD66b markers. (A) Whole peripheral blood was treated with vehicle (control) or nigericin (5 μM) for 30 minutes and CD66b$^+$CD16$^{dim}$ granulocytes were analyzed for FAM-FLICA MFI (caspase-1 activation). (B) Histogram of FAM-FLICA signal in CD66b$^+$CD16$^{dim}$ cells. Light colors, FAM-FLICA in the control condition; dark colors, FAM-FLICA in the nigericin-treated condition. The dotted line represents the gate used to determine the percentage of FAM-FLICA$^+$ cells. (C) Whole peripheral blood was treated with vehicle (control) or nigericin (5 μM) for 30 minutes and CD14$^{dim}$CD16$^+$ were analyzed for FAM-FLICA MFI (caspase-1 activation).

nigericin-triggered caspase-1 response, still had a profile with numerous CD66b$^+$CD16$^{dim}$CD45$^{dim}$ cells (Figure 5H).

## Inflammasome myeloid cell response as a biomarker of COVID-19 evolution

We here identified biological parameters significantly associated with the level of disease severity at inclusion. The severity biomarkers we identified as statistically robust were the decreased number of nonclassical monocytes and the decreased nigericin-triggered caspase-1 activation in CD66b$^+$CD16$^{dim}$ granulocytes (Figures 2C and 3B). We next evaluated whether these parameters can be used as biomarkers to predict both the evolution of the patient during the 2 days following inclusion and the final outcome. The immediate evolution of the disease was evaluated by the patient's oxygen requirement, calculated by the $Spo_2/Fio_2$ ratio on the day of inclusion (day 1) (Figure 6A-C) and 48 hours later (day 3) (Figure 6D-F). For this purpose, only hospitalized patients were included in this analysis. Both the decreased number of nonclassical monocytes (Figure 6A,D) and the nigericin-triggered caspase-1 activation in CD66b$^+$CD16$^{dim}$ granulocytes (Figure 6B,E) correlate with the $Spo_2/Fio_2$ ratio at day 1 and day 3 after inclusion. However, the correlation with the $Spo_2/Fio_2$ ratio was stronger with our caspase-1–based score (C1B score) defined as: (the percentage of CD14$^{dim}$CD16$^+$ monocytes) × (fold FAM-FLICA in CD66b$^+$CD16$^{dim}$ granulocytes) (Figure 6C,F).

We thus investigated whether the biological values obtained at day 1 of inclusion could predict the final outcome. Unfavorable outcome was defined as patient death, ICU transfer, or requirement of mechanical ventilation for patients directly admitted to the ICU. Taken alone, the decreased number of nonclassical monocytes was significantly associated with the final outcome of the patients (Figure 6G) and this association was statistically reinforced when

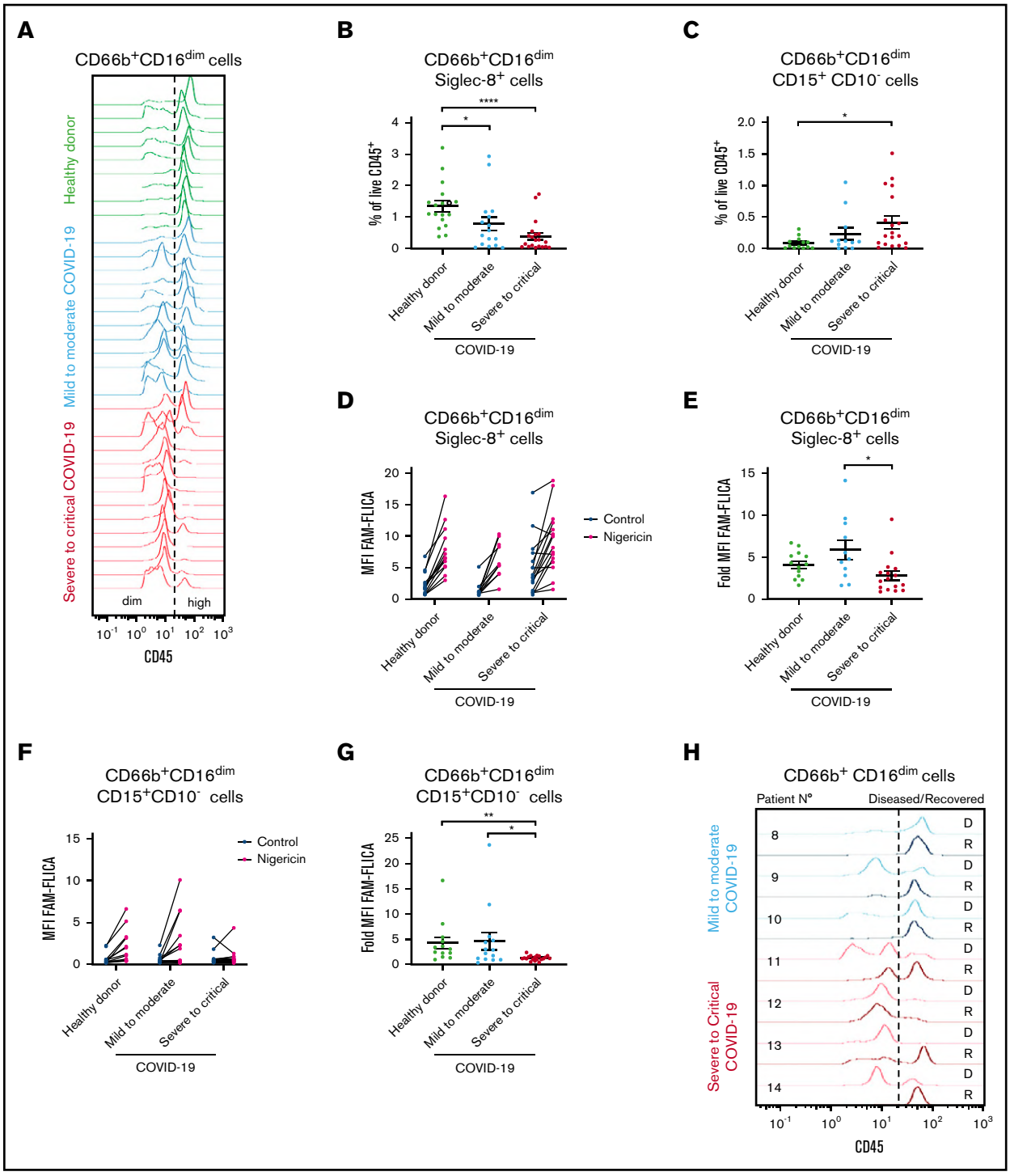


**Figure 5. Severe COVID-19 is associated with eosinophil disappearance and accumulation of immature neutrophils with impaired nigericin-triggered caspase-1 activation.** Whole peripheral blood cells of healthy donors or COVID-19 patients were analyzed by flow cytometry using CD45, CD66b, CD16, and Siglec-8 or CD45, CD66b, CD16, CD10, and CD15 markers. (A) $CD66b^{+}CD16^{dim}$ cells were analyzed for CD45 expression. (B) $CD66b^{+}CD16^{dim}$ cells were analyzed for CD66b and Siglec-8 (eosinophil marker) and the frequency of $CD66b^{+}CD16^{dim}Siglec8^{+}$ eosinophils among leukocytes was determined. (C) $CD66b^{+}CD16^{dim}$ cells were analyzed for CD10 (marker of mature neutrophil) and CD15 (neutrophil marker) and the frequency of $CD66b^{+}CD16^{dim}CD15^{+}CD10^{-}$ immature neutrophils among leukocytes was determined. (D-G) Whole peripheral blood was treated with vehicle (control) or nigericin (5 μM) for 30 minutes and eosinophils or immature neutrophils were analyzed for FAM-FLICA MFI (caspase-1 activation) (D,F) and nigericin-induced fold of FAM-FLICA MFI compared with control (E,G). (H) Peripheral blood cells of recovered COVID-19 patients were collected 30 to 50 days after the first analysis. Whole peripheral blood cells of recovered COVID-19 patients were analyzed by flow cytometry using CD45, CD16, and CD66b markers. $CD66b^{+}CD16^{dim}$ cells were analyzed for CD45 expression. $^{*}P \leq .05$; $^{**}P \leq .01$; $^{****}P < .001$. D, diseased; R, recovered.

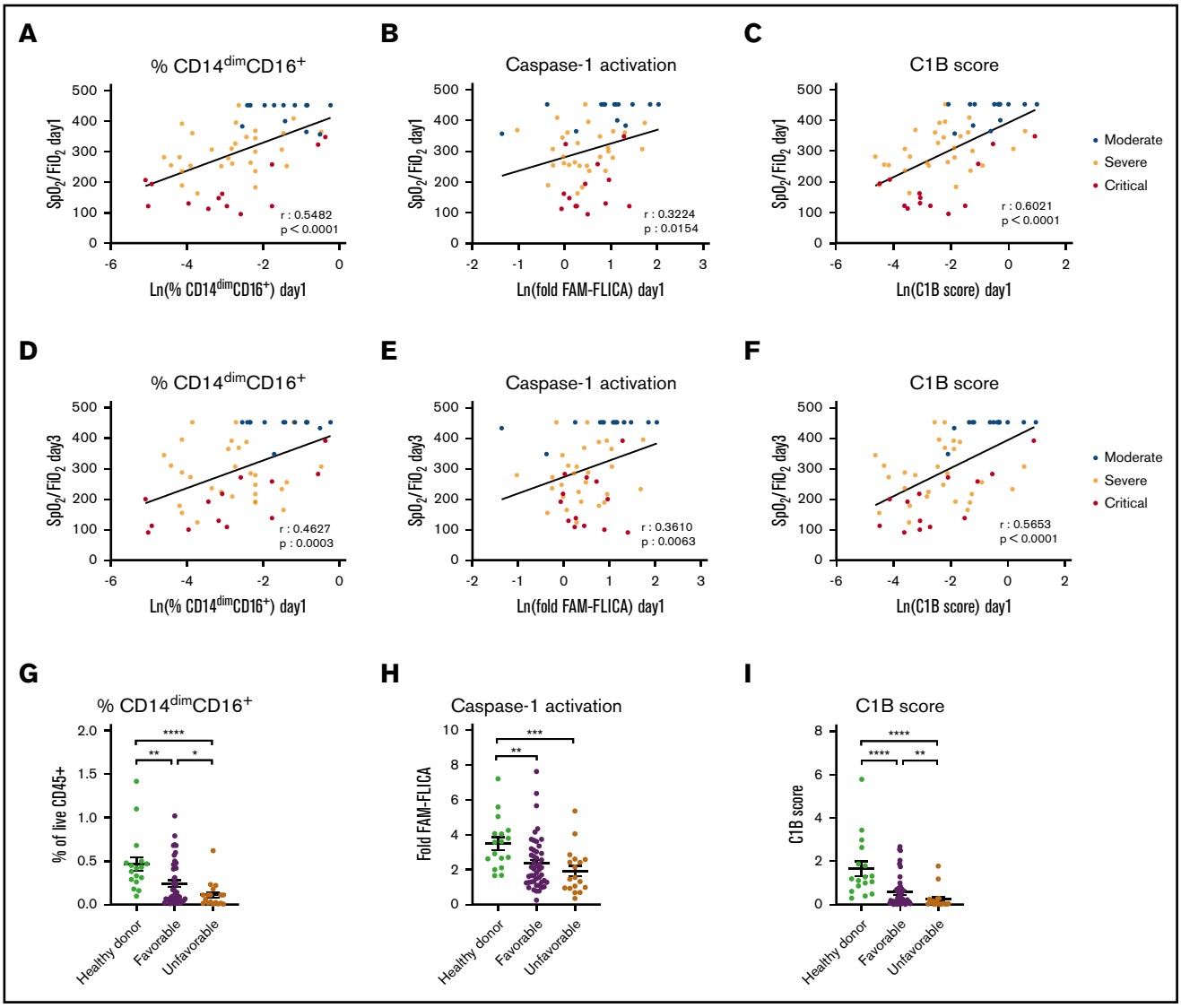


**Figure 6. C1B score is associated with the final outcome of the patient and predicts patients' evolution.** (A-F) Correlation between (A,D) the percentage of $CD14^{dim}CD16^{+}$ nonclassical monocytes of live $CD45^{+}$ cells, (B,E) the nigericin-triggered fold of FAM-FLICA in $CD66b^{+}C16^{dim}$ cells compared with control, (C,F) the C1B score (defined as the percentage of $CD14^{dim}CD16^{+}$ × fold FAM-FLICA in $CD66b^{+}CD16^{dim}$ cells) and the $Spo_2/Fio_2$ ratio at (A-C) day 1 and (D-F) day 3 of inclusion. The line represents the linear regression. Each dot represents a COVID-19 patient and the color its condition at the day of inclusion (blue, moderate; orange, severe; and red, critical). (G-I) Nigericin-triggered fold of FAM-FLICA in $CD66b^{+}C16^{dim}$ cells compared with control (H), percentage of $CD14^{dim}CD16^{+}$ nonclassical monocytes of live $CD45^{+}$ cells (G) and C1B score (I) as previously defined, observed in healthy donors or COVID-19 patients with favorable or unfavorable outcome. $^{*}P < .05$; $^{**}P < .01$; $^{***}P < .001$; $^{****}P < .0001$. r, Spearman coefficient.

the nigericin-triggered caspase-1 activation in $CD66b^{+}$ $CD16^{dim}$ granulocytes was used in the C1B score (Figure 6H-I).

In conclusion, we here described an assay that allows either the monitoring of basal caspase-1 activation or the activation of the NLRP3 inflammasome triggered by nigericin in blood myeloid cells obtained from healthy donors and COVID-19 patients. This assay allowed us to determine nonclassical monocytes as major NLRP3-responsive myeloid cells specifically in severe forms of COVID-19. Our results showed that the $CD66b^{+}CD16^{dim}$ cells of COVID-19 patients were decreased both in the basal level of caspase-1 activation as well as in nigericin-triggered caspase-1 activation in severe to critical patients. We show that patients who recovered from COVID-19 had restored nigericin-triggered caspase-1 activation potential in $CD66b^{+}CD16^{dim}$ cells. Finally, we specifically identify the emergence of immature neutrophils that display a strong defect of NLRP3 inflammasome activation in response to nigericin in these patients. Importantly, we provide proof of concept that caspase-1 and NLRP3 inflammasome monitoring in circulating myeloid cells could be used to stratify COVID-19 patients and predict their evolution.

## Discussion

The involvement of inflammasomes controlling IL-1β maturation during the COVID-19 cytokine storm is under extensive investigation, and

drugs inhibiting inflammasomes are expected to dampen this detrimental inflammation. Strategies directly targeting the inflammasome components or the IL-1β–signaling pathways are currently being evaluated in clinical trials.[3] Among them, the use of IL-1R antagonist anakinra in COVID-19 patients has been reported to reduce both mortality and ICU admission, providing first evidence of the importance of this pathway during the COVID-19 cytokine storm.[27] Here, by using a probe that labels active caspase-1, we investigated whether myeloid cells in the blood of COVID-19 patients had modulated caspase-1 activation, a hallmark of inflammation, and whether this response is related to the severity of COVID-19 symptoms.

Recent studies have shown increased NLRP3 inflammasome activation in patients with severe COVID-19 by measuring either the increased caspase-1 activity or pyroptotic cell death in peripheral blood mononuclear cells.[19,20] Here, we extended this finding and precisely defined nonclassical monocytes of COVID-19 patients as the NLRP3 inflammasome most responsive to myeloid cells. Indeed, our study revealed that both basal and triggered inflammasome activation differ among myeloid cell populations. We identified nonclassical monocytes as a myeloid population with a COVID-19 severity signature. Indeed, the nigericin-triggered NLRP3 inflammasome activation of nonclassical monocytes was increased in severe forms. Our data indicated nonclassical monocytes as the major NLRP3 inflammasome–responsive/primed cells in COVID-19 patients and suggest that their decreased proportion in severe forms may be a consequence of pyroptotic cell death occurring downstream of caspase-1 activation. In contrast, we measured lower basal caspase-1 activation in granulocytes of COVID-19 patients. As a major result of our study, we observed that the nigericin-triggered caspase-1 activation of $CD66b^{+}CD16^{dim}$ granulocytes inversely correlated with the severity of the symptoms of COVID-19 patients. Here, our data indicated that, in severe and critical patients, $CD66b^{+}CD16^{dim}$ granulocytes are not able to respond to the NLRP3 inflammasome stimulation. This result suggests that $CD66b^{+}CD16^{dim}$ granulocyte cells could be either exhausted or paralyzed. Interestingly, paralysis of the NLRP3 inflammasome was previously observed in patients during sepsis.[23] Another possibility to explain this absence of responsiveness is that severe or critical COVID-19 patients exhibited a more immature subset of neutrophils associated with an altered response. Such a situation was previously observed during sepsis: $CD66b^{+}CD16^{dim}$ neutrophils are released from the bone marrow and display less immune functionality.[28] Interestingly, in severe and critical COVID-19 patients, we identified the emergence of $CD66b^{+}CD16^{dim}CD15^{+}CD10^{-}$ immature neutrophils favoring this hypothesis, reinforcing the parallel between the cytokine storm observed in the severe forms of COVID-19 and that seen during sepsis. Recent reports have indicated the increased number of immature neutrophils in severe forms of COVID-19.[29-31] Complementing these studies, we here provide evidence for impaired function of these cells in correlation with the severity of COVID-19.

Strikingly, in patients who recovered from COVID-19, we found that $CD66b^{+}CD16^{dim}$ granulocytes had restored a normal response to nigericin treatment. These data show that the tested COVID-19 patients did not constitutively exhibit an NLRP3 inflammasome impairment; rather, this reduced response is a consequence of SARS-CoV-2 infection. This observation is in agreement with the occurrence of the NLRP3 inflammasome transient paralysis observed during sepsis.[23] Additionally, these data suggest that bone marrow stem cells, responsible for neutrophil generation, are not altered in recovered COVID-19 patients.

An interesting hypothesis that might explain the heterogeneous cell response of the NLRP3 inflammasome is differential expression of NLRP3 in COVID-19 patients. Supporting this hypothesis, single-cell RNA-sequencing data comparing healthy donors to COVID-19 patients showed increased NLRP3 expression in monocytes.[32,33] Further studies will be necessary to precisely investigate the transcriptional regulation of inflammasome components with regard to the different myeloid cell population and the severity of the disease.

We here identified the C1B score by combining the parameters our test determined as the most correlated with COVID-19 severity. The analysis of these parameters allowed us to identify the C1B score. For patients included in our cohort, we found that the C1B score predicted the worsening of a patient's clinical status in the next 2 days as well as their final outcome, using a rapid flow cytometry–based test requiring only 100 μL of blood. We believe that the test should be validated in various conditions and geographic areas for the strength of its prognosis value in various contexts.

By monitoring caspase-1 activation directly in the myeloid cells of COVID-19 patients, we provide first evidence of the involvement of myeloid cells, caspase-1, and the NLRP3 inflammasome complex during COVID-19 disease. We believe that our results will serve as a springboard for future development of a clinical test to be used for personalized medicine or to analyze biomarkers to predict COVID-19 severity. Such a test would have an important impact on the management of COVID-19 patient flow at hospitals during the pandemic period and would be helpful in therapeutic decisions involving immunomodulatory drugs.

## Acknowledgments

The authors acknowledge Jeanick Brisswalter and the staff of the University Côte d'Azur for their support. The authors thank Irit Touitou for help in data recording. The authors also thank the REDPIT Association and the members of the Centre Hospitalier Universitaire (CHU) de Nice Microbiology Department as well as the Emergency and Intensive Care Units of Nice University Hospital and Hospital of Cannes. The authors acknowledge FIP l'Objet PUB and Beijing Genomics Institute for their kind gift of surgical masks. The authors are indebted to the Etablissement Français du Sang of Marseille (EFS PACA–Corse, M. Sebastien Linossier) for providing human blood from healthy donors.

This work was supported by Université Côte d'Azur, IDEX Action 6.1 Fonds Excellence COVID-19, Inserm, and CHU de Nice (University Hospital of Nice) for regulatory and ethical submission.

## Authorship

Contribution: J. Courjon, D.C., J.D., J. Contenti, and A.R. recruited patients and collected patient samples; J. Courjon, O.D., D.C., C.T., A.D., C.L., S.V., R.L., C.P.-E., G.G., S.I., and A.J. performed and analyzed experiments; J. Courjon, O.D., A.R., L. Bailly, L.Y.-C., P.M., O.V., J.D., V.G., M.C., P.A., S.I., A.J., and L. Boyer interpreted the results; J. Courjon, O.D., and L. Boyer wrote the manuscript; L.Y.-C., S.I., P.A., and A.J. reviewed the manuscript; all authors edited the manuscript; and A.J. and L. Boyer supervised the project.

Conflict-of-interest disclosure: The authors declare no competing financial interests.

ORCID profiles: O.D., 0000-0001-7076-969X; A.R., 0000-0003-1360-2513; L. Bailly, 0000-0002-6565-8212; D.C., 0000-0002-7186-2818; J. Contenti, 0000-0002-1532-6180; S.V., 0000-0002-6102-9873; C.P.-E., 0000-0002-6192-3293; O.V., 0000-0001-7719-5836; J.D., 0000-0002-2681-8260; M.C., 0000-0001-5485-1511; P.A., 0000-0002-2481-8275; L. Boyer, 0000-0002-1375-1706.

Correspondence: Laurent Boyer, Centre Méditerranéen de Médecine Moléculaire, INSERM U1065, Bâtiment ARCHIMED, Hôpital l'Archet, 06204 Nice Cedex 3, France; e-mail: laurent.boyer@univ-cotedazur.fr.

## References

1. Li Q, Guan X, Wu P, et al. Early transmission dynamics in Wuhan, China, of novel coronavirus-infected pneumonia. *N Engl J Med*. 2020;382(13):1199-1207.
2. Chan JF, Yuan S, Kok KH, et al. A familial cluster of pneumonia associated with the 2019 novel coronavirus indicating person-to-person transmission: a study of a family cluster. *Lancet*. 2020;395(10223):514-523.
3. Jamilloux Y, Henry T, Belot A, et al. Should we stimulate or suppress immune responses in COVID-19? Cytokine and anti-cytokine interventions. *Autoimmun Rev*. 2020;19(7):102567.
4. Vabret N, Britton GJ, Gruber C, et al; Sinai Immunology Review Project. Immunology of COVID-19: current state of the science. *Immunity*. 2020;52(6):910-941.
5. Lamkanfi M, Dixit VM. Mechanisms and functions of inflammasomes. *Cell*. 2014;157(5):1013-1022.
6. Iwasaki A, Medzhitov R. Control of adaptive immunity by the innate immune system. *Nat Immunol*. 2015;16(4):343-353.
7. Medzhitov R. Approaching the asymptote: 20 years later. *Immunity*. 2009;30(6):766-775.
8. Takeuchi O, Akira S. Innate immunity to virus infection. *Immunol Rev*. 2009;227(1):75-86.
9. Chow KT, Gale M Jr., Loo YM. RIG-I and other RNA sensors in antiviral immunity. *Annu Rev Immunol*. 2018;36:667-694.
10. Huang C, Wang Y, Li X, et al. Clinical features of patients infected with 2019 novel coronavirus in Wuhan, China. *Lancet*. 2020;395(10223):497-506.
11. Wen W, Su W, Tang H, et al. Immune cell profiling of COVID-19 patients in the recovery stage by single-cell sequencing [published correction appears in *Cell Discov*. 2020;6:41]. *Cell Discov*. 2020;6:31.
12. Conti P, Ronconi G, Caraffa A, et al. Induction of pro-inflammatory cytokines (IL-1 and IL-6) and lung inflammation by coronavirus-19 (COVI-19 or SARS-CoV-2): anti-inflammatory strategies. *J Biol Regul Homeost Agents*. 2020;34(2):327-331.
13. Vabret N, Samstein R, Fernandez N, Merad M; Sinai Immunology Review Project; Trainees; Faculty. Advancing scientific knowledge in times of pandemics. *Nat Rev Immunol*. 2020;20(6):338.
14. Chen IY, Moriyama M, Chang MF, Ichinohe T. Severe acute respiratory syndrome coronavirus viroporin 3a activates the NLRP3 inflammasome. *Front Microbiol*. 2019;10:50.
15. Merad M, Martin JC. Pathological inflammation in patients with COVID-19: a key role for monocytes and macrophages [published corrections appear in *Nat Rev Immunol*. 2020;20(7):448]. *Nat Rev Immunol*. 2020;20(6):355-362.
16. Deftereos SG, Siasos G, Giannopoulos G, et al. The Greek study in the effects of colchicine in COvid-19 complications prevention (GRECCO-19 study): rationale and study design. *Hellenic J Cardiol*. 2020;61(1):42-45.
17. Parisi V, Leosco D. Precision medicine in COVID-19: IL-1β a potential target. *JACC Basic Transl Sci*. 2020;5(5):543-544.
18. Cheong DHJ, Tan DWS, Wong FWS, Tran T. Anti-malarial drug, artemisinin and its derivatives for the treatment of respiratory diseases. *Pharmacol Res*. 2020;158:104901.
19. Rodrigues TS, de Sá KSG, Ishimoto AY, et al. Inflammasomes are activated in response to SARS-CoV-2 infection and are associated with COVID-19 severity in patients. *J Exp Med*. 2021;218(3):e20201707.
20. Ferreira AC, Soares VC, de Azevedo-Quintanilha IG, et al SARS-CoV-2 induces inflammasome-dependent pyroptosis and downmodulation of HLA-DR in human monocytes. www.medrxiv.org/content/10.1101/2020.08.25.20182055v2. Accessed 10 January 2021.
21. World Health Organization (WHO). *Clinical Management of COVID-19: Interim Guidance*. Geneva, Switzerland: WHO; 2020.
22. Frat JP, Thille AW, Mercat A, et al; REVA Network. High-flow oxygen through nasal cannula in acute hypoxemic respiratory failure. *N Engl J Med*. 2015;372(23):2185-2196.
23. Martínez-García JJ, Martínez-Banaclocha H, Angosto-Bazarra D, et al. P2X7 receptor induces mitochondrial failure in monocytes and compromises NLRP3 inflammasome activation during sepsis. *Nat Commun*. 2019;10(1):2711.

24. Zhao Y, Qin L, Zhang P, et al. Longitudinal COVID-19 profiling associates IL-1RA and IL-10 with disease severity and RANTES with mild disease. *JCI Insight*. 2020;5(13):e139834.

25. Groslambert M, Py BF. Spotlight on the NLRP3 inflammasome pathway. *J Inflamm Res*. 2018;11:359-374.

26. Grieshaber-Bouyer R, Nigrovic PA. Neutrophil heterogeneity as therapeutic opportunity in immune-mediated disease. *Front Immunol*. 2019;10:346.

27. Cavalli G, De Luca G, Campochiaro C, et al. Interleukin-1 blockade with high-dose anakinra in patients with COVID-19, acute respiratory distress syndrome, and hyperinflammation: a retrospective cohort study. *Lancet Rheumatol*. 2020;2(6):e325-e331.

28. Pillay J, Ramakers BP, Kamp VM, et al. Functional heterogeneity and differential priming of circulating neutrophils in human experimental endotoxemia. *J Leukoc Biol*. 2010;88(1):211-220.

29. Silvin A, Chapuis N, Dunsmore G, et al. Elevated calprotectin and abnormal myeloid cell subsets discriminate severe from mild COVID-19. *Cell*. 2020; 182(6):1401-1418.e18.

30. Schulte-Schrepping J, Reusch N, Paclik D, et al; Deutsche COVID-19 OMICS Initiative (DeCOI). Severe COVID-19 is marked by a dysregulated myeloid cell compartment. *Cell*. 2020;182(6):1419-1440.e23.

31. Vitte J, Diallo AB, Boumaza A, et al. A granulocytic signature identifies COVID-19 and its severity. *J Infect Dis*. 2020;222(12):1985-1996.

32. Immunological Genome Project. ImmGen at 15. *Nat Immunol*. 2020;21(7):700-703.

33. Wilk AJ, Rustagi A, Zhao NQ, et al. A single-cell atlas of the peripheral immune response in patients with severe COVID-19. *Nat Med*. 2020;26(7): 1070-1076.

# Discussion

## 1. Détection de l'activité des facteurs de virulence ciblant les Rho-GTPases

La détection des microbes et plus particulièrement la détermination de leur pouvoir pathogène par le système immunitaire inné est essentielle pour la mise en place d'une réponse immunitaire adaptée. En effet, une trop faible activation du système immunitaire ne permettrait pas l'élimination des pathogènes alors qu'une réponse inflammatoire trop importante mènerait à des dommages de l'hôte.

La théorie des PRRs permet au système immunitaire d'estimer la quantité de microbes. Cependant, ce paramètre ne permet pas d'établir si le microbe est virulent ou non. Plusieurs modèles sont venus compléter ce lui des PRRs chez les métazoaires. Il a été proposé la notion de la détection de pattern de pathogénicité (Vance et al., 2009), la notion de la reconnaissance des DAMPs (Matzinger, 2002b) ou plus récemment de la détection de l'activité des facteurs de virulence (Fischer et al., 2020; Stuart et al., 2013). Chez la plante, en parallèle de l'immunité induite par les PRRs nommée « pattern-triggered immunity », il existe un système capable de détecter l'activité des facteurs de virulence et ainsi de déterminer la virulence du microbe et y répondre de manière proportionnée. Cette théorie nommée « effector-triggered immunity » fait intervenir des gènes de résistance codant pour des protéines de type NB-LRR (nucleotide-binding, leucine-rich repeat) qui partagent une similarité de structure frappante avec les récepteurs formant des inflammasomes chez les métazoaires (Jones et al., 2016). Il existe une autre similarité, ces protéines forment également un complexe, nommé résistosome, capable de s'ancrer dans la membrane plasmique pour induire une mort cellulaire protectrice (Wang et al., 2019). Il semblerait donc que ce mécanisme de défense pendant l'infection soit conservé au cours de l'évolution.

L'étude de la détection des toxines activant les Rho-GTPases, et plus particulièrement la toxine CNF1 des *E. coli* uropathogènes, nous a permis de mieux comprendre comment le système immunitaire distingue les bactéries pathogènes des non-pathogènes. Nous avons pu montrer qu'en activant la GTPase Rac2, CNF1 induit l'activation de la kinase Pak1 qui phosphoryle le récepteur NLRP3 sur la Thr659 afin de permettre son activation et son oligomérisation en un inflammasome. La Thr659 est hautement conservée au cours de l'évolution et nous avons pu montrer l'importance de ce résidu dans l'activation de l'inflammasome NLRP3 par CNF1 dans des macrophages primaires humains.

L'inflammasome NLRP3 est régulé par de nombreuses modifications post-traductionelles (ubiquitination, SUMOylation, phosphorylation…). Ces modifications interviennent au cours du priming, de l'activation ou après l'activation comme signal de rétrocontrôle négatif et semblent être régulées de façon spatiotemporelle. Il serait intéressant d'étudier la cinétique et la localisation subcellulaire de la phosphorylation de la Thr659 de NLRP3 par la kinase Pak1. La phosphorylation de ce résidu semble se produire en amont du recrutement de la protéine régulatrice Nek7 puisque la mutation Thr659Ala

empêche ce recrutement. La Thr659 est située dans un domaine nommé « LRR de transition » (652-742) en amont des LRR classiques (Hochheiser et al., 2021). Cependant la fonction de ce domaine n'est pas encore connue. La mutation Thr659Ala pourrait dénaturer la structure de NLRP3. Cependant cela est peu probable puisque le mutant Thr659Asp (phospho-mimétique) est actif et la mutation Ser658Ala (résidu voisin de la Thr659, non publié) n'affecte pas l'activité de NLRP3.

Contrairement à de nombreux activateurs de l'inflammasome NLRP3, nous n'avons pas observé avec la toxine CNF1 d'activation de la GSDMD ni de mort par pyroptose. De plus, la sécrétion d'IL-1ß en aval de l'activation de NLRP3 par CNF1 est indépendante de la GSDMD. Nous avons également montré que la clairance bactérienne au cours de la bactériémie est dépendante de l'IL-1ß (Diabate et al., 2015) mais indépendante de la GSDMD. Cela pose deux questions : comment l'IL-1ß est-il sécrété lors de la stimulation par CNF1 et pourquoi Caspase-1 activée par CNF1 ne clive pas la GSDMD ?

- *Comment l'IL-1ß est-il sécrété ?*

La toxine CNF1 n'est pas le premier exemple d'activateur d'inflammasome n'induisant pas de pyroptose. L'activation non canonique de l'inflammasome NLRP3 par des phospholipides oxydés (oxPAPC) ou par la *N*-acetylglucosamine (dérivée du peptidoglycane) induit une sécrétion d'IL-1ß dépendante de la GSDMD mais n'induisant pas de pyroptose des cellules (Evavold et al., 2018; Wolf et al., 2016; Zanoni et al., 2016). Les auteurs ont nommé cet état « hyperactivation » (Evavold et al., 2018; Zanoni et al., 2016). Cependant, dans le cas de CNF1, la sécrétion d'IL-1ß ne semble pas impliquer ce mécanisme puisque les macrophages invalidés pour la GSDMD sont toujours capables de sécréter l'IL-1ß. Nous n'observons pas d'entrée d'iodure de propidium (PI) dans les macrophages traités par CNF1 cependant, cela ne signifie pas qu'une autre GSDM ne puisse pas être à l'origine de la sécrétion d'IL-1ß. En effet, dans l'étude de Wolf et al., les auteurs n'ont pas observé d'entrée de PI alors qu'il a été ensuite montré que la GSDMD était impliquée dans la sécrétion d'IL-1ß en aval de la détection de *N*-acetylglucosamine sans pyroptose (Evavold et al., 2018; Wolf et al., 2016).

D'autres mécanismes, indépendants d'un pore de GSDM, pourraient être impliqués dans la sécrétion d'IL-1ß comme la fusion de lysosomes ou de vésicules d'autophagie avec la membrane plasmique, la libération d'exosomes, ou encore la libération de microvésicules (Figure 15). Il a notamment été montré que l'IL-1ß mature (chargée positivement) est relocalisée à la membrane plasmique dans des ondulations membranaires riches en PIP2 (phosphatidylinositol-4,5-bisphosphate). Ce mécanisme serait impliqué dans la sécrétion lente de l'IL-1ß de façon GSDMD-indépendante (Monteleone et al., 2018). En activant la Rho-GTPase Rac, la toxine CNF1 induit des ondulations membranaires qui pourraient favoriser ce phénomène (Ridley et al., 1992). De plus, les Rho-GTPases Cdc42 et Rac2,

activées par CNF1, ont été montrées pour jouer un rôle dans l'exocytose de granules chez les mastocytes, neutrophiles et éosinophiles (Brown et al., 1998; Mitchell et al., 2008; Shamri et al., 2019).

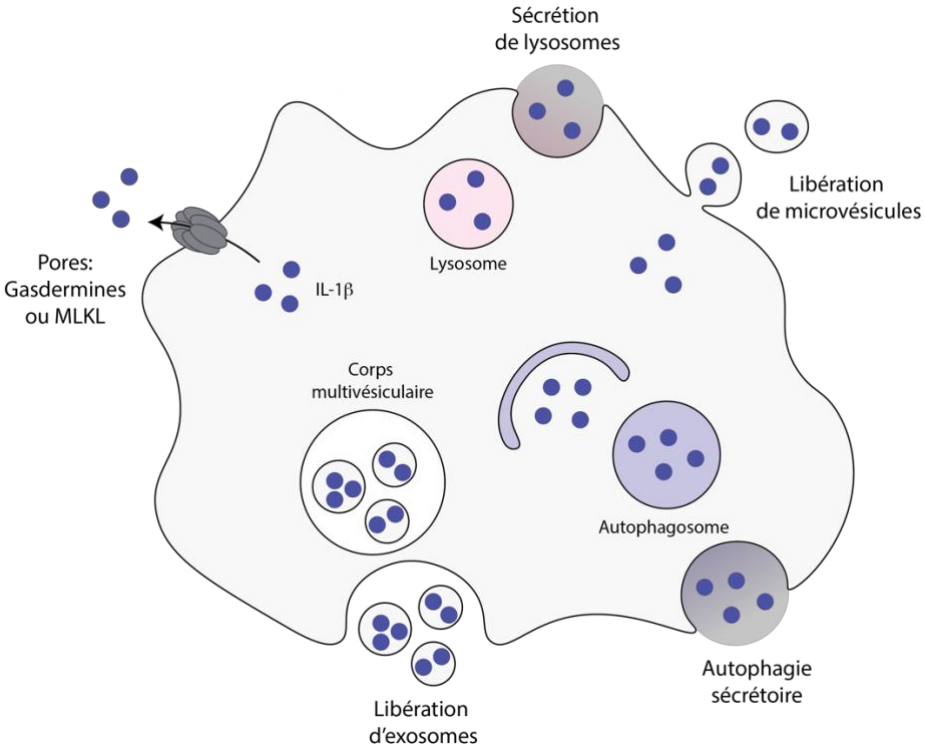


*Figure 15 : Mécanismes de sécrétion potentiels de l'IL-1ß*

Schéma adapté de (Monteleone et al., 2015)

- *Pourquoi la Caspase-1 active ne clive pas la GSDMD ?*

Contrairement à d'autres stimuli menant à la pyroptose ou à l'hyperactivation, nous n'avons pas détecté de clivage de la GSDMD dans les macrophages traités avec la toxine CNF1. L'absence de détection de ce clivage peut d'une part être dû au fait que le signal en western-blot soit en dessous du seuil de détection de l'anticorps et d'autre part que la GSDMD n'est en réalité pas clivée. L'activation de la Caspase-1 induite en aval de la détection de la toxine CNF1 que nous avons observé est faible quand elle est comparée à d'autres activateurs comme l'ATP ou la Nigéricine. Cela pourrait expliquer pourquoi le pool de Caspase-1 active est suffisant pour cliver la pro-IL-1ß mais insuffisant pour induire un clivage de la GSDMD. Pour cela, il faudrait que la Caspase-1 ait une meilleure affinité pour la pro-IL-1ß que pour la GSDMD. Une autre hypothèse serait que CNF1 induise l'activation de voies de signalisation anti-pyroptotique, cependant le pré-traitement des macrophages avec la toxine CNF1 puis l'ajout de Nigéricine ne réduit pas la pyroptose induite par la Nigéricine.

*D'un point de vue évolutif…*

Les récepteurs formant des inflammasomes de type NLRP, NLRC, Pyrin ou AIM2 sont classifiés comme des récepteurs de motifs microbiens (PRR). Cependant, tous les récepteurs formant un inflammasome ne semblent pas correspondre à cette classification. En effet, alors que NLRP6, AIM2, et NLRC4 détectent des motifs microbiens par liaison directe (Figure 16A), d'autres récepteurs comme NLRP3, Pyrin et NLRP1/1b détectent l'activité des facteurs de virulence microbiens et ne semblent pas correspondre à la définition d'un PRR mais plutôt à celle d'une protéine de résistance comme celles trouvées chez les plantes.

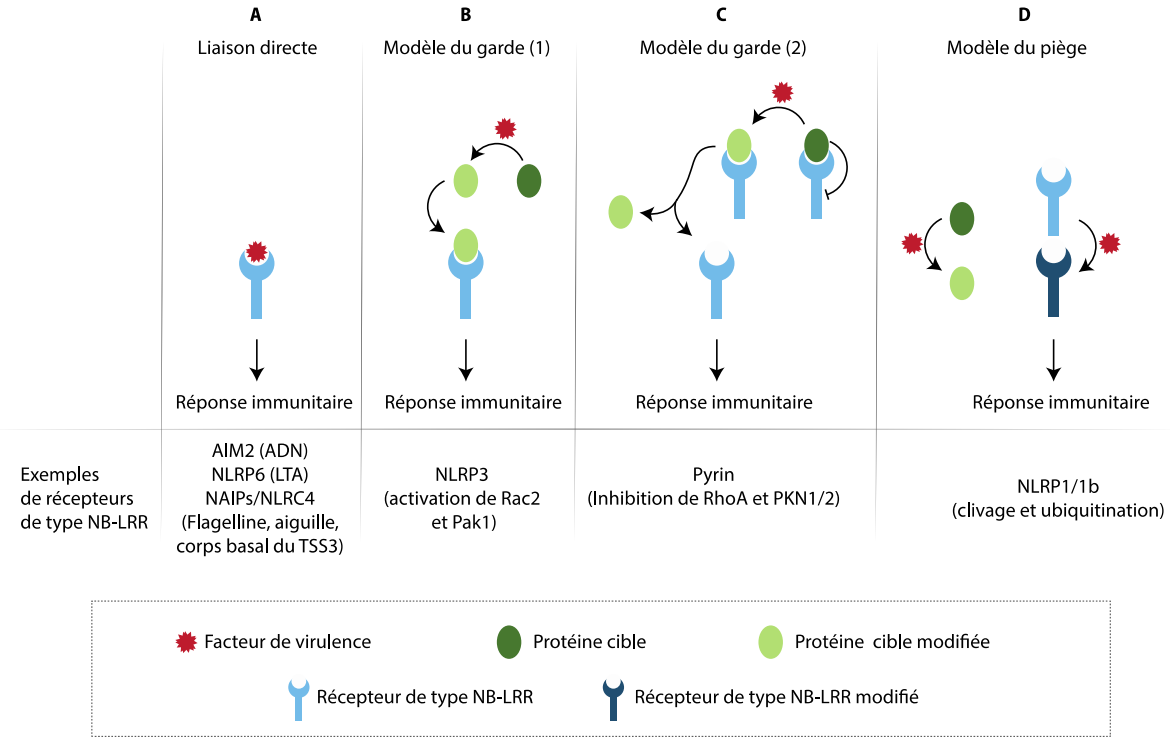


*Figure 16 : Immunité médiée par les effecteurs (ETI) : des plantes aux métazoaires*
Schéma adapté de (Stuart et al., 2013). Les exemples de récepteurs concernent les mammifères.

Chez les plantes, les protéines de type NB-LRR sont classifiées en fonction de leur mécanisme de détection du danger (Figure 16) (Khan et al., 2016). La compréhension du mécanisme de détection de la virulence microbienne par les inflammasomes indique que ces modes de détection des facteurs de virulence semblent être conservés (Figure 16). Plus particulièrement, la détection des facteurs de virulence ciblant les Rho-GTPases implique deux mécanismes distincts mais permettant de surveiller l'activation anormale des Rho-GTPases. Premièrement, la détection de l'inhibition microbienne de RhoA semble correspondre au deuxième modèle de garde (Figure 16C). En effet, à l'état basal, Pyrin est maintenu inactif grâce à l'activation de RhoA qui active ces effecteurs PKN1/2 qui phosphorylent Pyrin,

permettant son interaction avec les protéines chaperonnes 14-3-3 qui maintiennent le récepteur inactif (Jamilloux et al., 2018). L'inactivation de RhoA par des facteurs de virulence libère Pyrin qui peut alors s'activer (Figure 17). Deuxièmement, nous avons pu montrer que l'activation de la Rho-GTPase Rac2 par des toxines bactériennes mène à l'activation des kinases effectrices Pak1/2 qui phosphorylent NLRP3 pour l'activer (Dufies et al., 2021). Cette détection semble correspondre au premier modèle de garde (Figure 16B). Il est intéressant de noter que la détection des toxines ciblant les Rho-GTPases fait intervenir des phosphorylations qui dans un cas sont inhibitrices et dans l'autre activatrices (Figure 17).

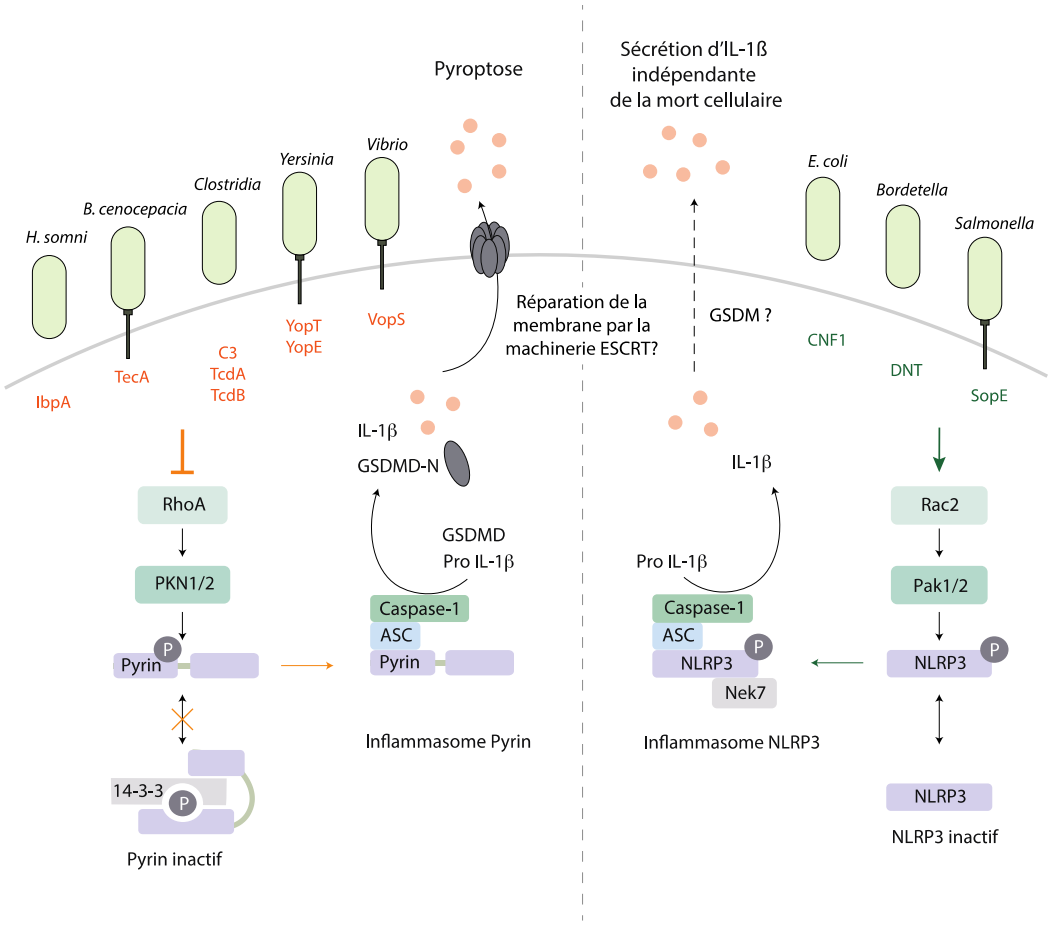


*Figure 17 : Détection de la modification des Rho-GTPases par les inflammasomes Pyrin et NLRP3*

Schéma adapté de (Dufies and Boyer, 2021).

Il semble y avoir une co-évolution entre l'hôte et les *Escherichia coli* uropathogènes correspondant au modèle en zig-zag initialement décrit chez les plantes (Jones and Dangl, 2006). Le modèle en zig-zag dérive de l'hypothèse de « la reine rouge » mentionnant que la co-évolution peut paraître comme une course à l'armement dont la forte pression de sélection maintient une co-évolution étroite. Le modèle en zig-zag stipule que face à l'infection par un microbe, l'hôte a mis en place le système de détection des MAMPs par les PRRs (PTI), puis le pathogène a cherché à inhiber la réponse immunitaire induite en modulant l'activité des protéines de l'hôte avec des effecteurs, rendant l'hôte susceptible. L'évolution

aurait sélectionné chez l'hôte un système de détection de ces effecteurs, correspondant à la théorie de l'ETI.

Nous pouvons retrouver ce modèle en zig-zag dans la relation hôte – *Escherichia coli* (Figure 18A). En effet, les MAMPs associés à *E. coli* sont détectés par les PRRs, rendant l'hôte résistant. Cependant l'activation des Rho-GTPases Rac, Cdc42 et Rho par la toxine CNF1 inhibe la phagocytose des bactéries par les phagocytes professionnels (Hofman et al., 2000). Avec l'évolution, un système de détection de l'activation anormale des Rho-GTPases impliquant l'inflammasome NLRP3 aurait été sélectionné en permettant à l'hôte de devenir résistant. Le gène codant pour CNF1 est localisé dans un opéron (*hlyCABD*) codant également pour l'hémolysine $\alpha$ (HlyA). Il a été montré que l'hémolysine $\alpha$ inhibe la réponse anti-virulence induite par la toxine CNF1 (Diabate et al., 2015). Il est important de noter que chez les souches d'*E. coli* uropathogènes retrouvées en clinique, la toxine CNF1 est systématiquement co-exprimée avec l'hémolysine $\alpha$, conférant un avantage à la bactérie mais rendant l'hôte susceptible (Landraud et al., 2003).

Certaines bactéries comme *Salmonella* ou *Yersinia* possèdent à la fois des facteurs de virulence qui inhibent les RhoGTPases et d'autres qui les activent. Certains mécanismes d'inhibition/activation sont réversibles (GEF, GAP, GDI bactériennes) alors que d'autres sont irréversibles (ADP-ribosylation, transglutamination, déamidation, clivage du motif CAAX…). D'un point de vue évolutif ces différences *pourrait* s'expliquer par une adaptation mutuelle entre l'hôte et le pathogène. D'une part le pathogène modulerait l'activation des RhoGTPases pour se disséminer, puis le pathogène pourrait contrecarrer cette activation/inhibition des Rho-GTPases afin d'éviter l'activation d'un inflammasome. Enfin, l'hôte s'adapterait pour détecter cette stratégie de contournement de la réponse immunitaire (Figure 18).

L'étude de la cinétique de la sécrétion des toxines et de l'injection des effecteurs concomitante avec l'étude de l'activation des inflammasomes Pyrin et NLRP3 permettrait d'étudier ce phénomène.

Il a été montré que les toxines Sptp (GAP) et SopE (GEF) de *Salmonella* sont injectées dans la cellule cible simultanément, cependant SopE est plus rapidement dégradé par le protéasome (Kubori and Galán, 2003). En activant les Rho-GTPases Rho, Rac et Cdc42, SopE induit des ondulations membranaires nécessaires à la phagocytose des Salmonelles par les cellules épithéliales. Cependant nous avons montré que l'activation de Rac2 induit l'activation de l'inflammasome NLRP3. SopE est alors dégradé et Sptp, ayant une demi-vie plus longue, inhibe les Rho-GTPases Rac et Cdc42. Il est intéressant de noter que Sptp n'inhibe pas RhoA et donc ne devrait pas activer l'inflammasome Pyrin (Figure 18B).

*Yersinia* est l'exemple le plus frappant d'une potentielle co-évolution hôte-pathogène. En effet, ce bacille possède 4 facteurs de virulence ciblant les Rho-GTPases, chacun employant un mécanisme différent pour moduler l'activité des Rho-GTPases. Concernant *Yersinia*, mon hypothèse est que dans

un premier temps les GAP et GDI bactériennes YopE et YopO inhiberait Rho, Rac et Cdc42 afin de d'augmenter la perméabilité de la barrière épithéliale intestinale et ainsi de permettre la dissémination bactérienne (Figure 18C). Cependant, l'inhibition de RhoA mènerait à l'activation de l'inflammasome Pyrin. *Yersinia* pourrait alors injecter CNFY, une déamidase homologue à CNF1, qui activerait constitutivement les GTPases Rho, Rac et Cdc42. Cependant, cette modification activerait cette fois l'inflammasome NLRP3.

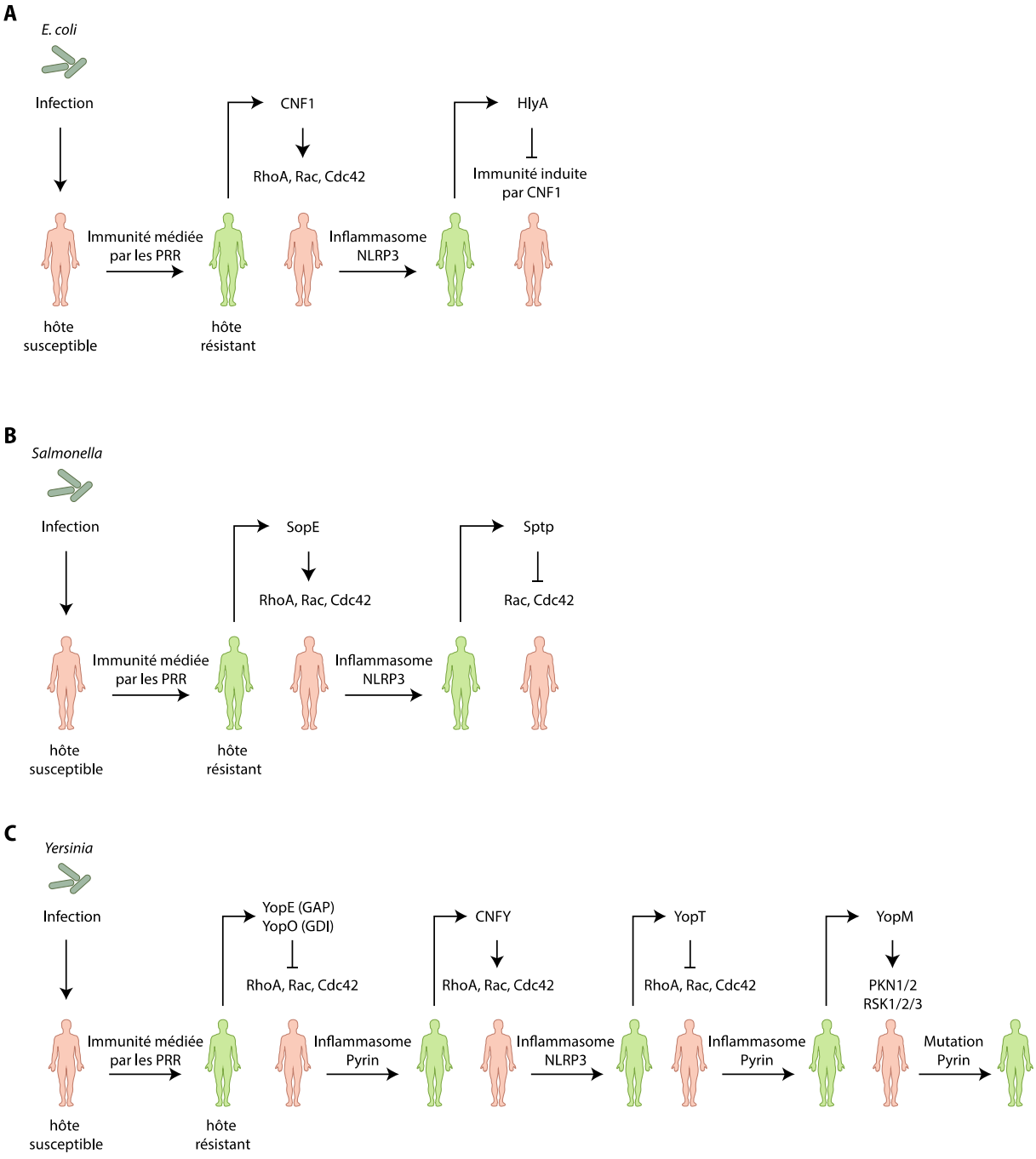


*Figure 18 : Modèle en zig-zag de l'évolution hôte-pathogène impliquant les Rho-GTPases*

Schéma inspiré de (Stuart et al., 2013).

Modèles en zig-zag concernant (A) les *E. coli* uropathogènes, (B) *Salmonella* et (C) *Yersinia*.

La déamidation étant une modification irréversible, seul un clivage du motif CAAX permettant aux Rho-GTPases de s'ancrer à la membrane plasmique afin d'interagir avec leurs effecteurs permettrait de contrecarrer l'action de CNFY. Ce serait le rôle de la protéase YopT qui inhiberait Rac mais également RhoA donc activerait l'inflammasome Pyrin. Cependant, *Yersinia* possède l'effecteur YopM qui active directement PKN1/2 et RSK1/2/3 pour inhiber Pyrin alors même que RhoA est inactivé (Chung et al., 2016; Park et al., 2020; Ratner et al., 2016).

Au cours de l'évolution, des mutations de gènes impliqués dans l'ETI et ayant conféré un avantage à l'hôte ont été sélectionnées. Cependant, certaines de ces mutations sont aujourd'hui associées à des pathologies auto-inflammatoires. C'est notamment le cas de mutations du gène *mefv* codant pour Pyrin. En effet, des mutations du domaine B30.2 de Pyrin conférant une résistance à *Yersinia* auraient été sélectionnées au cours d'épidémies de peste bubonique dans le bassin méditerranéen. Aujourd'hui, ces mutations sont associées à des cas de fièvre méditerranéenne familiale (FMF) (Park et al., 2020).

Des mutations associées aux Rho-GTPases sont également à l'origine pathologies affectant le système immunitaire (El Masri and Delon, 2021; Hashim and Ahmad Mokhtar, 2021). Ces mutations n'ont pas été associées à une co-évolution hôte-pathogène, mais il est intéressant de considérer cette possibilité.

Les Rho-GTPases sont situées au carrefour de grandes voies de signalisation cellulaire et représentent donc une cible idéale pour les bactéries pathogènes. L'étude de la détection de l'activité des facteurs de virulence ciblant les Rho-GTPases indique qu'il existe chez les mammifères une ETI responsable de la surveillance du cycle activation/inhibition anormal des Rho-GTPases.

L'activation de l'inflammasome NLRP3 induite par la toxine CNF1 au cours de la bactériémie joue un rôle bénéfique pour l'hôte en permettant l'élimination bactérienne. Cependant, l'activation des inflammasomes n'est pas systématiquement associée à un bénéfice pour l'hôte et peut parfois être à l'origine d'une inflammation délétère comme dans les pathologies auto-inflammatoires ou encore au cours du sepsis.

### 2. Activation de l'inflammasome NLRP3 au cours du COVID-19

Les premières études de la réponse immunitaire au cours du COVID-19 ont établi une élévation plasmatique de cytokines liées aux inflammasomes telles que l'IL-1ß, l'IL-18 ou encore l'IL-1RA chez les patients présentant une forme sévère (Del Valle et al., 2020; Lucas et al., 2020; Rodrigues et al., 2021; Theobald et al., 2021; Vora et al., 2021).

A l'aide de la sonde FAM-FLICA-fmk nous avons analysé l'activation de la Caspase-1 au sein des cellules myéloïdes circulantes. Nous n'avons pas observé de différence d'activation de la Caspase-1 au sein des monocytes circulants, que ce soit en fonction de l'infection des patients par le SARS-CoV-2 ou de la

sévérité de la maladie. D'autres études réalisées sur la même période ont néanmoins détecté une activation de la Caspase-1 et la formation de speck contenant l'adaptateur ASC et le récepteur NLRP3 dans les cellules mononuclées circulantes (PBMC) des patients infectés par le SARS-CoV-2 (Rodrigues et al., 2021). Il existe une différence majeure entre ces deux études pouvant être à l'origine de leur divergence en termes d'activation d'un inflammasome. En effet, au cours de notre étude, nous avons analysé l'activation de la Caspase-1 en incubant la sonde FAM-FLICA-fmk directement en sang total puis analysé l'activation de la Caspase-1 dans les différentes populations cellulaires par cytométrie en flux tandis que dans l'étude montrant une activation de la Caspase-1, les auteurs isolent les PBMCs par gradient de centrifugation (Ficoll) avant d'incuber les cellules avec la sonde FAM-FLICA-fmk. D'une part, la fraction contenant les PBMC regroupe plusieurs types cellulaires (monocytes, cellules dendritiques, lymphocytes B et T, cellules NK) et sa composition varie en fonction de l'état physiologique du patient. En effet, les granulocytes sont normalement absents de cette fraction mais lors d'états inflammatoires, il a été décrit que des neutrophiles de basse densité sont retrouvés dans la fraction « PBMC » (Silvestre-Roig et al., 2019). D'autre part, l'isolation des PMBC par gradient de centrifugation n'est pas neutre vis-à-vis des cellules. Il est donc difficile de comparer les résultats que nous avons obtenus avec ceux obtenus au cours de l'étude menée par Rodrigues et al.

D'autre part, nous avons pu montrer que les monocytes non classiques, en plus d'être meilleurs répondeurs à la Nigéricine chez les patients sévères, étaient fortement diminués dans la circulation. La proportion diminuée de ces cellules au niveau sanguin pourrait avoir plusieurs explications : la mortalité de ces cellules ou encore une infiltration tissulaire. En effet, ces cellules pourraient mourir par pyroptose après une activation facilitée de l'inflammasome NLRP3. De plus, une infiltration de monocytes intermédiaires et non classiques dans les voies respiratoires basses a été observée chez les patients atteints d'une forme sévère de COVID-19 (Sánchez-Cerrillo et al., 2020). Du fait de l'activation facilitée de l'inflammasome NLRP3, ces cellules pourraient être à l'origine de l'activation de cet inflammasome observé dans les poumons des patients atteints de forme sévères (Rodrigues et al., 2021).

Concernant les granulocytes, nous avons observé, en accord avec d'autres études, une diminution de la proportion des éosinophiles et une forte augmentation de la proportion de neutrophiles et plus particulièrement de neutrophiles immatures chez les patients COVID-19 sévères (Carissimo et al., 2020; Combadière et al., 2021; Lourda et al., 2021; Schulte-Schrepping et al., 2020; Silvin et al., 2020; Wilk et al., 2020). Cela est également observé au cours du sepsis bactérien et est dû à une granulopoïèse d'urgence (Boettcher and Manz, 2017; Yvan-Charvet and Ng, 2019). Des études ont observé une augmentation de la NETose intravasculaire et pulmonaire au cours du COVID-19 sévère (Middleton et al., 2020; Radermecker et al., 2020; Veras et al., 2020). La granulopoïèse d'urgence observée pourrait venir combler le pool de neutrophiles morts par NETose. Plusieurs signaux décrits pour être à l'origine

de l'induction de la granulopoïèse d'urgence au cours du sepsis comme le G-CSF, GM-CSF ou encore l'IL-6 et l'IL-1ß sont augmentés au cours du COVID-19 (Cabaro et al., 2021; Sinha et al., 2021).

Il a été décrit qu'au cours du sepsis bactérien, les neutrophiles immatures présentent des fonctions altérées comme une diminution de la production de ROS et une élimination bactérienne altérée (Hotchkiss et al., 2013). Chez les patients sévères, les neutrophiles immatures présentaient une perte d'activation de l'inflammasome NLRP3 induite par la Nigéricine alors que ces cellules répondaient à la Nigéricine chez les sujets sains et les patients atteints d'une forme modérée de COVID-19. Cela semble indiquer que ce n'est pas seulement l'immaturité de ces cellules qui est responsable de leur anergie face à la stimulation par la Nigéricine. L'anergie des neutrophiles immatures spécifiquement chez les patients atteints de COVID-19 sévère pourrait s'expliquer par un défaut intrinsèque du patient ou bien pourrait être provoquée par l'infection. Nous avons pu montrer que les patients guéris d'un COVID-19 sévère récupèrent leur capacité d'activation de l'inflammasome NLRP3. Il semblerait donc que cette incapacité d'activation de l'inflammasome NLRP3 au sein des neutrophiles immatures pourrait être due à l'infection. Cela pourrait s'inscrire dans l'immunosuppression observée dans un second temps au cours du sepsis (Hotchkiss et al., 2013).

Nous avons utilisé les principaux paramètres caractérisant les formes sévères de COVID-19 pour établir le score basé sur la mesure de l'activation de la Caspase-1 (C1B). Ce score est significativement plus faible chez les patients ayant une issue défavorable (admission en réanimation ou décès). Il serait nécessaire de valider l'utilisation de ce score au cours d'une étude clinique multicentrique. Cependant, son utilisation pourrait permettre une prise en charge personnalisée des patients.

Une limitation de notre étude est qu'une forte proportion de patients atteints de COVID-19 sévère étaient traités par dexaméthasone, traitement devenu la référence chez les patients COVID-19 hospitalisés atteints d'une pneumonie (The RECOVERY Collaborative Group, 2021). Cependant, lorsque nous analysons les principaux paramètres des patients sévères comme la proportion de monocytes non classiques et de neutrophiles immatures, ou encore l'activation de l'inflammasome NLRP3 par la Nigéricine chez les neutrophiles immatures, la corticothérapie ne semble pas affecter ces paramètres au sein des patients sévères.

---

### *Cibler l'IL-1ß au cours du COVID-19*

Il a été décrit que les patients souffrant d'une forme sévère de COVID-19 présentaient un retard de la production d'IFNs de type I et de l'induction des ISGs. Cela pourrait être en lien avec la production d'IL-1ß observée au cours du COVID-19. En effet, ces cytokines semblent jouer un rôle antagoniste l'une envers l'autre (Mayer-Barber and Yan, 2017). Cette régulation pourrait jouer un rôle dans

l'établissement soit d'une immunité antivirale effective observée chez les patients atteints d'une forme modéré ou bien d'une inflammation excessive retrouvée chez les patients atteints d'une forme sévère. Il serait intéressant de connaître la cinétique des évènements menant à une forme sévère. Est-ce le retard de production d'IFNs de type I qui induit une production d'IL-1ß puis d'autres cytokines pro-inflammatoires ou est-ce la présence excessive d'IL-1ß qui empêche la production d'IFN de type I et la mise en place d'une immunité antivirale adaptée ?

La réponse à cette question permettrait d'administrer des IFNs de type I ou des thérapies ciblant l'IL-1ß au bon moment. Une étude semble indiquer que l'administration d'Anakinra (IL-1RA recombinant) de façon précoce (suite à l'admission du patient) permettrait de réduire la sévérité 7 jours plus tard en comparaison avec le groupe « placebo » (Kyriazopoulou et al., 2021). Cette étude utilise également les taux circulants de suPAR (soluble urokinase plasminogen activator receptor), dont des taux élevés ont été associés à une sévérité accrue, afin de stratifier les patients et d'administrer ou non l'Anakinra. Cependant, certaines études ciblant l'IL-1ß (Anakinra ou anticorps dirigés contre l'IL-1ß – Canakinumab) au cours du COVID-19 n'ont pas démontré d'efficacité du traitement sur l'aggravation de l'état des patients ou sur la mortalité (Caricchio et al., 2021; CORIMUNO-19 Collaborative group, 2021). Ces résultats mitigés pourraient s'expliquer par le moment choisit pour l'administration et semblent renforcer la nécessité de prendre en compte la cinétique de la maladie pour choisir le traitement adapté.

# Conclusion

Au cours d'une infection il est crucial pour l'hôte de mettre en place une réponse immunitaire innée efficace. Cependant cette réponse doit être adaptée au stimuli et contrôlée pour résoudre l'inflammation et éviter les dommages liés à une réponse immunitaire aberrante.

Les Rho-GTPases sont des interrupteurs moléculaires situés au carrefour de grandes voies de signalisations. Pour cette raison, elles sont la cible d'un grand nombre de bactéries pathogènes. La détection des facteurs de virulence ciblant les Rho-GTPases par les inflammasome Pyrin et NLRP3 constitue un nouvel exemple de la capacité des mammifères à déclencher une immunité en réponse à la manipulation des voies de signalisations cellulaires par les bactéries pathogènes. Au cours de l'évolution, deux mécanismes de détection de la dérégulation des Rho-GTPases ont été sélectionnés. Il est saisissant de constater que ces mécanismes surveillent à la fois l'activation et l'inactivation des Rho-GTPases et font intervenir tous deux des inflammasomes dont la régulation semble diamétralement opposée. En effet, la détection de l'inactivation de la GTPase RhoA repose sur l'inhibition de ses kinases effectrices PKN1 et 2 et l'absence de phosphorylation du récepteur Pyrin. A l'inverse, la détection de l'activation de la GTPase Rac2 fait intervenir l'activation de ses kinases effectrices Pak1 et 2 et la phosphorylation du récepteur NLRP3. La découverte de cette ETI surveillant l'état d'activation des Rho-GTPases démontre l'importance d'une régulation contrôlée de ces protéines. Cependant, la sélection de mutations de ces voies au cours de la co-évolution hôte – pathogène s'avère impliquée dans des pathologies auto-inflammatoires comme la fièvre familiale méditerranéenne dans le cas de l'inflammasome Pyrin. Cela démontre que l'activation des inflammasomes n'est pas toujours bénéfique pour l'hôte et qu'il est nécessaire que ceux-ci sont étroitement régulés.

L'hyperinflammation constatée au cours des formes sévères de COVID-19 témoigne de l'importance d'une réponse immunitaire adaptée au cours de l'infection. Au cours des deux dernières années, des études ont suggéré que l'activation des inflammasomes pourraient être, pour partie, à l'origine d'une réponse inflammatoire délétère. Notre étude semble indiquer que la capacité d'activation de l'inflammasome NLRP3 varie en fonction de la sévérité des patients mais également du type cellulaire. Il est aussi probable que cet inflammasome soit activé différemment en fonction de la localisation (compartiment sanguin, voies respiratoires hautes et basses) mais également en fonction de la cinétique de la maladie. La meilleure compréhension de cette régulation spatio-temporelle permettrait de cibler l'inflammasome NLRP3 ou l'IL-1ß/IL-18 de façon localisée et à un moment précis de l'histoire de la maladie.

Les résultats obtenus au cours de ma thèse ont permis une meilleure compréhension de la régulation de la réponse immunitaire innée au cours de l'infection et ouvre la voie vers de nouvelles cibles thérapeutiques. En effet, l'inflammasome NLRP3 est impliqué dans de nombreuses pathologies inflammatoires et infectieuses. La modulation de l'activité de cet inflammasome pourrait permettre dans un cas, de l'inhiber au cours des pathologies où l'hyperinflammation est délétère et dans l'autre cas l'activer afin de stimuler la réponse immunitaire protectrice au cours d'infections. Le sepsis bactérien et viral démontre cependant que l'intensité de cette stimulation devra être finement contrôlée et la fenêtre d'action devra être ciblée spécifiquement dans le temps.

# Bibliographie

Ablasser, A., Goldeck, M., Cavlar, T., Deimling, T., Witte, G., Röhl, I., Hopfner, K.-P., Ludwig, J., and Hornung, V. (2013). cGAS produces a 2′-5′-linked cyclic dinucleotide second messenger that activates STING. Nature *498*, 380–384.

Acosta, M.I., Urbach, S., Doye, A., Ng, Y.-W., Boudeau, J., Mettouchi, A., Debant, A., Manser, E., Visvikis, O., and Lemichez, E. (2018). Group-I PAKs-mediated phosphorylation of HACE1 at serine 385 regulates its oligomerization state and Rac1 ubiquitination. Sci. Rep. *8*, 1410.

Aktories, K. (1997). Bacterial toxins that target Rho proteins. J. Clin. Invest. *99*, 827–829.

Aktories, K., Braun, U., Rösener, S., Just, I., and Hall, A. (1989). The rho gene product expressed in E. Coli is a substrate of botulinum ADP-ribosyltransferase C3. Biochem. Biophys. Res. Commun. *158*, 209–213.

Alexopoulou, L., Holt, A.C., Medzhitov, R., and Flavell, R.A. (2001). Recognition of double-stranded RNA and activation of NF-κB by Toll-like receptor 3. Nature *413*, 732–738.

Alto, N.M., Shao, F., Lazar, C.S., Brost, R.L., Chua, G., Mattoo, S., McMahon, S.A., Ghosh, P., Hughes, T.R., Boone, C., et al. (2006). Identification of a bacterial type III effector family with G protein mimicry functions. Cell *124*, 133–145.

Ambruso, D.R., Knall, C., Abell, A.N., Panepinto, J., Kurkchubasche, A., Thurman, G., Gonzalez-Aller, C., Hiester, A., deBoer, M., Harbeck, R.J., et al. (2000). Human neutrophil immunodeficiency syndrome is associated with an inhibitory Rac2 mutation. Proc. Natl. Acad. Sci. U. S. A. *97*, 4654–4659.

Anand, P.K., Malireddi, R.K.S., Lukens, J.R., Vogel, P., Bertin, J., Lamkanfi, M., and Kanneganti, T.-D. (2012). NLRP6 negatively regulates innate immunity and host defence against bacterial pathogens. Nature *488*, 389–393.

Andersson, U., Wang, H., Palmblad, K., Aveberger, A.C., Bloom, O., Erlandsson-Harris, H., Janson, A., Kokkola, R., Zhang, M., Yang, H., et al. (2000). High mobility group 1 protein (HMG-1) stimulates proinflammatory cytokine synthesis in human monocytes. J. Exp. Med. *192*, 565–570.

Andrei, C., Dazzi, C., Lotti, L., Torrisi, M.R., Chimini, G., and Rubartelli, A. (1999). The secretory route of the leaderless protein interleukin 1beta involves exocytosis of endolysosome-related vesicles. Mol. Biol. Cell *10*, 1463–1475.

Arbeloa, A., Garnett, J., Lillington, J., Bulgin, R.R., Berger, C.N., Lea, S.M., Matthews, S., and Frankel, G. (2010). EspM2 is a RhoA guanine nucleotide exchange factor. Cell. Microbiol. *12*, 654–664.

Asano, T., Boisson, B., Onodi, F., Matuozzo, D., Moncada-Velez, M., Maglorius Renkilaraj, M.R.L., Zhang, P., Meertens, L., Bolze, A., Materna, M., et al. (2021). X-linked recessive TLR7 deficiency in ~1% of men under 60 years old with life-threatening COVID-19. Sci. Immunol. *6*, eabl4348.

Aspenström, P. (1999). The Rho GTPases have multiple effects on the actin cytoskeleton. Exp. Cell Res. *246*, 20–25.

Aubert, D.F., Xu, H., Yang, J., Shi, X., Gao, W., Li, L., Bisaro, F., Chen, S., Valvano, M.A., and Shao, F. (2016). A Burkholderia Type VI Effector Deamidates Rho GTPases to Activate the Pyrin Inflammasome and Trigger Inflammation. Cell Host Microbe *19*, 664–674.

Ausubel, F.M. (2005). Are innate immune signaling pathways in plants and animals conserved? Nat. Immunol. *6*, 973–979.

Ball, D.P., Taabazuing, C.Y., Griswold, A.R., Orth, E.L., Rao, S.D., Kotliar, I.B., Vostal, L.E., Johnson, D.C., and Bachovchin, D.A. (2020). Caspase-1 interdomain linker cleavage is required for pyroptosis. Life Sci. Alliance *3*, e202000664.

Bambouskova, M., Potuckova, L., Paulenda, T., Kerndl, M., Mogilenko, D.A., Lizotte, K., Swain, A., Hayes, S., Sheldon, R.D., Kim, H., et al. (2021). Itaconate confers tolerance to late NLRP3 inflammasome

activation. Cell Rep. *34*, 108756.

Barry, R., John, S.W., Liccardi, G., Tenev, T., Jaco, I., Chen, C.-H., Choi, J., Kasperkiewicz, P., Fernandes-Alnemri, T., Alnemri, E., et al. (2018). SUMO-mediated regulation of NLRP3 modulates inflammasome activity. Nat. Commun. *9*, 3001.

Bastard, P., Rosen, L.B., Zhang, Q., Michailidis, E., Hoffmann, H.-H., Zhang, Y., Dorgham, K., Philippot, Q., Rosain, J., Béziat, V., et al. (2020). Autoantibodies against type I IFNs in patients with life-threatening COVID-19. Science *370*, eabd4585.

Bastard, P., Gervais, A., Le Voyer, T., Rosain, J., Philippot, Q., Manry, J., Michailidis, E., Hoffmann, H.-H., Eto, S., Garcia-Prat, M., et al. (2021). Autoantibodies neutralizing type I IFNs are present in ~4% of uninfected individuals over 70 years old and account for ~20% of COVID-19 deaths. Sci. Immunol. *6*, eabl4340.

Bauernfried, S., Scherr, M.J., Pichlmair, A., Duderstadt, K.E., and Hornung, V. (2021). Human NLRP1 is a sensor for double-stranded RNA. Science.

Beyer, D.K., and Forero, A. (2021). Mechanisms of Antiviral Immune Evasion of SARS-CoV-2. J. Mol. Biol. 167265.

Bhavsar, A.P., Guttman, J.A., and Finlay, B.B. (2007). Manipulation of host-cell pathways by bacterial pathogens. Nature *449*, 827–834.

Bishop, A.L., and Hall, A. (2000). Rho GTPases and their effector proteins. Biochem. J. *348*, 241–255.

Bjanes, E., Sillas, R.G., Matsuda, R., Demarco, B., Fettrelet, T., DeLaney, A.A., Kornfeld, O.S., Lee, B.L., López, E.M.R., Grubaugh, D., et al. (2021). Genetic targeting of Card19 is linked to disrupted NINJ1 expression, impaired cell lysis, and increased susceptibility to Yersinia infection. PLOS Pathog. *17*, e1009967.

Blanco-Melo, D., Nilsson-Payant, B.E., Liu, W.-C., Uhl, S., Hoagland, D., Møller, R., Jordan, T.X., Oishi, K., Panis, M., Sachs, D., et al. (2020). Imbalanced Host Response to SARS-CoV-2 Drives Development of COVID-19. Cell *181*, 1036-1045.e9.

Boettcher, S., and Manz, M.G. (2017). Regulation of Inflammation- and Infection-Driven Hematopoiesis. Trends Immunol. *38*, 345–357.

Bokoch, G.M., and Knaus, U.G. (2003). NADPH oxidases: not just for leukocytes anymore! Trends Biochem. Sci. *28*, 502–508.

Bost, P., Giladi, A., Liu, Y., Bendjelal, Y., Xu, G., David, E., Blecher-Gonen, R., Cohen, M., Medaglia, C., Li, H., et al. (2020). Host-Viral Infection Maps Reveal Signatures of Severe COVID-19 Patients. Cell *181*, 1475-1488.e12.

Boucher, D., Monteleone, M., Coll, R.C., Chen, K.W., Ross, C.M., Teo, J.L., Gomez, G.A., Holley, C.L., Bierschenk, D., Stacey, K.J., et al. (2018). Caspase-1 self-cleavage is an intrinsic mechanism to terminate inflammasome activity. J. Exp. Med. *215*, 827–840.

Boyer, L., Magoc, L., Dejardin, S., Cappillino, M., Paquette, N., Hinault, C., Charriere, G.M., Ip, W.E., Fracchia, S., Hennessy, E., et al. (2011). Pathogen-derived effectors trigger protective immunity via activation of the Rac2 enzyme and the IMD or Rip kinase signaling pathway. Immunity *35*, 536–549.

Brown, G.D., and Gordon, S. (2001). A new receptor for β-glucans. Nature *413*, 36–37.

Brown, A.M., O'Sullivan, A.J., and Gomperts, B.D. (1998). Induction of exocytosis from permeabilized mast cells by the guanosine triphosphatases Rac and Cdc42. Mol. Biol. Cell *9*, 1053–1063.

Broz, P., von Moltke, J., Jones, J.W., Vance, R.E., and Monack, D.M. (2010). Differential requirement for Caspase-1 autoproteolysis in pathogen-induced cell death and cytokine processing. Cell Host Microbe *8*, 471–483.

Brubaker, S.W., Bonham, K.S., Zanoni, I., and Kagan, J.C. (2015). Innate immune pattern recognition: a cell biological perspective. Annu. Rev. Immunol. *33*, 257–290.

Bruno, V.M., Hannemann, S., Lara-Tejero, M., Flavell, R.A., Kleinstein, S.H., and Galán, J.E. (2009). Salmonella Typhimurium Type III Secretion Effectors Stimulate Innate Immune Responses in Cultured Epithelial Cells. PLOS Pathog. *5*, e1000538.

Budunova, I.V., and Mittelman, L.A. (1992). The effect of K+/H+ antiporter nigericin on gap junction permeability. Cell Biol. Toxicol. *8*, 63–73.

Bulgin, R.R., Arbeloa, A., Chung, J.C.S., and Frankel, G. (2009). EspT triggers formation of lamellipodia and membrane ruffles through activation of Rac-1 and Cdc42. Cell. Microbiol. *11*, 217–229.

Bürckstümmer, T., Baumann, C., Blüml, S., Dixit, E., Dürnberger, G., Jahn, H., Planyavsky, M., Bilban, M., Colinge, J., Bennett, K.L., et al. (2009). An orthogonal proteomic-genomic screen identifies AIM2 as a cytoplasmic DNA sensor for the inflammasome. Nat. Immunol. *10*, 266–272.

Burridge, K., and Wennerberg, K. (2004). Rho and Rac Take Center Stage. Cell *116*, 167–179.

Cabaro, S., D'Esposito, V., Di Matola, T., Sale, S., Cennamo, M., Terracciano, D., Parisi, V., Oriente, F., Portella, G., Beguinot, F., et al. (2021). Cytokine signature and COVID-19 prediction models in the two waves of pandemics. Sci. Rep. *11*, 20793.

Campbell, G.R., To, R.K., Hanna, J., and Spector, S.A. (2021). SARS-CoV-2, SARS-CoV-1, and HIV-1 derived ssRNA sequences activate the NLRP3 inflammasome in human macrophages through a non-classical pathway. IScience *24*, 102295.

Caricchio, R., Abbate, A., Gordeev, I., Meng, J., Hsue, P.Y., Neogi, T., Arduino, R., Fomina, D., Bogdanov, R., Stepanenko, T., et al. (2021). Effect of Canakinumab vs Placebo on Survival Without Invasive Mechanical Ventilation in Patients Hospitalized With Severe COVID-19: A Randomized Clinical Trial. JAMA *326*, 230–239.

Carissimo, G., Xu, W., Kwok, I., Abdad, M.Y., Chan, Y.-H., Fong, S.-W., Puan, K.J., Lee, C.Y.-P., Yeo, N.K.-W., Amrun, S.N., et al. (2020). Whole blood immunophenotyping uncovers immature neutrophil-to-VD2 T-cell ratio as an early marker for severe COVID-19. Nat. Commun. *11*, 5243.

Casadevall, A., and Pirofski, L.-A. (2019). Benefits and Costs of Animal Virulence for Microbes. MBio *10*, e00863-19.

Centola, M., Aksentijevich, I., and Kastner, D.L. (1998). The Hereditary Periodic Fever Syndromes: Molecular Analysis of a New Family of Inflammatory Diseases. Hum. Mol. Genet. *7*, 1581–1588.

Chavarría-Smith, J., and Vance, R.E. (2015). The NLRP1 inflammasomes. Immunol. Rev. *265*, 22–34.

Chen, J., and Chen, Z.J. (2018). PtdIns4P on dispersed trans-Golgi network mediates NLRP3 inflammasome activation. Nature *564*, 71–76.

Chen, G., Wu, D., Guo, W., Cao, Y., Huang, D., Wang, H., Wang, T., Zhang, X., Chen, H., Yu, H., et al. (2020). Clinical and immunological features of severe and moderate coronavirus disease 2019. J. Clin. Invest. *130*, 2620–2629.

Chen, P.Z., Bobrovitz, N., Premji, Z.A., Koopmans, M., Fisman, D.N., and Gu, F.X. (2021). SARS-CoV-2 shedding dynamics across the respiratory tract, sex, and disease severity for adult and pediatric COVID-19. ELife *10*, e70458.

Chua, R.L., Lukassen, S., Trump, S., Hennig, B.P., Wendisch, D., Pott, F., Debnath, O., Thürmann, L., Kurth, F., Völker, M.T., et al. (2020). COVID-19 severity correlates with airway epithelium–immune cell interactions identified by single-cell analysis. Nat. Biotechnol. *38*, 970–979.

Chui, A.J., Okondo, M.C., Rao, S.D., Gai, K., Griswold, A.R., Johnson, D.C., Ball, D.P., Taabazuing, C.Y., Orth, E.L., Vittimberga, B.A., et al. (2019). N-terminal degradation activates the NLRP1B inflammasome.

Science *364*, 82–85.

Chung, J.W., Hong, S.J., Kim, K.J., Goti, D., Stins, M.F., Shin, S., Dawson, V.L., Dawson, T.M., and Kim, K.S. (2003). 37-kDa laminin receptor precursor modulates cytotoxic necrotizing factor 1-mediated RhoA activation and bacterial uptake. J. Biol. Chem. *278*, 16857–16862.

Chung, L.K., Park, Y.H., Zheng, Y., Brodsky, I.E., Hearing, P., Kastner, D.L., Chae, J.J., and Bliska, J.B. (2016). The Yersinia Virulence Factor YopM Hijacks Host Kinases to Inhibit Type III Effector-Triggered Activation of the Pyrin Inflammasome. Cell Host Microbe *20*, 296–306.

Cocconcelli, E., Castelli, G., Onelia, F., Lavezzo, E., Giraudo, C., Bernardinello, N., Fichera, G., Leoni, D., Trevenzoli, M., Saetta, M., et al. (2021). Disease Severity and Prognosis of SARS-CoV-2 Infection in Hospitalized Patients Is Not Associated With Viral Load in Nasopharyngeal Swab. Front. Med. *8*, 1527.

Combadière, B., Adam, L., Guillou, N., Quentric, P., Rosenbaum, P., Dorgham, K., Bonduelle, O., Parizot, C., Sauce, D., Mayaux, J., et al. (2021). LOX-1-Expressing Immature Neutrophils Identify Critically-Ill COVID-19 Patients at Risk of Thrombotic Complications. Front. Immunol. *12*, 3907.

Combes, A.J., Courau, T., Kuhn, N.F., Hu, K.H., Ray, A., Chen, W.S., Chew, N.W., Cleary, S.J., Kushnoor, D., Reeder, G.C., et al. (2021). Global absence and targeting of protective immune states in severe COVID-19. Nature *591*, 124–130.

Conos, S.A., Lawlor, K.E., Vaux, D.L., Vince, J.E., and Lindqvist, L.M. (2016). Cell death is not essential for caspase-1-mediated interleukin-1β activation and secretion. Cell Death Differ. *23*, 1827–1838.

CORIMUNO-19 Collaborative group (2021). Effect of anakinra versus usual care in adults in hospital with COVID-19 and mild-to-moderate pneumonia (CORIMUNO-ANA-1): a randomised controlled trial. Lancet Respir. Med. *9*, 295–304.

Del Valle, D.M., Kim-Schulze, S., Huang, H.-H., Beckmann, N.D., Nirenberg, S., Wang, B., Lavin, Y., Swartz, T.H., Madduri, D., Stock, A., et al. (2020). An inflammatory cytokine signature predicts COVID-19 severity and survival. Nat. Med. *26*, 1636–1643.

Deng, M., Tang, Y., Li, W., Wang, X., Zhang, R., Zhang, X., Zhao, X., Liu, J., Tang, C., Liu, Z., et al. (2018). The Endotoxin Delivery Protein HMGB1 Mediates Caspase-11-Dependent Lethality in Sepsis. Immunity *49*, 740-753.e7.

Desai, N., Neyaz, A., Szabolcs, A., Shih, A.R., Chen, J.H., Thapar, V., Nieman, L.T., Solovyov, A., Mehta, A., Lieb, D.J., et al. (2020). Temporal and spatial heterogeneity of host response to SARS-CoV-2 pulmonary infection. Nat. Commun. *11*, 6319.

Diabate, M., Munro, P., Garcia, E., Jacquel, A., Michel, G., Obba, S., Goncalves, D., Luci, C., Marchetti, S., Demon, D., et al. (2015). Escherichia coli α-Hemolysin Counteracts the Anti-Virulence Innate Immune Response Triggered by the Rho GTPase Activating Toxin CNF1 during Bacteremia. PLOS Pathog. *11*, e1004732.

Dick, M.S., Sborgi, L., Rühl, S., Hiller, S., and Broz, P. (2016). ASC filament formation serves as a signal amplification mechanism for inflammasomes. Nat. Commun. *7*, 1–13.

Diebold, S.S., Kaisho, T., Hemmi, H., Akira, S., and Reis e Sousa, C. (2004). Innate Antiviral Responses by Means of TLR7-Mediated Recognition of Single-Stranded RNA. Science *303*, 1529–1531.

D'Osualdo, A., Weichenberger, C.X., Wagner, R.N., Godzik, A., Wooley, J., and Reed, J.C. (2011). CARD8 and NLRP1 undergo autoproteolytic processing through a ZU5-like domain. PloS One *6*, e27396.

Drenth, J.P.H., Cuisset, L., Grateau, G., Vasseur, C., van de Velde-Visser, S.D., de Jong, J.G.N., Beckmann, J.S., van der Meer, J.W.M., and Delpech & contributing members of the International Hyper-IgD Study Group, M. (1999). Mutations in the gene encoding mevalonate kinase cause hyper-IgD and periodic fever syndrome. Nat. Genet. *22*, 178–181.

Dufies, O., and Boyer, L. (2021). RhoGTPases and inflammasomes: Guardians of effector-triggered

immunity. PLOS Pathog. *17*, e1009504.

Dufies, O., Doye, A., Courjon, J., Torre, C., Michel, G., Loubatier, C., Jacquel, A., Chaintreuil, P., Majoor, A., Guinamard, R.R., et al. (2021). Escherichia coli Rho GTPase-activating toxin CNF1 mediates NLRP3 inflammasome activation via p21-activated kinases-1/2 during bacteraemia in mice. Nat. Microbiol. *6*, 401–412.

Duncan, J.A., Bergstralh, D.T., Wang, Y., Willingham, S.B., Ye, Z., Zimmermann, A.G., and Ting, J.P.-Y. (2007). Cryopyrin/NALP3 binds ATP/dATP, is an ATPase, and requires ATP binding to mediate inflammatory signaling. Proc. Natl. Acad. Sci. U. S. A. *104*, 8041–8046.

Eisfeld, H.S., Simonis, A., Winter, S., Chhen, J., Ströh, L.J., Krey, T., Koch, M., Theobald, S.J., and Rybniker, J. (2021). Viral Glycoproteins Induce NLRP3 Inflammasome Activation and Pyroptosis in Macrophages. Viruses *13*, 2076.

El Masri, R., and Delon, J. (2021). RHO GTPases: from new partners to complex immune syndromes. Nat. Rev. Immunol. *21*, 499–513.

Evavold, C.L., Ruan, J., Tan, Y., Xia, S., Wu, H., and Kagan, J.C. (2018). The Pore-Forming Protein Gasdermin D Regulates Interleukin-1 Secretion from Living Macrophages. Immunity *48*, 35-44.e6.

Evrard, M., Kwok, I.W.H., Chong, S.Z., Teng, K.W.W., Becht, E., Chen, J., Sieow, J.L., Penny, H.L., Ching, G.C., Devi, S., et al. (2018). Developmental Analysis of Bone Marrow Neutrophils Reveals Populations Specialized in Expansion, Trafficking, and Effector Functions. Immunity *48*, 364-379.e8.

Feinberg, H., Mitchell, D.A., Drickamer, K., and Weis, W.I. (2001). Structural basis for selective recognition of oligosaccharides by DC-SIGN and DC-SIGNR. Science *294*, 2163–2166.

Fernandes-Alnemri, T., Yu, J.-W., Datta, P., Wu, J., and Alnemri, E.S. (2009). AIM2 activates the inflammasome and cell death in response to cytoplasmic DNA. Nature *458*, 509–513.

Fernandes-Alnemri, T., Kang, S., Anderson, C., Sagara, J., Fitzgerald, K.A., and Alnemri, E.S. (2013). Cutting Edge: TLR Signaling Licenses IRAK1 for Rapid Activation of the NLRP3 Inflammasome. J. Immunol. *191*, 3995–3999.

Ferreira, A.C., Soares, V.C., de Azevedo-Quintanilha, I.G., Dias, S. da S.G., Fintelman-Rodrigues, N., Sacramento, C.Q., Mattos, M., de Freitas, C.S., Temerozo, J.R., Teixeira, L., et al. (2021). SARS-CoV-2 engages inflammasome and pyroptosis in human primary monocytes. Cell Death Discov. *7*, 1–12.

Finger, J.N., Lich, J.D., Dare, L.C., Cook, M.N., Brown, K.K., Duraiswami, C., Bertin, J.J., and Gough, P.J. (2012). Autolytic Proteolysis within the Function to Find Domain (FIIND) Is Required for NLRP1 Inflammasome Activity *. J. Biol. Chem. *287*, 25030–25037.

Fiorentini, C., Falzano, L., Fabbri, A., Stringaro, A., Logozzi, M., Travaglione, S., Contamin, S., Arancia, G., Malorni, W., and Fais, S. (2001). Activation of rho GTPases by cytotoxic necrotizing factor 1 induces macropinocytosis and scavenging activity in epithelial cells. Mol. Biol. Cell *12*, 2061–2073.

Fischer, F.A., Mies, L.F.M., Nizami, S., Pantazi, E., Danielli, S., Demarco, B., Ohlmeyer, M., Lee, M.S.J., Coban, C., Kagan, J.C., et al. (2021). TBK1 and IKKε act like an OFF switch to limit NLRP3 inflammasome pathway activation. Proc. Natl. Acad. Sci. *118*.

Fischer, N.L., Naseer, N., Shin, S., and Brodsky, I.E. (2020). Effector-triggered immunity and pathogen sensing in metazoans. Nat. Microbiol. *5*, 14–26.

Fitzgerald, K.A., and Kagan, J.C. (2020). Toll-like Receptors and the Control of Immunity. Cell *180*, 1044–1066.

Flatau, G., Lemichez, E., Gauthier, M., Chardin, P., Paris, S., Fiorentini, C., and Boquet, P. (1997). Toxin-induced activation of the G protein p21 Rho by deamidation of glutamine. Nature *387*, 729–733.

Frew, B.C., Joag, V.R., and Mogridge, J. (2012). Proteolytic processing of Nlrp1b is required for

inflammasome activity. PLoS Pathog. *8*, e1002659.

Friebel, A., Ilchmann, H., Aepfelbacher, M., Ehrbar, K., Machleidt, W., and Hardt, W.D. (2001). SopE and SopE2 from Salmonella typhimurium activate different sets of RhoGTPases of the host cell. J. Biol. Chem. *276*, 34035–34040.

Fu, Y., and Galán, J.E. (1999). A Salmonella protein antagonizes Rac-1 and Cdc42 to mediate host-cell recovery after bacterial invasion. Nature *401*, 293–297.

Gaidt, M.M., Ebert, T.S., Chauhan, D., Ramshorn, K., Pinci, F., Zuber, S., O'Duill, F., Schmid-Burgk, J.L., Hoss, F., Buhmann, R., et al. (2017). The DNA Inflammasome in Human Myeloid Cells Is Initiated by a STING-Cell Death Program Upstream of NLRP3. Cell *171*, 1110-1124.e18.

Galani, I.-E., Rovina, N., Lampropoulou, V., Triantafyllia, V., Manioudaki, M., Pavlos, E., Koukaki, E., Fragkou, P.C., Panou, V., Rapti, V., et al. (2021). Untuned antiviral immunity in COVID-19 revealed by temporal type I/III interferon patterns and flu comparison. Nat. Immunol. *22*, 32–40.

Gando, S., Shiraishi, A., Yamakawa, K., Ogura, H., Saitoh, D., Fujishima, S., Mayumi, T., Kushimoto, S., Abe, T., Shiino, Y., et al. (2019). Role of disseminated intravascular coagulation in severe sepsis. Thromb. Res. *178*, 182–188.

Gao, W., Yang, J., Liu, W., Wang, Y., and Shao, F. (2016). Site-specific phosphorylation and microtubule dynamics control Pyrin inflammasome activation. Proc. Natl. Acad. Sci. U. S. A. *113*, E4857-4866.

Gernez, Y., de Jesus, A.A., Alsaleem, H., Macaubas, C., Roy, A., Lovell, D., Jagadeesh, K.A., Alehashemi, S., Erdman, L., Grimley, M., et al. (2019). Severe autoinflammation in 4 patients with C-terminal variants in cell division control protein 42 homolog (CDC42) successfully treated with IL-1β inhibition. J. Allergy Clin. Immunol. *144*, 1122-1125.e6.

Goehring, U.-M., Schmidt, G., Pederson, K.J., Aktories, K., and Barbieri, J.T. (1999). The N-terminal Domain of Pseudomonas aeruginosaExoenzyme S Is a GTPase-activating Protein for Rho GTPases. J. Biol. Chem. *274*, 36369–36372.

Gomes, I., Karmirian, K., Oliveira, J.T., Pedrosa, C. da S.G., Mendes, M.A., Rosman, F.C., Chimelli, L., and Rehen, S. (2021). SARS-CoV-2 infection of the central nervous system in a 14-month-old child: A case report of a complete autopsy. Lancet Reg. Health – Am. *2*.

Green, J.P., Yu, S., Martín-Sánchez, F., Pelegrin, P., Lopez-Castejon, G., Lawrence, C.B., and Brough, D. (2018). Chloride regulates dynamic NLRP3-dependent ASC oligomerization and inflammasome priming. Proc. Natl. Acad. Sci. *115*, E9371–E9380.

Groß, C.J., Mishra, R., Schneider, K.S., Médard, G., Wettmarshausen, J., Dittlein, D.C., Shi, H., Gorka, O., Koenig, P.-A., Fromm, S., et al. (2016). K + Efflux-Independent NLRP3 Inflammasome Activation by Small Molecules Targeting Mitochondria. Immunity *45*, 761–773.

Guan, Y., Ranoa, D.R.E., Jiang, S., Mutha, S.K., Li, X., Baudry, J., and Tapping, R.I. (2010). Human TLRs 10 and 1 share common mechanisms of innate immune sensing but not signaling. J. Immunol. Baltim. Md 1950 *184*, 5094–5103.

Guo, C., Xie, S., Chi, Z., Zhang, J., Liu, Y., Zhang, L., Zheng, M., Zhang, X., Xia, D., Ke, Y., et al. (2016). Bile Acids Control Inflammation and Metabolic Disorder through Inhibition of NLRP3 Inflammasome. Immunity *45*, 802–816.

Gurung, P., Lukens, J.R., and Kanneganti, T.-D. (2015). Mitochondria: diversity in the regulation of the NLRP3 inflammasome. Trends Mol. Med. *21*, 193–201.

Hadjadj, J., Yatim, N., Barnabei, L., Corneau, A., Boussier, J., Smith, N., Péré, H., Charbit, B., Bondet, V., Chenevier-Gobeaux, C., et al. (2020). Impaired type I interferon activity and inflammatory responses in severe COVID-19 patients. Science *369*, 718–724.

Hagar, J.A., Powell, D.A., Aachoui, Y., Ernst, R.K., and Miao, E.A. (2013). Cytoplasmic LPS Activates

Caspase-11: Implications in TLR4-Independent Endotoxic Shock. Science *341*, 1250–1253.

Hall, A. (1998). Rho GTPases and the Actin Cytoskeleton. *279*, 7.

Han, S., Lear, T.B., Jerome, J.A., Rajbhandari, S., Snavely, C.A., Gulick, D.L., Gibson, K.F., Zou, C., Chen, B.B., and Mallampalli, R.K. (2015). Lipopolysaccharide Primes the NALP3 Inflammasome by Inhibiting Its Ubiquitination and Degradation Mediated by the SCFFBXL2 E3 Ligase. J. Biol. Chem. *290*, 18124–18133.

Hansen, J.M., Jong, M.F. de, Wu, Q., Zhang, L.-S., Heisler, D.B., Alto, L.T., and Alto, N.M. (2021). Pathogenic ubiquitination of GSDMB inhibits NK cell bactericidal functions. Cell *0*.

Hara, H., Seregin, S.S., Yang, D., Fukase, K., Chamaillard, M., Alnemri, E.S., Inohara, N., Chen, G.Y., and Núñez, G. (2018). The NLRP6 Inflammasome Recognizes Lipoteichoic Acid and Regulates Gram-Positive Pathogen Infection. Cell *175*, 1651-1664.e14.

Hardt, W.D., Chen, L.M., Schuebel, K.E., Bustelo, X.R., and Galán, J.E. (1998). S. typhimurium encodes an activator of Rho GTPases that induces membrane ruffling and nuclear responses in host cells. Cell *93*, 815–826.

Hashim, I.F., and Ahmad Mokhtar, A.M. (2021). Small Rho GTPases and their associated RhoGEFs mutations promote immunological defects in primary immunodeficiencies. Int. J. Biochem. Cell Biol. *137*, 106034.

Hauwermeiren, F.V., and Lamkanfi, M. (2016). The NEK-sus of the NLRP3 inflammasome. Nat. Immunol. *17*, 223.

Hayashi, F., Smith, K.D., Ozinsky, A., Hawn, T.R., Yi, E.C., Goodlett, D.R., Eng, J.K., Akira, S., Underhill, D.M., and Aderem, A. (2001). The innate immune response to bacterial flagellin is mediated by Toll-like receptor 5. Nature *410*, 1099–1103.

Hazuda, D.J., Lee, J.C., and Young, P.R. (1988). The kinetics of interleukin 1 secretion from activated monocytes. Differences between interleukin 1 alpha and interleukin 1 beta. J. Biol. Chem. *263*, 8473–8479.

He, W., Wan, H., Hu, L., Chen, P., Wang, X., Huang, Z., Yang, Z.-H., Zhong, C.-Q., and Han, J. (2015). Gasdermin D is an executor of pyroptosis and required for interleukin-1β secretion. Cell Res. *25*, 1285–1298.

He, Y., Zeng, M.Y., Yang, D., Motro, B., and Núñez, G. (2016). Nek7 is an essential mediator of NLRP3 activation downstream of potassium efflux. Nature *530*, 354–357.

Heil, F., Hemmi, H., Hochrein, H., Ampenberger, F., Kirschning, C., Akira, S., Lipford, G., Wagner, H., and Bauer, S. (2004). Species-Specific Recognition of Single-Stranded RNA via Toll-like Receptor 7 and 8. Science.

Hemmi, H., Takeuchi, O., Kawai, T., Kaisho, T., Sato, S., Sanjo, H., Matsumoto, M., Hoshino, K., Wagner, H., Takeda, K., et al. (2000). A Toll-like receptor recognizes bacterial DNA. Nature *408*, 740–745.

Hernandez-Cuellar, E., Tsuchiya, K., Hara, H., Fang, R., Sakai, S., Kawamura, I., Akira, S., and Mitsuyama, M. (2012). Cutting Edge: Nitric Oxide Inhibits the NLRP3 Inflammasome. J. Immunol. *189*, 5113–5117.

Hidmark, A., Paul, A. von S., and Dalpke, A.H. (2012). Cutting Edge: TLR13 Is a Receptor for Bacterial RNA. J. Immunol. *189*, 2717–2721.

Higgs, H.N., and Pollard, T.D. (2001). Regulation of actin filament network formation through ARP2/3 complex: activation by a diverse array of proteins. Annu. Rev. Biochem. *70*, 649–676.

Hochheiser, I.V., Pilsl, M., Hagelueken, G., Moecking, J., Marleaux, M., Brinkschulte, R., Latz, E., Engel, C., and Geyer, M. (2021). Cryo-EM structure of the NLRP3 decamer bound to the cytokine release inhibitory drug CRID3. BioRxiv 2021.07.22.453353.

Hoffmann, C., Pop, M., Leemhuis, J., Schirmer, J., Aktories, K., and Schmidt, G. (2004). The Yersinia

pseudotuberculosis Cytotoxic Necrotizing Factor (CNFY) Selectively Activates RhoA. J. Biol. Chem. *279*, 16026–16032.

Hofman, P., Le Negrate, G., Mograbi, B., Hofman, V., Brest, P., Alliana-Schmid, A., Flatau, G., Boquet, P., and Rossi, B. (2000). Escherichia coli cytotoxic necrotizing factor-1 (CNF-1) increases the adherence to epithelia and the oxidative burst of human polymorphonuclear leukocytes but decreases bacteria phagocytosis. J. Leukoc. Biol. *68*, 522–528.

Hollingsworth, L.R., Sharif, H., Griswold, A.R., Fontana, P., Mintseris, J., Dagbay, K.B., Paulo, J.A., Gygi, S.P., Bachovchin, D.A., and Wu, H. (2021). DPP9 sequesters the C terminus of NLRP1 to repress inflammasome activation. Nature *592*, 778–783.

Hooftman, A., Angiari, S., Hester, S., Corcoran, S.E., Runtsch, M.C., Ling, C., Ruzek, M.C., Slivka, P.F., McGettrick, A.F., Banahan, K., et al. (2020). The Immunomodulatory Metabolite Itaconate Modifies NLRP3 and Inhibits Inflammasome Activation. Cell Metab. *32*, 468-478.e7.

Horiguchi, Y., Inoue, N., Masuda, M., Kashimoto, T., Katahira, J., Sugimoto, N., and Matsuda, M. (1997). Bordetella bronchiseptica dermonecrotizing toxin induces reorganization of actin stress fibers through deamidation of Gln-63 of the GTP-binding protein Rho. Proc. Natl. Acad. Sci. U. S. A. *94*, 11623–11626.

Hornung, V., Bauernfeind, F., Halle, A., Samstad, E.O., Kono, H., Rock, K.L., Fitzgerald, K.A., and Latz, E. (2008). Silica crystals and aluminum salts mediate NALP-3 inflammasome activation via phagosomal destabilization. Nat. Immunol. *9*, 847–856.

Hornung, V., Ablasser, A., Charrel-Dennis, M., Bauernfeind, F., Horvath, G., Caffrey, D.R., Latz, E., and Fitzgerald, K.A. (2009). AIM2 recognizes cytosolic dsDNA and forms a caspase-1-activating inflammasome with ASC. Nature *458*, 514–518.

Hotchkiss, R.S., Monneret, G., and Payen, D. (2013). Sepsis-induced immunosuppression: from cellular dysfunctions to immunotherapy. Nat. Rev. Immunol. *13*, 862–874.

Hsu, A.P., Donkó, A., Arrington, M.E., Swamydas, M., Fink, D., Das, A., Escobedo, O., Bonagura, V., Szabolcs, P., Steinberg, H.N., et al. (2019). Dominant activating RAC2 mutation with lymphopenia, immunodeficiency and cytoskeletal defects. Blood blood-2018-11-886028.

Hu, Z., Zhou, Q., Zhang, C., Fan, S., Cheng, W., Zhao, Y., Shao, F., Wang, H.-W., Sui, S.-F., and Chai, J. (2015). Structural and biochemical basis for induced self-propagation of NLRC4. Science *350*, 399–404.

Huang, C., Wang, Y., Li, X., Ren, L., Zhao, J., Hu, Y., Zhang, L., Fan, G., Xu, J., Gu, X., et al. (2020). Clinical features of patients infected with 2019 novel coronavirus in Wuhan, China. The Lancet *395*, 497–506.

Huang, M., Zhang, X., Toh, G.A., Gong, Q., Wang, J., Han, Z., Wu, B., Zhong, F., and Chai, J. (2021). Structural and biochemical mechanisms of NLRP1 inhibition by DPP9. Nature *592*, 773–777.

Humphries, F., Bergin, R., Jackson, R., Delagic, N., Wang, B., Yang, S., Dubois, A.V., Ingram, R.J., and Moynagh, P.N. (2018). The E3 ubiquitin ligase Pellino2 mediates priming of the NLRP3 inflammasome. Nat. Commun. *9*, 1560.

Humphries, F., Shmuel-Galia, L., Ketelut-Carneiro, N., Li, S., Wang, B., Nemmara, V.V., Wilson, R., Jiang, Z., Khalighinejad, F., Muneeruddin, K., et al. (2020). Succination inactivates gasdermin D and blocks pyroptosis. Science *369*, 1633–1637.

Imlay, J.A., and Linn, S. (1988). DNA damage and oxygen radical toxicity. Science *240*, 1302–1309.

Iyer, S.S., He, Q., Janczy, J.R., Elliott, E.I., Zhong, Z., Olivier, A.K., Sadler, J.J., Knepper-Adrian, V., Han, R., Qiao, L., et al. (2013). Mitochondrial cardiolipin is required for Nlrp3 inflammasome activation. Immunity *39*, 311–323.

Jamilloux, Y., Magnotti, F., Belot, A., and Henry, T. (2018). The pyrin inflammasome: from sensing RhoA GTPases-inhibiting toxins to triggering autoinflammatory syndromes. Pathog. Dis. *76*.

Jamilloux, Y., Henry, T., Belot, A., Viel, S., Fauter, M., El Jammal, T., Walzer, T., François, B., and Sève, P. (2020). Should we stimulate or suppress immune responses in COVID-19? Cytokine and anti-cytokine interventions. Autoimmun. Rev. *19*, 102567.

Janeway, C.A. (1989). Approaching the asymptote? Evolution and revolution in immunology. Cold Spring Harb. Symp. Quant. Biol. *54 Pt 1*, 1–13.

Jin, T., Perry, A., Jiang, J., Smith, P., Curry, J.A., Unterholzner, L., Jiang, Z., Horvath, G., Rathinam, V.A., Johnstone, R.W., et al. (2012). Structures of the HIN domain:DNA complexes reveal ligand binding and activation mechanisms of the AIM2 inflammasome and IFI16 receptor. Immunity *36*, 561–571.

Johnson, D.C., Okondo, M.C., Orth, E.L., Rao, S.D., Huang, H.-C., Ball, D.P., and Bachovchin, D.A. (2020). DPP8/9 inhibitors activate the CARD8 inflammasome in resting lymphocytes. Cell Death Dis. *11*, 628.

Jones, J.D.G., and Dangl, J.L. (2006). The plant immune system. Nature *444*, 323–329.

Jones, J.D.G., Vance, R.E., and Dangl, J.L. (2016). Intracellular innate immune surveillance devices in plants and animals. Science *354*.

Just, I., Schallehn, G., and Aktories, K. (1992). ADP-ribosylation of small GTP-binding proteins by Bacillus cereus. Biochem. Biophys. Res. Commun. *183*, 931–936.

Just, I., Wilm, M., Selzer, J., Rex, G., Eichel-Streiber, C. von, Mann, M., and Aktories, K. (1995a). The Enterotoxin from Clostridium difficile (ToxA) Monoglucosylates the Rho Proteins. J. Biol. Chem. *270*, 13932–13936.

Just, I., Selzer, J., Wilm, M., Eichel-Streiber, C. von, Mann, M., and Aktories, K. (1995b). Glucosylation of Rho proteins by Clostridium difficile toxin B. Nature *375*, 500–503.

Kaneko, N., Kuo, H.-H., Boucau, J., Farmer, J.R., Allard-Chamard, H., Mahajan, V.S., Piechocka-Trocha, A., Lefteri, K., Osborn, M., Bals, J., et al. (2020). Loss of Bcl-6-Expressing T Follicular Helper Cells and Germinal Centers in COVID-19. Cell *183*, 143-157.e13.

Kato, H., Takeuchi, O., Sato, S., Yoneyama, M., Yamamoto, M., Matsui, K., Uematsu, S., Jung, A., Kawai, T., Ishii, K.J., et al. (2006). Differential roles of MDA5 and RIG-I helicases in the recognition of RNA viruses. Nature *441*, 101–105.

Katsnelson, M., Smith, C., and Dubyak, G. (2012). Cytosolic K+ and extracellular ATP as regulators of NLRP3 inflammasome activation and the IL-1β secretion response of macrophages to crystalline stimuli. (114.9). J. Immunol. *188*, 114.9-114.9.

Kawashima, A., Karasawa, T., Tago, K., Kimura, H., Kamata, R., Usui-Kawanishi, F., Watanabe, S., Ohta, S., Funakoshi-Tago, M., Yanagisawa, K., et al. (2017). ARIH2 Ubiquitinates NLRP3 and Negatively Regulates NLRP3 Inflammasome Activation in Macrophages. J. Immunol. Baltim. Md 1950 *199*, 3614–3622.

Kayagaki, N., Wong, M.T., Stowe, I.B., Ramani, S.R., Gonzalez, L.C., Akashi-Takamura, S., Miyake, K., Zhang, J., Lee, W.P., Muszyński, A., et al. (2013). Noncanonical Inflammasome Activation by Intracellular LPS Independent of TLR4. Science *341*, 1246–1249.

Kayagaki, N., Stowe, I.B., Lee, B.L., O'Rourke, K., Anderson, K., Warming, S., Cuellar, T., Haley, B., Roose-Girma, M., Phung, Q.T., et al. (2015). Caspase-11 cleaves gasdermin D for non-canonical inflammasome signalling. Nature *526*, 666–671.

Kayagaki, N., Kornfeld, O.S., Lee, B.L., Stowe, I.B., O'Rourke, K., Li, Q., Sandoval, W., Yan, D., Kang, J., Xu, M., et al. (2021). NINJ1 mediates plasma membrane rupture during lytic cell death. Nature *591*, 131–136.

Keestra, A.M., Winter, M.G., Auburger, J.J., Fräßle, S.P., Xavier, M.N., Winter, S.E., Kim, A., Poon, V., Ravesloot, M.M., Waldenmaier, J.F.T., et al. (2013). Manipulation of small Rho GTPases is a pathogen-induced process detected by NOD1. Nature *496*, 233–237.

Kern, W.V., and Rieg, S. (2020). Burden of bacterial bloodstream infection—a brief update on epidemiology and significance of multidrug-resistant pathogens. Clin. Microbiol. Infect. *26*, 151–157.

Khan, M., Subramaniam, R., and Desveaux, D. (2016). Of guards, decoys, baits and traps: pathogen perception in plants by type III effector sensors. Curr. Opin. Microbiol. *29*, 49–55.

Khare, S., Ratsimandresey, R.A., de Almeida, L., Cuda, C.M., Rellick, S.L., Misharin, A.V., Wallin, M.C., Gangopadhyay, A., Forte, E., Gottwein, E., et al. (2014). The PYRIN domain–only protein POP3 inhibits ALR inflammasomes and regulates responses to infection with DNA viruses. Nat. Immunol. *15*, 343–353.

Kim, M.-J., Bae, S.H., Ryu, J.-C., Kwon, Y., Oh, J.-H., Kwon, J., Moon, J.-S., Kim, K., Miyawaki, A., Lee, M.G., et al. (2016). SESN2/sestrin2 suppresses sepsis by inducing mitophagy and inhibiting NLRP3 activation in macrophages. Autophagy *12*, 1272–1291.

Klink, B.U., Barden, S., Heidler, T.V., Borchers, C., Ladwein, M., Stradal, T.E.B., Rottner, K., and Heinz, D.W. (2010). Structure of Shigella IpgB2 in Complex with Human RhoA IMPLICATIONS FOR THE MECHANISM OF BACTERIAL GUANINE NUCLEOTIDE EXCHANGE FACTOR MIMICRY. J. Biol. Chem. *285*, 17197–17208.

Knust, Z., Blumenthal, B., Aktories, K., and Schmidt, G. (2009). Cleavage of Escherichia coli cytotoxic necrotizing factor 1 is required for full biologic activity. Infect. Immun. *77*, 1835–1841.

Koblansky, A.A., Jankovic, D., Oh, H., Hieny, S., Sungnak, W., Mathur, R., Hayden, M.S., Akira, S., Sher, A., and Ghosh, S. (2013). Recognition of profilin by Toll-like receptor 12 is critical for host resistance to Toxoplasma gondii. Immunity *38*, 119–130.

Kofoed, E.M., and Vance, R.E. (2011). Innate immune recognition of bacterial ligands by NAIPs determines inflammasome specificity. Nature *477*, 592–595.

Krall, R., Schmidt, G., Aktories, K., and Barbieri, J.T. (2000). Pseudomonas aeruginosa ExoT Is a Rho GTPase-Activating Protein. Infect. Immun. *68*, 6066–6068.

Kubori, T., and Galán, J.E. (2003). Temporal Regulation of Salmonella Virulence Effector Function by Proteasome-Dependent Protein Degradation. Cell *115*, 333–342.

Kudo, S., Mizuno, K., Hirai, Y., and Shimizu, T. (1990). Clearance and tissue distribution of recombinant human interleukin 1 beta in rats. Cancer Res. *50*, 5751–5755.

Kupper, T.S., and Groves, R.W. (1995). The interleukin-1 axis and cutaneous inflammation. J. Invest. Dermatol. *105*, 62S-66S.

Kureishy, N., Sapountzi, V., Prag, S., Anilkumar, N., and Adams, J.C. (2002). Fascins, and their roles in cell structure and function. BioEssays News Rev. Mol. Cell. Dev. Biol. *24*, 350–361.

Kvedaraite, E., Hertwig, L., Sinha, I., Ponzetta, A., Myrberg, I.H., Lourda, M., Dzidic, M., Akber, M., Klingström, J., Folkesson, E., et al. (2021). Major alterations in the mononuclear phagocyte landscape associated with COVID-19 severity. Proc. Natl. Acad. Sci. *118*.

Kyriazopoulou, E., Poulakou, G., Milionis, H., Metallidis, S., Adamis, G., Tsiakos, K., Fragkou, A., Rapti, A., Damoulari, C., Fantoni, M., et al. (2021). Early treatment of COVID-19 with anakinra guided by soluble urokinase plasminogen receptor plasma levels: a double-blind, randomized controlled phase 3 trial. Nat. Med. *27*, 1752–1760.

Lagrange, B., Benaoudia, S., Wallet, P., Magnotti, F., Provost, A., Michal, F., Martin, A., Di Lorenzo, F., Py, B.F., Molinaro, A., et al. (2018). Human caspase-4 detects tetra-acylated LPS and cytosolic Francisella and functions differently from murine caspase-11. Nat. Commun. *9*, 1–14.

Lam, M.T., Coppola, S., Krumbach, O.H.F., Prencipe, G., Insalaco, A., Cifaldi, C., Brigida, I., Zara, E., Scala, S., Di Cesare, S., et al. (2019). A novel disorder involving dyshematopoiesis, inflammation, and HLH due to aberrant CDC42 function. J. Exp. Med. *216*, 2778–2799.

Lamkanfi, M., and Dixit, V.M. (2014). Mechanisms and functions of inflammasomes. Cell *157*, 1013–1022.

Landraud, L., Gauthier, M., Fosse, T., and Boquet, P. (2000). Frequency of Escherichia coli strains producing the cytotoxic necrotizing factor (CNF1) in nosocomial urinary tract infections. Lett. Appl. Microbiol. *30*, 213–216.

Landraud, L., Gibert, M., Popoff, M.R., Boquet, P., and Gauthier, M. (2003). Expression of cnf1 by Escherichia coli J96 involves a large upstream DNA region including the hlyCABD operon, and is regulated by the RfaH protein. Mol. Microbiol. *47*, 1653–1667.

Langereis, J.D., Pickkers, P., de Kleijn, S., Gerretsen, J., de Jonge, M.I., and Kox, M. (2017). Spleen-derived IFN-γ induces generation of PD-L1+-suppressive neutrophils during endotoxemia. J. Leukoc. Biol. *102*, 1401–1409.

Lazear, H.M., Schoggins, J.W., and Diamond, M.S. (2019). Shared and Distinct Functions of Type I and Type III Interferons. Immunity *50*, 907–923.

Lee, G.-S., Subramanian, N., Kim, A.I., Aksentijevich, I., Goldbach-Mansky, R., Sacks, D.B., Germain, R.N., Kastner, D.L., and Chae, J.J. (2012). The calcium-sensing receptor regulates the NLRP3 inflammasome through Ca2+ and cAMP. Nature *492*, 123–127.

Lei, X., Zhang, Z., Xiao, X., Qi, J., He, B., and Wang, J. (2017). Enterovirus 71 Inhibits Pyroptosis through Cleavage of Gasdermin D. J. Virol. *91*, e01069-17.

Lemaitre, B., Nicolas, E., Michaut, L., Reichhart, J.M., and Hoffmann, J.A. (1996). The dorsoventral regulatory gene cassette spätzle/Toll/cactus controls the potent antifungal response in Drosophila adults. Cell *86*, 973–983.

Lemonnier, M., Landraud, L., and Lemichez, E. (2007). Rho GTPase-activating bacterial toxins: from bacterial virulence regulation to eukaryotic cell biology. FEMS Microbiol. Rev. *31*, 515–534.

Levinsohn, J.L., Newman, Z.L., Hellmich, K.A., Fattah, R., Getz, M.A., Liu, S., Sastalla, I., Leppla, S.H., and Moayeri, M. (2012). Anthrax Lethal Factor Cleavage of Nlrp1 Is Required for Activation of the Inflammasome. PLOS Pathog. *8*, e1002638.

Li, F., and Higgs, H.N. (2003). The mouse Formin mDia1 is a potent actin nucleation factor regulated by autoinhibition. Curr. Biol. CB *13*, 1335–1340.

Li, H., Liu, L., Zhang, D., Xu, J., Dai, H., Tang, N., Su, X., and Cao, B. (2020a). SARS-CoV-2 and viral sepsis: observations and hypotheses. The Lancet *395*, 1517–1520.

Li, Q., Guan, X., Wu, P., Wang, X., Zhou, L., Tong, Y., Ren, R., Leung, K.S.M., Lau, E.H.Y., Wong, J.Y., et al. (2020b). Early Transmission Dynamics in Wuhan, China, of Novel Coronavirus–Infected Pneumonia. N. Engl. J. Med.

Li, X., Thome, S., Ma, X., Amrute-Nayak, M., Finigan, A., Kitt, L., Masters, L., James, J.R., Shi, Y., Meng, G., et al. (2017). MARK4 regulates NLRP3 positioning and inflammasome activation through a microtubule-dependent mechanism. Nat. Commun. *8*, 15986.

Liao, M., Liu, Y., Yuan, J., Wen, Y., Xu, G., Zhao, J., Cheng, L., Li, J., Wang, X., Wang, F., et al. (2020). Single-cell landscape of bronchoalveolar immune cells in patients with COVID-19. Nat. Med. *26*, 842–844.

Linder, A., Bauernfried, S., Cheng, Y., Albanese, M., Jung, C., Keppler, O.T., and Hornung, V. (2020). CARD8 inflammasome activation triggers pyroptosis in human T cells. EMBO J. *39*, e105071.

Liu, J., Li, Y., Liu, Q., Yao, Q., Wang, X., Zhang, H., Chen, R., Ren, L., Min, J., Deng, F., et al. (2021). SARS-CoV-2 cell tropism and multiorgan infection. Cell Discov. *7*, 1–4.

Liu, T., Tang, Q., Liu, K., Xie, W., Liu, X., Wang, H., Wang, R.-F., and Cui, J. (2016a). TRIM11 Suppresses AIM2 Inflammasome by Degrading AIM2 via p62-Dependent Selective Autophagy. Cell Rep. *16*, 1988–

2002.

Liu, X., Zhang, Z., Ruan, J., Pan, Y., Magupalli, V.G., Wu, H., and Lieberman, J. (2016b). Inflammasome-activated gasdermin D causes pyroptosis by forming membrane pores. Nature *535*, 153–158.

Lopez, J., Mommert, M., Mouton, W., Pizzorno, A., Brengel-Pesce, K., Mezidi, M., Villard, M., Lina, B., Richard, J.-C., Fassier, J.-B., et al. (2021). Early nasal type I IFN immunity against SARS-CoV-2 is compromised in patients with autoantibodies against type I IFNs. J. Exp. Med. *218*.

Lopez-Castejon, G., and Brough, D. (2011). Understanding the mechanism of IL-1β secretion. Cytokine Growth Factor Rev. *22*, 189–195.

Lourda, M., Dzidic, M., Hertwig, L., Bergsten, H., Palma Medina, L.M., Sinha, I., Kvedaraite, E., Chen, P., Muvva, J.R., Gorin, J.-B., et al. (2021). High-dimensional profiling reveals phenotypic heterogeneity and disease-specific alterations of granulocytes in COVID-19. Proc. Natl. Acad. Sci. U. S. A. *118*, e2109123118.

Lu, Q., Liu, J., Zhao, S., Gomez Castro, M.F., Laurent-Rolle, M., Dong, J., Ran, X., Damani-Yokota, P., Tang, H., Karakousi, T., et al. (2021). SARS-CoV-2 exacerbates proinflammatory responses in myeloid cells through C-type lectin receptors and Tweety family member 2. Immunity *54*, 1304-1319.e9.

Lucas, C., Wong, P., Klein, J., Castro, T.B.R., Silva, J., Sundaram, M., Ellingson, M.K., Mao, T., Oh, J.E., Israelow, B., et al. (2020). Longitudinal analyses reveal immunological misfiring in severe COVID-19. Nature *584*, 463–469.

Luchetti, G., Roncaioli, J.L., Chavez, R.A., Schubert, A.F., Kofoed, E.M., Reja, R., Cheung, T.K., Liang, Y., Webster, J.D., Lehoux, I., et al. (2021). Shigella ubiquitin ligase IpaH7.8 targets gasdermin D for degradation to prevent pyroptosis and enable infection. Cell Host Microbe *29*, 1521-1530.e10.

Lugrin, J., and Martinon, F. (2018). The AIM2 inflammasome: Sensor of pathogens and cellular perturbations. Immunol. Rev. *281*, 99–114.

Lupfer, C., Thomas, P.G., Anand, P.K., Vogel, P., Milasta, S., Martinez, J., Huang, G., Green, M., Kundu, M., Chi, H., et al. (2013). Receptor interacting protein kinase 2–mediated mitophagy regulates inflammasome activation during virus infection. Nat. Immunol. *14*, 480–488.

Luster, A.D. (2009). Chemokines — Chemotactic Cytokines That Mediate Inflammation (Massachusetts Medical Society).

Ma, J., Zhu, F., Zhao, M., Shao, F., Yu, D., Ma, J., Zhang, X., Li, W., Qian, Y., Zhang, Y., et al. (2021). SARS-CoV-2 nucleocapsid suppresses host pyroptosis by blocking Gasdermin D cleavage. EMBO J. *40*, e108249.

Machesky, L.M., and Insall, R.H. (1998). Scar1 and the related Wiskott–Aldrich syndrome protein, WASP, regulate the actin cytoskeleton through the Arp2/3 complex. Curr. Biol. *8*, 1347–1356.

van der Made, C.I., Simons, A., Schuurs-Hoeijmakers, J., van den Heuvel, G., Mantere, T., Kersten, S., van Deuren, R.C., Steehouwer, M., van Reijmersdal, S.V., Jaeger, M., et al. (2020). Presence of Genetic Variants Among Young Men With Severe COVID-19. JAMA *324*, 663–673.

Magnotti, F., Lefeuvre, L., Benezech, S., Malsot, T., Waeckel, L., Martin, A., Kerever, S., Chirita, D., Desjonqueres, M., Duquesne, A., et al. (2019). Pyrin dephosphorylation is sufficient to trigger inflammasome activation in familial Mediterranean fever patients. EMBO Mol. Med. *11*, e10547.

Magupalli, V.G., Negro, R., Tian, Y., Hauenstein, A.V., Di Caprio, G., Skillern, W., Deng, Q., Orning, P., Alam, H.B., Maliga, Z., et al. (2020). HDAC6 mediates an aggresome-like mechanism for NLRP3 and pyrin inflammasome activation. Science *369*, eaas8995.

Mariathasan, S., Weiss, D.S., Newton, K., McBride, J., O'Rourke, K., Roose-Girma, M., Lee, W.P., Weinrauch, Y., Monack, D.M., and Dixit, V.M. (2006). Cryopyrin activates the inflammasome in response to toxins and ATP. Nature *440*, 228–232.

Marshall, J.D., Aste-Amézaga, M., Chehimi, S.S., Murphy, M., Olsen, H., and Trinchieri, G. (1999). Regulation of human IL-18 mRNA expression. Clin. Immunol. Orlando Fla *90*, 15–21.

Martinon, F., Burns, K., and Tschopp, J. (2002). The Inflammasome: A Molecular Platform Triggering Activation of Inflammatory Caspases and Processing of proIL-β. Mol. Cell *10*, 417–426.

Masuda, M., Betancourt, L., Matsuzawa, T., Kashimoto, T., Takao, T., Shimonishi, Y., and Horiguchi, Y. (2000). Activation of Rho through a cross-link with polyamines catalyzed by Bordetella dermonecrotizing toxin. EMBO J. *19*, 521–530.

Matono, R., Miyano, K., Kiyohara, T., and Sumimoto, H. (2014). Arachidonic Acid Induces Direct Interaction of the p67phox-Rac Complex with the Phagocyte Oxidase Nox2, Leading to Superoxide Production. J. Biol. Chem. *289*, 24874–24884.

Matusiak, M., Opdenbosch, N.V., Walle, L.V., Sirard, J.-C., Kanneganti, T.-D., and Lamkanfi, M. (2015). Flagellin-induced NLRC4 phosphorylation primes the inflammasome for activation by NAIP5. Proc. Natl. Acad. Sci. *112*, 1541–1546.

Matzinger, P. (2002a). The danger model: a renewed sense of self. Science *296*, 301–305.

Matzinger, P. (2002b). An innate sense of danger. Ann. N. Y. Acad. Sci. *961*, 341–342.

Mayer-Barber, K.D., and Yan, B. (2017). Clash of the Cytokine Titans: counter-regulation of interleukin-1 and type I interferon-mediated inflammatory responses. Cell. Mol. Immunol. *14*, 22–35.

Mayes-Hopfinger, L., Enache, A., Xie, J., Huang, C.-L., Köchl, R., Tybulewicz, V.L.J., Fernandes-Alnemri, T., and Alnemri, E.S. (2021). Chloride sensing by WNK1 regulates NLRP3 inflammasome activation and pyroptosis. Nat. Commun. *12*, 4546.

McElvaney, O.J., McEvoy, N.L., McElvaney, O.F., Carroll, T.P., Murphy, M.P., Dunlea, D.M., Ní Choileáin, O., Clarke, J., O'Connor, E., Hogan, G., et al. (2020). Characterization of the Inflammatory Response to Severe COVID-19 Illness. Am. J. Respir. Crit. Care Med. *202*, 812–821.

Medici, N.P., Rashid, M., and Bliska, J.B. (2019). Characterization of Pyrin Dephosphorylation and Inflammasome Activation in Macrophages as Triggered by the Yersinia Effectors YopE and YopT. Infect. Immun. *87*.

Medzhitov, R. (2009). Approaching the asymptote: 20 years later. Immunity *30*, 766–775.

Medzhitov, R., Preston-Hurlburt, P., and Janeway, C.A. (1997). A human homologue of the Drosophila Toll protein signals activation of adaptive immunity. Nature *388*, 394–397.

Meunier, E., Dick, M.S., Dreier, R.F., Schürmann, N., Kenzelmann Broz, D., Warming, S., Roose-Girma, M., Bumann, D., Kayagaki, N., Takeda, K., et al. (2014). Caspase-11 activation requires lysis of pathogen-containing vacuoles by IFN-induced GTPases. Nature *509*, 366–370.

Miao, E.A., Leaf, I.A., Treuting, P.M., Mao, D.P., Dors, M., Sarkar, A., Warren, S.E., Wewers, M.D., and Aderem, A. (2010). Caspase-1-induced pyroptosis is an innate immune effector mechanism against intracellular bacteria. Nat. Immunol. *11*, 1136–1142.

Middleton, E.A., He, X.-Y., Denorme, F., Campbell, R.A., Ng, D., Salvatore, S.P., Mostyka, M., Baxter-Stoltzfus, A., Borczuk, A.C., Loda, M., et al. (2020). Neutrophil extracellular traps contribute to immunothrombosis in COVID-19 acute respiratory distress syndrome. Blood *136*, 1169–1179.

Mills, E.L., Ryan, D.G., Prag, H.A., Dikovskaya, D., Menon, D., Zaslona, Z., Jedrychowski, M.P., Costa, A.S.H., Higgins, M., Hams, E., et al. (2018). Itaconate is an anti-inflammatory metabolite that activates Nrf2 via alkylation of KEAP1. Nature *556*, 113.

Mishra, B.B., Rathinam, V.A.K., Martens, G.W., Martinot, A.J., Kornfeld, H., Fitzgerald, K.A., and Sassetti, C.M. (2013). Nitric oxide controls the immunopathology of tuberculosis by inhibiting NLRP3 inflammasome–dependent processing of IL-1β. Nat. Immunol. *14*, 52–60.

Mitchell, T., Lo, A., Logan, M.R., Lacy, P., and Eitzen, G. (2008). Primary granule exocytosis in human neutrophils is regulated by Rac-dependent actin remodeling. Am. J. Physiol. Cell Physiol. *295*, C1354-1365.

Monteleone, M., Stow, J.L., and Schroder, K. (2015). Mechanisms of unconventional secretion of IL-1 family cytokines. Cytokine *74*, 213–218.

Monteleone, M., Stanley, A.C., Chen, K.W., Brown, D.L., Bezbradica, J.S., von Pein, J.B., Holley, C.L., Boucher, D., Shakespear, M.R., Kapetanovic, R., et al. (2018). Interleukin-1β Maturation Triggers Its Relocation to the Plasma Membrane for Gasdermin-D-Dependent and -Independent Secretion. Cell Rep. *24*, 1425–1433.

Moreno, E., Planells, I., Prats, G., Planes, A.M., Moreno, G., and Andreu, A. (2005). Comparative study of Escherichia coli virulence determinants in strains causing urinary tract bacteremia versus strains causing pyelonephritis and other sources of bacteremia. Diagn. Microbiol. Infect. Dis. *53*, 93–99.

Mosley, B., Urdal, D.L., Prickett, K.S., Larsen, A., Cosman, D., Conlon, P.J., Gillis, S., and Dower, S.K. (1987). The interleukin-1 receptor binds the human interleukin-1 alpha precursor but not the interleukin-1 beta precursor. J. Biol. Chem. *262*, 2941–2944.

Mukherjee, S., Kumar, R., Tsakem Lenou, E., Basrur, V., Kontoyiannis, D.L., Ioakeimidis, F., Mosialos, G., Theiss, A.L., Flavell, R.A., and Venuprasad, K. (2020). Deubiquitination of NLRP6 inflammasome by Cyld critically regulates intestinal inflammation. Nat. Immunol. *21*, 626–635.

Mullins, B., and Chen, J. (2021). NLRP9 in innate immunity and inflammation. Immunology *162*, 262–267.

Muñoz-Planillo, R., Kuffa, P., Martínez-Colón, G., Smith, B.L., Rajendiran, T.M., and Núñez, G. (2013). $K^+$ efflux is the common trigger of NLRP3 inflammasome activation by bacterial toxins and particulate matter. Immunity *38*, 1142–1153.

Murakami, T., Ockinger, J., Yu, J., Byles, V., McColl, A., Hofer, A.M., and Horng, T. (2012). Critical role for calcium mobilization in activation of the NLRP3 inflammasome. Proc. Natl. Acad. Sci. U. S. A. *109*, 11282–11287.

Newton, K., Dixit, V.M., and Kayagaki, N. (2021). Dying cells fan the flames of inflammation. Science *374*, 1076–1080.

Niu, T., De Rosny, C., Chautard, S., Rey, A., Patoli, D., Groslambert, M., Cosson, C., Lagrange, B., Zhang, Z., Visvikis, O., et al. (2021). NLRP3 phosphorylation in its LRR domain critically regulates inflammasome assembly. Nat. Commun. *12*, 5862.

Ohya, K., Handa, Y., Ogawa, M., Suzuki, M., and Sasakawa, C. (2005). IpgB1 is a novel Shigella effector protein involved in bacterial invasion of host cells. Its activity to promote membrane ruffling via Rac1 and Cdc42 activation. J. Biol. Chem. *280*, 24022–24034.

O'Neill, L. a. J. (2002). Signal transduction pathways activated by the IL-1 receptor/toll-like receptor superfamily. Curr. Top. Microbiol. Immunol. *270*, 47–61.

O'Neill, L.A.J., Kishton, R.J., and Rathmell, J. (2016). A guide to immunometabolism for immunologists. Nat. Rev. Immunol. *16*, 553–565.

Oroz, J., Barrera-Vilarmau, S., Alfonso, C., Rivas, G., and de Alba, E. (2016). ASC Pyrin Domain Self-associates and Binds NLRP3 Protein Using Equivalent Binding Interfaces. J. Biol. Chem. *291*, 19487–19501.

Orzalli, M.H., Prochera, A., Payne, L., Smith, A., Garlick, J.A., and Kagan, J.C. (2021). Virus-mediated inactivation of anti-apoptotic Bcl-2 family members promotes Gasdermin-E-dependent pyroptosis in barrier epithelial cells. Immunity S1074761321001746.

Otten, E.G., Werner, E., Crespillo-Casado, A., Boyle, K.B., Dharamdasani, V., Pathe, C., Santhanam, B.,

and Randow, F. (2021). Ubiquitylation of lipopolysaccharide by RNF213 during bacterial infection. Nature *594*, 111–116.

Ozen, S., Demirkaya, E., Erer, B., Livneh, A., Ben-Chetrit, E., Giancane, G., Ozdogan, H., Abu, I., Gattorno, M., Hawkins, P.N., et al. (2016). EULAR recommendations for the management of familial Mediterranean fever. Ann. Rheum. Dis. *75*, 644–651.

Ozinsky, A., Underhill, D.M., Fontenot, J.D., Hajjar, A.M., Smith, K.D., Wilson, C.B., Schroeder, L., and Aderem, A. (2000). The repertoire for pattern recognition of pathogens by the innate immune system is defined by cooperation between toll-like receptors. Proc. Natl. Acad. Sci. U. S. A. *97*, 13766–13771.

Pan, P., Shen, M., Yu, Z., Ge, W., Chen, K., Tian, M., Xiao, F., Wang, Z., Wang, J., Jia, Y., et al. (2021). SARS-CoV-2 N protein promotes NLRP3 inflammasome activation to induce hyperinflammation. Nat. Commun. *12*, 1–17.

Park, J.S., Svetkauskaite, D., He, Q., Kim, J.-Y., Strassheim, D., Ishizaka, A., and Abraham, E. (2004). Involvement of Toll-like Receptors 2 and 4 in Cellular Activation by High Mobility Group Box 1 Protein*. J. Biol. Chem. *279*, 7370–7377.

Park, Y.H., Wood, G., Kastner, D.L., and Chae, J.J. (2016). Pyrin inflammasome activation and RhoA signaling in the autoinflammatory diseases FMF and HIDS. Nat. Immunol. *17*, 914–921.

Park, Y.H., Remmers, E.F., Lee, W., Ombrello, A.K., Chung, L.K., Shilei, Z., Stone, D.L., Ivanov, M.I., Loeven, N.A., Barron, K.S., et al. (2020). Ancient familial Mediterranean fever mutations in human pyrin and resistance to Yersinia pestis. Nat. Immunol. *21*, 857–867.

Pawel-Rammingen, U.V., Telepnev, M.V., Schmidt, G., Aktories, K., Wolf-Watz, H., and Rosqvist, R. (2000). GAP activity of the Yersinia YopE cytotoxin specifically targets the Rho pathway: a mechanism for disruption of actin microfilament structure. Mol. Microbiol. *36*, 737–748.

Pétrilli, V., Papin, S., Dostert, C., Mayor, A., Martinon, F., and Tschopp, J. (2007). Activation of the NALP3 inflammasome is triggered by low intracellular potassium concentration. Cell Death Differ. *14*, 1583–1589.

Planès, R., Pinilla, M., Santoni, K., Hessel, A., Lay, K., Paillette, P., Valadao, A.-L., Robinson, K.S., Bastard, P., Rossi, I., et al. (2021). Human NLRP1 Is a Sensor of 3CL Proteases from Pathogenic Coronaviruses in Lung Epithelial Cells (Rochester, NY: Social Science Research Network).

van der Poll, T., Shankar-Hari, M., and Wiersinga, W.J. (2021). The immunology of sepsis. Immunity *54*, 2450–2464.

Poltorak, A., He, X., Smirnova, I., Liu, M.Y., Van Huffel, C., Du, X., Birdwell, D., Alejos, E., Silva, M., Galanos, C., et al. (1998). Defective LPS signaling in C3H/HeJ and C57BL/10ScCr mice: mutations in Tlr4 gene. Science *282*, 2085–2088.

Popoff, M.R., Chaves-Olarte, E., Lemichez, E., von Eichel-Streiber, C., Thelestam, M., Chardin, P., Cussac, D., Antonny, B., Chavrier, P., Flatau, G., et al. (1996). Ras, Rap, and Rac Small GTP-binding Proteins Are Targets for *Clostridium sordellii* Lethal Toxin Glucosylation. J. Biol. Chem. *271*, 10217–10224.

Prehna, G., Ivanov, M.I., Bliska, J.B., and Stebbins, C.E. (2006). Yersinia Virulence Depends on Mimicry of Host Rho-Family Nucleotide Dissociation Inhibitors. Cell *126*, 869–880.

Py, B.F., Kim, M.-S., Vakifahmetoglu-Norberg, H., and Yuan, J. (2013). Deubiquitination of NLRP3 by BRCC3 critically regulates inflammasome activity. Mol. Cell *49*, 331–338.

Qi, X., Yu, Y., Sun, R., Huang, J., Liu, L., Yang, Y., Rui, T., and Sun, B. (2021). Identification and characterization of neutrophil heterogeneity in sepsis. Crit. Care *25*, 50.

Qin, Y., Li, Q., Liang, W., Yan, R., Tong, L., Jia, M., Zhao, C., and Zhao, W. (2021). TRIM28 SUMOylates and stabilizes NLRP3 to facilitate inflammasome activation. Nat. Commun. *12*, 4794.

Qu, J., Cammarano, M.S., Shi, Q., Ha, K.C., de Lanerolle, P., and Minden, A. (2001). Activated PAK4 regulates cell adhesion and anchorage-independent growth. Mol. Cell. Biol. *21*, 3523–3533.

Qu, Y., Misaghi, S., Izrael-Tomasevic, A., Newton, K., Gilmour, L.L., Lamkanfi, M., Louie, S., Kayagaki, N., Liu, J., Kömüves, L., et al. (2012). Phosphorylation of NLRC4 is critical for inflammasome activation. Nature *490*, 539–542.

Radermecker, C., Detrembleur, N., Guiot, J., Cavalier, E., Henket, M., d'Emal, C., Vanwinge, C., Cataldo, D., Oury, C., Delvenne, P., et al. (2020). Neutrophil extracellular traps infiltrate the lung airway, interstitial, and vascular compartments in severe COVID-19. J. Exp. Med. *217*, e20201012.

Rane, C.K., and Minden, A. (2014). P21 activated kinases: structure, regulation, and functions. Small GTPases *5*.

Ratner, D., Orning, M.P.A., Proulx, M.K., Wang, D., Gavrilin, M.A., Wewers, M.D., Alnemri, E.S., Johnson, P.F., Lee, B., Mecsas, J., et al. (2016). The Yersinia pestis Effector YopM Inhibits Pyrin Inflammasome Activation. PLOS Pathog. *12*, e1006035.

Reibel, L., Dorseuil, O., Stancou, R., Bertoglio, J., and Gacon, G. (1991). A hemopoietic specific gene encoding a small GTP binding protein is overexpressed during T cell activation. Biochem. Biophys. Res. Commun. *175*, 451–458.

Ren, G., Zhang, X., Xiao, Y., Zhang, W., Wang, Y., Ma, W., Wang, X., Song, P., Lai, L., Chen, H., et al. (2019). ABRO1 promotes NLRP3 inflammasome activation through regulation of NLRP3 deubiquitination. EMBO J. *38*.

Reppin, F., Cochet, S., El Nemer, W., Fritz, G., and Schmidt, G. (2018). High Affinity Binding of Escherichia coli Cytotoxic Necrotizing Factor 1 (CNF1) to Lu/BCAM Adhesion Glycoprotein. Toxins *10*, 3.

Reutershan, J., and Ley, K. (2004). Bench-to-bedside review: Acute respiratory distress syndrome – how neutrophils migrate into the lung. Crit. Care *8*, 453.

Ridley, A.J., and Hall, A. (1992). The small GTP-binding protein rho regulates the assembly of focal adhesions and actin stress fibers in response to growth factors. Cell *70*, 389–399.

Ridley, A.J., Paterson, H.F., Johnston, C.L., Diekmann, D., and Hall, A. (1992). The small GTP-binding protein rac regulates growth factor-induced membrane ruffling. Cell *70*, 401–410.

Robert Hollingsworth, L., David, L., Li, Y., Griswold, A.R., Ruan, J., Sharif, H., Fontana, P., Orth-He, E.L., Fu, T.-M., Bachovchin, D.A., et al. (2021). Mechanism of filament formation in UPA-promoted CARD8 and NLRP1 inflammasomes. Nat. Commun. *12*, 1–13.

Roberts, T.L., Idris, A., Dunn, J.A., Kelly, G.M., Burnton, C.M., Hodgson, S., Hardy, L.L., Garceau, V., Sweet, M.J., Ross, I.L., et al. (2009). HIN-200 Proteins Regulate Caspase Activation in Response to Foreign Cytoplasmic DNA. Science *323*, 1057–1060.

Robinson, K.S., Teo, D.E.T., Tan, K.S., Toh, G.A., Ong, H.H., Lim, C.K., Lay, K., Au, B.V., Lew, T.S., Chu, J.J.H., et al. (2020). Enteroviral 3C protease activates the human NLRP1 inflammasome in airway epithelia. Science *370*, eaay2002.

Rodrigues, T.S., de Sá, K.S.G., Ishimoto, A.Y., Becerra, A., Oliveira, S., Almeida, L., Gonçalves, A.V., Perucello, D.B., Andrade, W.A., Castro, R., et al. (2021). Inflammasomes are activated in response to SARS-CoV-2 infection and are associated with COVID-19 severity in patients. J. Exp. Med. *218*, e20201707.

Rothenfusser, S., Goutagny, N., DiPerna, G., Gong, M., Monks, B.G., Schoenemeyer, A., Yamamoto, M., Akira, S., and Fitzgerald, K.A. (2005). The RNA helicase Lgp2 inhibits TLR-independent sensing of viral replication by retinoic acid-inducible gene-I. J. Immunol. Baltim. Md 1950 *175*, 5260–5268.

Ruan, Q., Yang, K., Wang, W., Jiang, L., and Song, J. (2020). Clinical predictors of mortality due to COVID-19 based on an analysis of data of 150 patients from Wuhan, China. Intensive Care Med. *46*, 846–848.

Rühl, S., and Broz, P. (2015). Caspase-11 activates a canonical NLRP3 inflammasome by promoting K(+) efflux. Eur. J. Immunol. *45*, 2927–2936.

Rühl, S., Shkarina, K., Demarco, B., Heilig, R., Santos, J.C., and Broz, P. (2018). ESCRT-dependent membrane repair negatively regulates pyroptosis downstream of GSDMD activation. Science *362*, 956–960.

Saijo, S., Ikeda, S., Yamabe, K., Kakuta, S., Ishigame, H., Akitsu, A., Fujikado, N., Kusaka, T., Kubo, S., Chung, S., et al. (2010). Dectin-2 recognition of alpha-mannans and induction of Th17 cell differentiation is essential for host defense against Candida albicans. Immunity *32*, 681–691.

Saito, T., and Gale, M. (2008). Differential recognition of double-stranded RNA by RIG-I–like receptors in antiviral immunity. J. Exp. Med. *205*, 1523–1527.

Salvi, V., Nguyen, H.O., Sozio, F., Schioppa, T., Gaudenzi, C., Laffranchi, M., Scapini, P., Passari, M., Barbazza, I., Tiberio, L., et al. (2021). SARS-CoV-2-associated ssRNAs activate inflammation and immunity via TLR7/8. JCI Insight *6*, e150542.

Sánchez-Cerrillo, I., Landete, P., Aldave, B., Sánchez-Alonso, S., Sánchez-Azofra, A., Marcos-Jiménez, A., Ávalos, E., Alcaraz-Serna, A., de Los Santos, I., Mateu-Albero, T., et al. (2020). COVID-19 severity associates with pulmonary redistribution of CD1c+ DCs and inflammatory transitional and nonclassical monocytes. J. Clin. Invest. *130*, 6290–6300.

Sanders, L.C., Matsumura, F., Bokoch, G.M., and de Lanerolle, P. (1999). Inhibition of myosin light chain kinase by p21-activated kinase. Science *283*, 2083–2085.

Sandstrom, A., Mitchell, P.S., Goers, L., Mu, E.W., Lesser, C.F., and Vance, R.E. (2019). Functional degradation: A mechanism of NLRP1 inflammasome activation by diverse pathogen enzymes. Science *364*, eaau1330.

Sanman, L.E., Qian, Y., Eisele, N.A., Ng, T.M., van der Linden, W.A., Monack, D.M., Weerapana, E., and Bogyo, M. (2016). Disruption of glycolytic flux is a signal for inflammasome signaling and pyroptotic cell death. ELife *5*, e13663.

Santos, J.C., Boucher, D., Schneider, L.K., Demarco, B., Dilucca, M., Shkarina, K., Heilig, R., Chen, K.W., Lim, R.Y.H., and Broz, P. (2020). Human GBP1 binds LPS to initiate assembly of a caspase-4 activating platform on cytosolic bacteria. Nat. Commun. *11*, 1–15.

Schmidt, G., Sehr, P., Wilm, M., Selzer, J., Mann, M., and Aktories, K. (1997). Gln 63 of Rho is deamidated by Escherichia coli cytotoxic necrotizing factor-1. Nature *387*, 725–729.

Schulte-Schrepping, J., Reusch, N., Paclik, D., Baßler, K., Schlickeiser, S., Zhang, B., Krämer, B., Krammer, T., Brumhard, S., Bonaguro, L., et al. (2020). Severe COVID-19 Is Marked by a Dysregulated Myeloid Cell Compartment. Cell *182*, 1419-1440.e23.

Schultze, J.L., and Aschenbrenner, A.C. (2021). COVID-19 and the human innate immune system. Cell *184*, 1671–1692.

Shamri, R., Young, K.M., and Weller, P.F. (2019). Rho and Rac, but not ROCK, are required for secretion of human and mouse eosinophil-associated RNases. Clin. Exp. Allergy J. Br. Soc. Allergy Clin. Immunol. *49*, 190–198.

Shao, F., Merritt, P.M., Bao, Z., Innes, R.W., and Dixon, J.E. (2002). A Yersinia Effector and a Pseudomonas Avirulence Protein Define a Family of Cysteine Proteases Functioning in Bacterial Pathogenesis. Cell *109*, 575–588.

Shao, L., Liu, Y., Wang, W., Li, A., Wan, P., Liu, W., Shereen, M.A., Liu, F., Zhang, W., Tan, Q., et al. (2020). SUMO1 SUMOylates and SENP3 deSUMOylates NLRP3 to orchestrate the inflammasome activation. FASEB J. *34*, 1497–1515.

Sharapova, S.O., Haapaniemi, E., Sakovich, I.S., Kostyuchenko, L.V., Donkó, A., Dulau-Florea, A., Malko,

O., Bondarenko, A.V., Stegantseva, M.V., Leto, T.L., et al. (2019). Heterozygous activating mutation in RAC2 causes infantile-onset combined immunodeficiency with susceptibility to viral infections. Clin. Immunol. Orlando Fla *205*, 1–5.

Sharif, H., Wang, L., Wang, W.L., Magupalli, V.G., Andreeva, L., Qiao, Q., Hauenstein, A.V., Wu, Z., Núñez, G., Mao, Y., et al. (2019). Structural mechanism for NEK7-licensed activation of NLRP3 inflammasome. Nature *570*, 338–343.

Sharif, H., Hollingsworth, L.R., Griswold, A.R., Hsiao, J.C., Wang, Q., Bachovchin, D.A., and Wu, H. (2021). Dipeptidyl peptidase 9 sets a threshold for CARD8 inflammasome formation by sequestering its active C-terminal fragment. Immunity *54*, 1392-1404.e10.

Sharp, F.A., Ruane, D., Claass, B., Creagh, E., Harris, J., Malyala, P., Singh, M., O'Hagan, D.T., Pétrilli, V., Tschopp, J., et al. (2009). Uptake of particulate vaccine adjuvants by dendritic cells activates the NALP3 inflammasome. Proc. Natl. Acad. Sci. U. S. A. *106*, 870–875.

Shen, C., Li, R., Negro, R., Cheng, J., Vora, S.M., Fu, T.-M., Wang, A., He, K., Andreeva, L., Gao, P., et al. (2021). Phase separation drives RNA virus-induced activation of the NLRP6 inflammasome. Cell.

Shi, C.-S., Shenderov, K., Huang, N.-N., Kabat, J., Abu-Asab, M., Fitzgerald, K.A., Sher, A., and Kehrl, J.H. (2012). Activation of autophagy by inflammatory signals limits IL-1β production by targeting ubiquitinated inflammasomes for destruction. Nat. Immunol. *13*, 255–263.

Shi, H., Wang, Y., Li, X., Zhan, X., Tang, M., Fina, M., Su, L., Pratt, D., Bu, C.H., Hildebrand, S., et al. (2016). NLRP3 activation and mitosis are mutually exclusive events coordinated by NEK7, a new inflammasome component. Nat. Immunol. *17*, 250.

Shi, J., Zhao, Y., Wang, Y., Gao, W., Ding, J., Li, P., Hu, L., and Shao, F. (2014). Inflammatory caspases are innate immune receptors for intracellular LPS. Nature *514*, 187–192.

Shi, J., Zhao, Y., Wang, K., Shi, X., Wang, Y., Huang, H., Zhuang, Y., Cai, T., Wang, F., and Shao, F. (2015). Cleavage of GSDMD by inflammatory caspases determines pyroptotic cell death. Nature *526*, 660–665.

Shi, J., Gao, W., and Shao, F. (2017). Pyroptosis: Gasdermin-Mediated Programmed Necrotic Cell Death. Trends Biochem. Sci. *42*, 245–254.

Shimada, K., Crother, T.R., Karlin, J., Dagvadorj, J., Chiba, N., Chen, S., Ramanujan, V.K., Wolf, A.J., Vergnes, L., Ojcius, D.M., et al. (2012). Oxidized mitochondrial DNA activates the NLRP3 inflammasome during apoptosis. Immunity *36*, 401–414.

Silvestre-Roig, C., Fridlender, Z.G., Glogauer, M., and Scapini, P. (2019). Neutrophil Diversity in Health and Disease. Trends Immunol. *40*, 565–583.

Silvin, A., Chapuis, N., Dunsmore, G., Goubet, A.-G., Dubuisson, A., Derosa, L., Almire, C., Hénon, C., Kosmider, O., Droin, N., et al. (2020). Elevated Calprotectin and Abnormal Myeloid Cell Subsets Discriminate Severe from Mild COVID-19. Cell *182*, 1401-1418.e18.

Singer, M., Deutschman, C.S., Seymour, C.W., Shankar-Hari, M., Annane, D., Bauer, M., Bellomo, R., Bernard, G.R., Chiche, J.-D., Coopersmith, C.M., et al. (2016). The Third International Consensus Definitions for Sepsis and Septic Shock (Sepsis-3). JAMA *315*, 801–810.

Sinha, S., Rosin, N.L., Arora, R., Labit, E., Jaffer, A., Cao, L., Farias, R., Nguyen, A.P., de Almeida, L.G.N., Dufour, A., et al. (2021). Dexamethasone modulates immature neutrophils and interferon programming in severe COVID-19. Nat. Med. 1–11.

Sironi, M., Breviario, F., Proserpio, P., Biondi, A., Vecchi, A., Damme, J.V., Dejana, E., and Mantovani, A. (1989). IL-1 stimulates IL-6 production in endothelial cells. J. Immunol. *142*, 549–553.

Song, H., Liu, B., Huai, W., Yu, Z., Wang, W., Zhao, J., Han, L., Jiang, G., Zhang, L., Gao, C., et al. (2016). The E3 ubiquitin ligase TRIM31 attenuates NLRP3 inflammasome activation by promoting proteasomal degradation of NLRP3. Nat. Commun. *7*.

Song, N., Liu, Z.-S., Xue, W., Bai, Z.-F., Wang, Q.-Y., Dai, J., Liu, X., Huang, Y.-J., Cai, H., Zhan, X.-Y., et al. (2017). NLRP3 Phosphorylation Is an Essential Priming Event for Inflammasome Activation. Mol. Cell *68*, 185-197.e6.

Spalinger, M.R., Kasper, S., Gottier, C., Lang, S., Atrott, K., Vavricka, S.R., Scharl, S., Gutte, P.M., Grütter, M.G., Beer, H.-D., et al. (2016). NLRP3 tyrosine phosphorylation is controlled by protein tyrosine phosphatase PTPN22 (American Society for Clinical Investigation).

Sposito, B., Broggi, A., Pandolfi, L., Crotta, S., Clementi, N., Ferrarese, R., Sisti, S., Criscuolo, E., Spreafico, R., Long, J.M., et al. (2021). The interferon landscape along the respiratory tract impacts the severity of COVID-19. Cell *184*, 4953-4968.e16.

Stender, S., Friebel, A., Linder, S., Rohde, M., Mirold, S., and Hardt, W.D. (2000). Identification of SopE2 from Salmonella typhimurium, a conserved guanine nucleotide exchange factor for Cdc42 of the host cell. Mol. Microbiol. *36*, 1206–1221.

Stevens, M.P., Friebel, A., Taylor, L.A., Wood, M.W., Brown, P.J., Hardt, W.-D., and Galyov, E.E. (2003). A Burkholderia pseudomallei Type III Secreted Protein, BopE, Facilitates Bacterial Invasion of Epithelial Cells and Exhibits Guanine Nucleotide Exchange Factor Activity. J. Bacteriol. *185*, 4992–4996.

Stevenson, F.T., Torrano, F., Locksley, R.M., and Lovett, D.H. (1992). Interleukin 1: the patterns of translation and intracellular distribution support alternative secretory mechanisms. J. Cell. Physiol. *152*, 223–231.

Stoll, T., Markwirth, G., Reipschläger, S., and Schmidt, G. (2009). A new member of a growing toxin family--Escherichia coli cytotoxic necrotizing factor 3 (CNF3). Toxicon Off. J. Int. Soc. Toxinology *54*, 745–753.

Stuart, L.M., Paquette, N., and Boyer, L. (2013). Effector-triggered versus pattern-triggered immunity: how animals sense virulent pathogens. Nat. Rev. Immunol. *13*, 199–206.

Stutz, A., Kolbe, C.-C., Stahl, R., Horvath, G.L., Franklin, B.S., Ray, O. van, Brinkschulte, R., Geyer, M., Meissner, F., and Latz, E. (2017). NLRP3 inflammasome assembly is regulated by phosphorylation of the pyrin domain. J. Exp. Med. jem.20160933.

Sugai, M., Hashimoto, K., Kikuchi, A., Inoue, S., Okumura, H., Matsumoto, K., Goto, Y., Ohgai, H., Moriishi, K., and Syuto, B. (1992). Epidermal cell differentiation inhibitor ADP-ribosylates small GTP-binding proteins and induces hyperplasia of epidermis. J. Biol. Chem. *267*, 2600–2604.

Sun, H., Kamanova, J., Lara-Tejero, M., and Galán, J.E. (2018). Salmonella stimulates pro-inflammatory signalling through p21-activated kinases bypassing innate immune receptors. Nat. Microbiol. *3*, 1122–1130.

Sun, L., Wu, J., Du, F., Chen, X., and Chen, Z.J. (2013). Cyclic GMP-AMP Synthase Is a Cytosolic DNA Sensor That Activates the Type I Interferon Pathway. Science.

Swanson, K.V., Deng, M., and Ting, J.P.-Y. (2019). The NLRP3 inflammasome: molecular activation and regulation to therapeutics. Nat. Rev. Immunol. *19*, 477–489.

Takeda, K., and Akira, S. (2015). Toll-like receptors. Curr. Protoc. Immunol. *109*, 14.12.1-10.

Takeuchi, O., Sato, S., Horiuchi, T., Hoshino, K., Takeda, K., Dong, Z., Modlin, R.L., and Akira, S. (2002). Cutting Edge: Role of Toll-Like Receptor 1 in Mediating Immune Response to Microbial Lipoproteins. J. Immunol. *169*, 10–14.

Tang, J., Tu, S., Lin, G., Guo, H., Yan, C., Liu, Q., Huang, L., Tang, N., Xiao, Y., Pope, R.M., et al. (2020). Sequential ubiquitination of NLRP3 by RNF125 and Cbl-b limits inflammasome activation and endotoxemia. J. Exp. Med. *217*, e20182091.

Tang, T., Lang, X., Xu, C., Wang, X., Gong, T., Yang, Y., Cui, J., Bai, L., Wang, J., Jiang, W., et al. (2017). CLICs-dependent chloride efflux is an essential and proximal upstream event for NLRP3 inflammasome

activation. Nat. Commun. *8*, 1–12.

Tapia-Abellán, A., Angosto-Bazarra, D., Alarcón-Vila, C., Baños, M.C., Hafner-Bratkovič, I., Oliva, B., and Pelegrín, P. (2021). Sensing low intracellular potassium by NLRP3 results in a stable open structure that promotes inflammasome activation. Sci. Adv. *7*, eabf4468.

The RECOVERY Collaborative Group (2021). Dexamethasone in Hospitalized Patients with Covid-19. N. Engl. J. Med. *384*, 693–704.

Theobald, S.J., Simonis, A., Georgomanolis, T., Kreer, C., Zehner, M., Eisfeld, H.S., Albert, M.-C., Chhen, J., Motameny, S., Erger, F., et al. (2021). Long-lived macrophage reprogramming drives spike protein-mediated inflammasome activation in COVID-19. EMBO Mol. Med. *n/a*, e14150.

Thompson, E.A., Cascino, K., Ordonez, A.A., Zhou, W., Vaghasia, A., Hamacher-Brady, A., Brady, N.R., Sun, I.-H., Wang, R., Rosenberg, A.Z., et al. (2021). Metabolic programs define dysfunctional immune responses in severe COVID-19 patients. Cell Rep. *34*, 108863.

Thorne, L.G., Reuschl, A.-K., Zuliani-Alvarez, L., Whelan, M.V.X., Turner, J., Noursadeghi, M., Jolly, C., and Towers, G.J. (2021). SARS-CoV-2 sensing by RIG-I and MDA5 links epithelial infection to macrophage inflammation. EMBO J. *40*, e107826.

Thurston, T.L.M., Wandel, M.P., von Muhlinen, N., Foeglein, Á., and Randow, F. (2012). Galectin 8 targets damaged vesicles for autophagy to defend cells against bacterial invasion. Nature *482*, 414–418.

Tosato, G., and Jones, K.D. (1990). Interleukin-1 Induces Interleukin-6 Production in Peripheral Blood Monocytes. Blood *75*, 1305–1310.

Tsu, B.V., Beierschmitt, C., Ryan, A.P., Agarwal, R., Mitchell, P.S., and Daugherty, M.D. (2021). Diverse viral proteases activate the NLRP1 inflammasome. ELife *10*, e60609.

Van Gorp, H., Saavedra, P.H.V., de Vasconcelos, N.M., Van Opdenbosch, N., Vande Walle, L., Matusiak, M., Prencipe, G., Insalaco, A., Van Hauwermeiren, F., Demon, D., et al. (2016). Familial Mediterranean fever mutations lift the obligatory requirement for microtubules in Pyrin inflammasome activation. Proc. Natl. Acad. Sci. U. S. A. *113*, 14384–14389.

Vance, R.E. (2015). The NAIP/NLRC4 Inflammasomes. Curr. Opin. Immunol. *0*, 84–89.

Vance, R.E., Isberg, R.R., and Portnoy, D.A. (2009). Patterns of pathogenesis: discrimination of pathogenic and nonpathogenic microbes by the innate immune system. Cell Host Microbe *6*, 10–21.

Veras, F.P., Pontelli, M.C., Silva, C.M., Toller-Kawahisa, J.E., de Lima, M., Nascimento, D.C., Schneider, A.H., Caetité, D., Tavares, L.A., Paiva, I.M., et al. (2020). SARS-CoV-2–triggered neutrophil extracellular traps mediate COVID-19 pathologySARS-CoV-2 directly triggers ACE-dependent NETs. J. Exp. Med. *217*, e20201129.

Vicente-Manzanares, M., and Sánchez-Madrid, F. (2004). Role of the cytoskeleton during leukocyte responses. Nat. Rev. Immunol. *4*, 110–122.

Vincent, J.-L., Sakr, Y., Sprung, C.L., Ranieri, V.M., Reinhart, K., Gerlach, H., Moreno, R., Carlet, J., Le Gall, J.-R., Payen, D., et al. (2006). Sepsis in European intensive care units: results of the SOAP study. Crit. Care Med. *34*, 344–353.

Vora, S.M., Lieberman, J., and Wu, H. (2021). Inflammasome activation at the crux of severe COVID-19. Nat. Rev. Immunol. *21*, 694–703.

Wan, P., Zhang, Q., Liu, W., Jia, Y., Ai, S., Wang, T., Wang, W., Pan, P., Yang, G., Xiang, Q., et al. (2019). Cullin1 binds and promotes NLRP3 ubiquitination to repress systematic inflammasome activation. FASEB J. *33*, 5793–5807.

Wandel, M.P., Kim, B.-H., Park, E.-S., Boyle, K.B., Nayak, K., Lagrange, B., Herod, A., Henry, T., Zilbauer, M., Rohde, J., et al. (2020). Guanylate-binding proteins convert cytosolic bacteria into caspase-4

signaling platforms. Nat. Immunol. *21*, 880–891.

Wang, F., Nie, J., Wang, H., Zhao, Q., Xiong, Y., Deng, L., Song, S., Ma, Z., Mo, P., and Zhang, Y. (2020). Characteristics of Peripheral Lymphocyte Subset Alteration in COVID-19 Pneumonia. J. Infect. Dis. *221*, 1762–1769.

Wang, J., Hu, M., Wang, J., Qi, J., Han, Z., Wang, G., Qi, Y., Wang, H.-W., Zhou, J.-M., and Chai, J. (2019). Reconstitution and structure of a plant NLR resistosome conferring immunity. Science *364*, eaav5870.

Wang, P., Zhu, S., Yang, L., Cui, S., Pan, W., Jackson, R., Zheng, Y., Rongvaux, A., Sun, Q., Yang, G., et al. (2015). Nlrp6 regulates intestinal antiviral innate immunity. Science *350*, 826–830.

Wang, P.-H., Ye, Z.-W., Deng, J.-J., Siu, K.-L., Gao, W.-W., Chaudhary, V., Cheng, Y., Fung, S.-Y., Yuen, K.-S., Ho, T.-H., et al. (2018). Inhibition of AIM2 inflammasome activation by a novel transcript isoform of IFI16. EMBO Rep. *19*.

Wang, Q., Gao, H., Clark, K.M., Mugisha, C.S., Davis, K., Tang, J.P., Harlan, G.H., DeSelm, C.J., Presti, R.M., Kutluay, S.B., et al. (2021a). CARD8 is an inflammasome sensor for HIV-1 protease activity. Science *371*, eabe1707.

Wang, S., Narendran, S., Hirahara, S., Varshney, A., Pereira, F., Apicella, I., Ambati, M., Ambati, V.L., Yerramothu, P., Ambati, K., et al. (2021b). DDX17 is an essential mediator of sterile NLRC4 inflammasome activation by retrotransposon RNAs. Sci. Immunol. *6*, eabi4493.

Wauters, E., Van Mol, P., Garg, A.D., Jansen, S., Van Herck, Y., Vanderbeke, L., Bassez, A., Boeckx, B., Malengier-Devlies, B., Timmerman, A., et al. (2021). Discriminating mild from critical COVID-19 by innate and adaptive immune single-cell profiling of bronchoalveolar lavages. Cell Res. *31*, 272–290.

Weber, A., Wasiliew, P., and Kracht, M. (2010). Interleukin-1 (IL-1) pathway. Sci. Signal. *3*, cm1.

Wennerberg, K., Rossman, K.L., and Der, C.J. (2005). The Ras superfamily at a glance. J. Cell Sci. *118*, 843–846.

Wilde, C., Chhatwal, G.S., Schmalzing, G., Aktories, K., and Just, I. (2001). A Novel C3-like ADP-ribosyltransferase fromStaphylococcus aureus Modifying RhoE and Rnd3. J. Biol. Chem. *276*, 9537–9542.

Wilk, A.J., Rustagi, A., Zhao, N.Q., Roque, J., Martínez-Colón, G.J., McKechnie, J.L., Ivison, G.T., Ranganath, T., Vergara, R., Hollis, T., et al. (2020). A single-cell atlas of the peripheral immune response in patients with severe COVID-19. Nat. Med. *26*, 1070–1076.

Williams, D.A., Tao, W., Yang, F., Kim, C., Gu, Y., Mansfield, P., Levine, J.E., Petryniak, B., Derrow, C.W., Harris, C., et al. (2000). Dominant negative mutation of the hematopoietic-specific Rho GTPase, Rac2, is associated with a human phagocyte immunodeficiency. Blood *96*, 1646–1654.

Winheim, E., Rinke, L., Lutz, K., Reischer, A., Leutbecher, A., Wolfram, L., Rausch, L., Kranich, J., Wratil, P.R., Huber, J.E., et al. (2021). Impaired function and delayed regeneration of dendritic cells in COVID-19. PLOS Pathog. *17*, e1009742.

Wolf, A.J., Reyes, C.N., Liang, W., Becker, C., Shimada, K., Wheeler, M.L., Cho, H.C., Popescu, N.I., Coggeshall, K.M., Arditi, M., et al. (2016). Hexokinase Is an Innate Immune Receptor for the Detection of Bacterial Peptidoglycan. Cell *166*, 624–636.

Wolters, M., Boyle, E.C., Lardong, K., Trülzsch, K., Steffen, A., Rottner, K., Ruckdeschel, K., and Aepfelbacher, M. (2013). Cytotoxic necrotizing factor-Y boosts Yersinia effector translocation by activating Rac protein. J. Biol. Chem. *288*, 23543–23553.

Worby, C.A., Mattoo, S., Kruger, R.P., Corbeil, L.B., Koller, A., Mendez, J.C., Zekarias, B., Lazar, C., and Dixon, J.E. (2009). The fic domain: regulation of cell signaling by adenylylation. Mol. Cell *34*, 93–103.

Xian, H., Liu, Y., Rundberg Nilsson, A., Gatchalian, R., Crother, T.R., Tourtellotte, W.G., Zhang, Y., Aleman-

Muench, G.R., Lewis, G., Chen, W., et al. (2021). Metformin inhibition of mitochondrial ATP and DNA synthesis abrogates NLRP3 inflammasome activation and pulmonary inflammation. Immunity *54*, 1463-1477.e11.

Xu, G., Qi, F., Li, H., Yang, Q., Wang, H., Wang, X., Liu, X., Zhao, J., Liao, X., Liu, Y., et al. (2020). The differential immune responses to COVID-19 in peripheral and lung revealed by single-cell RNA sequencing. Cell Discov. *6*, 73.

Xu, H., Yang, J., Gao, W., Li, L., Li, P., Zhang, L., Gong, Y.-N., Peng, X., Xi, J.J., Chen, S., et al. (2014). Innate immune sensing of bacterial modifications of Rho GTPases by the Pyrin inflammasome. Nature *513*, 237–241.

Xu, H., Shi, J., Gao, H., Liu, Y., Yang, Z., Shao, F., and Dong, N. (2019). The N-end rule ubiquitin ligase UBR2 mediates NLRP1B inflammasome activation by anthrax lethal toxin. EMBO J. *38*, e101996.

Yamada, T., Sato, S., Sotoyama, Y., Orba, Y., Sawa, H., Yamauchi, H., Sasaki, M., and Takaoka, A. (2021). RIG-I triggers a signaling-abortive anti-SARS-CoV-2 defense in human lung cells. Nat. Immunol. *22*, 820–828.

Yan, Y., Jiang, W., Liu, L., Wang, X., Ding, C., Tian, Z., and Zhou, R. (2015). Dopamine controls systemic inflammation through inhibition of NLRP3 inflammasome. Cell *160*, 62–73.

Yang, J., Zhao, Y., Shi, J., and Shao, F. (2013). Human NAIP and mouse NAIP1 recognize bacterial type III secretion needle protein for inflammasome activation. Proc. Natl. Acad. Sci. U. S. A. *110*, 14408–14413.

Yang, X., Cheng, X., Tang, Y., Qiu, X., Wang, Y., Kang, H., Wu, J., Wang, Z., Liu, Y., Chen, F., et al. (2019a). Bacterial Endotoxin Activates the Coagulation Cascade through Gasdermin D-Dependent Phosphatidylserine Exposure. Immunity *51*, 983-996.e6.

Yang, X., Yu, Y., Xu, J., Shu, H., Xia, J., Liu, H., Wu, Y., Zhang, L., Yu, Z., Fang, M., et al. (2020a). Clinical course and outcomes of critically ill patients with SARS-CoV-2 pneumonia in Wuhan, China: a single-centered, retrospective, observational study. Lancet Respir. Med. *8*, 475–481.

Yang, Y., Wang, H., Kouadir, M., Song, H., and Shi, F. (2019b). Recent advances in the mechanisms of NLRP3 inflammasome activation and its inhibitors. Cell Death Dis. *10*, 128.

Yang, Y., Shen, C., Li, J., Yuan, J., Wei, J., Huang, F., Wang, F., Li, G., Li, Y., Xing, L., et al. (2020b). Plasma IP-10 and MCP-3 levels are highly associated with disease severity and predict the progression of COVID-19. J. Allergy Clin. Immunol. *146*, 119-127.e4.

Yarbrough, M.L., Li, Y., Kinch, L.N., Grishin, N.V., Ball, H.L., and Orth, K. (2009). AMPylation of Rho GTPases by Vibrio VopS Disrupts Effector Binding and Downstream Signaling. Science *323*, 269–272.

Yarovinsky, F., Zhang, D., Andersen, J.F., Bannenberg, G.L., Serhan, C.N., Hayden, M.S., Hieny, S., Sutterwala, F.S., Flavell, R.A., Ghosh, S., et al. (2005). TLR11 activation of dendritic cells by a protozoan profilin-like protein. Science *308*, 1626–1629.

Yin, Q., Sester, D.P., Tian, Y., Hsiao, Y.-S., Lu, A., Cridland, J.A., Sagulenko, V., Thygesen, S.J., Choubey, D., Hornung, V., et al. (2013). Molecular Mechanism for p202-mediated Specific Inhibition of AIM2 Inflammasome Activation. Cell Rep. *4*, 327.

Yoneyama, M., Kikuchi, M., Natsukawa, T., Shinobu, N., Imaizumi, T., Miyagishi, M., Taira, K., Akira, S., and Fujita, T. (2004). The RNA helicase RIG-I has an essential function in double-stranded RNA-induced innate antiviral responses. Nat. Immunol. *5*, 730–737.

Yvan-Charvet, L., and Ng, L.G. (2019). Granulopoiesis and Neutrophil Homeostasis: A Metabolic, Daily Balancing Act. Trends Immunol. *40*, 598–612.

Zanoni, I., Tan, Y., Di Gioia, M., Broggi, A., Ruan, J., Shi, J., Donado, C.A., Shao, F., Wu, H., Springstead, J.R., et al. (2016). An endogenous caspase-11 ligand elicits interleukin-1 release from living dendritic cells. Science *352*, 1232–1236.

Zhang, A., Xing, J., Xia, T., Zhang, H., Fang, M., Li, S., Du, Y., Li, X.C., Zhang, Z., and Zeng, M.-S. (2020a). EphA2 phosphorylates NLRP3 and inhibits inflammasomes in airway epithelial cells. EMBO Rep. *21*, e49666.

Zhang, J., Wu, H., Yao, X., Zhang, D., Zhou, Y., Fu, B., Wang, W., Li, H., Wang, Z., Hu, Z., et al. (2021). Pyroptotic macrophages stimulate the SARS-CoV-2-associated cytokine storm. Cell. Mol. Immunol. *18*, 1305–1307.

Zhang, L., Krachler, A.M., Broberg, C.A., Li, Y., Mirzaei, H., Gilpin, C.J., and Orth, K. (2012). Type III effector VopC mediates invasion for Vibrio species. Cell Rep. *1*, 453–460.

Zhang, L., Chen, S., Ruan, J., Wu, J., Tong, A.B., Yin, Q., Li, Y., David, L., Lu, A., Wang, W.L., et al. (2015). Cryo-EM structure of the activated NAIP2-NLRC4 inflammasome reveals nucleated polymerization. Science *350*, 404–409.

Zhang, Q., Bastard, P., Liu, Z., Le Pen, J., Moncada-Velez, M., Chen, J., Ogishi, M., Sabli, I.K.D., Hodeib, S., Korol, C., et al. (2020b). Inborn errors of type I IFN immunity in patients with life-threatening COVID-19. Science *370*, eabd4570.

Zhang, Z., Meszaros, G., He, W., Xu, Y., Magliarelli, H. de F., Mailly, L., Mihlan, M., Liu, Y., Gámez, M.P., Goginashvili, A., et al. (2017). Protein kinase D at the Golgi controls NLRP3 inflammasome activation. J. Exp. Med. *214*, 2671–2693.

Zhao, W., Shi, C.-S., Harrison, K., Hwang, I.-Y., Nabar, N.R., Wang, M., and Kehrl, J.H. (2020a). AKT Regulates NLRP3 Inflammasome Activation by Phosphorylating NLRP3 Serine 5. J. Immunol. *205*, 2255–2264.

Zhao, Y., Yang, J., Shi, J., Gong, Y.-N., Lu, Q., Xu, H., Liu, L., and Shao, F. (2011). The NLRC4 inflammasome receptors for bacterial flagellin and type III secretion apparatus. Nature *477*, 596–600.

Zhao, Y., Qin, L., Zhang, P., Li, K., Liang, L., Sun, J., Xu, B., Dai, Y., Li, X., Zhang, C., et al. (2020b). Longitudinal COVID-19 profiling associates IL-1RA and IL-10 with disease severity and RANTES with mild disease. JCI Insight *5*, 139834.

Zheng, M., Karki, R., Williams, E.P., Yang, D., Fitzpatrick, E., Vogel, P., Jonsson, C.B., and Kanneganti, T.-D. (2021). TLR2 senses the SARS-CoV-2 envelope protein to produce inflammatory cytokines. Nat. Immunol. *22*, 829–838.

Zheng, S., Fan, J., Yu, F., Feng, B., Lou, B., Zou, Q., Xie, G., Lin, S., Wang, R., Yang, X., et al. (2020). Viral load dynamics and disease severity in patients infected with SARS-CoV-2 in Zhejiang province, China, January-March 2020: retrospective cohort study. BMJ *369*, m1443.

Zhong, F.L., Mamaï, O., Sborgi, L., Boussofara, L., Hopkins, R., Robinson, K., Szeverényi, I., Takeichi, T., Balaji, R., Lau, A., et al. (2016). Germline NLRP1 Mutations Cause Skin Inflammatory and Cancer Susceptibility Syndromes via Inflammasome Activation. Cell *167*, 187-202.e17.

Zhong, Z., Liang, S., Sanchez-Lopez, E., He, F., Shalapour, S., Lin, X., Wong, J., Ding, S., Seki, E., Schnabl, B., et al. (2018). New mitochondrial DNA synthesis enables NLRP3 inflammasome activation. Nature *560*, 198–203.

Zhou, Z., Ren, L., Zhang, L., Zhong, J., Xiao, Y., Jia, Z., Guo, L., Yang, J., Wang, C., Jiang, S., et al. (2020). Heightened Innate Immune Responses in the Respiratory Tract of COVID-19 Patients. Cell Host Microbe *27*, 883-890.e2.

Zhu, K., Jin, X., Chi, Z., Chen, S., Wu, S., Sloan, R.D., Lin, X., Neculai, D., Wang, D., Hu, H., et al. (2021). Priming of NLRP3 inflammasome activation by Msn kinase MINK1 in macrophages. Cell. Mol. Immunol. 1–11.

Zhu, S., Ding, S., Wang, P., Wei, Z., Pan, W., Palm, N.W., Yang, Y., Yu, H., Li, H.-B., Wang, G., et al. (2017). Nlrp9b inflammasome restricts rotavirus infection in intestinal epithelial cells. Nature *546*, 667–670.

Ziegler, C.G.K., Miao, V.N., Owings, A.H., Navia, A.W., Tang, Y., Bromley, J.D., Lotfy, P., Sloan, M., Laird, H., Williams, H.B., et al. (2021). Impaired local intrinsic immunity to SARS-CoV-2 infection in severe COVID-19. Cell *184*, 4713-4733.e22.

Zumbihl, R., Aepfelbacher, M., Andor, A., Jacobi, C.A., Ruckdeschel, K., Rouot, B., and Heesemann, J. (1999). The Cytotoxin YopT of *Yersinia enterocolitica* Induces Modification and Cellular Redistribution of the Small GTP-binding Protein RhoA. J. Biol. Chem. *274*, 29289–29293.

# Annexes

1. Rho-GTPases et inflammasomes : gardiens de l'ETI

2. Articles en collaboration :

   - Propriété anti-inflammatoire des acides gras polyinsaturés ω au niveau du tissu adipeux
   - Rôle des adipocytes bruns et blancs dans la réponse inflammatoire au LPS

PLOS PATHOGENS

PEARLS

# RhoGTPases and inflammasomes: Guardians of effector-triggered immunity

**Océane Dufies, Laurent Boyer***

Université Côte d'Azur, Inserm, C3M, Nice, France

* laurent.boyer@univ-cotedazur.fr

## Abstract

Pathogens have evolved smart strategies to invade hosts and hijack their immune responses. One such strategy is the targeting of the host RhoGTPases by toxins or virulence factors to hijack the cytoskeleton dynamic and immune processes. In response to this microbial attack, the host has evolved an elegant strategy to monitor the function of virulence factors and toxins by sensing the abnormal activity of RhoGTPases. This innate immune strategy of sensing bacterial effector targeting RhoGTPase appears to be a bona fide example of effector-triggered immunity (ETI). Here, we review recently discovered mechanisms by which the host can sense the activity of these toxins through NOD and NOD-like receptors (NLRs).





**Citation:** Dufies O, Boyer L (2021) RhoGTPases and inflammasomes: Guardians of effector-triggered immunity. PLoS Pathog 17(4): e1009504. https://doi.org/10.1371/journal.ppat.1009504

**Editor:** Neal Silverman, University of Massachusetts, Worcester, UNITED STATES

**Published:** April 29, 2021



**Funding:** This work was supported by grants from Inserm (inserm.fr), Université Côte d'Azur (univ-cotedazur.fr), ANR (anr.fr) (ANR-17-CE15-0001) to L.B.. O.D. is supported by a fellowship from Inserm and Université Côte d'Azur. The funders had no role in study design, data collection and analysis, decision to publish, or preparation of the manuscript.

**Competing interests:** The authors have declared that no competing interests exist.

## Introduction

The detection of microbes by the innate immune system is central to host immunity. Recent studies have highlighted the role of the innate immune monitoring of RhoGTPases activity to sense virulence factors targeting RhoGTPases. This is in contrast to the detection of microbial-associated molecular patterns (MAMPs) via pattern recognition receptors (PRRs) which monitors the structural motifs of microbes [1]. The sensing of virulence factors targeting RhoGTPases is based on the detection of the abnormal activity of the host RhoGTPases. This feature is related to effector-triggered immunity (ETI) that initially emerged from phytopathology studies [2,3]. Both systems play critical roles: While the sensing of microbial structural motifs expressed by most microbes would enable to sense all kinds of microbes, the detection of microbial virulence factors expressed by pathogens would enable an increased immune response specifically against pathogens.

ETI was proposed to monitor the function of microbial virulence factors (i.e., effectors and toxins) by sensing their activity [3–7]. Over the last 10 years, a major contribution to the identification of ETI in animals came from the study of virulence factors targeting RhoGTPases and their interplay with innate immune sensors such as NOD and NOD-like receptor (NLR) family members.

More than 30 virulence factors target RhoGTPases [8,9]. The mammalian RhoGTPase family consists of about 20 members, and the best characterized subfamilies are Rho, Rac, and Cdc42 [10]. Rho proteins are molecular switches that control a wide range of cellular processes including inflammation, cell death as well as tissue homeostasis [11]. Mutations of RhoGTPases or dysregulation of their activities have been linked to immune deficiencies, neurological

disorders, or cancers [12–14]. The targeting of RhoGTPases by virulence factors was firstly shown to confer to pathogens a selective advantage by counteracting the innate immune responses. This encompasses the inhibition of phagocytosis and migration as well as modulation of innate immune pathways [15]. Pathogens have evolved multiple strategies to manipulate the RhoGTPase cycle. These can be divided in 2 groups: the RhoGTPase-activating toxins and the toxins inactivating RhoGTPases. Here, we review the molecular mechanism by which the host immune system senses the virulence factors that target RhoGTPases and discuss the implications of these sensing mechanisms.

## RhoGTPase-targeting toxins and virulence factors: Hijacking cellular signaling

RhoGTPases are one of the preferential targets of virulence factors, probably because of their critical role in innate immune responses. RhoGTPases have been shown to be critical regulators of the innate immune response via their contribution to phagocytosis and migration as well as the production of reactive oxygen species via NADPH oxidase [16]. RhoGTPases cycle between an active GTP-bound and an inactive GDP-bound stage which is regulated by the GTPase-activating protein (GAP), guanine nucleotide exchange factor (GEF), and guanosine nucleotide dissociation inhibitor (GDI) [17].

Bacteria use 2 types of strategies to manipulate the host RhoGTPases: (1) they use virulence factors mimicking the RhoGTPases regulators (GAP, GEF, or GDI); and (2) they utilize virulence factors endowed with enzymatic activities modifying host RhoGTPases [18]. These modifications result in either activation or inhibition of RhoGTPases, both of which affect the actin cytoskeleton and the bacterial uptake by phagocytic or non-phagocytic cells. The advantages of manipulating RhoGTPases for pathogens have been extensively studied [19–21]. Here, going through the looking glass, we will describe how these manipulations of RhoGTPases are sensed by the innate immune system.

## Sensing RhoGTPase activation to trigger a transcriptional antimicrobial response

Microbial activation of RhoGTPases induces the transcription of pro-inflammatory cytokine- and chemokine-coding genes. Interestingly, the *Salmonella* virulence factor SopE, a GEF for Rac and Cdc42, has been found to activate different signaling pathways converging on gene transcription. Firstly, *Salmonella* expressing SopE and SopE2 activates JNK, p38, and Erk MAPK, leading to NF-κB activation [22]. Interestingly, by activating Rac1 and Cdc42, SopE was shown to trigger the activation of NOD1 and Rip2 which drives cytokine production [23]. More recently, SopE has been found to activate a Cdc42-Pak1 axis leading to TAK1- and TRAF6-dependent NF-κB activation [24]. Further studies would be required to determine whether these 3 pathways are interlinked or occur separately during infection. An interesting example of an antimicrobial response triggered by RhoGTPases activation is the CNF1 toxin. The CNF1 toxin of uropathogenic *Escherichia coli* is a deamidase that was shown to trigger a protective antimicrobial response by activating the Rac2GTPase, which, in turn, activates the IMD-Relish and Rip1/2 kinases-NF-κB signaling pathways in *Drosophila* and mammalian cells, respectively [4,25].

## Sensing the inactivation of RhoGTPases by the Pyrin inflammasome

The *mefv* gene (coding for the Pyrin protein) was discovered through its involvement in auto-inflammatory syndromes such as familial Mediterranean fever (FMF) [26,27]. Recent studies

have shown a host protective function for the Pyrin inflammasome by monitoring the activity of virulence factors that inactivate RhoGTPases. The immune detection of bacterial toxins that modify the host RhoGTPases is of major importance to restrain bacterial infection. This detection system was first suggested by studies showing that TcdA and TcdB toxins from *Clostridium difficile* were able to induce Caspase-1 activation and interleukin (IL)-1ß maturation [28]. The Pyrin inflammasome was later shown by Shao and colleagues to be the sensor for RhoGTPase-inhibiting toxins. They revealed that not only TcdA and TcdB toxins but also VopS (from *Vibrio parahaemolyticus*), IbpA (from *Histophilus somni*), TecA (from *Burkholderia cenocepacia*) are detected by the Pyrin inflammasome. It is noteworthy that these toxins inactivate the RhoGTPases via 4 different mechanisms: glycosylation, ADP ribosylation, AMPylation, and deamidation [29–32]. Shao and colleagues reported that the catalytically inactive mutant of TcdB failed to activate the inflammasome, indicating the importance of sensing activity rather than conserved structural motifs. Interestingly, the toxin TcsL (from *Clostridium sordellii*) that inactivates Rac and Cdc42 but not RhoA failed to activate the Pyrin inflammasome, suggesting that Pyrin monitors the activation status of RhoA specifically [30]. It is now accepted that the Pyrin inflammasome senses the activity of RhoGTPase-inactivating virulence factors via a signaling cascade involving Ser/Thr kinases and modifications of microtubule stability. At steady state, Pyrin interacts with 14-3-3 proteins which maintain the receptor in an inactive form. RhoA inhibition by toxins results in 14-3-3 dissociation from Pyrin in a Pyrin phosphorylation status-dependent manner [31]. Park and colleagues revealed that the RhoA-interacting kinases, protein kinase N1 (PKN1) and N2 (PKN2), phosphorylate human Pyrin on Ser208 and Ser242 (Ser205 and Ser241 on murine Pyrin) and trigger 14-3-3-Pyrin interaction to maintain the inactive status of the Pyrin inflammasome [32]. Inactivation of RhoA by bacterial toxins abolishes the Pyrin phosphorylation on Ser205/Ser241 by PKN1/2 and the subsequent 14-3-3 interaction and, as a consequence, activates the Pyrin inflammasome and triggers IL-1ß secretion [31,32] (Fig 1). Interestingly, macrophage infection by *C. difficile*, expressing TcdA and TcdB, triggers pyroptotic cell death in a GSDMD-dependent manner [33]. Other virulence factors inactivating RhoGTPases have been shown to be sensed by the Pyrin inflammasome (Table 1). Murine macrophages infected with *Yersinia pseudotuberculosis* expressing YopE and YopT, 2 virulence factors inhibiting RhoA, trigger Ser205 dephosphorylation of Pyrin and IL-1ß secretion [34]. *Yersinia* provides a striking example of the virulence factor interplay that probably resulted from host–pathogen coevolution. Indeed, *Yersinia* injects the effector YopM that binds and activates PKN1/2 and RSK kinases to trigger Pyrin phosphorylation, thus preventing Pyrin inflammasome activation and thereby counteracting the Pyrin sensing of RhoGTPase-inactivating toxins [35–37]. Interestingly, the YopO virulence factor (YpkA in *Yersinia pestis*) has a RhoGDI domain that inhibits RhoA as well as Rac [38,39]. Further studies would determine whether it could participate to this interplay by triggering the activation of Pyrin. Another step in this host–pathogen coevolution process is the selection of human Pyrin mutations. These mutations render Pyrin insensitive to YopM and may have been evolutionarily selected to resist infection by *Y. pestis*, the causative agent of the plague [36]. In individuals carrying activating Pyrin mutations, the increased activity might have conferred a selective advantage against pathogens [40]. However, these mutations are also responsible for Pyrin-dependent autoinflammatory disorders [32]. The microtubule dynamics also play a role in the Pyrin inflammasome activation. Microtubules act downstream of Pyrin dephosphorylation and dissociation from 14-3-3 proteins [31,41]. Despite the clinical importance of drug targeting microtubules (such as colchicine) in Pyrin-dependent autoinflammatory disorders, the mechanisms involved in microtubule regulation of the Pyrin inflammasome are not fully understood.

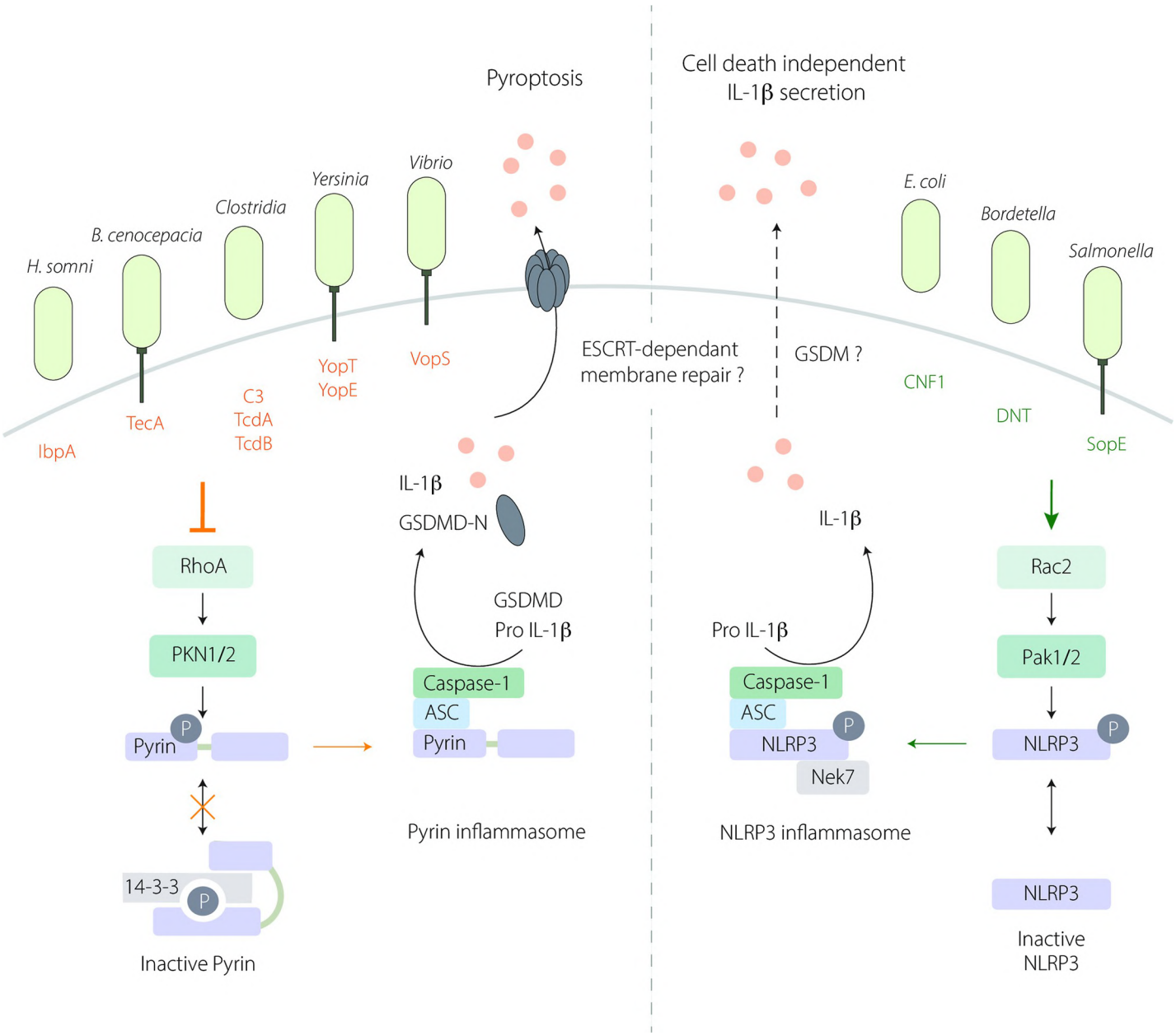


**Fig 1. Sensing of RhoGTPase-modifying toxins by Pyrin and NLRP3 inflammasomes.** (Left) The Pyrin inflammasome is activated in response to RhoA inhibition by several bacterial toxins. At steady state, active RhoA induces the activation of PKN1/2 that phosphorylates (P) Pyrin (on Ser205 and Ser241) and triggers 14-3-3—Pyrin interaction to maintain Pyrin inactive. Inhibition of RhoA by virulence factors disrupts this interaction leading to Pyrin inflammasome activation and subsequent IL-1ß maturation and GSDMD cleavage into GSDMD-N. GSDMD-N anchors to the plasma membrane and triggers IL-1ß secretion and pyroptotic cell death. The involvement of ESCRT-mediated membrane repair during Pyrin-dependent pyroptosis is not yet defined. (Right) The NLRP3 inflammasome senses Rac2 activation by bacterial virulence factors. Downstream of Rac2 activation, the Pak1/2 kinases phosphorylate (P) NLRP3 on Thr659 allowing the inflammasome assembly, and subsequent IL-1ß maturation. Is this context, IL-1ß secretion is GSDMD independent and does not trigger cell death but may involve another GSDM and/or an ESCRT-dependent membrane repair mechanism. GSDM, gasdermin; GSDMD, gasdermin D; IL, interleukin.

https://doi.org/10.1371/journal.ppat.1009504.g001

## Sensing of RhoGTPase activation through the NLRP3 inflammasome

In 2004, Tschopp and colleagues established that NLRP3 is able to assemble into an NLRP3-ASC-Caspase-1 inflammasome that is responsible for autoinflammatory disorders

**Table 1. Inflammasome sensing of RhoGTPase-targeting by bacterial toxins.**

| | Toxin | Pathogen | Host target | Modification | Reference |
|---|---|---|---|---|---|
| Pyrin inflammasome | **RhoGTPase-inactivating toxins** | | | | |
| | C3 | *Clostridium botulinum*<br>*Clostridium limosum*<br>*Bacillus cereus*<br>*Bacillus thuringiensis* | Rho | ADP ribosylation | Xu et al. (2014) [30] |
| | TcdA | *C. difficile* | Rho, Rac, Cdc42 | Glucosylation | Gao et al. (2016) [31] |
| | TcdB | *C. difficile* | Rho, Rac, Cdc42 | Glucosylation | Xu et al. (2014) [30] |
| | VopS | *V. parahaemolyticus* | Rho, Rac, Cdc42 | AMPylation | Xu et al. (2014) [30] |
| | IbpA | *H. somni* | Rho, Rac, Cdc42 | AMPylation | Xu et al. 2014 [30] |
| | TecA | *B. cenocepacia* | Rho, Rac, Cdc42 | Deamidation | Aubert et al. (2016) [29] |
| | YopT | *Y. pestis*<br>*Y. pseudotuberculosis*<br>*Yersinia enterocolitica* | Rho, Rac, Cdc42 | CAAX cleavage | Medici et al. (2019) [34] |
| | YopE | *Y. pestis*<br>*Y. pseudotuberculosis*<br>*Y. enterocolitica* | Rho, Rac, Cdc42 | GAP | Medici et al. (2019) [34] |
| NLRP3 inflammasome | **RhoGTPase-activating toxins** | | | | |
| | CNF1 | *E. coli* | Rho, Rac, Cdc42 | Deamidation | Dufies et al. (2021) [47] |
| | DNT | *Bordetella pertussis*<br>*Bordetella parapertussis*<br>*Bordetella bronchiseptica* | Rho, Rac, Cdc42 | Transglutamination | Dufies et al. (2021) [47] |
| | SopE | *Salmonella* spp. | Rac, Cdc42 | GEF | Dufies et al. (2021) [47] |

GAP, RhoGTPase-activating protein; GEF, guanine nucleotide exchange factor.

https://doi.org/10.1371/journal.ppat.1009504.t001

[42]. Further studies reveal that NLRP3 inflammasome plays a role in metabolic diseases such as diabetes, atherosclerosis, and gouty arthritis [43–46]. It is thought that the main physiological function of NLRP3 inflammasome is to sense pathogen- and metabolic-triggered danger signals. The contribution of the NLRP3 inflammasome in protecting the host against infectious agents has recently emerged. The NLRP3 inflammasome is activated by several triggers such as pore-forming toxins, extracellular ATP, crystalline structures, and mitochondrial damage, but its role in ETI only recently emerged from study of RhoGTPase-activating toxins [45,47–50]. NLRP3 is regulated by phosphorylation and ubiquitination, which control its stability and subcellular localization, conformational changes, and its interaction with inflammasome-related proteins such as the adaptor protein ASC and the regulator protein Nek7 [51]. Nek7 interacts with the carboxyl terminus leucin-rich repeat (LRR) of NLRP3 and triggers a conformational change that is essential for NLRP3 oligomerization and inflammasome assembly [52–54].

The CNF1 toxin is a bona fide RhoGTPase-activating toxin encoded by uropathogenic *E. coli*. Interestingly, CNF1 has been shown to trigger an inflammatory immune response in vivo and in cellulo using multiple models including *Drosophila*, mouse, and human [4,25,55,56]. This CNF1-triggered protective immunity and induced bacterial clearance was observed during both *Drosophila* systemic infections and during mice bacteremia. While the CNF1-immune response in *Drosophila* was restricted to the transcriptional antimicrobial peptide expression, the CNF1-expressing *E. coli* triggered response in mice depended on Caspase-1 and IL-1 signaling [4,25]. Both CNF1 toxin and SopE virulence factor activating RhoGTPases have been reported to trigger Caspase-1 activation and IL-1ß maturation and secretion, but the inflammasome involved was only recently identified. The NLRP3 inflammasome has been found to be the sensor of RhoGTPase activation induced by CNF1, SopE, and DNT toxins [47]

(Table 1). The NLRP3 inflammasome specifically senses the activation of Rac2. Downstream of Rac2 activation, the p21-activated kinase (Pak) 1, and Pak2 are necessary for NLRP3 inflammasome sensing of CNF1, SopE, and DNT activities. The kinases Pak1/2 regulation of NLRP3 inflammasome activation was dependent on $K^+$ efflux and occurred through NLRP3 phosphorylation on Thr659 which enables the recruitment of Nek7 and inflammasome assembly and activation. During mice infections, both NLRP3 and Pak1 chemical inhibition or gene knock-out prevented CNF1-induced bacterial clearance during bacteremia. In contrast to other NLRP3 inflammasome activators, CNF1-triggered IL-1ß secretion was GSDMD independent and did not induce pyroptotic cell death (Fig 1). Further studies will be necessary to determine the mechanisms involved in IL-1ß secretion downstream of toxin-induced RhoGTPase activation. An exciting possibility would be the involvement of other GSDM in the CNF1-triggered IL-1ß secretion coupled with a cell death inhibition mechanism to control the balance between cell death and inflammation as described for GSDMD and ESCRT machinery that controls membrane repair [57,58]. In human monocyte-derived macrophages, the sensing of the CNF1 toxin via the Pak/NLRP3 axis is conserved. However, further studies are needed to determine the role of Pak and NLRP3 during infection in humans and whether Pak/NLRP3 signaling axis deficiencies are associated with increased susceptibility to infection. The NLRP3 sensing of virulence factors activating RacGTPases could better explain the coexistence within the same bacteria of virulence factors with antagonistic activities toward RacGTPases such as in *Salmonella* with SopE and SptP, respectively, GEF and GAP for RacGTPases [59].

## Concluding remarks

Pyrin and NLRP3 inflammasome guarding of RhoGTPases share striking molecular similarities such as the involvement of Ser/Thr kinases and precise phosphorylation sites to control inflammasome activation. Interestingly, PKN phosphorylation inhibits the inflammasome, while Pak phosphorylation activates the inflammasome. The fine-tuning of these Rho-regulated innate immune sensing mechanisms is probably essential for the host in order to cope with microbial infection and inflammation. The reason why the host innate immune system uses 2 different inflammasomes to monitor RhoGTPase activity remains an open question. The only easy answer is that the guarding of RhoGTPases is critical for host survival during infection.

## Acknowledgments

We thank Patrick Munro for critical reading of the manuscript. We acknowledge Abby Cuttriss of the Office of International Scientific Visibility of Université Côte d'Azur for professional language editing.

## References

1. Janeway CA. Approaching the asymptote? Evolution and revolution in immunology. Cold Spring Harb Symp Quant Biol. 1989; 54(Pt 1):1–13. https://doi.org/10.1101/sqb.1989.054.01.003 PMID: 2700931
2. Jones JDG, Dangl JL. The plant immune system. Nature. 2006; 444:323–329. https://doi.org/10.1038/nature05286 PMID: 17108957
3. Stuart LM, Paquette N, Boyer L. Effector-triggered versus pattern-triggered immunity: how animals sense pathogens. Nat Rev Immunol. 2013; 13:199–206. https://doi.org/10.1038/nri3398 PMID: 23411798
4. Diabate M, Munro P, Garcia E, Jacquel A, Michel G, Obba S, et al. Escherichia coli α-hemolysin counteracts the anti-virulence innate immune response triggered by the Rho GTPase activating toxin CNF1 during bacteremia. PLoS Pathog. 2015; 11:e1004732. https://doi.org/10.1371/journal.ppat.1004732 PMID: 25781937

5. Fischer NL, Naseer N, Shin S, Brodsky IE. Effector-triggered immunity and pathogen sensing in metazoans. Nat Microbiol. 2020; 5: 14–26. https://doi.org/10.1038/s41564-019-0623-2 PMID: 31857733
6. Stuart LM, Boyer L. RhoGTPases—NODes for effector-triggered immunity in animals. Cell Res. 2013; 23:980–981. https://doi.org/10.1038/cr.2013.68 PMID: 23689278
7. Vance RE, Isberg RR, Portnoy DA. Patterns of pathogenesis: discrimination of pathogenic and non-pathogenic microbes by the innate immune system. Cell Host Microbe 2009; 6: 10–21. https://doi.org/10.1016/j.chom.2009.06.007 PMID: 19616762
8. Aktories K. Bacterial protein toxins that modify host regulatory GTPases. Nat Rev Microbiol. 2011; 9: 487–498. https://doi.org/10.1038/nrmicro2592 PMID: 21677684
9. Galán JE. Common Themes in the Design and Function of Bacterial Effectors. Cell Host Microbe. 2009; 5:571–579. https://doi.org/10.1016/j.chom.2009.04.008 PMID: 19527884
10. Burridge K, Wennerberg K. Rho Rac Take Center Stage. Cell. 2004; 116:167–179. https://doi.org/10.1016/s0092-8674(04)00003-0 PMID: 14744429
11. Jaffe AB, Hall A. RHO GTPASES: Biochemistry and Biology. Annu Rev Cell Dev Biol. 2005; 21:247–269. https://doi.org/10.1146/annurev.cellbio.21.020604.150721 PMID: 16212495
12. Lougaris V, Baronio M, Gazzurelli L, Benvenuto A, Plebani A. RAC2 and primary human immune deficiencies. J Leukoc Biol. 2020; 108:687–696. https://doi.org/10.1002/JLB.5MR0520-194RR PMID: 32542921
13. El Masri R, Delon J. RHO GTPases: from new partners to complex immune syndromes. Nat Rev Immunol. 2021. https://doi.org/10.1038/s41577-021-00500-7 PMID: 33547421
14. Clayton NS, Ridley AJ. Targeting Rho GTPase Signaling Networks in Cancer. Front Cell Dev Biol. 2020; 8:222. https://doi.org/10.3389/fcell.2020.00222 PMID: 32309283
15. Brodsky IE, Medzhitov R. Targeting of immune signalling networks by bacterial pathogens. Nat Cell Biol. 2009; 11:521–526. https://doi.org/10.1038/ncb0509-521 PMID: 19404331
16. Bokoch GM. Regulation of innate immunity by Rho GTPases. Trends Cell Biol. 2005; 15:163–171. https://doi.org/10.1016/j.tcb.2005.01.002 PMID: 15752980
17. Bishop AL, Hall A. Rho GTPases and their effector proteins. Biochem J. 2000; 348:241–255. PMID: 10816416
18. Popoff MR. Bacterial factors exploit eukaryotic Rho GTPase signaling cascades to promote invasion and proliferation within their host. Small GTPases. 2014; 5. https://doi.org/10.4161/sgtp.28209 PMID: 25203748
19. Finlay BB. Bacterial virulence strategies that utilize Rho GTPases. Curr Top Microbiol Immunol. 2005; 291:1–10. https://doi.org/10.1007/3-540-27511-8_1 PMID: 15981456
20. Schlumberger MC, Hardt WD. Triggered phagocytosis by Salmonella: bacterial molecular mimicry of RhoGTPase activation/deactivation. Curr Top Microbiol Immunol. 2005; 291:29–42. https://doi.org/10.1007/3-540-27511-8_3 PMID: 15981458
21. Boquet P, Lemichez E. Bacterial virulence factors targeting Rho GTPases: parasitism or symbiosis? Trends Cell Biol. 2003; 13:238–246. https://doi.org/10.1016/s0962-8924(03)00037-0 PMID: 12742167
22. Bruno VM, Hannemann S, Lara-Tejero M, Flavell RA, Kleinstein SH, Galán JE. Salmonella Typhimurium Type III Secretion Effectors Stimulate Innate Immune Responses in Cultured Epithelial Cells. PLoS Pathog 2009; 5:e1000538. https://doi.org/10.1371/journal.ppat.1000538 PMID: 19662166
23. Keestra AM, Winter MG, Auburger JJ, Fräßle SP, Xavier MN, Winter SE, et al. Manipulation of small Rho GTPases is a pathogen-induced process detected by NOD1. Nature. 2013; 496:233–237. https://doi.org/10.1038/nature12025 PMID: 23542589
24. Sun H, Kamanova J, Lara-Tejero M, Galán JE. Salmonella stimulates pro-inflammatory signalling through p21-activated kinases bypassing innate immune receptors. Nat Microbiol. 2018; 3:1122–1130. https://doi.org/10.1038/s41564-018-0246-z PMID: 30224799
25. Boyer L, Magoc L, Dejardin S, Cappillino M, Paquette N, Hinault C, et al. Pathogen-derived effectors trigger protective immunity via activation of the Rac2 enzyme and the IMD or Rip kinase signaling pathway. Immunity. 2011; 35:536–549. https://doi.org/10.1016/j.immuni.2011.08.015 PMID: 22018470
26. Jamilloux Y, Magnotti F, Belot A, Henry T. The pyrin inflammasome: from sensing RhoA GTPases-inhibiting toxins to triggering autoinflammatory syndromes. Pathog Dis. 2018; 76. https://doi.org/10.1093/femspd/fty020 PMID: 29718184
27. Centola M, Aksentijevich I, Kastner DL. The Hereditary Periodic Fever Syndromes: Molecular Analysis of a New Family of Inflammatory Diseases. Hum Mol Genet. 1998; 7:1581–1588. https://doi.org/10.1093/hmg/7.10.1581 PMID: 9735379

28. Ng J, Hirota SA, Gross O, Li Y, Ulke-Lemee A, Potentier MS, et al. Clostridium difficile toxin-induced inflammation and intestinal injury are mediated by the inflammasome. Gastroenterology. 2010; 139:542–552, 552.e1–3. https://doi.org/10.1053/j.gastro.2010.04.005 PMID: 20398664

29. Aubert DF, Xu H, Yang J, Shi X, Gao W, Li L, et al. A Burkholderia Type VI Effector Deamidates Rho GTPases to Activate the Pyrin Inflammasome and Trigger Inflammation. Cell Host Microbe. 2016; 19:664–674. https://doi.org/10.1016/j.chom.2016.04.004 PMID: 27133449

30. Xu H, Yang J, Gao W, Li L, Li P, Zhang L, et al. Innate immune sensing of bacterial modifications of Rho GTPases by the Pyrin inflammasome. Nature. 2014; 513:237–241. https://doi.org/10.1038/nature13449 PMID: 24919149

31. Gao W, Yang J, Liu W, Wang Y, Shao F. Site-specific phosphorylation and microtubule dynamics control Pyrin inflammasome activation. Proc Natl Acad Sci U S A. 2016; 113:E4857–4866. https://doi.org/10.1073/pnas.1601700113 PMID: 27482109

32. Park YH, Wood G, Kastner DL, Chae JJ. Pyrin inflammasome activation and RhoA signaling in the autoinflammatory diseases FMF and HIDS. Nat Immunol. 2016; 17:914–921. https://doi.org/10.1038/ni.3457 PMID: 27270401

33. Kanneganti A, Malireddi RKS, Saavedra PHV, Vande Walle L, Van Gorp H, Kambara H, et al. GSDMD is critical for autoinflammatory pathology in a mouse model of Familial Mediterranean Fever. J Exp Med. 2018; 215:1519–1529. https://doi.org/10.1084/jem.20172060 PMID: 29793924

34. Medici NP, Rashid M, Bliska JB. Characterization of Pyrin Dephosphorylation and Inflammasome Activation in Macrophages as Triggered by the Yersinia Effectors YopE and YopT. Infect Immun. 2019; 87. https://doi.org/10.1128/IAI.00822-18 PMID: 30602502

35. Chung LK, Park YH, Zheng Y, Brodsky IE, Hearing P, Kastner DL, et al. The Yersinia Virulence Factor YopM Hijacks Host Kinases to Inhibit Type III Effector-Triggered Activation of the Pyrin Inflammasome. Cell Host Microbe. 2016; 20:296–306. https://doi.org/10.1016/j.chom.2016.07.018 PMID: 27569559

36. Park YH, Remmers EF, Lee W, Ombrello AK, Chung LK, Shilei Z, et al. Ancient familial Mediterranean fever mutations in human pyrin and resistance to Yersinia pestis. Nat Immunol. 2020; 21:857–867. https://doi.org/10.1038/s41590-020-0705-6 PMID: 32601469

37. Ratner D, Orning MPA, Proulx MK, Wang D, Gavrilin MA, Wewers MD, et al. The Yersinia pestis Effector YopM Inhibits Pyrin Inflammasome Activation. PLoS Pathog. 2016; 12:e1006035. https://doi.org/10.1371/journal.ppat.1006035 PMID: 27911947

38. Dukuzumuremyi JM, Rosqvist R, Hallberg B, Akerström B, Wolf-Watz H, Schesser K. The Yersinia protein kinase A is a host factor inducible RhoA/Rac-binding virulence factor. J Biol Chem. 2000; 275:35281–35290. https://doi.org/10.1074/jbc.M003009200 PMID: 10950948

39. Dominguez R. Subversive bacteria reveal new tricks in their cytoskeleton-hijacking arsenal. Nat Struct Mol Biol. 2015; 22:178–179. https://doi.org/10.1038/nsmb.2976 PMID: 25736086

40. Schnappauf O, Chae JJ, Kastner DL, Aksentijevich I. The Pyrin Inflammasome in Health and Disease. Front Immunol. 2019; 10:1745. https://doi.org/10.3389/fimmu.2019.01745 PMID: 31456795

41. Van Gorp H, Saavedra PHV, de Vasconcelos NM, Van Opdenbosch N, Vande Walle L, Matusiak M, et al. Familial Mediterranean fever mutations lift the obligatory requirement for microtubules in Pyrin inflammasome activation. Proc Natl Acad Sci U S A. 2016; 113:14384–14389. https://doi.org/10.1073/pnas.1613156113 PMID: 27911804

42. Agostini L, Martinon F, Burns K, McDermott MF, Hawkins PN, Tschopp J. NALP3 Forms an IL-1β-Processing Inflammasome with Increased Activity in Muckle-Wells Autoinflammatory Disorder. Immunity. 2004; 20:319–325. https://doi.org/10.1016/s1074-7613(04)00046-9 PMID: 15030775

43. Ridker PM, Everett BM, Thuren T, MacFadyen JG, Chang WH, Ballantyne C, et al. Antiinflammatory Therapy with Canakinumab for Atherosclerotic Disease. N Engl J Med. 2017; 377:1119–1131. https://doi.org/10.1056/NEJMoa1707914 PMID: 28845751

44. Masters SL, Dunne A, Subramanian SL, Hull RL, Tannahill GM, Sharp FA, et al. Activation of the NLRP3 inflammasome by islet amyloid polypeptide provides a mechanism for enhanced IL-1β in type 2 diabetes. Nat Immunol. 2010; 11:897–904. https://doi.org/10.1038/ni.1935 PMID: 20835230

45. Martinon F, Pétrilli V, Mayor A, Tardivel A, Tschopp J. Gout-associated uric acid crystals activate the NALP3 inflammasome. Nature. 2006; 440:237–241. https://doi.org/10.1038/nature04516 PMID: 16407889

46. Alena Grebe, Florian Hoss, Eicke Latz. NLRP3 Inflammasome and the IL-1 Pathway in Atherosclerosis. Circ Res. 2018; 122:1722–1740. https://doi.org/10.1161/CIRCRESAHA.118.311362 PMID: 29880500

47. Dufies O, Doye A, Courjon J, Torre C, Michel G, Loubatier C, et al. Escherichia coli Rho GTPase-activating toxin CNF1 mediates NLRP3 inflammasome activation via p21-activated kinases-1/2 during bacteraemia in mice. Nat Microbiol. 2021;1–12. https://doi.org/10.1038/s41564-020-00847-y PMID: 33349680

48. Hornung V, Bauernfeind F, Halle A, Samstad EO, Kono H, Rock KL, et al. Silica crystals and aluminum salts mediate NALP-3 inflammasome activation via phagosomal destabilization. Nat Immunol. 2008; 9:847–856. https://doi.org/10.1038/ni.1631 PMID: 18604214

49. Mariathasan S, Weiss DS, Newton K, McBride J, O'Rourke K, Roose-Girma M, et al. Cryopyrin activates the inflammasome in response to toxins and ATP. Nature. 2006; 440:228–232. https://doi.org/10.1038/nature04515 PMID: 16407890

50. Zhou R, Yazdi AS, Menu P, Tschopp J. A role for mitochondria in NLRP3 inflammasome activation. Nature. 2011; 469:221–225. https://doi.org/10.1038/nature09663 PMID: 21124315

51. Yang Y, Wang H, Kouadir M, Song H, Shi F. Recent advances in the mechanisms of NLRP3 inflammasome activation and its inhibitors. Cell Death Dis. 2019; 10:128. https://doi.org/10.1038/s41419-019-1413-8 PMID: 30755589

52. He Y, Zeng MY, Yang D, Motro B, Núñez G. Nek7 is an essential mediator of NLRP3 activation downstream of potassium efflux. Nature. 2016; 530:354–357. https://doi.org/10.1038/nature16959 PMID: 26814970

53. Sharif H, Wang L, Wang WL, Magupalli VG, Andreeva L, Qiao Q, et al. Structural mechanism for NEK7-licensed activation of NLRP3 inflammasome. Nature. 2019; 570:338–343. https://doi.org/10.1038/s41586-019-1295-z PMID: 31189953

54. Shi H, Wang Y, Li X, Zhan X, Tang M, Fina M, et al. NLRP3 activation and mitosis are mutually exclusive events coordinated by NEK7, a new inflammasome component. Nat Immunol. 2016; 17:250. https://doi.org/10.1038/ni.3333 PMID: 26642356

55. Müller AJ, Hoffmann C, Galle M, Broeke AVD, Heikenwalder M, Falter L, et al. The S. Typhimurium Effector SopE Induces Caspase-1 Activation in Stromal Cells to Initiate Gut Inflammation. Cell Host Microbe. 2009; 6:125–136. https://doi.org/10.1016/j.chom.2009.07.007 PMID: 19683679

56. Hoffmann C, Galle M, Dilling S, Käppeli R, Müller AJ, Songhet P, et al. In Macrophages, Caspase-1 Activation by SopE and the Type III Secretion System-1 of S. Typhimurium Can Proceed in the Absence of Flagellin. PLoS ONE. 2010; 5. https://doi.org/10.1371/journal.pone.0012477 PMID: 20814576

57. Rühl S, Shkarina K, Demarco B, Heilig R, Santos JC, Broz P. ESCRT-dependent membrane repair negatively regulates pyroptosis downstream of GSDMD activation. Science. 2018; 362:956–960. https://doi.org/10.1126/science.aar7607 PMID: 30467171

58. Evavold CL, Ruan J, Tan Y, Xia S, Wu H, Kagan JC. The Pore-Forming Protein Gasdermin D Regulates Interleukin-1 Secretion from Living Macrophages. Immunity. 2018; 48:35–44.e6. https://doi.org/10.1016/j.immuni.2017.11.013 PMID: 29195811

59. Fu Y, Galán JE. A salmonella protein antagonizes Rac-1 and Cdc42 to mediate host-cell recovery after bacterial invasion. Nature. 1999; 401:293–297. https://doi.org/10.1038/45829 PMID: 10499590

*nutrients*

MDPI

*Article*

# Diet Supplementation in ω3 Polyunsaturated Fatty Acid Favors an Anti-Inflammatory Basal Environment in Mouse Adipose Tissue

**Cecilia Colson [1], Rayane A. Ghandour [1], Océane Dufies [2], Samah Rekima [1], Agnès Loubat [1], Patrick Munro [2], Laurent Boyer [2] and Didier F. Pisani [1,3,*]**

1 Université Côte d'Azur, CNRS, Inserm, iBV, 06107 Nice, France; Ceciclia.Colson@unice.fr (C.C.); ghandourrayane@hotmail.com (R.A.G.); Samah.Rekima@unice.fr (S.R.); Agnes.Loubat@unice.fr (A.L.)
2 Université Côte d'Azur, Inserm, C3M, 06107 Nice, France; oceane.dufies@unice.fr (O.D.); Patrick.Munro@unice.fr (P.M.); Laurent.Boyer@unice.fr (L.B.)
3 Didier Pisani, Laboratoire de PhysioMédecine Moléculaire—LP2M, Univ. Nice Sophia Antipolis, 28 Avenue de Valombrose, 06107 Nice CEDEX 2, France
* Correspondence: pisani@unice.fr; Tel.:+33-0493377037

Received: 14 January 2019; Accepted: 15 February 2019; Published: 20 February 2019


**Abstract:** Oxylipins are metabolized from dietary ω3 and ω6 polyunsaturated fatty acids and are involved in an inflammatory response. Adipose tissue inflammatory background is a key factor of metabolic disorders and it is accepted that dietary fatty acids, in terms of quality and quantity, modulate oxylipin synthesis in this tissue. Moreover, it has been reported that diet supplementation in ω3 polyunsaturated fatty acids resolves some inflammatory situations. Thus, it is crucial to assess the influence of dietary polyunsaturated fatty acids on oxylipin synthesis and their impact on adipose tissue inflammation. To this end, mice fed an ω6- or ω3-enriched standard diet (*ω6/ω3* ratio of 30 and 3.75, respectively) were analyzed for inflammatory phenotype and adipose tissue oxylipin content. Diet enrichment with an ω3 polyunsaturated fatty acid induced an increase in the oxylipins derived from ω6 linoleic acid, ω3 eicosapentaenoic, and ω3 docosahexaenoic acids in brown and white adipose tissues. Among these, the level of pro-resolving mediator intermediates, as well as anti-inflammatory metabolites, were augmented. Concomitantly, expressions of M2 macrophage markers were increased without affecting inflammatory cytokine contents. In vitro, these metabolites did not activate macrophages but participated in macrophage polarization by inflammatory stimuli. In conclusion, we demonstrated that an ω3-enriched diet, in non-obesogenic non-inflammatory conditions, induced synthesis of oxylipins which were involved in an anti-inflammatory response as well as enhancement of the M2 macrophage molecular signature, without affecting inflammatory cytokine secretion.

**Keywords:** oxylipins; brown adipose tissue; white adipose tissue; macrophages; inflammation

## 1. Introduction

ω6 linoleic acid (LA), a precursor of dihomo-γ-linolenic acid (DGLA) and arachidonic acid (ARA), and ω3 α-linolenic acid, a precursor of eicosapentaenoic (EPA) and docosahexaenoic (DHA) acids are essential polyunsaturated fatty acids (PUFAs) only supplied by food. These PUFAs are required for healthy development from embryonic steps to adult life and are involved in a variety of biological processes, especially, in adipose tissue [1,2]. It is now well accepted that insufficient intakes of ω3 PUFAs, as well as an excess of ω6 PUFAs, correlate with various diseases; especially, metabolic diseases [3–5]. For example, ARA intake correlates positively with being overweight/obese, inflammatory diseases, and associated metabolic syndrome [6–10]. Indeed, ω6 oxylipins (oxygenated

derivatives of PUFAs) are known to favor inflammatory responses [11], as well as to promote energy storage [12] and to inhibit energy expenditure [13,14]. The dietary *ω6/ω3* PUFAs ratio is more important than the total amount of PUFA intake as it determines the level of synthesized ω6-derived oxylipins. Indeed, ω3 PUFAs modulate ω6-derived oxylipins synthesis [15]. Mechanistically this is characterized by (i) the capacity of ω6 and ω3 PUFAs to compete at the level of lipoxygenase (LOX) and cyclooxygenase (COX), their two major metabolization pathways and ii) the capacity of various ω3 PUFAs to inhibit these pathways.

The increase in the number of overweight or obese people has reached an epidemic stage in the 21st century. More than 2 billion adults are overweight (body mass index (BMI) > 25 kg/m$^2$) and at least 600 million are clinically obese (BMI > 30 kg/m$^2$). Obesity and being overweight are the consequences of a positive energy balance that leads to an increase in the mass of subcutaneous and visceral white adipose tissue. White adipocytes are storing energy under the form of triglycerides whereas brown adipocytes dissipate energy from triglycerides by producing heat (=thermogenesis). In addition, white and brown adipocytes are able to secrete molecules acting on their environment, and especially, on immune cells [16]. For example, white adipocytes secrete adipokines (e.g., adiponectin) and pro-inflammatory factors (e.g., PAI-1, MCP-1, or IL-6) which are able to recruit and activate macrophages [17]. Furthermore, it has also been shown that the white adipose tissue of obese subjects is characterized by low-grade inflammation that can lead to metabolic disorders such as insulin resistance [18]. This inflammation, characterized by an increase in inflammatory markers such as TNFα, PAI-1, or interleukins 1 and 6 (IL-1, IL-6), promotes the macrophage infiltration of adipose tissue and the polarization of macrophages of the alternative M2 type in classic pro-inflammatory M1 type [19].

The macrophages respond to environmental cues by acquiring specific functional phenotypes. Pro-inflammatory M1 macrophages are involved in the fight against many infections. They are activated by Toll-like receptor (TLR) ligands such as lipopolysaccharide and saturated fatty acids, but also by IFNγ and TNFα. They participate in the inflammatory environment by secreting many cytokines such as IL-1, IL-6, IL-12, IL-23, and TNFα, and by participating in the chemo-attraction of other immune cells [20]. M2 macrophages are more heterogeneous at functional and secretory levels. Considered as anti-inflammatory or inactive, they normally reside in tissues and are involved in tissue homeostasis by participating in the remodeling, repair, and activation of certain metabolic functions. They can be activated by cytokines such as IL-4, IL-10, and IL-13, but also by more specific signals from the tissue environment [21].

The accumulation of immune cells, especially that of macrophages, as well as their inflammatory phenotype, affect adipose tissue homeostasis and, more specifically, the recruitment and function of adipocytes in white and brown adipose tissues [16]. It has been shown that TNFα secreted by M1 macrophages inhibited adipocyte differentiation [22] and that IL-1β blocked insulin signaling [23], thus favoring insulin-resistance. Recently, it has also been shown that IL-1β and TNFα can affect the thermogenic function of brown adipocyte [24–26]. These inflammatory cytokines thus participate in the deregulation of tissue homeostasis by limiting its ability to dissipate an excessive supply of substrate in the form of heat. On the contrary, it was shown that M2 macrophages, via the secretion of factors such as IL-4 or IL-13 favored the formation of brown adipocytes and their activation [27,28]. In addition, immune cells can modulate insulin sensitivity and local secretion of catecholamines [29]. This secretion, that represents the preferential inducer of lipolysis and thermogenesis through the activation of the β-adrenergic pathway, appears to be crucial during prolonged exposure to cold or aging [28,30].

Similarly to adipokines, the oxygenated derivatives of ω6 PUFAs such as the *n*-2 series prostaglandins or the *n*-4 series leukotrienes, which are synthesized and secreted by adipocytes, participate in the inflammatory state of the tissue [31,32]. Furthermore, adipocytes are able to metabolize ω3 PUFAs, in the same way as ω6, to produce oxygenated anti-inflammatory derivatives such as *n*-3 series prostaglandins (PG), *n*-5 series leukotrienes (LT), as well as resolvins (Rv) and

protectins (PD) [32]. For example, the administration of ω3 PUFAs to obese mice as well as resolvin D1 (RvD1), an oxygenated derivative of DHA, limits macrophage infiltration, favors their polarization toward the M2 phenotype, and rescues adipocyte metabolic dysfunction [33,34]. Thus, ω6- and ω3-derived oxylipins are able to modulate the inflammatory phenotype of immune cells, especially macrophages [11,35]. As dietary ω6 and ω3 PUFAs directly affect the quality and the quantity of oxylipins synthesized and secreted by the adipocytes, it is of high interest to characterize the impact of ω3 PUFA diet supplementation on the inflammatory state of adipose tissue.

## 2. Materials and Methods

### *2.1. Reagents*

Culture media and buffer solutions were purchased from Lonza (Ozyme, St-Quentin en Yvelines, France), fetal bovine serum (FBS) from Eurobio (Courtaboeuf, France), insulin and trypsin from InVitrogen (Cergy Pontoise, France). Oxylipins and inhibitors were purchased from Cayman (BertinPharma, Montigny le Bretonneux, France). Other culture reagents were from Sigma-Aldrich Chimie (Saint-Quentin Fallavier, France).

### *2.2. Animals and Diets*

The experiments were conducted in accordance with the French and European regulations (Directive 2010/63/EU) for the care and use of research animals and were approved by national experimentation committees (MESR 01947.03). Ten-week-old C57BL/6J male mice from Janvier Laboratory (France) were maintained at thermoneutrality (28 ± 2 °C) and 12:12-h light-dark cycles, with ad libitum access to food and water to not hide any behavioral modification. Mice were fed for 12 weeks with isocaloric isoenergetic (3.2 kCal/g–13.5 kJ/g) ω6- or ω3-enriched diets (12% energy content as lipids). The diets were prepared by Harlan (WI, USA) from standard chow diets (reference number 2016) by the addition of specific fatty acid ethyl-esters from NuChekPrep (Elysian, MIN, USA). Detailed compositions are displayed in Table 1. Blood, interscapular brown adipose tissue (iBAT), epididymal (eWAT), and inguinal subcutaneous (scWAT) white adipose tissues were sampled and used for different analyses.

**Table 1.** Diet compositions.

| | ω6-Enriched Diet | ω3-Enriched Diet |
|---|---|---|
| Protein [% by weight] | 16 | |
| Carbohydrate [% by weight] | 52 | |
| Fat [% by weight] | 5 | |
| Saturated fatty acids (FAs) [% of total FAs] | 12 | |
| Monounsaturated FAs [% of total FAs] | 26 | 14 |
| Polyunsaturated FAs [% of total FAs] | 62 | 74 |
| Linoleic acid [% by weight] | 3 | |
| α-linolenic acid [% by weight] | 0.1 | 0.64 |
| EPA [% by weight] | - | 0.08 |
| DHA [% by weight] | - | 0.08 |
| *ω6/ω3* PUFA ratio | 30 | 3.75 |

### *2.3. Cell Culture*

THP-1, a human pro-monocytic cell line, was cultured in RPMI GlutaMax medium, supplemented with 10% FBS and 10 mM sodium pyruvate, at 37 °C and 5% $CO_2$. Differentiation in macrophages-like cells was induced by treatment with 20 nmol/L phorbol 12-myristate 13-acetate (PMA) for 72 h. Then, media were replaced and polarization was induced for 48 h either with lipopolysaccharides (LPS, 100 ng/mL) for M1 like-phenotype or with IL-4/IL-10 (10 ng/mL each) for M2 like-phenotype acquisition. Treatments with a LOX inhibitor (=carnosic acid (CA), 10 µM), and/or with 9-HODE and 13-HODE (50 nmol/L + 50 nmol/L), were performed during the 48 h polarization step.

### *2.4. Oxylipin Quantification*

For quantification of unesterified oxylipins, tissues were snap-frozen with liquid nitrogen immediately after retrieval and stored at −80 °C. Extraction and analysis by mass spectrometry were performed at METATOUL platform (MetaboHUB, INSERM UMR 1048, I2MC, Toulouse, France) as previously described [13,36].

### *2.5. Cytokine Quantification*

For blood analysis, plasmas were diluted twice and analysis following manufacturer's instructions using the mouse V-PLEX Proinflammatory Panel 1 Kit (Meso Scale Discovery, # K15048D) on a QuickPlex SQ 120 apparatus (Meso Scale Discovery).

For tissue analysis, proteins were extracted from frozen organs using an ULTRA TURRAX T25 (Ika, Germany) and lysis buffer (25 mM Tris-Cl (pH 7.4), 100 mM NaCl, 1 mM EDTA, 1% Triton X-100, 0.5% Nonidet P40 and protease inhibitors (Roche Diagnostics, Meylan, France)). Protein concentration was evaluated by BCA assay (Sigma-Aldrich Chimie, Saint-Quentin Fallavier, France). 10 µg proteins were used to evaluate cytokine concentration using the same kit and apparatus as those used for blood cytokine analysis.

### *2.6. Histology*

Freshly sampled tissues were fixed in 4% paraformaldehyde overnight at RT and then paraffin-embedded. Embedded tissues were cut into 5-µm sections and dried overnight at 37 °C. For immunohistochemistry, sections were then deparaffinized in xylene, rehydrated using alcohol, and washed in phosphate-buffered saline (PBS).

For histology analysis, sections were stained with hematoxylin-eosin and mounted in Mowiol.

For immunohistochemistry analysis, antigen unmasking was performed in boiling citrate buffer (10 mM, pH 6.0) for 6 minutes. Sections were then permeabilized in PBS with 0.2% Triton X-100 at room temperature for 20 minutes and blocked in the same buffer containing 3% BSA for 30 min. Sections were co-incubated with rat anti-F4/80 antibody (Biorad, clone Cl:A3-1, dilution 1:100) and rabbit anti-Arginase-1 (ThermoFisher Scientific, #PA5-29645, dilution 1:100) overnight at 4 °C.

Following a 30-min incubation with biotinylated anti-rat and TRITC-coupled anti-rabbit secondary antibodies, the sections were incubated for another 30 min at room temperature with avidin–biotin complex (Vector Lab, VECTASTAIN ABC Kit, PK-4000), and were then labeled with 3,3′-diaminobenzidine solution (Vector Lab, DAB, SK-4100). Nuclear staining was performed with DAPI and sections were mounted in Mowiol.

Visualization was performed with an Axiovert microscope. Pictures were captured using AxioVision software (Carl Zeiss, Jena, Germany).

### *2.7. Isolation and Analysis of RNA*

Procedures follow MIQE recommendations [37]. Total RNA was extracted using a TRI-Reagent kit (Euromedex, Souffelweyersheim, France) according to the manufacturer's instructions. For RNA isolation from organs, tissues were homogenized in TRI-Reagent using a dispersing instrument (ULTRA TURRAX T25). A reverse transcription-polymerase chain reaction (RT-PCR) was performed using M-MLV-RT (Promega). SYBR qPCR premix Ex TaqII from Takara (Ozyme, France) was used for quantitative PCR (qPCR), and assays were run on a StepOne Plus ABI real-time PCR machine (PerkinElmer Life and Analytical Sciences, Boston). The expression of selected genes was normalized to that of the TATA-box binding protein (TBP) and 36B4 housekeeping genes and then quantified using the comparative-ΔCt method. Primer sequences are available upon request.

### *2.8. Statistical Analysis*

Data were expressed as mean values ± standard error of the mean (SEM). Data were analyzed using InStat software (GraphPad Software) by one-way ANOVA followed by a Mann-Whitney (for in vivo experiments) or a Student-Newman-Keuls (for in vitro experiments) post-test to assess statistical differences between experimental groups. Differences were considered statistically significant with $p < 0.01$.

## 3. Results

### *3.1. Impact of ω3 PUFA Supplementation on General Parameters of Mice*

#### 3.1.1. General Metabolic Parameters

Ten-week-old male mice were fed for 12 weeks with an isocaloric isoenergetic standard diet enriched in ω6 PUFAs (ω6-enriched diet, *ω6/ω3* = 30), or supplemented with ω3 PUFAs (ω3-enriched diet, *ω6/ω3* = 3.7), see Table 1. Mice were housed at 28 °C, near thermoneutrality, in order to limit energy expenditure due to thermogenic metabolism and to avoid any effect of this activity on inflammatory response, as demonstrated previously [38].

Mice body weight, see Figure 1a, as well as food intake (ω6-enriched diet, 4.49 g/day; ω3-enriched diet, 4.46 g/day per mouse) were similar between the two groups. Epididymal white adipose tissue mean weight, see Figure 1b, and fed glycaemia, see Figure 1c, were not different after 12 weeks of the diets. Altogether, these results indicated that the *ω6/ω3* ratio of a standard diet, equilibrated in carbohydrate, protein, and fat quantities (respectively, 20.1%, 65.4%, and 14.5% of energy supply), did not modify general metabolic parameters of mice.

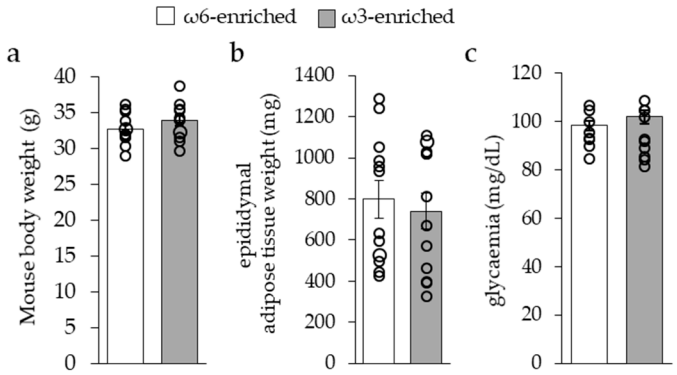


**Figure 1.** Mice general metabolic parameters. (**a**) Mouse body weight, (**b**) epididymal white adipose tissue weight, and (**c**) blood glycaemia evaluated after 12 weeks of ω6- or ω3-enriched diet. Results are displayed as independent mouse values (dots) and mean ± SEM (histograms). $n = 12$.

#### 3.1.2. Plasmatic Inflammatory Phenotype

To characterize the systemic inflammatory effect of a PUFA-enriched diet, we evaluated the blood circulating level of a panel of cytokines, see Figure 2.

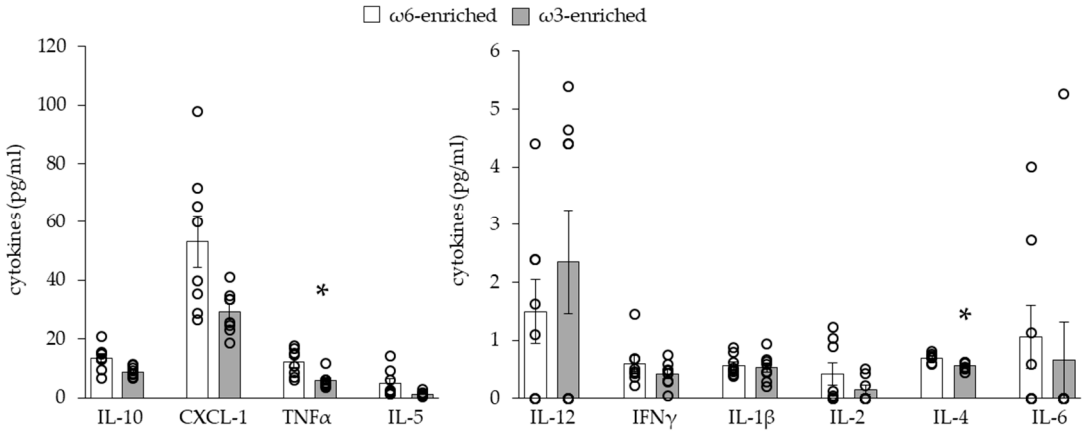


**Figure 2.** Analysis of blood cytokines. Results are displayed as independent mouse values (dots) and mean ± SEM (histograms). $n = 8$. *, $p < 0.01$.

As expected, the level of most of the pro-inflammatory and anti-inflammatory cytokines was unchanged between the two groups of mice. Only TNFα (pro-inflammatory cytokine) and IL-4 (anti-inflammatory cytokine) levels slightly but significantly decreased in mice fed an ω3-enriched diet.

### 3.1.3. Impact of ω3 PUFA Supplementation on Adipose Tissue Oxylipin Content

To investigate the modification induced by the two different diets within adipose tissues, we quantified the levels of 33 PUFA-metabolites within iBAT, see Figure 3, and scWAT, see Figure 4, of mice. These oxylipins were analyzed by groups following their PUFA origin, see Figures 3a and 4a, or separately, see Figures 3b and 4b. In the iBAT, ω3 PUFA supplementation led to a significant increase of the oxylipins deriving from ω3 PUFAs EPA (PGE3, LTB5, 18-HEPE) and DHA (RvD2, RvD1, MaR1, PDx, 17-HDoHE, 14-HDoHE), but did not affect ω6-derived metabolites (6kPGF1a, TxB2, 11B-PGF2a, PGF2a, PGE2, PGD2, 8isoPGA2, 15dPGJ2, LxB4, LxA4, LTB4, 5,6-DiHETE, 15-HETE, 8-HETE, 12-HETE, 5-HETE, 5oxoETE, 14,15-EET, 11,12-EET, 8,9-EET, 5,6-EET derived from ARA; 13-HODE, 9-HODE derived from LA), see Figure 3a.

In scWAT, while similar results were found for ω3 PUFA-derived and ARA-derived oxylipins, LA-derived metabolites were highly increased, as shown in Figure 4a.

LA and ω3-PUFA derived oxylipins are considered as anti-inflammatory and pro-resolving mediators, especially through the modulation of macrophage function. Along with these oxylipins, we have found that 14- and 17-HDoHEs and 18-HEPE levels were increased in iBAT and scWAT of mice fed the ω3-enriched diet, and 9- and 13-HODEs were increased only in scWAT, see Figures 3b and 4b. 14- and 17-HDoHE are metabolized in pro-resolving mediators as RvD1, RvD2, Mar1, PDx, and PD1, while 18-HEPE leads to RvE1 synthesis. It is interesting to note that these final metabolites were barely (PDx) or not detected within the tissue, see Figures 3b and 4b.

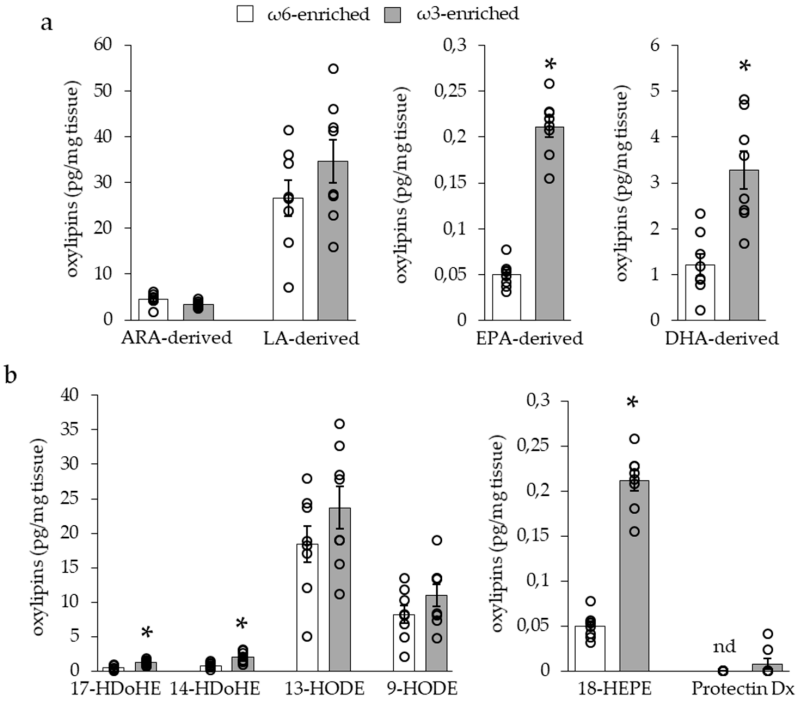


**Figure 3.** Quantities of oxylipins derived from dietary polyunsaturated fatty acids (PUFAs) in interscapular brown adipose tissue (iBAT). (**a**) Quantities of oxylipins derived from arachidonic acid (ARA) and linoleic acid (LA) ω6 PUFAS or eicosapentaenoic acid (EPA) and docosahexaenoic acid (DHA) ω3 PUFAs. (**b**) Quantities of oxylipins considered as anti-inflammatory or pro-resolving mediator intermediates. Results are displayed as independent mouse values (dots) and mean ± SEM (histograms). $n = 8$. *, $p < 0.01$.

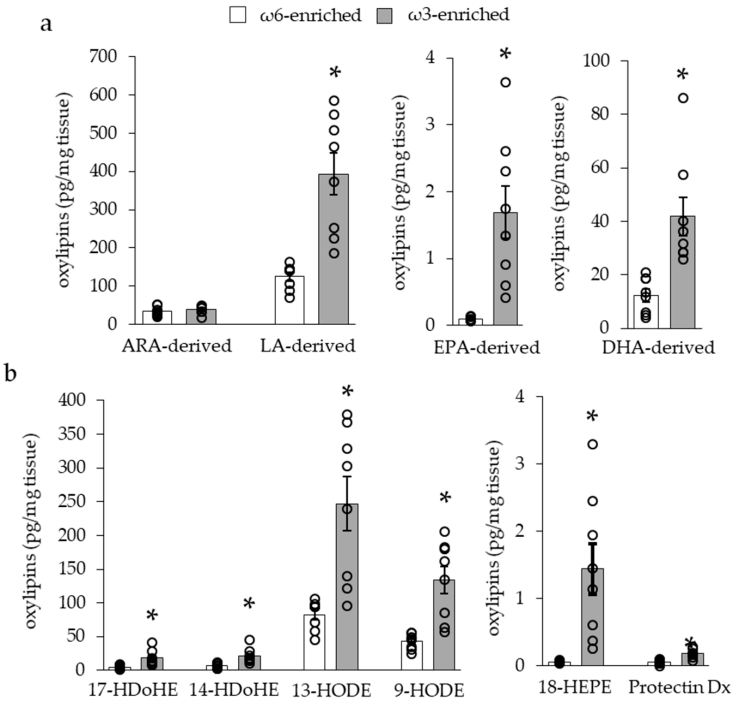


**Figure 4.** Quantities of oxylipins derived from dietary PUFAs in inguinal subcutaneous white adipose tissues (scWAT). (**a**) Quantities of oxylipins derived from ARA and LA ω6 PUFAS or EPA and DHA ω3 PUFAs. (**b**) Quantities of oxylipins considered as anti-inflammatory or pro-resolving mediator intermediates. Results are displayed as independent mouse values (dots) and mean ± SEM (histograms). $n = 8$. *, $p < 0.01$.

### *3.2. Effect on Inflammatory Phenotype of Adipose Tissue*

#### 3.2.1. Histology and Cytokine Content

The histological analysis of iBAT and scWAT, see Figure 5a, revealed neither cell infiltration nor crown structure that were typical of an adipose tissue inflammatory response in both groups of mice.

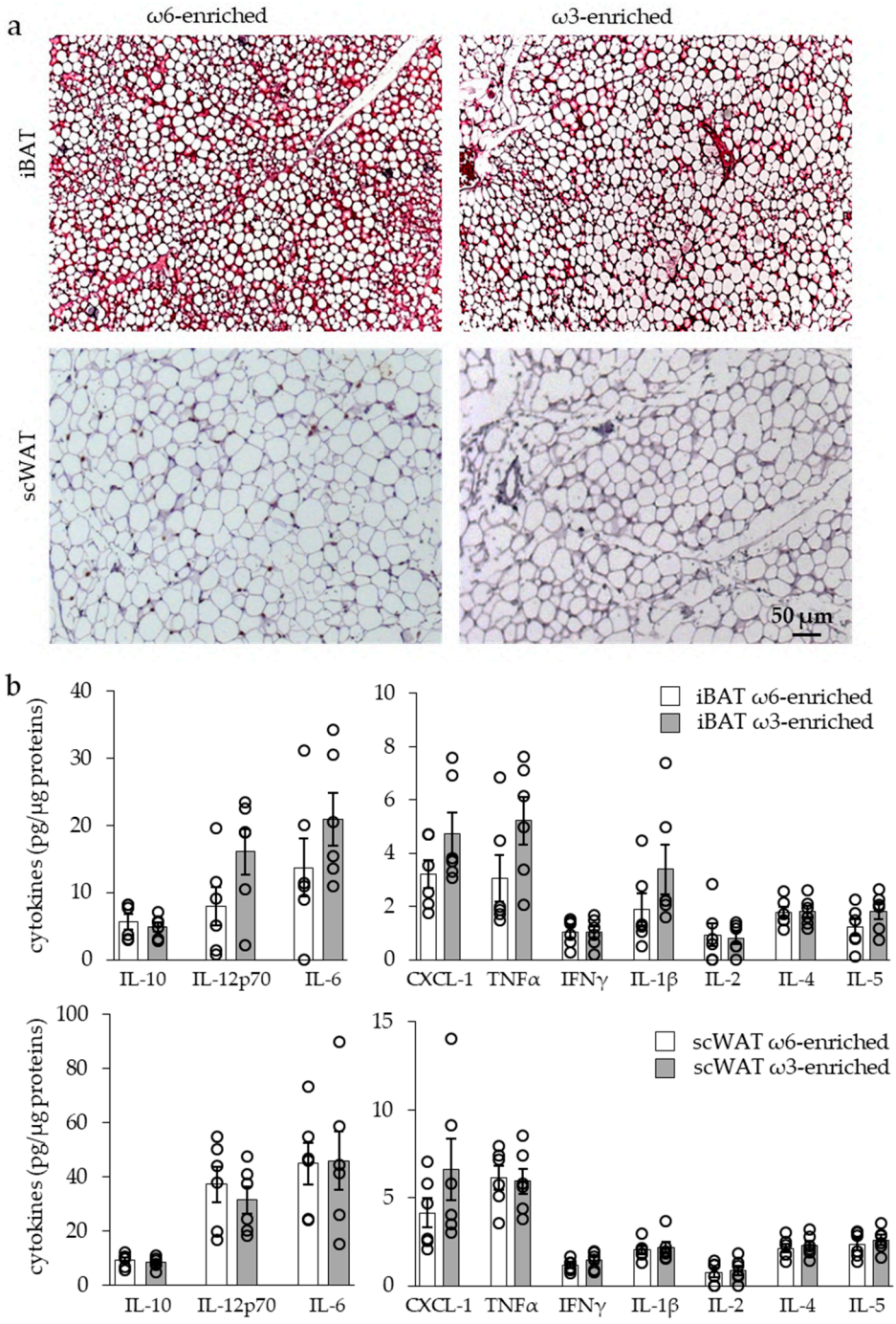


**Figure 5.** Inflammatory profile of iBAT and scWAT of mice submitted to ω6- or ω3-enriched diet. (**a**) Hematoxylin and eosin staining of tissue sections. (**b**) Analysis of adipose tissue cytokine levels. Results are displayed as independent mouse values (dots) and mean ± SEM (histograms). $n = 6$. *, $p < 0.01$.

In the same way, analysis of the iBAT and scWAT cytokine contents showed similar levels of both pro- and anti-inflammatory cytokines in the two groups of mice, as shown in Figure 5b.

### 3.2.2. Expression of Inflammatory Markers

As we did not find any modulation of cytokine levels, we analyzed marker expression of specialized macrophages to evaluate the inflammatory background of the tissue, see Figure 6.

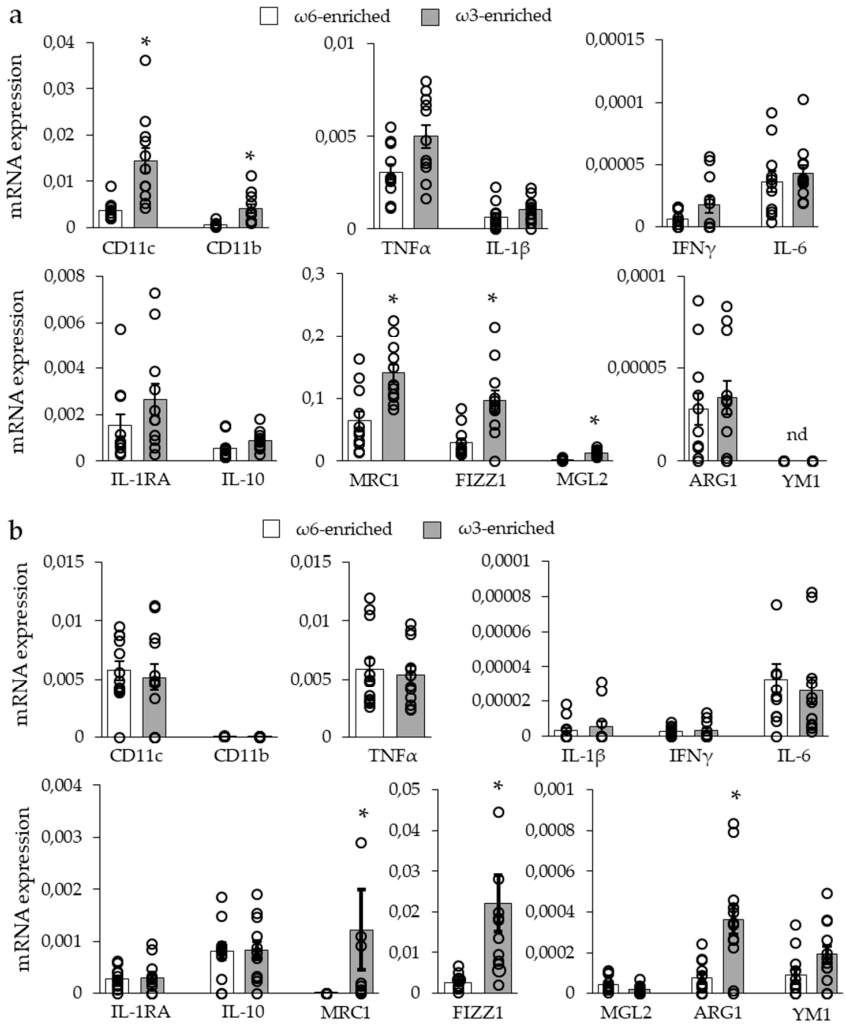


**Figure 6.** Macrophage marker expression in adipose tissue of mice submitted to ω6- or ω3-enriched diet. mRNA level analysis of general (CD11c, CD11b), M1 (TNFα, IL-1β, IFNγ, IL-6) and M2 (IL-1RA, IL-10, MRC1, FIZZ1, MGL2, ARG1, YM1) macrophage markers in (**a**) iBAT and (**b**) scWAT. Histograms display mean ± SEM. $n = 12$. *, $p < 0.01$.

The analysis of macrophage markers in iBAT derived from the ω3-enriched diet group, see Figure 6a, revealed an increase in CD11b (or ITGAM, integrin αM) and CD11c (or ITGAX, integrin αX) mRNA expression, concomitantly to an increase in major M2 macrophage markers, namely MRC1 (mannose receptor 1), FIZZ1 (found in inflammatory zone 1 or RELMα), and MGL2 (macrophage galactose N-acetyl-galactosamine specific lectin 2). No change was found for other M2 macrophage markers or for M1 macrophage markers. To note, ARG1 (arginase 1) and Ym1 (chitinase 3-like 3) were either barely detected or undetected in this tissue.

The analysis of the scWAT, see Figure 6b, from ω3-supplemented mice, showed an increased the expression of the M2 macrophage markers MRC1 and FIZZ1 (not MGL2), but no increase of CD11c (CD11b was undetected). In contrast to iBAT, our data revealed an increase of ARG1 mRNA expression

and the induction of YM1 mRNA expression. Finally, as for iBAT, no change was found for mRNA expression of M1 macrophage markers.

Altogether, these results demonstrated that an ω3-enriched diet led to a general increase in M2 anti-inflammatory macrophage marker expression without modification in M1 pro-inflammatory markers. This was correlated and perhaps due to the increased amount of substrates for pro-resolving mediator synthesis, as well as an increased quantity of M2 polarizing oxylipins.

### *3.3. Effect of Potential Anti-Inflammatory Oxylipins Modified in an ω3-Enriched Diet on THP1 Monocyte Cells*

The oxylipins 9- and 13-HODEs (LA-derived oxylipins metabolized by LOX) are not known to be precursors of pro-resolving mediators but display high contents in iBAT, see Figure 3b, and scWAT, see Figure 4b, and are strongly increased in scWAT after the implementation of an ω3-enriched diet. In order to investigate the role of 9- and 13-HODEs on macrophage polarization, we used THP-1 macrophage cell lines activated in pro-inflammatory M1 (LPS 100 ng/mL, Figure 7a) or anti-inflammatory M2-like phenotype (IL4 + IL-10 10 ng/mL each, Figure 7b). THP-1 cells were treated with 9- and 13-HODEs (9/13-HODEs, 50 nmol/L each) or with carnosic acid (CA, 10 μM), a lipoxygenase inhibitor [39], or a combination of both.

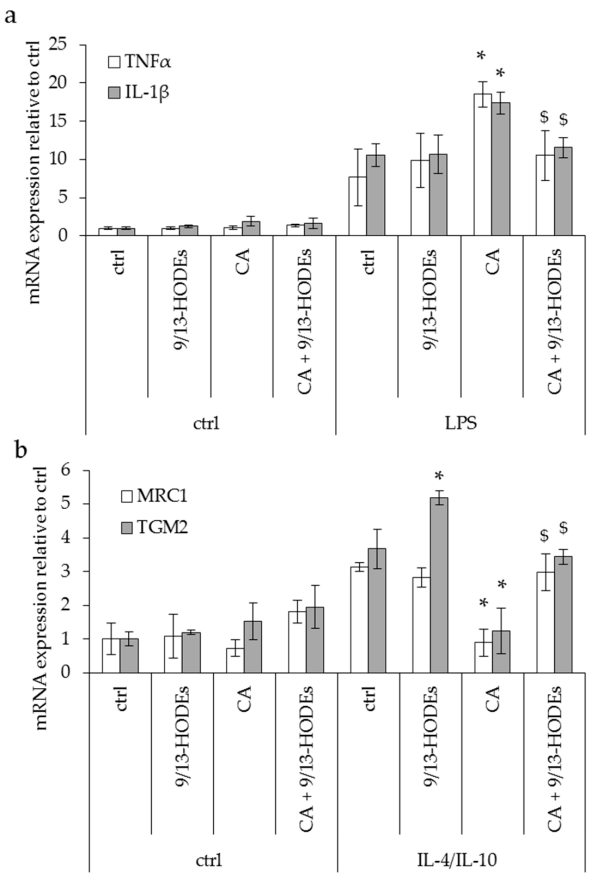


**Figure 7.** Macrophage marker expression in THP-1 cells under 9- and 13-HODE treatment. mRNA level analysis by RT-qPCR of M1 (TNFα, IL-1β) and M2 (MRC1, TGM2) macrophage markers in control, lipopolysaccharides (LPS) (upper panel) or IL-4/IL-10 (lower panel) treated THP-1 macrophages. Cells were co-treated for 48 h with carnosic acid (CA, 10 μM) and or 9- and 13-HODEs. (**a**) CA treatment induced opposite effects in M1- and M2-like macrophages as it increased inflammatory markers in THP-1 M1-like macrophages, and (**b**) decreased M2-like macrophages' markers. Histograms display mean ± SEM. $n = 3$. *, $p < 0.01$ vs. ctrl and $, $p < 0.01$ vs. CA.

None of the treatments modulated non-polarized THP-1, see Figure 7. Treatment with 9/13-HODEs alone showed no effect on macrophages' M1-like phenotype but increased TGM2 expression on M2-like macrophages. Remarkably, CA treatment induced opposite effects in M1- and M2-like macrophages as it increased inflammatory markers in THP-1 M1-like macrophages, see Figure 7a, and decreased M2-like macrophages' markers, see Figure 7b. Interestingly, 9/13-HODEs supplementation reversed CA effects, see Figure 7.

## 4. Discussion

Dietary fats are the source of essential PUFAs that are required for fetal and newborn development and trigger a variety of biological responses in adults, especially, in adipose tissue. New dietary recommendations warn against the insufficient intake of ω3 PUFAs and the excess of ω6 PUFAs which correlate with various disease developments [3,4]. In the first year of life, a high dietary *ω6/ω3* ratio is positively associated with adiposity of infants [40–42]. In the same way, in adults, a high *ω6/ω3* ratio can correlate to an increase of fat mass and the development of metabolic complications [6–10].

Conversely, it has been described that a low *ω6/ω3* ratio seems to be correlated with metabolic disorder protection in different populations [43]. On a metabolic point of view, diets exhibiting a high *ω6/ω3* ratio allow a higher ARA bioavailability for the synthesis of ω6-derived eicosanoids due to an insufficient compensatory effect of EPA and DHA [15]. Indeed, both ω6 and ω3 PUFAs are metabolized using the same enzymatic pathways. First, LA and LNA are modified by common Δ-desaturases and elongases [44]; then, their metabolites, i.e., ARA, DGLA, EPA, and DHA, are metabolized in oxygenated derivatives also using common pathways involving cyclooxygenases, lipoxygenases, and CYP450 enzymatic reactions. Here, we provided evidence that, compared to a high *ω6/ω3* PUFA ratio, an equilibrated ratio of four allows the synthesis of LA and EPA/DHA oxylipins instead of ARA oxylipins. As LA and LNA use a common pathway (Δ-desaturase) to be transformed, respectively, into DGLA/ARA and EPA/DHA, we hypothesize that LNA supplementation could limit LA desaturation and thus increase LA bioavailability and metabolization in oxylipins through the LOX pathways. Thus, these competitive phenomena, in addition to dietary intake, determine PUFA availability in oxylipins synthesis and, in turn, their various metabolic effects, especially for inflammatory responses [45].

It has already been described in rodents that an increase of white adipose tissue mass can be related to an ω6 PUFA-enriched high-fat diet and can be prevented by ω3 PUFA supplementation [12, 46]. It is suggested that this could only be due to a specific subset of ω3 PUFA such as EPA [47]. Moreover, eicosanoids derived from ω6 PUFA inhibit adipocyte thermogenic activity both in vitro and in vivo [11,13,48]. We and others demonstrated previously, using the same nutritional approach as in the present work, that an ω3 PUFA diet supplementation improved the thermogenic adipocyte function by promoting a more oxidative phenotype in response to β-adrenergic stimulation [14,49]. In the present study, ω3 PUFA supplementation does not induce any change in body mass, glycaemia, or white and brown adipose tissue morphologies since the mice were fed diets with normal fat content and did not receive any β-adrenergic challenge.

Most studies concerning ω3 PUFA supplementations were carried out in a context of obesity (high-fat diet) or infection (LPS treatment) and demonstrate a positive effect of ω3 PUFA supplementation on the analyzed parameters [35]. Nevertheless, other studies demonstrate the inability of ω3 PUFAs to modulate inflammation after LPS treatment [50] or in obese mice [51,52]. These discrepancies are essentially due to the differences in the experimental approaches (diet composition, mouse strain, challenge . . . .) and in the analyzed parameters (cytokine concentration, mRNA expression, histology . . . ). In humans, several experimental approaches have tried to link an ω3 PUFA intake to inflammatory response, again with inconsistent conclusions. For example, a one-year dietary supplementation in ω3 PUFA does not modify the circulating cytokine levels in healthy volunteers [53]. Conversely, other studies show a decrease of blood inflammatory markers after ω3 PUFA supplementation [54,55]. It is important to note that a plasma inflammatory mediator profile seems to be less representative compared to the one of adipose tissue [56]. The same discrepancy

is found for studies analyzing adipose tissue inflammation. Although one human trial (4g ω3 PUFAs/day; 12 weeks) on insulin-resistant adults demonstrates a decrease in the crown-like structure number [57], corresponding to phagocytic activity of macrophage on adipocyte, another trial on the same type of patients (4.2g ω3 PUFAs/day; 6 months) demonstrates no effect of ω3 PUFA supplementation on the same parameter [58]. Moreover, a recent paper establishes that the oxylipin profile in rat adipose tissue after dietary ω3 PUFA supplementation (ratio *ω6/ω3* of 0.6) is dependent of (i) the kind of ω3 PUFA used, (ii) the kind of adipose tissue analyzed, and (iii) the sex [59].

In view of these heterogeneities, we decided to analyze the effect of PUFA intake in normal physiological conditions (thermoneutrality, no β-adrenergic challenge) using an isocaloric, isoenergetic standard diet supplemented with ethyl esters of fatty acids (instead of classic oil supplementation) and various technical approaches to characterize the inflammatory profile. With this strategy, we characterize fatty acid metabolism within subcutaneous and brown adipose tissues and the related inflammatory phenotype. Our results linking ω3 PUFA supplementation and M2 macrophage are in line with other studies, such as a recent one demonstrating that (i) treatment of human adipose tissue explants with ω3 PUFAs lead to an anti-inflammatory phenotype characterized by a decrease of M1 marker expression, and (ii) treatment of THP-1 cells increased expression of M2 markers [60]. In the same way, DHA supplementation in a high-fat diet context promotes mRNA expression of M2 markers within white adipose tissue without affecting the total macrophage number [61]. In this study, the authors describe the same effect for RvD1, DHA metabolites, and conclude that DHA leads to an anti-inflammatory phenotype via RvD1 synthesis. Unfortunately, they never quantify RvD1 production in vivo and thus do not link DHA supplementation to RvD1 synthesis [61]. In our study, we have not been able to detect resolvins but only their substrates. We assume that without a specific inflammatory signal, intermediates of pro-resolving mediators are synthesized but not metabolized. Indeed, these mediators are involved in the resolution of inflammation and appeared late in the process as they are not required before, differently to prostaglandins and leukotrienes which appear early [62].

In our study, we measure a defined set of oxylipins. Even if this panel includes oxylipins deriving from all pathways and PUFAs, we cannot exclude that unmeasured oxylipins triggered the anti-inflammatory effect of ω3 PUFA supplementation found in our model. In this way, epoxide and diol metabolites derived from CYP epoxygenase/soluble epoxide hydrolase activity [63], as well as endocannabinoids, are known and interesting potential mediators of the inflammatory effect of PUFA [64]. In addition, the esterification of oxylipins, especially of eicosanoids, was described as an active and major mechanism in various cell biological responses including inflammation [65]. These esterified oxylipins can represent the majority of cell oxylipins and can be hydrolyzed from the membrane under specific stimuli [66]. In this way, it could be interesting to quantify all oxylipins (unesterified and esterified) in adipose tissue under ω3 PUFA diet supplementation and to evaluate their hydrolysis under inflammatory conditions. Nevertheless, our unexhaustive analysis allowed a correlation between the synthesis of several oxylipins and the expression of M2 macrophage markers. We propose that 9- and 13-HODEs could drive this effect. In our in vitro results on the THP-1 cell line, we demonstrate that 9- and 13-HODEs are not enough to directly drive the polarization of THP-1 macrophage but are required to maintain the phenotype. Indeed, their supplementation restores control level expression of M1-like and M2-like markers after CA treatment. Moreover, 9- and 13-HODEs seem to play a role in the anti-inflammatory effects since they are able to increase M2 markers such as TGM2. These results are consistent with some studies describing 9- and 13-HODEs as known mediators of macrophage polarization [67] in a PPARγ-dependent manner [68]. Of course, other oxylipins could be involved in the anti-inflammatory environment found in our mice. For example, the study of Fat-1 mouse, which is able to synthesize ω3 PUFAs itself, displays a lowered inflammatory environment induced by obesity, correlatively to 17-HDoHE synthesis [69]. In addition to oxylipins involvement, we cannot exclude a direct action of ω3 PUFAs on the membrane receptor. Indeed, it is shown that DHA is able to directly activate, via GPR120, an anti-inflammatory response driven by macrophage within adipose tissue [33]. This activity could be linked to the recent characterization of the DHA

inhibitory effect on NLRP3 inflammasome activity, an effect triggered by GPR40/GPR120 pathways and leading to a decreased production of mature IL-1β [70]. As NLRP3 is activated essentially in response to an infectious environment, we do not correlate ω3 PUFA supplementation with a decrease in IL-1β production in our physiological context.

It is interesting to note that the ω3 PUFA intake finely drives the kind of oxylipins synthesized. A recent study analyzed the effect of an ω3 PUFA dietary supplementation of an already equilibrated diet (ratio *ω6/ω3* = 6.7) to reach an *ω6/ω3* ratio of 0.8. Thus, differently to our situation, LA and LNA are already desaturated equivalently, and the increase in ω3 PUFA intake leads to a decrease of LA-derived oxylipins (9/13-HODEs) in favor of EPA and DHA derived oxylipins in the brain. Moreover, this "over"-supplementation ameliorates against an inflammatory response [71].

## 5. Conclusions

Previous studies have demonstrated the positive effect of ω3 PUFA intake to counteract the adverse consequences of a high-fat diet or inflammatory situation. Herein, our study was conducted in non-obesogenic non-inflammatory conditions and also showed a beneficial influence of ω3 PUFA dietary supplementation on the adipose tissue inflammatory phenotype. Moreover, while ω3 PUFA metabolites have been involved in this effect, we additionally highlighted the unsuspected role of LA-derived metabolites. Finally, this already assumed beneficial outcome of ω3 PUFA supplementation is in line with a human situation where a high *ω6/ω3* ratio is correlated with the development of inflammatory diseases in metabolic tissue.

**Author Contributions:** The author(s) have made the following declarations about their contributions: Conceived and designed the experiments: L.B., D.F.P. Performed the experiments: C.C., R.A.G., O.D., S.R., A.L., D.F.P. Analyzed the data: C.C., L.B., D.F.P. Wrote the manuscript: C.C., L.B., D.F.P.

**Funding:** This research was funded by French Agence Nationale de la Recherche (ANR/DFG-15-CE14-0033 "Nutribrite"), INSERM, Region PACA, Nutricia Research Foundation ("2015-26") and Société Francophone du Diabète (SFD)/Pierre Fabre Médicament 2017.

**Acknowledgments:** The authors greatly acknowledge the IRCAN Animal core facility and the IBV histology platform. We thank Pauline Le Faouder, Justine Bertrand-Michel, and the METATOUL platform (MetaboHUB, INSERM UMR 1048, I2MC, Toulouse, France) for oxylipins analysis. We acknowledge OCTALIA Technologies to English editing.

**Conflicts of Interest:** The authors declare no conflict of interests. The funders had no role in the design of the study; in the collection, analyses, or interpretation of data; in the writing of the manuscript, or in the decision to publish the results.

## References

1. Simopoulos, A.P. The importance of the ratio of omega-6/omega-3 essential fatty acids. *Biomed. Pharmacother.* **2002**, *56*, 365–379. [CrossRef]
2. Simopoulos, A.P. An Increase in the Omega-6/Omega-3 Fatty Acid Ratio Increases the Risk for Obesity. *Nutrients* **2016**, *8*, 128. [CrossRef]
3. Ailhaud, G.; Massiera, F.; Weill, P.; Legrand, P.; Alessandri, J.M.; Guesnet, P. Temporal changes in dietary fats: Role of *n*-6 polyunsaturated fatty acids in excessive adipose tissue development and relationship to obesity. *Prog. Lipid Res.* **2006**, *45*, 203–236. [CrossRef] [PubMed]
4. Muhlhausler, B.S.; Ailhaud, G.P. Omega-6 polyunsaturated fatty acids and the early origins of obesity. *Curr. Opin. Endocrinol. Diabetes Obes.* **2013**, *20*, 56–61. [CrossRef] [PubMed]
5. Simopoulos, A.P.; DiNicolantonio, J.J. The importance of a balanced omega-6 to omega-3 ratio in the prevention and management of obesity. *Open Heart* **2016**, *3*, e000385. [CrossRef]
6. Inoue, K.; Kishida, K.; Hirata, A.; Funahashi, T.; Shimomura, I. Low serum eicosapentaenoic acid/arachidonic acid ratio in male subjects with visceral obesity. *Nutr. Metab. (Lond.)* **2013**, *10*, 25. [CrossRef] [PubMed]
7. Savva, S.C.; Chadjigeorgiou, C.; Hatzis, C.; Kyriakakis, M.; Tsimbinos, G.; Tornaritis, M.; Kafatos, A. Association of adipose tissue arachidonic acid content with BMI and overweight status in children from Cyprus and Crete. *Br. J. Nutr.* **2004**, *91*, 643–649. [CrossRef]

8. Williams, E.S.; Baylin, A.; Campos, H. Adipose tissue arachidonic acid and the metabolic syndrome in Costa Rican adults. *Clin. Nutr.* **2007**, *26*, 474–482. [CrossRef]
9. Claria, J.; Nguyen, B.T.; Madenci, A.L.; Ozaki, C.K.; Serhan, C.N. Diversity of lipid mediators in human adipose tissue depots. *Am. J. Physiol. Cell Physiol.* **2013**, *304*, C1141–C1149. [CrossRef]
10. Garaulet, M.; Perez-Llamas, F.; Perez-Ayala, M.; Martinez, P.; de Medina, F.S.; Tebar, F.J.; Zamora, S. Site-specific differences in the fatty acid composition of abdominal adipose tissue in an obese population from a Mediterranean area: Relation with dietary fatty acids, plasma lipid profile, serum insulin, and central obesity. *Am. J. Clin. Nutr.* **2001**, *74*, 585–591. [CrossRef]
11. Ghoshal, S.; Trivedi, D.B.; Graf, G.A.; Loftin, C.D. Cyclooxygenase-2 deficiency attenuates adipose tissue differentiation and inflammation in mice. *J. Biol. Chem.* **2011**, *286*, 889–898. [CrossRef] [PubMed]
12. Massiera, F.; Saint-Marc, P.; Seydoux, J.; Murata, T.; Kobayashi, T.; Narumiya, S.; Guesnet, P.; Amri, E.Z.; Negrel, R.; Ailhaud, G. Arachidonic acid and prostacyclin signaling promote adipose tissue development: A human health concern? *J. Lipid Res.* **2003**, *44*, 271–279. [CrossRef] [PubMed]
13. Pisani, D.F.; Ghandour, R.A.; Beranger, G.E.; Le Faouder, P.; Chambard, J.C.; Giroud, M.; Vegiopoulos, A.; Djedaini, M.; Bertrand-Michel, J.; Tauc, M.; et al. The omega6-fatty acid, arachidonic acid, regulates the conversion of white to brite adipocyte through a prostaglandin/calcium mediated pathway. *Mol. Metab.* **2014**, *3*, 834–847. [CrossRef] [PubMed]
14. Ghandour, R.A.; Colson, C.; Giroud, M.; Maurer, S.; Rekima, S.; Ailhaud, G.P.; Klingenspor, M.; Amri, E.Z.; Pisani, D.F. Impact of dietary omega3 polyunsaturated fatty acid supplementation on brown and brite adipocyte function. *J. Lipid Res.* **2018**. [CrossRef] [PubMed]
15. Fischer, R.; Konkel, A.; Mehling, H.; Blossey, K.; Gapelyuk, A.; Wessel, N.; von Schacky, C.; Dechend, R.; Muller, D.N.; Rothe, M.; et al. Dietary omega-3 fatty acids modulate the eicosanoid profile in man primarily via the CYP-epoxygenase pathway. *J. Lipid Res.* **2014**, *55*, 1150–1164. [CrossRef] [PubMed]
16. Odegaard, J.I.; Chawla, A. The immune system as a sensor of the metabolic state. *Immunity* **2013**, *38*, 644–654. [CrossRef] [PubMed]
17. Tilg, H.; Moschen, A.R. Adipocytokines: Mediators linking adipose tissue, inflammation and immunity. *Nat. Rev. Immunol.* **2006**, *6*, 772–783. [CrossRef] [PubMed]
18. Hotamisligil, G.S. Inflammation and metabolic disorders. *Nature* **2006**, *444*, 860–867. [CrossRef]
19. Lumeng, C.N.; Bodzin, J.L.; Saltiel, A.R. Obesity induces a phenotypic switch in adipose tissue macrophage polarization. *J. Clin. Investig.* **2007**, *117*, 175–184. [CrossRef]
20. Sica, A.; Mantovani, A. Macrophage plasticity and polarization: In vivo veritas. *J. Clin. Investig.* **2012**, *122*, 787–795. [CrossRef]
21. Roszer, T. Understanding the Mysterious M2 Macrophage through Activation Markers and Effector Mechanisms. *Mediat. Inflamm.* **2015**, *2015*, 816460. [CrossRef] [PubMed]
22. Hotamisligil, G.S.; Shargill, N.S.; Spiegelman, B.M. Adipose expression of tumor necrosis factor-alpha: Direct role in obesity-linked insulin resistance. *Science* **1993**, *259*, 87–91. [CrossRef] [PubMed]
23. Jager, J.; Gremeaux, T.; Cormont, M.; Le Marchand-Brustel, Y.; Tanti, J.F. Interleukin-1beta-induced insulin resistance in adipocytes through down-regulation of insulin receptor substrate-1 expression. *Endocrinology* **2007**, *148*, 241–251. [CrossRef] [PubMed]
24. Okla, M.; Zaher, W.; Alfayez, M.; Chung, S. Inhibitory Effects of Toll-Like Receptor 4, NLRP3 Inflammasome, and Interleukin-1beta on White Adipocyte Browning. *Inflammation* **2018**, *41*, 626–642. [CrossRef] [PubMed]
25. Goto, T.; Naknukool, S.; Yoshitake, R.; Hanafusa, Y.; Tokiwa, S.; Li, Y.; Sakamoto, T.; Nitta, T.; Kim, M.; Takahashi, N.; et al. Proinflammatory cytokine interleukin-1beta suppresses cold-induced thermogenesis in adipocytes. *Cytokine* **2016**, *77*, 107–114. [CrossRef] [PubMed]
26. Sakamoto, T.; Takahashi, N.; Sawaragi, Y.; Naknukool, S.; Yu, R.; Goto, T.; Kawada, T. Inflammation induced by RAW macrophages suppresses UCP1 mRNA induction via ERK activation in 10T1/2 adipocytes. *Am. J. Physiol. Cell Physiol.* **2013**, *304*, C729–C738. [CrossRef]
27. Lee, Y.H.; Kim, S.N.; Kwon, H.J.; Maddipati, K.R.; Granneman, J.G. Adipogenic role of alternatively activated macrophages in beta-adrenergic remodeling of white adipose tissue. *Am. J. Physiol. Regul. Integr. Comp. Physiol.* **2016**, *310*, R55–R65. [CrossRef]
28. Qiu, Y.; Nguyen, K.D.; Odegaard, J.I.; Cui, X.; Tian, X.; Locksley, R.M.; Palmiter, R.D.; Chawla, A. Eosinophils and type 2 cytokine signaling in macrophages orchestrate development of functional beige fat. *Cell* **2014**, *157*, 1292–1308. [CrossRef]

29. Bolus, W.R.; Hasty, A.H. Contributions of Innate Type 2 Inflammation to Adipose Function. *J. Lipid Res.* **2018**. [CrossRef]
30. Camell, C.D.; Sander, J.; Spadaro, O.; Lee, A.; Nguyen, K.Y.; Wing, A.; Goldberg, E.L.; Youm, Y.H.; Brown, C.W.; Elsworth, J.; et al. Inflammasome-driven catecholamine catabolism in macrophages blunts lipolysis during ageing. *Nature* **2017**, *550*, 119–123. [CrossRef]
31. Hardwick, J.P.; Eckman, K.; Lee, Y.K.; Abdelmegeed, M.A.; Esterle, A.; Chilian, W.M.; Chiang, J.Y.; Song, B.J. Eicosanoids in metabolic syndrome. *Adv. Pharmacol.* **2013**, *66*, 157–266. [CrossRef] [PubMed]
32. Masoodi, M.; Kuda, O.; Rossmeisl, M.; Flachs, P.; Kopecky, J. Lipid signaling in adipose tissue: Connecting inflammation & metabolism. *Biochim. Biophys. Acta* **2015**, *1851*, 503–518. [CrossRef] [PubMed]
33. Oh, D.Y.; Talukdar, S.; Bae, E.J.; Imamura, T.; Morinaga, H.; Fan, W.; Li, P.; Lu, W.J.; Watkins, S.M.; Olefsky, J.M. GPR120 is an omega-3 fatty acid receptor mediating potent anti-inflammatory and insulin-sensitizing effects. *Cell* **2010**, *142*, 687–698. [CrossRef] [PubMed]
34. Titos, E.; Claria, J. Omega-3-derived mediators counteract obesity-induced adipose tissue inflammation. *Prostaglandins Other Lipid Mediat.* **2013**, *107*, 77–84. [CrossRef] [PubMed]
35. Liddle, D.M.; Hutchinson, A.L.; Wellings, H.R.; Power, K.A.; Robinson, L.E.; Monk, J.M. Integrated Immunomodulatory Mechanisms through which Long-Chain *n*-3 Polyunsaturated Fatty Acids Attenuate Obese Adipose Tissue Dysfunction. *Nutrients* **2017**, *9*, 1289. [CrossRef] [PubMed]
36. Le Faouder, P.; Baillif, V.; Spreadbury, I.; Motta, J.P.; Rousset, P.; Chene, G.; Guigne, C.; Terce, F.; Vanner, S.; Vergnolle, N.; et al. LC-MS/MS method for rapid and concomitant quantification of pro-inflammatory and pro-resolving polyunsaturated fatty acid metabolites. *J. Chromatogr. B Analyt. Technol. Biomed. Life Sci.* **2013**, *932*, 123–133. [CrossRef] [PubMed]
37. Bustin, S.A.; Benes, V.; Garson, J.A.; Hellemans, J.; Huggett, J.; Kubista, M.; Mueller, R.; Nolan, T.; Pfaffl, M.W.; Shipley, G.L.; et al. The MIQE guidelines: Minimum information for publication of quantitative real-time PCR experiments. *Clin. Chem.* **2009**, *55*, 611–622. [CrossRef]
38. Tian, X.Y.; Ganeshan, K.; Hong, C.; Nguyen, K.D.; Qiu, Y.; Kim, J.; Tangirala, R.K.; Tontonoz, P.; Chawla, A. Thermoneutral Housing Accelerates Metabolic Inflammation to Potentiate Atherosclerosis but Not Insulin Resistance. *Cell Metab.* **2016**, *23*, 165–178. [CrossRef]
39. Poeckel, D.; Greiner, C.; Verhoff, M.; Rau, O.; Tausch, L.; Hornig, C.; Steinhilber, D.; Schubert-Zsilavecz, M.; Werz, O. Carnosic acid and carnosol potently inhibit human 5-lipoxygenase and suppress pro-inflammatory responses of stimulated human polymorphonuclear leukocytes. *Biochem. Pharmacol.* **2008**, *76*, 91–97. [CrossRef]
40. Donahue, S.M.; Rifas-Shiman, S.L.; Gold, D.R.; Jouni, Z.E.; Gillman, M.W.; Oken, E. Prenatal fatty acid status and child adiposity at age 3 y: Results from a US pregnancy cohort. *Am. J. Clin. Nutr.* **2011**, *93*, 780–788. [CrossRef]
41. Moon, R.J.; Harvey, N.C.; Robinson, S.M.; Ntani, G.; Davies, J.H.; Inskip, H.M.; Godfrey, K.M.; Dennison, E.M.; Calder, P.C.; Cooper, C.; et al. Maternal plasma polyunsaturated fatty acid status in late pregnancy is associated with offspring body composition in childhood. *J. Clin. Endocrinol. Metab.* **2013**, *98*, 299–307. [CrossRef]
42. Rudolph, M.C.; Young, B.E.; Lemas, D.J.; Palmer, C.E.; Hernandez, T.L.; Barbour, L.A.; Friedman, J.E.; Krebs, N.F.; MacLean, P.S. Early infant adipose deposition is positively associated with the *n*-6 to *n*-3 fatty acid ratio in human milk independent of maternal BMI. *Int. J. Obes. (Lond.)* **2017**, *41*, 510–517. [CrossRef] [PubMed]
43. Muley, A.; Muley, P.; Shah, M. ALA, fatty fish or marine *n*-3 fatty acids for preventing DM? A systematic review and meta-analysis. *Curr. Diabetes Rev.* **2014**, *10*, 158–165. [CrossRef] [PubMed]
44. D'Andrea, S.; Guillou, H.; Jan, S.; Catheline, D.; Thibault, J.N.; Bouriel, M.; Rioux, V.; Legrand, P. The same rat Delta6-desaturase not only acts on 18- but also on 24-carbon fatty acids in very-long-chain polyunsaturated fatty acid biosynthesis. *Biochem. J.* **2002**, *364*, 49–55. [CrossRef] [PubMed]
45. Monk, J.M.; Liddle, D.M.; Cohen, D.J.; Tsang, D.H.; Hillyer, L.M.; Abdelmagid, S.A.; Nakamura, M.T.; Power, K.A.; Ma, D.W.; Robinson, L.E. The delta 6 desaturase knock out mouse reveals that immunomodulatory effects of essential *n*-6 and *n*-3 polyunsaturated fatty acids are both independent of and dependent upon conversion. *J. Nutr. Biochem.* **2016**, *32*, 29–38. [CrossRef] [PubMed]

46. Muhlhausler, B.S.; Cook-Johnson, R.; James, M.; Miljkovic, D.; Duthoit, E.; Gibson, R. Opposing effects of omega-3 and omega-6 long chain polyunsaturated Fatty acids on the expression of lipogenic genes in omental and retroperitoneal adipose depots in the rat. *J. Nutr. Metab.* **2010**, *2010*. [CrossRef] [PubMed]
47. Pinel, A.; Pitois, E.; Rigaudiere, J.P.; Jouve, C.; De Saint-Vincent, S.; Laillet, B.; Montaurier, C.; Huertas, A.; Morio, B.; Capel, F. EPA prevents fat mass expansion and metabolic disturbances in mice fed with a Western diet. *J. Lipid Res.* **2016**, *57*, 1382–1397. [CrossRef] [PubMed]
48. Fjaere, E.; Aune, U.L.; Roen, K.; Keenan, A.H.; Ma, T.; Borkowski, K.; Kristensen, D.M.; Novotny, G.W.; Mandrup-Poulsen, T.; Hudson, B.D.; et al. Indomethacin Treatment Prevents High Fat Diet-induced Obesity and Insulin Resistance but Not Glucose Intolerance in C57BL/6J Mice. *J. Biol. Chem.* **2014**, *289*, 16032–16045. [CrossRef] [PubMed]
49. Zhao, M.; Chen, X. Eicosapentaenoic acid promotes thermogenic and fatty acid storage capacity in mouse subcutaneous adipocytes. *Biochem. Biophys. Res. Commun.* **2014**, *450*, 1446–1451. [CrossRef]
50. Shin, S.; Ajuwon, K.M. Lipopolysaccharide Alters Thermogenic and Inflammatory Genes in White Adipose Tissue in Mice Fed Diets with Distinct 18-Carbon Fatty-Acid Composition. *Lipids* **2018**, *53*, 885–896. [CrossRef]
51. Sundaram, S.; Bukowski, M.R.; Lie, W.R.; Picklo, M.J.; Yan, L. High-Fat Diets Containing Different Amounts of n3 and n6 Polyunsaturated Fatty Acids Modulate Inflammatory Cytokine Production in Mice. *Lipids* **2016**, *51*, 571–582. [CrossRef] [PubMed]
52. Todoric, J.; Loffler, M.; Huber, J.; Bilban, M.; Reimers, M.; Kadl, A.; Zeyda, M.; Waldhausl, W.; Stulnig, T.M. Adipose tissue inflammation induced by high-fat diet in obese diabetic mice is prevented by *n*-3 polyunsaturated fatty acids. *Diabetologia* **2006**, *49*, 2109–2119. [CrossRef] [PubMed]
53. Blok, W.L.; Deslypere, J.P.; Demacker, P.N.; van der Ven-Jongekrijg, J.; Hectors, M.P.; van der Meer, J.W.; Katan, M.B. Pro- and anti-inflammatory cytokines in healthy volunteers fed various doses of fish oil for 1 year. *Eur. J. Clin. Investig.* **1997**, *27*, 1003–1008. [CrossRef]
54. Cooper, A.L.; Gibbons, L.; Horan, M.A.; Little, R.A.; Rothwell, N.J. Effect of dietary fish oil supplementation on fever and cytokine production in human volunteers. *Clin. Nutr.* **1993**, *12*, 321–328. [CrossRef]
55. James, M.J.; Gibson, R.A.; Cleland, L.G. Dietary polyunsaturated fatty acids and inflammatory mediator production. *Am. J. Clin. Nutr.* **2000**, *71*, 343S–348S. [CrossRef] [PubMed]
56. Balvers, M.G.; Verhoeckx, K.C.; Meijerink, J.; Bijlsma, S.; Rubingh, C.M.; Wortelboer, H.M.; Witkamp, R.F. Time-dependent effect of in vivo inflammation on eicosanoid and endocannabinoid levels in plasma, liver, ileum and adipose tissue in C57BL/6 mice fed a fish-oil diet. *Int. Immunopharmacol.* **2012**, *13*, 204–214. [CrossRef]
57. Spencer, M.; Finlin, B.S.; Unal, R.; Zhu, B.; Morris, A.J.; Shipp, L.R.; Lee, J.; Walton, R.G.; Adu, A.; Erfani, R.; et al. Omega-3 fatty acids reduce adipose tissue macrophages in human subjects with insulin resistance. *Diabetes* **2013**, *62*, 1709–1717. [CrossRef]
58. Hames, K.C.; Morgan-Bathke, M.; Harteneck, D.A.; Zhou, L.; Port, J.D.; Lanza, I.R.; Jensen, M.D. Very-long-chain omega-3 fatty acid supplements and adipose tissue functions: A randomized controlled trial. *Am. J. Clin. Nutr.* **2017**, *105*, 1552–1558. [CrossRef]
59. Mendonca, A.M.; Cayer, L.G.J.; Pauls, S.D.; Winter, T.; Leng, S.; Taylor, C.G.; Zahradka, P.; Aukema, H.M. Distinct effects of dietary ALA, EPA and DHA on rat adipose oxylipins vary by depot location and sex. *Prostaglandins Leukot. Essent. Fatty Acids* **2018**, *129*, 13–24. [CrossRef]
60. Ferguson, J.F.; Roberts-Lee, K.; Borcea, C.; Smith, H.M.; Midgette, Y.; Shah, R. Omega-3 polyunsaturated fatty acids attenuate inflammatory activation and alter differentiation in human adipocytes. *J. Nutr. Biochem.* **2018**, *64*, 45–49. [CrossRef]
61. Titos, E.; Rius, B.; Gonzalez-Periz, A.; Lopez-Vicario, C.; Moran-Salvador, E.; Martinez-Clemente, M.; Arroyo, V.; Claria, J. Resolvin D1 and its precursor docosahexaenoic acid promote resolution of adipose tissue inflammation by eliciting macrophage polarization toward an M2-like phenotype. *J. Immunol.* **2011**, *187*, 5408–5418. [CrossRef] [PubMed]
62. Fredman, G.; Serhan, C.N. Specialized proresolving mediator targets for RvE1 and RvD1 in peripheral blood and mechanisms of resolution. *Biochem. J.* **2011**, *437*, 185–197. [CrossRef] [PubMed]
63. Fleming, I. The pharmacology of the cytochrome P450 epoxygenase/soluble epoxide hydrolase axis in the vasculature and cardiovascular disease. *Pharmacol. Rev.* **2014**, *66*, 1106–1140. [CrossRef] [PubMed]

64. Balvers, M.G.; Verhoeckx, K.C.; Bijlsma, S.; Rubingh, C.M.; Meijerink, J.; Wortelboer, H.M.; Witkamp, R.F. Fish oil and inflammatory status alter the *n*-3 to *n*-6 balance of the endocannabinoid and oxylipin metabolomes in mouse plasma and tissues. *Metabolomics* **2012**, *8*, 1130–1147. [CrossRef] [PubMed]
65. Hammond, V.J.; O'Donnell, V.B. Esterified eicosanoids: Generation, characterization and function. *Biochim. Biophys. Acta* **2012**, *1818*, 2403–2412. [CrossRef] [PubMed]
66. Quehenberger, O.; Dahlberg-Wright, S.; Jiang, J.; Armando, A.M.; Dennis, E.A. Quantitative determination of esterified eicosanoids and related oxygenated metabolites after base hydrolysis. *J. Lipid Res.* **2018**, *59*, 2436–2445. [CrossRef] [PubMed]
67. Vangaveti, V.N.; Jansen, H.; Kennedy, R.L.; Malabu, U.H. Hydroxyoctadecadienoic acids: Oxidised derivatives of linoleic acid and their role in inflammation associated with metabolic syndrome and cancer. *Eur. J. Pharmacol.* **2016**, *785*, 70–76. [CrossRef]
68. Nagy, L.; Tontonoz, P.; Alvarez, J.G.; Chen, H.; Evans, R.M. Oxidized LDL regulates macrophage gene expression through ligand activation of PPARgamma. *Cell* **1998**, *93*, 229–240. [CrossRef]
69. White, P.J.; Arita, M.; Taguchi, R.; Kang, J.X.; Marette, A. Transgenic restoration of long-chain *n*-3 fatty acids in insulin target tissues improves resolution capacity and alleviates obesity-linked inflammation and insulin resistance in high-fat-fed mice. *Diabetes* **2010**, *59*, 3066–3073. [CrossRef]
70. Yan, Y.; Jiang, W.; Spinetti, T.; Tardivel, A.; Castillo, R.; Bourquin, C.; Guarda, G.; Tian, Z.; Tschopp, J.; Zhou, R. Omega-3 fatty acids prevent inflammation and metabolic disorder through inhibition of NLRP3 inflammasome activation. *Immunity* **2013**, *38*, 1154–1163. [CrossRef]
71. Rey, C.; Delpech, J.C.; Madore, C.; Nadjar, A.; Greenhalgh, A.D.; Amadieu, C.; Aubert, A.; Pallet, V.; Vaysse, C.; Laye, S.; et al. Dietary *n*-3 long chain PUFA supplementation promotes a pro-resolving oxylipin profile in the brain. *Brain Behav. Immun.* **2019**, *76*, 17–27. [CrossRef] [PubMed]


*Am J Physiol Endocrinol Metab* 319: E912–E922, 2020.
First published September 21, 2020; doi:10.1152/ajpendo.00279.2020.

**RESEARCH ARTICLE** | *Browning and Beiging of Adipose Tissue: Its Role in the Regulation of Energy Homeostasis and as a Potential Target for Alleviating Metabolic Diseases*

# Modulation of the inflammatory response to LPS by the recruitment and activation of brown and brite adipocytes in mice

**Patrick Munro,[1] Océane Dufies,[1] Samah Rekima,[2] Agnès Loubat,[2] Christophe Duranton,[3] Laurent Boyer,[1*] and Didier F. Pisani[3*]**

[1]*Université Côte d'Azur, Inserm, C3M, Nice, France;* [2]*Université Côte d'Azur, CNRS, Inserm, IBV, Nice, France; and* [3]*Université Côte d'Azur, CNRS, LP2M, Nice, France*

Submitted 5 June 2020; accepted in final form 11 September 2020

**Munro P, Dufies O, Rekima S, Loubat A, Duranton C, Boyer L, Pisani DF.** Modulation of the inflammatory response to LPS by the recruitment and activation of brown and brite adipocytes in mice. *Am J Physiol Endocrinol Metab* 319: E912–E922, 2020. First published September 21, 2020; doi:10.1152/ajpendo.00279.2020.— Numerous studies have shown that the recruitment and activation of thermogenic adipocytes, which are brown and beige/brite, reduce the mass of adipose tissue and normalize abnormal glycemia and lipidemia. However, the impact of these adipocytes on the inflammatory state of adipose tissue is still not well understood, especially in response to endotoxemia, which is a major aspect of obesity and metabolic diseases. First, we analyzed the phenotype and metabolic function of white and brite primary adipocytes in response to lipopolysaccharide (LPS) treatment in vitro. Then, 8-wk-old male BALB/c mice were treated for 1 wk with a β3-adrenergic receptor agonist (CL316,243, 1 mg/kg/day) to induce recruitment and activation of brown and brite adipocytes and were subsequently injected with LPS (*Escherichia coli* lipopolysaccharide, 100 μg/mouse ip) to generate acute endotoxemia. The metabolic and inflammatory parameters of the mice were analyzed 6 h later. Our results showed that in response to LPS, thermogenic activity promoted a local anti-inflammatory environment with high secretion of IL-1 receptor antagonist (IL-1RA) without affecting other anti- or proinflammatory cytokines. Interestingly, activation of brite adipocytes reduced the LPS-induced secretion of leptin. However, thermogenic activity and adipocyte function were not altered by LPS treatment in vitro or by acute endotoxemia in vivo. In conclusion, these results suggest an IL-1RA-mediated immunomodulatory activity of thermogenic adipocytes specifically in response to endotoxemia. This encourages potential therapy involving brown and brite adipocytes for the treatment of obesity and associated metabolic diseases.

**NEW & NOTEWORTHY** Recruitment and activation of brown and brite adipocytes in the adipose tissue of mice lead to a local low-grade anti-inflammatory phenotype in response to acute endotoxemia without alteration of adipocyte phenotype and function.

brown adipose tissue; catecholamines; cytokines; inflammation; white adipose tissue

## INTRODUCTION

White adipocytes are specialized for the storage and release of energy (carbohydrates and lipids), whereas brown adipocytes dissipate this energy in the form of heat (thermogenesis) through the activity of uncoupling protein-1 (UCP1) (10). Brown adipocytes constitute brown adipose tissue (BAT) but can also be found within white adipose tissue (WAT). They are then called beige or brite adipocytes ("brown in white") and have a high thermogenesis capacity in response to conditions such as prolonged cold exposure (11).

Overweight (body mass index, BMI $\geq$ 25 kg/m$^2$) and obesity (BMI $\geq$ 30 kg/m$^2$) are the consequences of a positive energy balance (energetic substrate storage > expenditure) that leads to an increase in the mass of subcutaneous and visceral white adipose tissue. Obesity is a major risk factor for type 2 diabetes development, as 90% of patients suffering from type 2 diabetes are overweight or obese (16). It has also been shown that metabolic organs of obese subjects, especially WAT, are characterized by low-grade inflammation that can lead to metabolic disorders such as insulin resistance (20). Inflammation is characterized in WAT by an increase in inflammatory cytokines such as tumor necrosis factor alpha (TNF-α), plasminogen activator inhibitor-1 (PAI-1), or interleukin-1β and interleukin-6 (IL-1β and IL-6). This promotes immune cell infiltration of adipose tissue, particularly infiltration of inflammatory macrophages (29, 30). Immune cell accumulation and secretion of inflammatory cytokines affect adipose tissue homeostasis and, more specifically, the recruitment and function of adipocytes in WAT and BAT (32). Previous studies have shown that TNF-α inhibits adipocyte differentiation (21) and that IL-1β blocks insulin signaling, thus favoring insulin resistance (22). Recently, it has also been shown that IL-1β and TNF-α affect the thermogenic function of brown adipocytes (18, 34, 39). Altogether, these studies showed that inflammatory cytokines participate in the development of an inflammatory environment, leading to the deregulation of adipose tissue homeostasis. However, the origin of low-grade metabolic inflammation is still under debate. Growing evidence indicates that the gut microbiota are a major player in metabolic inflammation. The gut of obese patients is characterized by an alteration in the microbiota (dysbiosis) and a disruption of the intestinal barrier, increasing its permeability to microbiota

* L. Boyer and D. F. Pisani contributed equally to this work.
Correspondence: D. Pisani (didier.pisani@univ-cotedazur.fr).

metabolites and degradation products. Consequently, systemic endotoxin levels increase (endotoxemia), including the levels of lipopolysaccharides (LPS) (46). It has been demonstrated using germ-free rodent models that this endotoxemia is directly linked to adipose tissue inflammation (6, 7, 49). In this pathophysiological condition, LPS directly activates Toll-like receptor 4 (TLR-4), which is displayed by tissue macrophages and adipocytes (42). In response, white and brown/beige adipocytes exhibit an altered function (33, 34) and secrete inflammatory cytokines (TNF-α and IL-1β), which alter tissue homeostasis. Recently, it has been shown that brown and white adipocytes respond differently to in vitro LPS stimulation and mediate different inflammatory responses (13).

One of the strategies for treating type 2 diabetes associated with obesity is to increase energy expenditure by stimulating the recruitment and activity of brown and/or beige adipocytes (27). Although little is known about the impact of this strategy on the balance and functionality of the immune system, it is a key element in the pathology of metabolic syndrome, especially in low-grade inflammation and inherent insulin resistance. In this work, we investigated the response of white and brown/brite adipocytes to LPS treatment with regard to their impact on the inflammatory environment induced by LPS. Using ex vivo and in vivo approaches in mice, we demonstrated that recruitment/activation of brown/brite adipocytes by β-adrenergic receptor agonists was not affected by LPS treatment and led to a reduced inflammatory response to LPS, especially by the overexpression of an IL-1 receptor antagonist (IL-1RA), coded by *Il-1rn* gene, that is known to inhibit the action of IL-1β.

## MATERIALS AND METHODS

*Reagents.* Culture media and buffer solutions were purchased from Lonza (Ozyme, St-Quentin en Yvelines, France), fetal bovine serum (FBS) was purchased from Eurobio (Courtaboeuf, France), and insulin was purchased from Invitrogen (Cergy Pontoise, France). LPS (LPS-EK Ultrapure isolated from *Escherichia coli* K12 strain) was obtained from InvivoGen (Toulouse, France). Other reagents were obtained from Sigma-Aldrich (Saint-Quentin Fallavier, France).

*Animals.* The experiments were conducted in accordance with the French and European regulations (2010/63/EU directive) for the care and use of research animals and were approved by national experimentation committees (MESR No.: APAFIS#18322–2018121809427035 v2). Eight-week-old male BALB/c mice from Janvier Laboratory (France) were maintained at housing temperature (22°C) on a 12:12-h light/dark cycle, with ad libitum access to food and water.

The mice were treated daily with the β3-adrenergic receptor agonist CL316,243 (1 mg/kg in saline solution, ip, $n = 12$) (Sigma-Aldrich) or with vehicle only (saline solution, $n = 12$). To induce endotoxemia, six mice from each group were injected at *day 7* with LPS (100 μg/mouse in PBS, ip) or vehicle only and were euthanized 6 h later alternating one mouse from each group. At the end of the experiment, blood, interscapular brown adipose tissue (iBAT), epididymal white adipose tissue (eWAT), and inguinal subcutaneous white adipose tissue (scWAT) were sampled and used for different analyses. No mice were excluded.

*Cytokine and metabolic parameter quantification.* For blood analysis, freshly prepared plasma was diluted twice before analysis. For tissue analysis, freshly sampled WAT and BAT were washed in PBS, weighed, and incubated in free Dulbecco's modified Eagle's medium for 2 h at 37°C. The media were preserved for the analysis of various secreted proteins.

Leptin was assayed using a mouse leptin kit (Meso Scale Discovery, Cat No. K152BYC), and cytokines were measured using a mouse V-PLEX proinflammatory panel 1 kit (# K15048D) according to the manufacturer's instructions using a QuickPlex SQ 120 apparatus (Meso Scale Discovery, Rockville, MD). IL-1RA levels were assayed using a mouse IL-1RA ELISA kit (Cat. No. EMIL1RN) from Thermo Fisher Scientific (Courtaboeuf, France). Glycerol and triglyceride determinations were performed using a dedicated kit (free glycerol reagent and triglyceride reagent, Sigma-Aldrich).

*Histology.* Freshly sampled tissues were fixed in 4% paraformaldehyde overnight at room temperature (RT) and then paraffin embedded. Embedded tissues were cut into 5-μm sections and dried overnight at 37°C.

For histological analysis, the sections were stained with hematoxylin-eosin and mounted in VectaMount (Vector Laboratories).

For immunohistochemical analysis, antigen retrieval was performed using a low-pH buffer in a decloaking chamber (Dako, Cat. No. S2367). The sections were then permeabilized in PBS with 0.2% Triton X-100 at room temperature for 10 min and blocked in the same buffer containing 3% BSA for 1 h. The sections were incubated with rat anti-F4/80 antibody (Bio-Rad, clone Cl:A3–1, dilution 1:100) overnight at 4°C. Following a 1 h incubation with A568-coupled antirabbit secondary antibodies, nuclear staining was performed with DAPI, and the sections were mounted in PermaFluor mounting medium (Thermo Fisher).

Visualization was performed with an Axiovert microscope. Images were captured using AxioVision software (Carl Zeiss, Jena, Germany).

*Stromal vascular fraction cell isolation and culture.* Subcutaneous WAT (scWAT, inguinal) and interscapular BAT (iBAT) deposits were sampled from 8-wk-old BALB/c male mice, washed in PBS, and minced. Adipose tissue samples were digested for 45 min at 37°C in DMEM containing 2 mg/mL collagenase A (Roche Diagnostics, Meylan, France) and 20 mg/mL bovine serum albumin (Sigma-Aldrich Chimie, Saint-Quentin Fallavier, France). The samples were successively filtered through 250-, 100-, and 27-μm nylon sheets and centrifuged for 5 min at 500 *g*. The pellet containing stromal vascular fraction (SVF) cells was subjected to red blood cell lysis.

SVF cells were plated and maintained in DMEM containing 10% fetal calf serum until confluence. Differentiation was induced in the same medium supplemented with 1 μM dexamethasone, 0.5 mM isobutylmethylxanthine, and 860 nM insulin for 2 days. Then, the cells were maintained for 7 days in the presence of 860 nM insulin for white adipogenesis and 860 nM insulin, 1 μM rosiglitazone, and 2 nM triiodothyronine for brite and brown adipogenesis, as previously published (36). Media were changed every other day. On the final day, the differentiated preadipocytes were stimulated with or without 1 μM isoproterenol for 6 h.

*Isolation and analysis of RNA.* Procedures were performed according to MIQE (Minimum Information for Publication of Quantitative Real-Time PCR Experiment) recommendations (5). Total RNA was extracted using a TRI-Reagent kit (Euromedex, Souffelweyersheim, France), according to the manufacturer's instructions. For RNA isolation from organs, tissues were homogenized in TRI-Reagent using a dispersing instrument (ULTRA TURRAX T25). Reverse transcription-polymerase chain reaction (RT-PCR) was performed using M-MLV-RT (Promega). SYBR qPCR premix Ex Taq II from Takara (Ozyme, France) was used for quantitative PCR (qPCR), and assays were run on a StepOne Plus ABI real-time PCR instrument (PerkinElmer Life and Analytical Sciences, Boston). The expression of selected genes was normalized to that of the TATA-box binding protein (TBP) and 36B4 housekeeping genes and then quantified using the comparative-ΔCt method. Primer sequences are available upon request.

*Oxygen consumption analysis.* The oxygen consumption rate (OCR) and the extracellular acidification rate (ECAR) of 10-day-old differentiated SVF cells were determined using an XF24 Extracellular Flux Analyzer (Seahorse Bioscience, Agilent Technologies France, Courtaboeuf, France). Isoproterenol (1 μM) and/or LPS (100 ng/mL) were used to characterize inducible respiration. Uncoupled OCR and maximal OCR were determined using oligomycin (1.2 μM) and carbonyl-cyanide-4-(trifluoromethoxy)phenylhydrazone (FCCP, 1 μM). Rotenone and antimycin-A (2 μM each) were used to inhibit

mitochondrial respiration. All parameters were calculated as described previously (4).

*Statistical analysis.* Animal cohort size was determined using G*Power (14), and animals were allocated to experimental groups by randomization. The data were analyzed using GraphPad Prism 6 software and evaluated by ordinary one-way ANOVA followed by Tukey's multiple-comparison posttest to assess significant differences between experimental groups. Differences were considered statistically significant with $P < 0.05$. The data are displayed as scatter plots of independent values and group means ± SD.

## RESULTS

*In vitro phenotypic and functional metabolic response of white, brown, and brite differentiated preadipocytes to LPS treatment.* White and brite adipocytes were obtained after differentiation of preadipocytes that were isolated from the stromal vascular fraction of mouse subcutaneous white adipose tissue, and brown adipocytes were obtained from the stromal vascular fraction of mouse brown adipose tissue, as previously published (36). On the last day of differentiation, the differentiated preadipocytes were treated for 6 h with 1 μM isoproterenol (a nonspecific β-adrenergic receptor agonist that activates lipolysis and/or UCP1 activity) and/or 100 ng/mL LPS and were then used for mRNA expression (Fig. 1) or treated acutely with the same compounds for functional metabolism modification analysis (Fig. 2).

LPS treatment did not alter perilipin 1, adiponectin, and Glut4 mRNA expressions in all kinds of adipocytes. Leptin mRNA was scarcely detected in all adipocytes, limiting our interpretation about the strong inhibition found in white adipocytes under LPS and isoproterenol treatments (Fig. 1). White adipocytes barely expressed Ucp1 and perilipin 5 mRNA, and LPS and isoproterenol did not alter these expression levels. In brite adipocytes, perilipin 5 was slightly inhibited by LPS treatment independent of isoproterenol. Interestingly, LPS alone did not alter Ucp1 expression in brite adipocytes but blunted the increase in Ucp1 mRNA expression due to acute isoproterenol treatment (Fig. 1). In brown adipocytes, perilipin 5 and Ucp1 mRNA levels were increased by isoproterenol but were unaffected by LPS. Interestingly, in all kinds of adipocytes, Ppar-γ (peroxisome proliferator-activated receptor γ) mRNA levels were inhibited by LPS and by isoproterenol treatment (Fig. 1).

Analysis of Tnf-α and Il-6 mRNA levels showed that they were overexpressed after acute LPS treatment. Interestingly, isoproterenol completely inhibited Tnf-α overexpression in the three kinds of adipocytes. A more complex situation was found for Il-6 mRNA, which was positively affected by the combination of isoproterenol and LPS treatment in white adipocytes but inhibited by the same cotreatment in brite and brown adipocytes (Fig. 1). Analysis of Il-1β mRNA expression showed an increase after LPS treatment of adipocytes. Isoproterenol did not alter this expression, except when white adipocytes were treated with both isoproterenol and LPS. As Il-1β mRNA encodes the proform of the protein before its maturation and secretion, these results need to be analyzed with caution. mRNA expression of Il-1rn, which codes for the IL-1RA protein that counteracts the effect of IL-1β, was increased after LPS treatment, similar to that of Il-1β mRNA. Interestingly, brite adipocytes expressed more Il-1rn than white and brown adipocytes. This expression in brite adipocytes was increased by LPS treatment and, more importantly, by isoproterenol with or without LPS (Fig. 1).

At the metabolic level, isoproterenol treatment induced glycerol release (a reflection of lipolysis) in the three types of adipocytes, but cotreatment with LPS had no effect (Fig. 2*A*). Interestingly, LPS slightly but significantly increased glycerol release in white, brite, and brown adipocytes. The extracellular acidification rate (ECAR) (Fig. 2*B*) and oxygen consumption rate (OCR) (Fig. 2*C*) were analyzed concomitantly and were increased by acute isoproterenol treatment in brite and brown adipocytes, whereas only the OCR was increased in white adipocytes. Uncoupling mitochondrial oxygen consumption (the OCR due to proton leakage) was increased in brite and brown adipocytes after isoproterenol stimulation, which is a reflection of Ucp1 activity (Fig. 2*C*). Neither ECAR nor OCR was affected by LPS treatment (Fig. 2, *B* and *C*).

Taken together, these in vitro adipocyte experiments suggest that activation of adipocyte β-adrenergic receptors decreased the inflammatory phenotype and that LPS treatment did not clearly affect the thermogenic phenotype.

*In vivo effects of acute LPS treatment on browning and BAT activation induced by the β3-adrenergic receptor agonist (CL316,243).* Eight-week-old male BALB/c mice were treated daily with a β3-adrenergic receptor agonist (CL316,243, 1 mg/kg) that activates brown and brite adipocyte thermogenesis and adipocyte lipolysis and were finally treated with 100 μg of LPS for 6 h. Body weight was unaffected by treatment with CL316,243 or LPS (Fig. 3*A*). Different weights of epididymal WAT showed that fat mass was decreased after CL316,243 treatment but was unaffected by LPS treatment (Fig. 3*A*). Although the plasma glycerol level did not change, we found a decrease in plasma triglyceride levels, probably due to the high use of this substrate by activated brown and brite adipocytes (Fig. 3*B*). Interestingly, LPS treatment also decreased triglyceride levels, but no additive effect was found in the cotreated mouse group (Fig. 3*B*). Leptin plasma levels increased in LPS-treated mice, and the effect was blunted when the mice were pretreated with CL316,243 (Fig. 3*C*). Similar results were found for secreted leptin using scWAT explants sampled from these mice (Fig. 3*C*). Thus, in our experiment, leptin levels did not follow the fat mass of the animals and corresponded to an adipose tissue inflammatory response to LPS.

To assess the effects of acute LPS treatment on brown and brite adipocyte recruitment and activation, we performed histological and molecular analyses of WAT and BAT from mice in each group. As shown in Fig. 3*D*, CL316,243 decreased the quantity of lipid droplets in brown adipose tissue and slightly increased Ucp1 and Cpt1m (carnitine O-palmitoyltransferase 1M) mRNA expression, which is characteristic of activated BAT, without affecting perilipin 1 and 5 expressions as well as adiponectin, Glut4 (glucose transporter 4), and Ppar-γ mRNA expressions (Supplemental Fig. S1*A*; all Supplemental material is available at https://doi.org/10.6084/m9.figshare.12739874). scWAT histological sections from CL316,243-treated groups displayed massive recruitment of multiloculated adipocytes (Fig. 3*D*), which is a characteristic morphology of brite adipocytes. This was confirmed by the overexpression of Ucp1 and perilipin 5 mRNA (Supplemental Fig. S1*B*).

Perilipin 1, adiponectin, and leptin mRNA expression in scWAT did not change with LPS and/or CL316,243 treatment. This discrepancy between leptin secretory levels and mRNA

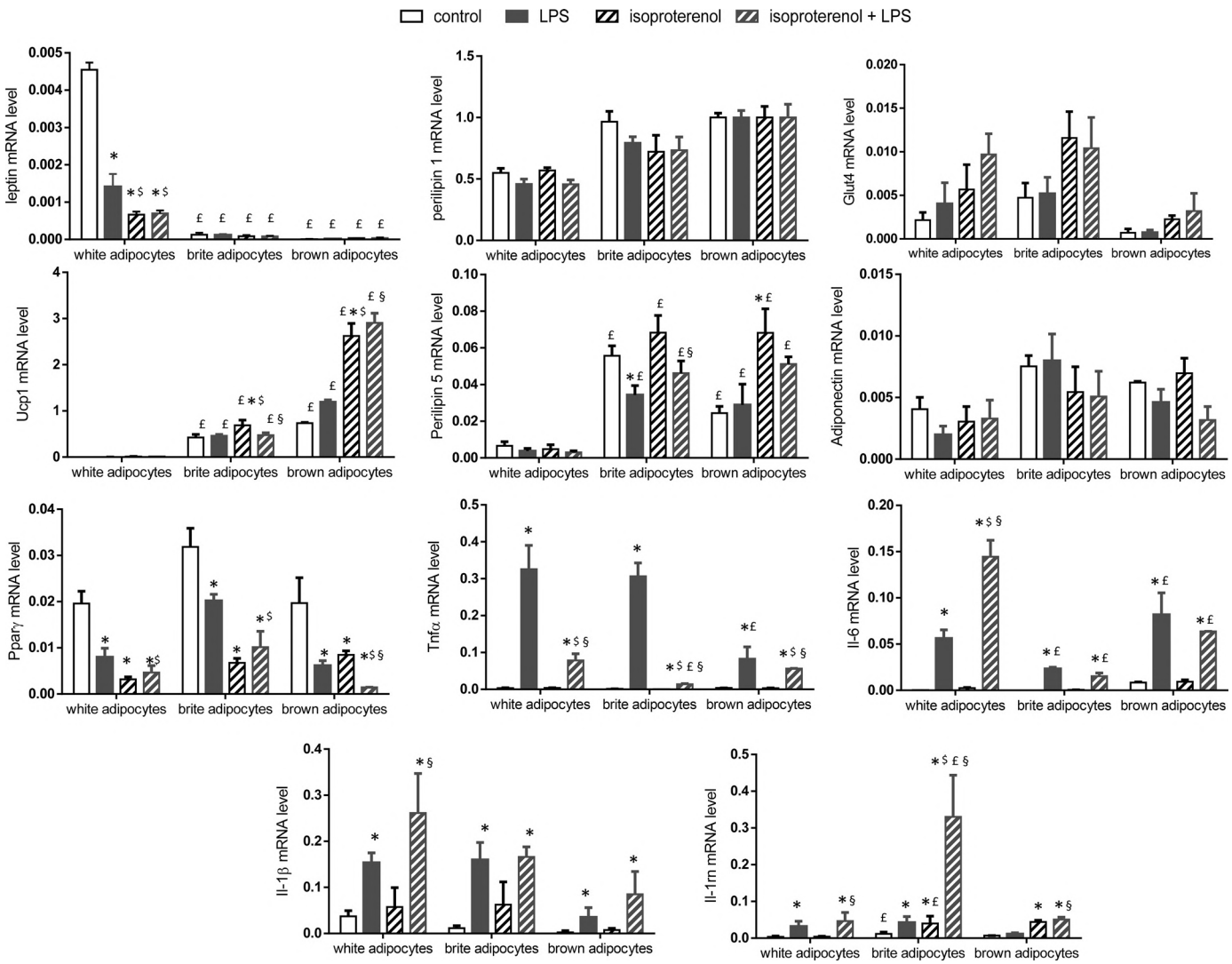


Fig. 1. Effect of LPS on white, brite, and brown differentiated preadipocytes in vitro. White and brite adipocytes were obtained after differentiation of stromal vascular fraction cells isolated from mouse scWAT, and brown adipocytes were obtained from the stromal vascular fraction of iBAT. mRNA expression analysis by quantitative PCR of white (leptin, perilipin 1, Ppar-γ, Glut4, and adiponectin), brite/brown (Ucp1 and perilipin 5), and inflammatory markers (Tnf-α, Il-6, Il-1β, and Il-1rn) after 6 h of treatment with isoproterenol (1 μM) and/or LPS (100 ng/mL). The results are displayed as means ± SE. $n = 6$ (2 replicates of 3 independent cultures). *$P < 0.05$ vs. control; $$P < 0.05$ vs. LPS; §$P < 0.05$ vs. isoproterenol; £$P < 0.05$ vs. white adipocytes. iBAT, interscapular brown adipose tissue; scWAT, subcutaneous white adipose tissue.

expression supports an acute response independent of fat mass change (Supplemental Fig. S1*B*). Different to Glut4 mRNA, which was increased after isoproterenol treatment and less affected by LPS treatment, Ppar-γ mRNA levels were strongly inhibited by LPS independent of isoproterenol exposition (Supplemental Fig. S1*B*). Interestingly, we did not detect cell infiltration or crown structure after LPS treatment by histological analysis (Fig. 3*D*), which was confirmed by negative staining for the macrophagic marker F4/80 (data not shown). Certainly, the time was too short between LPS treatment and analysis to allow infiltration of adipose tissue by immune cells.

*Acute LPS treatment induces an inflammatory response and secretion of anti-inflammatory cytokines.* Inflammation is mainly triggered by inflammatory cytokine secretion, followed by a resolution step that is characterized by the secretion of anti-inflammatory cytokines. This effect was observed in mice that were treated with LPS. Terminal LPS treatment induced an increase in the plasma level of IL-1β, as well as IL-1β secretion in BAT and scWAT explants, and CL316,243 did not alter this effect (Fig. 4*A*). IL-1RA plasma levels equivalently increased after administration of LPS to untreated and CL316,243-treated mice (Fig. 4*B*). In contrast, in scWAT and BAT, while LPS treatment increased IL-1RA secretion, CL316,243 also increased IL-1RA secretion, and this effect was additive in the presence of LPS (Fig. 4*B*).

In addition to IL-1β/IL-1RA, other cytokine levels were affected. TNF-α and IL-12 plasma levels were increased after LPS treatment independent of CL316,243 treatment, and the same trend was found for IL-6 (Supplemental Fig. S2). KC/GRO (CXCL-1) was detected in the plasma of mice but was not affected by the different treatments. Interestingly, LPS-induced IFN-γ and IL-2 plasma level increases were abrogated when the mice were treated with CL316,243 (Supplemental Fig. S2).

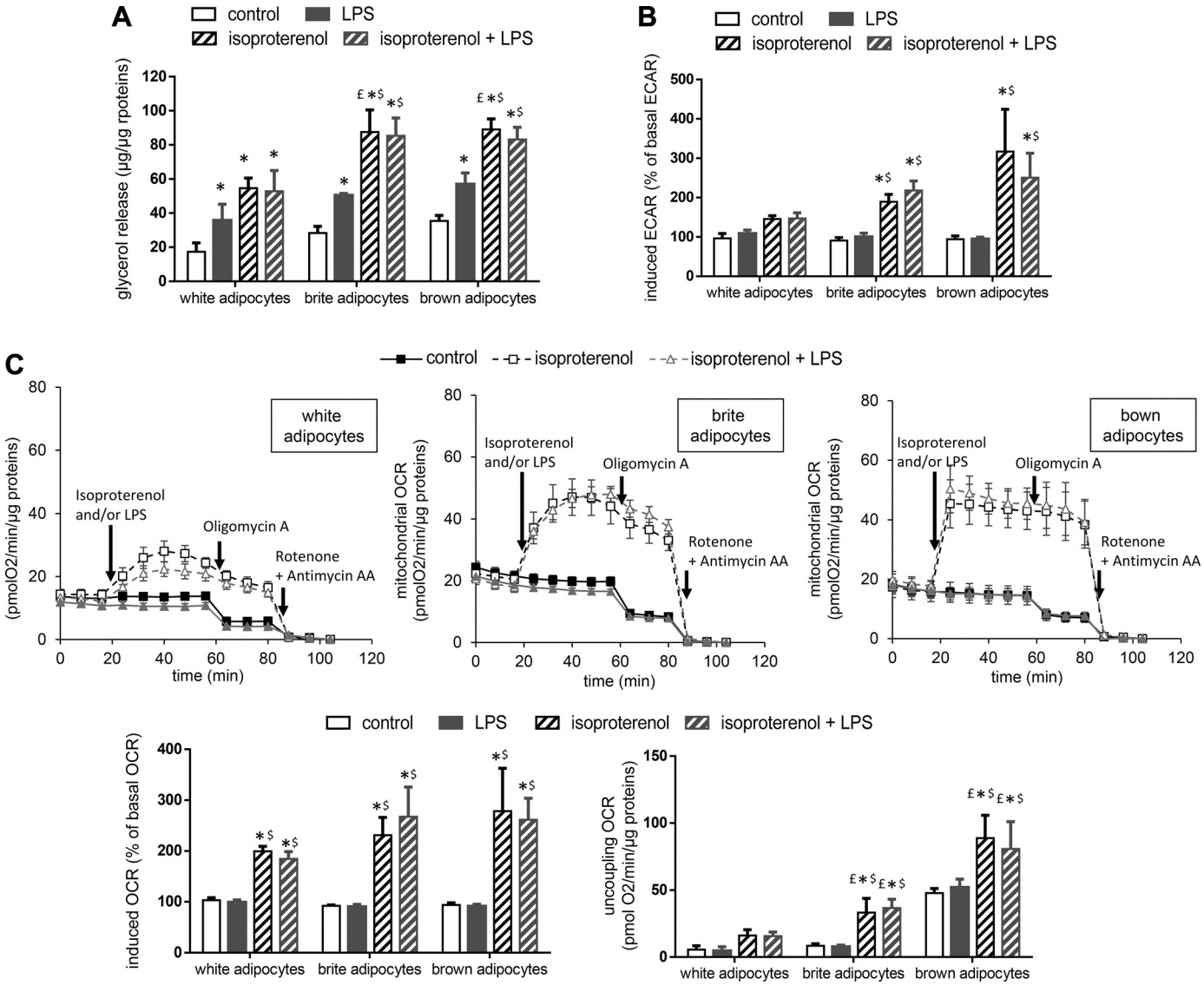


Fig. 2. Effect of LPS on white, brite, and brown differentiated preadipocytes in vitro. White and brite adipocytes were obtained after differentiation of stromal vascular fraction cells isolated from mouse scWAT, and brown adipocytes were obtained from the stromal vascular fraction of iBAT. *A*: glycerol levels were assayed in the supernatants of white and brite adipocytes that were treated for 2 h with LPS and/or isoproterenol. *B* and *C*: adipocytes were analyzed for oxygen consumption and extracellular acidification following sequential injection of isoproterenol and/or LPS, oligomycin A (1.2 µM), and rotenone/antimycin A (2 + 2 µM). *B*: ECAR in response to LPS and/or isoproterenol is displayed as % of basal ECAR. *C*: plots show mitochondrial OCR and the indicated injections. Histograms display mitochondrial OCR in response to LPS and/or isoproterenol (induced/basal mitochondrial OCR) and uncoupling mitochondrial respiration. The results are displayed as means ± SE. $n = 6$ (2 replicates of 3 independent cultures). *$P < 0.05$ vs. control; \$$P < 0.05$ vs. LPS; §$P < 0.05$ vs. isoproterenol; £$P < 0.05$ vs. white adipocytes. ECAR, extracellular acidification rate; LPS, lipopolysaccharide; iBAT, interscapular brown adipose tissue; OCR, oxygen consumption rate; scWAT, subcutaneous white adipose tissue.

A different profile of secreted cytokines was found in the adipose tissue explant media. IFN-γ was undetected, and IL-2 and IL-12 were barely detected (Fig. 5), with a slight increase only in the iBAT of LPS-treated mice (Fig. 5*A*). Secreted IL-6 increased in the iBAT of LPS-treated mice independent of CL316,243 treatment and only in LPS plus CL316,243 in scWAT (Fig. 5). In contrast, KC/GRO and TNF-α increased in all groups of LPS-treated mice independent of CL316,243 treatment and had the same trend (Fig. 5).

Although the anti-inflammatory cytokine IL-4 was barely detected in plasma and undetected in explants of adipose tissues, the plasma level of IL-10 was increased in response to LPS (Supplemental Fig. S3). None of these was altered by CL316,243. In contrast, local secretion of IL-10 by adipose tissue was not stimulated by LPS alone, but an increasing trend was observed after CL316,243 treatment, especially in BAT that was cotreated with LPS (Supplemental Fig. S3).

## DISCUSSION

Metabolic endotoxemia, found for example in obese patients and sepsis, appears after gut epithelium disturbance, which allows LPS from Gram-negative gut bacteria to enter the systemic circulation (8, 24). This leads to systemic and local

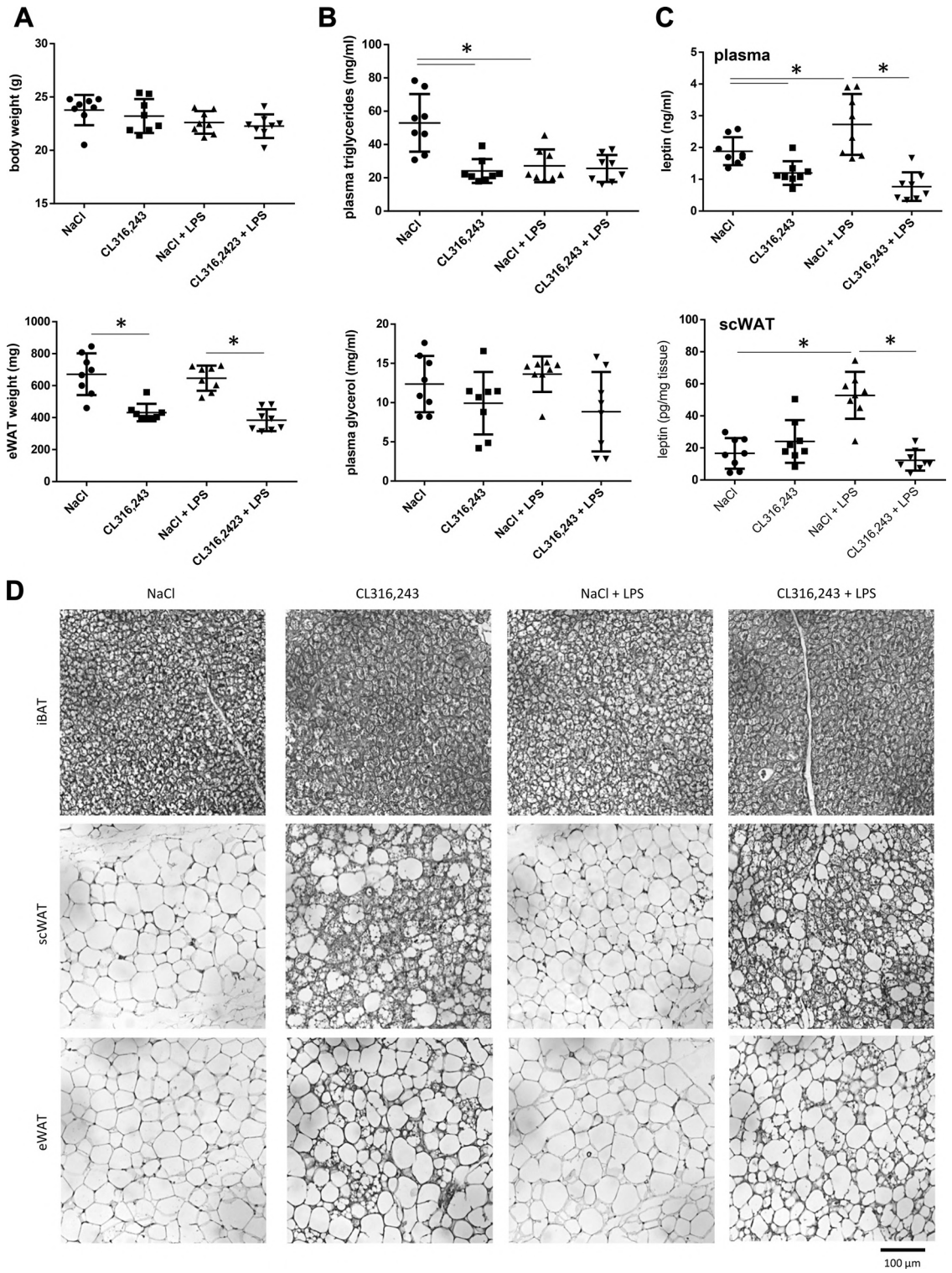


Fig. 3. Effect of CL316,243 and LPS on general mouse metabolic parameters. Mice were analyzed after 1 wk of treatment with CL316,243 daily (1 mg/kg/day) or vehicle only (NaCl) and with or without LPS treatment (1 mg/kg) during the final 6 h. Mouse body weights and epididymal white adipose tissue (eWAT) weights (*A*), triglycerides and glycerol plasma levels (*B*), and secreted leptin levels in plasma and subcutaneous white adipose tissue (scWAT) (*C*). *D*: hematoxylin-eosin staining of interscapular brown adipose tissue (iBAT), scWAT, and eWAT sections. The results are displayed as independent values (dots) and means ± SE. $n = 6$ (mice and plasma) or 8 (explant). *$P < 0.05$. LPS, lipopolysaccharide .

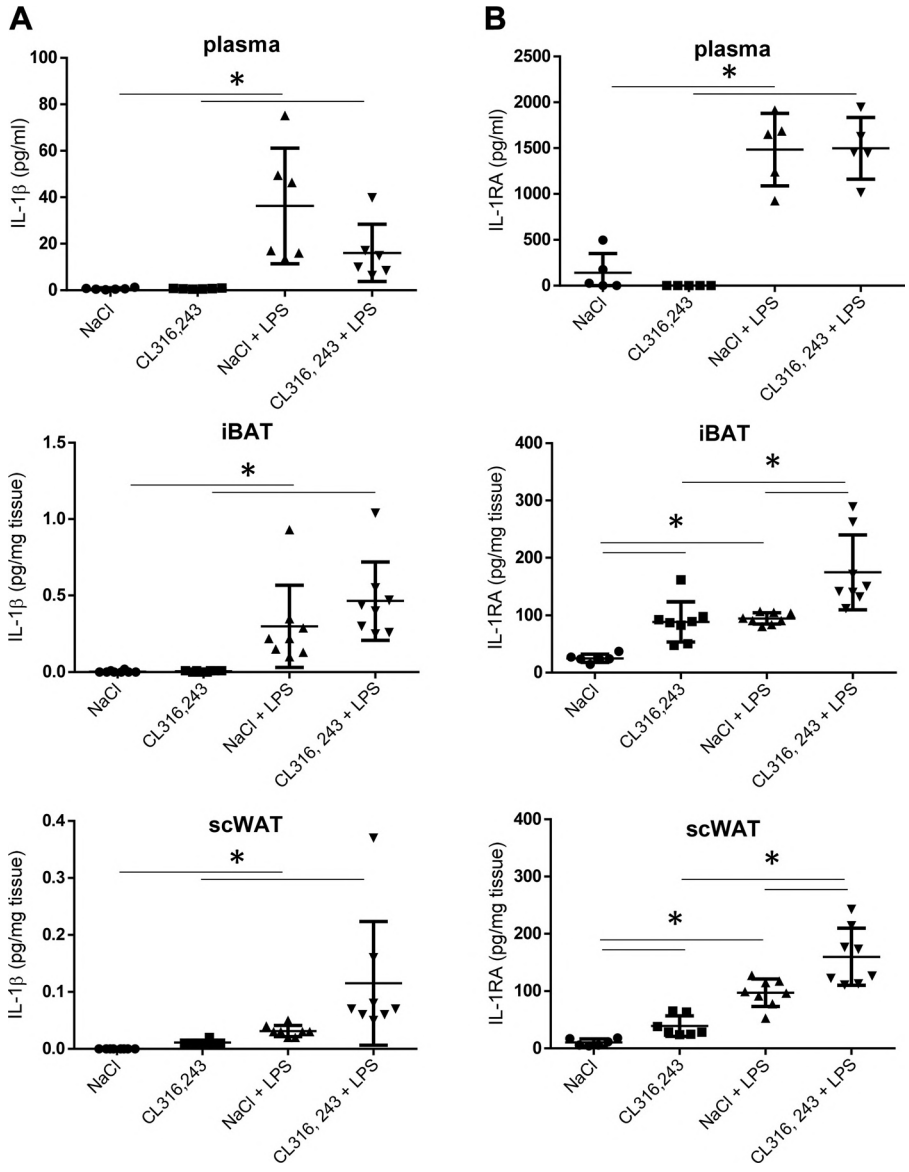


Fig. 4. Effect of CL316,243 and LPS on IL-1β/IL-1RA. IL-1β (*A*) and IL-1RA (*B*) protein levels were assessed in plasma (*top*) and in the media of iBAT (*middle*) and scWAT (*bottom*) explants from mice that were treated for 1 wk with CL316,243 daily (1 mg/kg/day) or vehicle only (NaCl) and with or without LPS treatment (1 mg/kg) for the final 6 h. The results are displayed as independent values (dots) and means ± SE. $n = 6$ (plasma) or 8 (explant). *$P < 0.05$. iBAT, interscapular brown adipose tissue; scWAT, subcutaneous white adipose tissue.

inflammation, which is, among others, a central feature of metabolic syndrome development (6). Several studies have shown the action of LPS on white and brown adipocyte differentiation and function. LPS modulates adipocyte functions directly via TLR-4 activation or indirectly, especially through macrophage activation, which in turn secrete cytokines that modulate adipocyte functions. In WAT, LPS directly induces lipolysis (51) and cytokine secretion by adipocytes and indirectly (mainly by macrophage-derived cytokines) inhibits differentiation and promotes insulin resistance (41, 50). In BAT, LPS has been suspected to be an activator of brown adipocyte thermogenesis (9), but recent studies demonstrated that acute (in vitro) and chronic (in vivo) exposure to LPS inhibits UCP1 expression and function in these adipocytes (1, 33). However, little is known about the influence of white and brite or brown adipocytes on local and systemic inflammation due to LPS exposure, especially the secretion of inflammatory mediators such as cytokines and adipokines. Herein, we analyzed the impact of brown and brite adipocyte recruitment and activation on systemic and local (adipose tissue) responses to acute LPS treatment, which mimics endotoxemia.

Leptin is a well-known modulator of pyrexia in response to LPS (15, 37, 38). As expected, we found an increase in plasma leptin level that correlated with the scWAT leptin level, a chief origin of this adipokine with others in adipose tissues (25), in mice that were stimulated with acute LPS treatment. This positive effect was not found at the mRNA level in the scWAT of these mice or in primary white adipocytes that were exposed to LPS. These results suggested that the modulation in leptin levels was not due to change in adipose tissue mass but that LPS stimulated adipocyte leptin secretion without affecting its mRNA expression. Interestingly, these increased leptin levels were completely abolished when the mice were pretreated with CL316,243, which induces brown/brite adipocyte recruitment and activation and thus thermogenesis. As leptin induces fever independent of thermogenesis (15), we suspect negative feedback that prevents hyperthermia due to the addition of thermogenesis and pyrexia. Unfortunately, leptin levels cannot be

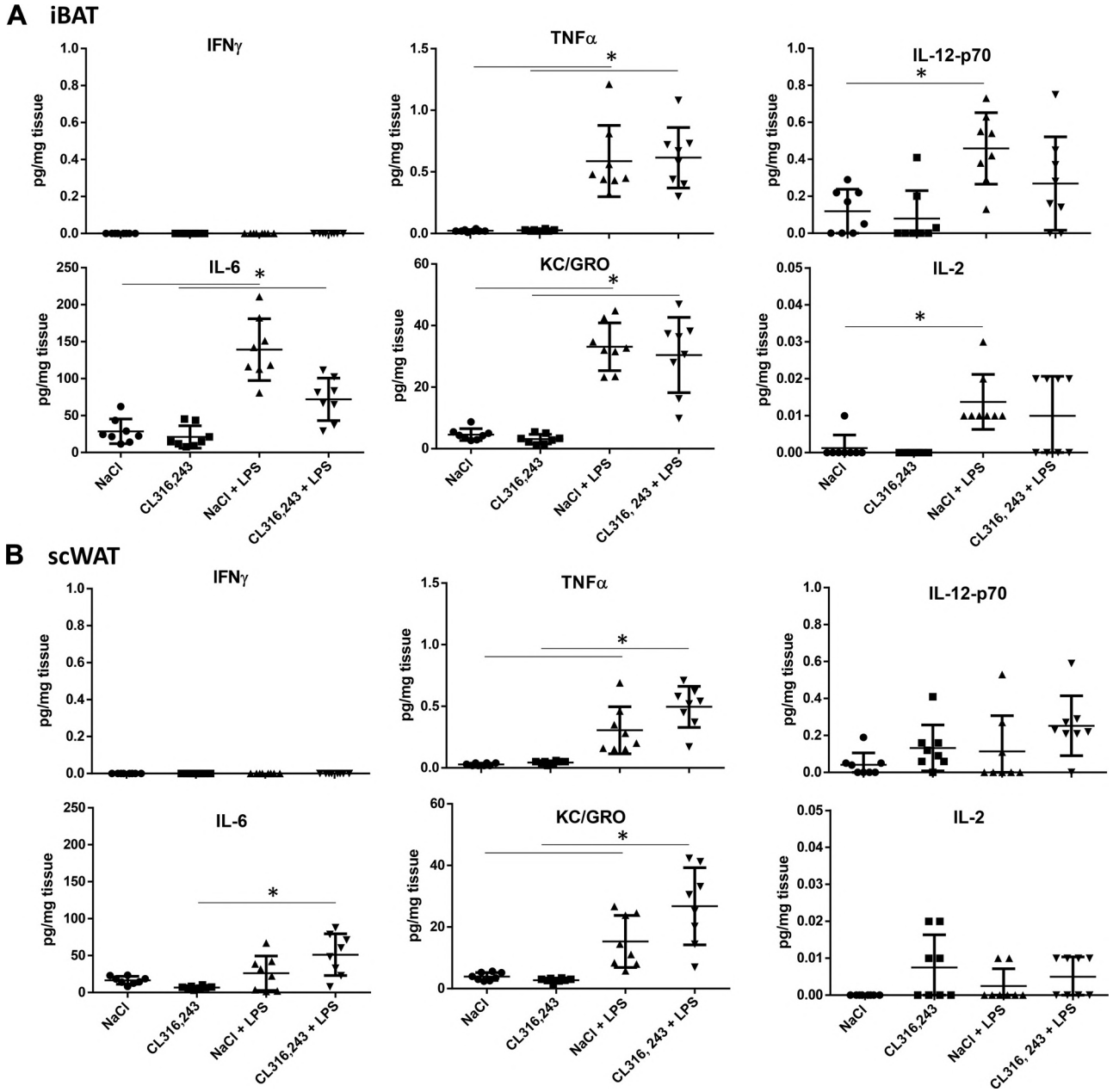


Fig. 5. Local inflammatory response to LPS. IFN-γ, TNF-α, IL-6, IL-12-p70, KC/GRO (CXCL-1), and IL-2 levels were assessed in the media of iBAT (*A*) and scWAT (*B*) explants from mice that were treated for 1 wk with CL316,243 daily (1 mg/kg/day) or vehicle only (NaCl) and with or without LPS treatment (1 mg/kg) for the final 6 h. The results are displayed as explant values (dots) and means ± SE. $n = 8$. *$P < 0.05$. iBAT, interscapular brown adipose tissue; scWAT, subcutaneous white adipose tissue.

related to fever, as body temperature was not available in our work. Inconsistently, numerous studies have shown an inhibitory effect of chronic LPS treatment on Ucp1 expression and function in vivo and thus on thermogenesis (33). In our work, we showed that LPS did not modify Ucp1 expression or the histology of BAT and scWAT after CL316,243 treatment, strongly suggesting that LPS does not affect thermogenesis. The difference between our results and those of Okla and colleagues (33) is probably due to the duration of LPS treatment (6 h vs. 2 wk). This was confirmed by an in vitro experiment on brite adipocytes showing that LPS slightly inhibited Ucp1 mRNA expression due to isoproterenol treatment but did not modify Ucp1 function, as demonstrated by oxygen consumption analysis. It is possible that a difference exists between brite and brown adipocytes, as LPS inhibits Ucp1 function in brown adipocytes in vitro (1).

As mentioned previously, LPS is a known inducer of lipolysis, which is confirmed in our in vitro experiment (51). In the same way, thermogenic activity induced by CL316,243 treatment involved a sustained lipolysis supplying fatty acids as the energy substrate to brown and brite adipocytes and releasing glycerol in circulation (47). In vivo, we did not detect any increase in glycerol plasma level after both LPS and CL316,243 treatment. Although the short treatment time with LPS can

explain this, it is not the case for chronic CL316,243 treatment. We hypothesized that, in this mouse strain, a higher uptake of glycerol by the liver or an active glycerol recycling by adipocytes could limit the level of circulating glycerol in the blood (3, 35).

Dowal and colleagues (13) used a coculture of human adipocytes and macrophage cell lines to show that brown adipocytes reduced macrophage IL-6 secretion in response to LPS compared with that of white adipocytes. Under similar conditions, mRNA expression of other inflammatory markers, including Il-10, in macrophages was inhibited by brown adipocytes. These results suggest that brown adipocytes and perhaps brite adipocytes display general immunomodulatory properties of interest. Our ex vivo analysis showed the same results, with decreased mRNA expression of Il-6 in brite adipocytes compared with that in white adipocytes and to a lesser extent for Tnf-α. We hypothesized that the inhibition of inflammatory cytokine expression in brown adipocytes participates in its immunomodulatory activity on macrophages. Unfortunately, this inhibition of proinflammatory and anti-inflammatory cytokine levels was not confirmed in vivo. Control mice and mice that were pretreated with CL316,243 displayed an equivalent increase in the secretion of TNF-α and IL-6 after LPS treatment. The same results were obtained for other pro- and anti-inflammatory cytokines in plasma and adipose tissue, except for IFN-γ and IL-2 plasma levels, which were strongly decreased in the CL316,243 group after LPS treatment. As no IFN-γ and very low quantities of IL-2 were found in BAT and scWAT, we can exclude the involvement of these tissues in this immunomodulatory effect. Moreover, the discrepancies between plasma and adipose tissue cytokine levels demonstrated that the local production of cytokines found in the adipose tissue had a limited impact on systemic inflammatory response to LPS. Nevertheless, in addition to cytokines, oxygenated derivatives of ω6 polyunsaturated fatty acids (n-2 series prostaglandins and n-4 series leukotrienes) and of ω3 polyunsaturated fatty acids (n-3 series prostaglandins, n-5 series leukotrienes, resolvins, and protectins) are highly synthesized and secreted by adipocytes and participate in the inflammatory and resolutive states of immune response (19, 31). As we have demonstrated previously that recruitment and activation of brown and brite adipocytes modulate these syntheses (12, 17), we can hypothesize that these metabolites could participate in the local, and even systemic, inflammatory response to LPS of the adipose tissue.

Along with proinflammatory cytokines, IL-1β has a central role in the immune response to LPS and in adipose tissue homeostasis (45). More specifically, IL-1β secretion induced by LPS treatment disrupts insulin signaling in WAT (2, 22, 26) and inhibits UCP1 function in BAT both in vitro and in vivo (9, 18). As expected, we found that LPS treatment induced IL-1β production in all conditions assayed, as shown by mRNA expression in white and brite adipocytes in vitro and secretion of the mature form of IL-1β in BAT and scWAT in vivo. In addition, we showed that recruitment and activation of brown and brite adipocytes did not modulate IL-1β levels and thus did not seem to prevent the inflammatory action of this cytokine. IL-1β is mainly regulated at the expression, maturation, and secretion levels, especially by modulation of the nuclear factor κB (NF-kB) transcription factor and activation of inflammasomes. Another pathway exists to modulate IL-1 activity, which is the production and secretion of IL-1RA. This cytokine antagonizes the biological effects of IL-1β by competing for binding to the IL-1 receptor without inducing a cellular response (43). Moreover, IL-1RA is highly produced by the adipose tissue (23). Interestingly, we demonstrated that Il-1rn mRNA was more highly expressed in brite adipocytes in vitro than in white adipocytes and that this difference was amplified when the cells were treated with a β-adrenergic receptor agonist. Importantly, these observations were confirmed in vivo, where CL316,243 treatment increased IL-1RA levels in WAT and BAT, with or without LPS treatment. In contrast, the plasma levels of IL-1RA increased only in the presence of LPS and independent of CL316,243 treatment. Taken together, these results clearly demonstrate that brite and brown adipocytes express and/or secrete more IL-1RA than white adipocytes, especially in response to acute LPS treatment and certainly via direct activation of TLR4 pathway. In addition to a potential anti-inflammatory role of IL-1RA, we hypothesize that the simultaneous secretion of IL-1RA and IL-1β corresponds to a protective mechanism to preserve adipocyte function in an inflammatory context.

Increased IL-1β or decreased IL-1RA levels are linked to the development of obesity and diabetes, and among therapeutic strategies developed to normalize these levels, some studies have focused on the use of exogenous IL-1RA (44, 45). In rodents, chronic IL-1RA treatment of mice that were fed a high-fat/high-sucrose diet prevented glucose metabolism alteration and normalized the metabolic parameters linked to obesity without affecting fat mass (40). In addition, using IL-1RA-overexpressing mice, we detected a normalization of inflammatory marker mRNA in the WAT of mice that were fed a high-fat diet (40). In humans, several clinical trials using anakinra (recombinant human IL-1RA) have been developed with obese and diabetic patients and have shown, among others, better pancreatic function and decreased systemic inflammation after treatment (28, 48). As we demonstrated that IL-1RA adipose levels are increased after β-adrenergic receptor agonist treatment, we suggest that increasing brown/brite adipocyte recruitment and activity in humans, in addition to decreasing fat mass, protects the adipose tissue from the adverse effects of IL-1β.

Our study was performed in lean BALB/c mice at ambient temperature. Thus, *i*) we cannot exclude that the results displayed herein were inherent to the model chosen; *ii*) we have a basal thermogenic activity due to ambient temperature, which could limit the difference between CL316,243 treated and untreated mice, and it will be interesting to reproduce this work at thermoneutrality to match the human situation more; and *iii*) as we have decided to develop our study on lean mice to exclude any additional effect of an obesogenic environment, it will be of interest to transpose now this study in an obese mouse model mimicking the human situation, where endotoxemia is mainly found.

Finally, we have demonstrated that recruitment and activation of brown and brite adipocytes in the adipose tissue of mice led to a local anti-inflammatory phenotype characterized by an increased IL-1RA level and decreased leptin secretion in response to endotoxemia without modulation of systemic inflammation.

**ACKNOWLEDGMENTS**

The authors greatly acknowledge the C3M Animal core facility, the IRCAN Cytomed platform, and the IBV histology platform.

## GRANTS

This research was funded by Inserm, Region PACA, and Société Francophone du Diabète/Pierre Fabre Médicament 2017.

## DISCLOSURE

No conflicts of interest, financial or otherwise, are declared by the authors.

## AUTHOR CONTRIBUTIONS

L.B. and D.F.P. conceived and designed research; P.M., O.D., S.R., A.L., C.D., and D.F.P. performed experiments; P.M., C.D., L.B., and D.F.P. analyzed data; P.M., L.B., and D.F.P. interpreted results of experiments; D.F.P. prepared figures; D.F.P. drafted manuscript; P.M., C.D., L.B., and D.F.P. edited and revised manuscript; P.M., O.D., S.R., A.L., C.D., L.B., and D.F.P. approved final version of manuscript.

## REFERENCES

1. **Bae J**, **Ricciardi CJ**, **Esposito D**, **Komarnytsky S**, **Hu P**, **Curry BJ**, **Brown PL**, **Gao Z**, **Biggerstaff JP**, **Chen J**, **Zhao L.** Activation of pattern recognition receptors in brown adipocytes induces inflammation and suppresses uncoupling protein 1 expression and mitochondrial respiration. *Am J Physiol Cell Physiol* 306: C918–C930, 2014. doi:10.1152/ajpcell.00249.2013.
2. **Ballak DB**, **Stienstra R**, **Tack CJ**, **Dinarello CA**, **van Diepen JA.** IL-1 family members in the pathogenesis and treatment of metabolic disease: Focus on adipose tissue inflammation and insulin resistance. *Cytokine* 75: 280–290, 2015. doi:10.1016/j.cyto.2015.05.005.
3. **Barquissau V**, **Beuzelin D**, **Pisani DF**, **Beranger GE**, **Mairal A**, **Montagner A**, **Roussel B**, **Tavernier G**, **Marques MA**, **Moro C**, **Guillou H**, **Amri EZ**, **Langin D.** White-to-brite conversion in human adipocytes promotes metabolic reprogramming towards fatty acid anabolic and catabolic pathways. *Mol Metab* 5: 352–365, 2016. doi:10.1016/j.molmet.2016.03.002.
4. **Brand MD**, **Nicholls DG.** Assessing mitochondrial dysfunction in cells. *Biochem J* 435: 297–312, 2011. doi:10.1042/BJ20110162.
5. **Bustin SA**, **Benes V**, **Garson JA**, **Hellemans J**, **Huggett J**, **Kubista M**, **Mueller R**, **Nolan T**, **Pfaffl MW**, **Shipley GL**, **Vandesompele J**, **Wittwer CT.** The MIQE guidelines: minimum information for publication of quantitative real-time PCR experiments. *Clin Chem* 55: 611–622, 2009. doi:10.1373/clinchem.2008.112797.
6. **Cani PD**, **Bibiloni R**, **Knauf C**, **Waget A**, **Neyrinck AM**, **Delzenne NM**, **Burcelin R.** Changes in gut microbiota control metabolic endotoxemia-induced inflammation in high-fat diet-induced obesity and diabetes in mice. *Diabetes* 57: 1470–1481, 2008. doi:10.2337/db07-1403.
7. **Cani PD**, **Delzenne NM.** Involvement of the gut microbiota in the development of low grade inflammation associated with obesity: focus on this neglected partner. *Acta Gastroenterol Belg* 73: 267–269, 2010.
8. **Cani PD**, **Delzenne NM**, **Amar J**, **Burcelin R.** Role of gut microflora in the development of obesity and insulin resistance following high-fat diet feeding. *Pathol Biol (Paris)* 56: 305–309, 2008. doi:10.1016/j.patbio.2007.09.008.
9. **Cannon B**, **Houstek J**, **Nedergaard J.** Brown adipose tissue. More than an effector of thermogenesis? *Ann N Y Acad Sci* 856: 171–187, 1998. doi:10.1111/j.1749-6632.1998.tb08325.x.
10. **Cannon B**, **Nedergaard J.** Brown adipose tissue: function and physiological significance. *Physiol Rev* 84: 277–359, 2004. doi:10.1152/physrev.00015.2003.
11. **Cinti S.** Transdifferentiation properties of adipocytes in the adipose organ. *Am J Physiol Endocrinol Metab* 297: E977–E986, 2009. doi:10.1152/ajpendo.00183.2009.
12. **Colson C**, **Ghandour RA**, **Dufies O**, **Rekima S**, **Loubat A**, **Munro P**, **Boyer L**, **Pisani DF.** Diet supplementation in ω3 polyunsaturated fatty acid favors an anti-inflammatory basal environment in mouse adipose tissue. *Nutrients* 11: 438, 2019. doi:10.3390/nu11020438.
13. **Dowal L**, **Parameswaran P**, **Phat S**, **Akella S**, **Majumdar ID**, **Ranjan J**, **Shah C**, **Mogre S**, **Guntur K**, **Thapa K**, **Gesta S**, **Vishnudas VK**, **Narain NR**, **Sarangarajan R.** Intrinsic properties of brown and white adipocytes have differential effects on macrophage inflammatory responses. *Mediators Inflamm* 2017: 9067049, 2017. doi:10.1155/2017/9067049.
14. **Faul F**, **Erdfelder E**, **Lang AG**, **Buchner A.** G*Power 3: a flexible statistical power analysis program for the social, behavioral, and biomedical sciences. *Behav Res Methods* 39: 175–191, 2007. doi:10.3758/BF03193146.
15. **Fischer AW**, **Hoefig CS**, **Abreu-Vieira G**, **de Jong JMA**, **Petrovic N**, **Mittag J**, **Cannon B**, **Nedergaard J.** leptin raises defended body temperature without activating thermogenesis. *Cell Reports* 14: 1621–1631, 2016. doi:10.1016/j.celrep.2016.01.041.
16. **Gatineau M**, **Hancock C**, **Holman N**, **Outhwaite H**, **Oldridge L**, **Christie A**, **Ells L.** *Adult Obesity and Type 2 Diabetes* (Online). London: Public Health England, 2014. https://assets.publishing.service.gov.uk/government/uploads/system/uploads/attachment_data/file/338934/Adult_obesity_and_type_2_diabetes_.pdf.
17. **Ghandour RA**, **Colson C**, **Giroud M**, **Maurer S**, **Rekima S**, **Ailhaud G**, **Klingenspor M**, **Amri EZ**, **Pisani DF.** Impact of dietary ω3 polyunsaturated fatty acid supplementation on brown and brite adipocyte function. *J Lipid Res* 59: 452–461, 2018. doi:10.1194/jlr.M081091.
18. **Goto T**, **Naknukool S**, **Yoshitake R**, **Hanafusa Y**, **Tokiwa S**, **Li Y**, **Sakamoto T**, **Nitta T**, **Kim M**, **Takahashi N**, **Yu R**, **Daiyasu H**, **Seno S**, **Matsuda H**, **Kawada T.** Proinflammatory cytokine interleukin-1β suppresses cold-induced thermogenesis in adipocytes. *Cytokine* 77: 107–114, 2016. doi:10.1016/j.cyto.2015.11.001.
19. **Hardwick JP**, **Eckman K**, **Lee YK**, **Abdelmegeed MA**, **Esterle A**, **Chilian WM**, **Chiang JY**, **Song BJ.** Eicosanoids in metabolic syndrome. *Adv Pharmacol* 66: 157–266, 2013. doi:10.1016/B978-0-12-404717-4.00005-6.
20. **Hotamisligil GS.** Inflammation and metabolic disorders. *Nature* 444: 860–867, 2006. doi:10.1038/nature05485.
21. **Hotamisligil GS**, **Shargill NS**, **Spiegelman BM.** Adipose expression of tumor necrosis factor-alpha: direct role in obesity-linked insulin resistance. *Science* 259: 87–91, 1993. doi:10.1126/science.7678183.
22. **Jager J**, **Grémeaux T**, **Cormont M**, **Le Marchand-Brustel Y**, **Tanti JF.** Interleukin-1beta-induced insulin resistance in adipocytes through down-regulation of insulin receptor substrate-1 expression. *Endocrinology* 148: 241–251, 2007. doi:10.1210/en.2006-0692.
23. **Juge-Aubry CE**, **Somm E**, **Giusti V**, **Pernin A**, **Chicheportiche R**, **Verdumo C**, **Rohner-Jeanrenaud F**, **Burger D**, **Dayer JM**, **Meier CA.** Adipose tissue is a major source of interleukin-1 receptor antagonist: upregulation in obesity and inflammation. *Diabetes* 52: 1104–1110, 2003. doi:10.2337/diabetes.52.5.1104.
24. **Karampela I**, **Christodoulatos GS**, **Dalamaga M.** The role of adipose tissue and adipokines in sepsis: inflammatory and metabolic considerations, and the obesity paradox. *Curr Obes Rep* 8: 434–457, 2019. doi:10.1007/s13679-019-00360-2.
25. **Kershaw EE**, **Flier JS.** Adipose tissue as an endocrine organ. *J Clin Endocrinol Metab* 89: 2548–2556, 2004. doi:10.1210/jc.2004-0395.
26. **Lagathu C**, **Yvan-Charvet L**, **Bastard JP**, **Maachi M**, **Quignard-Boulangé A**, **Capeau J**, **Caron M.** Long-term treatment with interleukin-1beta induces insulin resistance in murine and human adipocytes. *Diabetologia* 49: 2162–2173, 2006. doi:10.1007/s00125-006-0335-z.
27. **Langin D.** Recruitment of brown fat and conversion of white into brown adipocytes: strategies to fight the metabolic complications of obesity? *Biochim Biophys Acta* 1801: 372–376, 2010. doi:10.1016/j.bbalip.2009.09.008.
28. **Larsen CM**, **Faulenbach M**, **Vaag A**, **Vølund A**, **Ehses JA**, **Seifert B**, **Mandrup-Poulsen T**, **Donath MY.** Interleukin-1-receptor antagonist in type 2 diabetes mellitus. *N Engl J Med* 356: 1517–1526, 2007. doi:10.1056/NEJMoa065213.
29. **Locati M**, **Curtale G**, **Mantovani A.** Diversity, mechanisms, and significance of macrophage plasticity. *Annu Rev Pathol* 15: 123–147, 2020. doi:10.1146/annurev-pathmechdis-012418-012718.
30. **Lumeng CN**, **Bodzin JL**, **Saltiel AR.** Obesity induces a phenotypic switch in adipose tissue macrophage polarization. *J Clin Invest* 117: 175–184, 2007. doi:10.1172/JCI29881.
31. **Masoodi M**, **Kuda O**, **Rossmeisl M**, **Flachs P**, **Kopecky J.** Lipid signaling in adipose tissue: Connecting inflammation & metabolism. *Biochim Biophys Acta* 1851: 503–518, 2015. doi:10.1016/j.bbalip.2014.09.023.
32. **Odegaard JI**, **Chawla A.** The immune system as a sensor of the metabolic state. *Immunity* 38: 644–654, 2013. doi:10.1016/j.immuni.2013.04.001.
33. **Okla M**, **Wang W**, **Kang I**, **Pashaj A**, **Carr T**, **Chung S.** Activation of Toll-like receptor 4 (TLR4) attenuates adaptive thermogenesis via endoplasmic reticulum stress. *J Biol Chem* 290: 26476–26490, 2015. doi:10.1074/jbc.M115.677724.
34. **Okla M**, **Zaher W**, **Alfayez M**, **Chung S.** Inhibitory effects of toll-like receptor 4, NLRP3 inflammasome, and interleukin-1β on white adipocyte browning. *Inflammation* 41: 626–642, 2018. doi:10.1007/s10753-017-0718-y.

35. **Patsouris D**, **Mandard S**, **Voshol PJ**, **Escher P**, **Tan NS**, **Havekes LM**, **Koenig W**, **März W**, **Tafuri S**, **Wahli W**, **Müller M**, **Kersten S.** PPARalpha governs glycerol metabolism. *J Clin Invest* 114: 94–103, 2004. doi:10.1172/JCI200420468.
36. **Pisani DF**, **Beranger GE**, **Corinus A**, **Giroud M**, **Ghandour RA**, **Altirriba J**, **Chambard JC**, **Mazure NM**, **Bendahhou S**, **Duranton C**, **Michiels JF**, **Frontini A**, **Rohner-Jeanrenaud F**, **Cinti S**, **Christian M**, **Barhanin J**, **Amri EZ.** The K+ channel TASK1 modulates β-adrenergic response in brown adipose tissue through the mineralocorticoid receptor pathway. *FASEB J* 30: 909–922, 2016. doi:10.1096/fj.15-277475.
37. **Pohl J**, **Woodside B**, **Luheshi GN.** Leptin modulates the late fever response to LPS in diet-induced obese animals. *Brain Behav Immun* 42: 41–47, 2014. doi:10.1016/j.bbi.2014.07.017.
38. **Sachot C**, **Poole S**, **Luheshi GN.** Circulating leptin mediates lipopolysaccharide-induced anorexia and fever in rats. *J Physiol* 561: 263–272, 2004. doi:10.1113/jphysiol.2004.074351.
39. **Sakamoto T**, **Takahashi N**, **Sawaragi Y**, **Naknukool S**, **Yu R**, **Goto T**, **Kawada T.** Inflammation induced by RAW macrophages suppresses UCP1 mRNA induction via ERK activation in 10T1/2 adipocytes. *Am J Physiol Cell Physiol* 304: C729–C738, 2013. doi:10.1152/ajpcell.00312.2012.
40. **Sauter NS**, **Schulthess FT**, **Galasso R**, **Castellani LW**, **Maedler K.** The antiinflammatory cytokine interleukin-1 receptor antagonist protects from high-fat diet-induced hyperglycemia. *Endocrinology* 149: 2208–2218, 2008. doi:10.1210/en.2007-1059.
41. **Schäffler A**, **Schölmerich J.** Innate immunity and adipose tissue biology. *Trends Immunol* 31: 228–235, 2010. doi:10.1016/j.it.2010.03.001.
42. **Schäffler A**, **Schölmerich J**, **Salzberger B.** Adipose tissue as an immunological organ: Toll-like receptors, C1q/TNFs and CTRPs. *Trends Immunol* 28: 393–399, 2007. doi:10.1016/j.it.2007.07.003.
43. **Seckinger P**, **Lowenthal JW**, **Williamson K**, **Dayer JM**, **MacDonald HR.** A urine inhibitor of interleukin 1 activity that blocks ligand binding. *J Immunol* 139: 1546–1549, 1987.
44. **Stienstra R**, **Tack CJ**, **Kanneganti TD**, **Joosten LA**, **Netea MG.** The inflammasome puts obesity in the danger zone. *Cell Metab* 15: 10–18, 2012. doi:10.1016/j.cmet.2011.10.011.
45. **Tack CJ**, **Stienstra R**, **Joosten LA**, **Netea MG.** Inflammation links excess fat to insulin resistance: the role of the interleukin-1 family. *Immunol Rev* 249: 239–252, 2012. doi:10.1111/j.1600-065X.2012.01145.x.
46. **Tilg H**, **Zmora N**, **Adolph TE**, **Elinav E.** The intestinal microbiota fuelling metabolic inflammation. *Nat Rev Immunol* 20: 40–54, 2020. doi:10.1038/s41577-019-0198-4.
47. **Umekawa T**, **Yoshida T**, **Sakane N**, **Kondo M.** Effect of CL316,243, a highly specific beta(3)-adrenoceptor agonist, on lipolysis of epididymal, mesenteric and subcutaneous adipocytes in rats. *Endocr J* 44: 181–185, 1997. doi:10.1507/endocrj.44.181.
48. **van Asseldonk EJ**, **Stienstra R**, **Koenen TB**, **Joosten LA**, **Netea MG**, **Tack CJ.** Treatment with Anakinra improves disposition index but not insulin sensitivity in nondiabetic subjects with the metabolic syndrome: a randomized, double-blind, placebo-controlled study. *J Clin Endocrinol Metab* 96: 2119–2126, 2011. doi:10.1210/jc.2010-2992.
49. **Vijay-Kumar M**, **Aitken JD**, **Carvalho FA**, **Cullender TC**, **Mwangi S**, **Srinivasan S**, **Sitaraman SV**, **Knight R**, **Ley RE**, **Gewirtz AT.** Metabolic syndrome and altered gut microbiota in mice lacking Toll-like receptor 5. *Science* 328: 228–231, 2010. doi:10.1126/science.1179721.
50. **Wellen KE**, **Hotamisligil GS.** Obesity-induced inflammatory changes in adipose tissue. *J Clin Invest* 112: 1785–1788, 2003. doi:10.1172/JCI20514.
51. **Zu L**, **He J**, **Jiang H**, **Xu C**, **Pu S**, **Xu G.** Bacterial endotoxin stimulates adipose lipolysis via toll-like receptor 4 and extracellular signal-regulated kinase pathway. *J Biol Chem* 284: 5915–5926, 2009. doi:10.1074/jbc.M807852200.

# Implication de l'inflammasome NLRP3 dans la détection des toxines bactériennes et dans l'évolution du COVID-19

Lors d'une infection, la détection des microorganismes pathogènes est indispensable à la réponse immunitaire innée et à l'initiation de l'immunité adaptative. Une réponse immunitaire physiologique est définie comme une réponse proportionnelle et adaptée à la stimulation microbienne et doit conduire à une résolution de l'inflammation. Pour cela, l'hôte doit être capable de détecter quantitativement et qualitativement les micro-organismes. Du point de vue quantitatif, l'hôte détecte des motifs structuraux conservés au sein d'une classe de micro-organismes. D'autre part, la détection de l'activité des facteurs de virulence – spécifiques aux pathogènes – permet une détection qualitative.

La découverte des PRR et plus précisément des inflammasomes a permis une avancée majeure dans la compréhension des mécanismes de détection des pathogènes et des signaux de danger liés aux dommages cellulaires produits lors de l'infections. Les inflammasomes sont des complexes responsables de l'activation de la Caspase-1 et de la maturation de l'IL-1ß et IL-18. Initialement découverts pour leur implication dans des maladies auto-inflammatoires, les inflammasomes sont également impliqués dans la détection de l'activité des facteurs de virulence notamment ceux ciblant les Rho-GTPases.

Les Rho-GTPases sont situées au carrefour de grandes voies de signalisation cellulaire ; en régulant la migration cellulaire, la phagocytose ou encore la transcription des gènes, ceux sont des acteurs majeurs de l'immunité. Cela en fait des cibles préférentielles pour les bactéries pathogènes. En effet, plus de 30 facteurs de virulence bactériens manipulent les Rho GTPases en utilisant diverses stratégies menant à leur inhibition ou leur activation.

La bactérie E. coli uropathogène est la première cause de cystites, pyélonéphrites et dans les cas les plus graves de bactériémies. Plus de 30% des E. coli uropathogènes possèdent la toxine CNF1, une dé-amidase activant les Rho-GTPases.

Avant mon arrivée au laboratoire, l'équipe du Dr Laurent Boyer a montré que la toxine CNF1 induit une réponse immunitaire. En effet, au cours de la bactériémie chez la souris ou de l'infection systémique chez la drosophile, la détection de la toxine CNF1 induit la clairance bactérienne. Au niveau cellulaire, l'activation des Rho-GTPases par CNF1 est responsable de la production de cytokines pro-inflammatoires. En parallèle de cette réponse transcriptionnelle, la toxine CNF1 provoque la maturation de l'IL-1ß de façon dépendante de la Caspase-1, suggérant l'implication d'un inflammasome.

Mon projet de thèse était d'identifier l'inflammasome impliqué dans la détection de la toxine CNF1 et de caractériser la voie de signalisation menant à cette activation.

Nous avons identifié l'inflammasome NLRP3 comme étant responsable de la détection de l'activation de la GTPase Rac2 par la toxine CNF1. Nous avons ensuite étudié le rôle de la kinase Pak1, effecteur de Rac2, dans cette voie de signalisation et nous avons pu montrer que Pak1 joue un rôle crucial dans l'activation de l'inflammasome NLRP3 par CNF1. Pak1 phosphoryle la Thr659 du récepteur NLRP3 et cette phosphorylation est déterminante pour le recrutement de la protéine régulatrice Nek7 et l'activation de l'inflammasome NLRP3. Finalement, nous avons pu montrer le rôle majeur de la voie Pak1-NLRP3 dans la mise en place d'une réponse immunitaire anti-virulence au cours de la bactériémie.

De plus, nous avons utilisé notre expertise pour étudier l'activation de l'inflammasome NLRP3 chez les patients infectés par le SARS-CoV-2. Cette étude nous a permis d'établir la signature de la réponse NLRP3 dans les cellules myéloïdes circulantes des patients COVID-19 et d'utiliser ces paramètres pour définir un score permettant de prédire l'évolution des patients.

Mon travail sur l'implication de l'inflammasome NLRP3 dans la détection de la virulence a permis une meilleure compréhension des mécanismes impliqués lors d'une réponse immunitaire anti-infectieuse.